AD 742733

AD

USAAMRDL TECHNICAL REPORT 71-54

THE DESIGN, FABRICATION, AND TESTING OF AN INTEGRALLY ARMORED CRASHWORTHY CREW SEAT

By

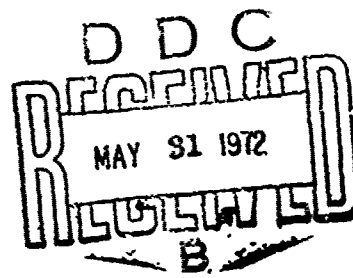Stanley P. Desjardins

Harold D. Harrison

January 1972

EUSTIS DIRECTORATE
U. S. ARMY AIR MOBILITY RESEARCH AND DEVELOPMENT LABORATORY
FORT EUSTIS, VIRGINIA

CONTRACT DAAJ02-69-C-0030
DYNAMIC SCIENCE ENGINEERING OPERATIONS
A DIVISION OF MARSHALL INDUSTRIES
PHOENIX, ARIZONA

Best Available Copy

DISCLAIMERS

The findings in this report are not to be construed as an official Department of the Army position unless so designated by other authorized documents.

When Government drawings, specifications, or other data are used for any purpose other than in connection with a definitely related Government procurement operation, the United States Government thereby incurs no responsibility nor any obligation whatsoever; and the fact that the Government may have formulated, furnished, or in any way supplied the said drawings, specifications, or other data is not to be regarded by implication or otherwise as in any manner licensing the holder or any other person or corporation, or conveying any rights or permission, to manufacture, use, or sell any patented invention that may in any way be related thereto.

Trade names cited in this report do not constitute an official endorsement or approval of the use of such commercial hardware or software.

DISPOSITION INSTRUCTIONS

Destroy this report when no longer needed. Do not return it to the originator.

DOCUMENT CONTROL DATA - R & D

(Security classification of title, body of abstract and indexing annotation must be entered when the overall report is classified)

1. ORIGINATING ACTIVITY (Corporate author)	2a. REPORT SECURITY CLASSIFICATION
Dynamic Science Engineering Operations A Division of Marshall Industries Phoenix, Arizona	Unclassified
	2b. GROUP

3. REPORT TITLE

THE DESIGN, FABRICATION, AND TESTING OF AN INTEGRALLY ARMORED
CRASHWORTHY CREW SEAT

4. DESCRIPTIVE NOTES (Type of report and inclusive dates)

Final

5. AUTHOR(S) (First name, middle initial, last name)

Stanley P. Desjardins
Harold D. Harrison

6. REPORT DATE	7a. TOTAL NO. OF PAGES	7b. NO. OF REFS
January 1972	316	25
8a. CONTRACT OR GRANT NO. DAAJ02-69-C-0030	9a. ORIGINATOR'S REPORT NUMBER(S)	
b. PROJECT NO. 1F162203A529	USAAMRDL Technical Report 71-54	
c.	9b. OTHER REPORT NO(S) (Any other numbers that may be assigned this report) Dynamic Science 1680-71-24	
d.		

10. DISTRIBUTION STATEMENT

Approved for public release; distribution unlimited.

11. SUPPLEMENTARY NOTES	12. SPONSORING MILITARY ACTIVITY
	Eustis Directorate, U. S. Army Air Mobility Research and Development Laboratory, Fort Eustis, Virginia

13. ABSTRACT

A program was conducted to develop design technology for integrally armored crashworthy crew seats. The effort included theoretical analysis, design, fabrication, and testing.

Dynamic analysis of an occupant seated in an integrally armored crew seat was conducted. Then a seat concept trade-off was performed, a concept was selected and designed, and prototype seats were fabricated. The seats were subjected to a combined static loading test including simultaneous longitudinal, lateral, and vertical components while mounted in a test fixture simulating warped floor conditions typical of crashing aircraft. The seats were then subjected to a series of 10 dynamic tests to investigate and to verify the seat integrity and performance when subjected to dynamic loading conditions up to and including the 95th percentile survivable crash as defined for present-day aircraft. Empirical data were gathered which enabled determination of the decelerative load factor for use in sizing the energy-absorbing limit load to produce tolerable loads on the occupant. Conclusions were drawn and recommendations made for the design of crashworthy integrally armored crew seats for use in improving the survivability of both future and existing aircraft.

DD FORM **1473** REPLACES DD FORM 1473, 1 JAN 64, WHICH IS
1 NOV 65 OBSOLETE FOR ARMY USE.

14. KEY WORDS	LINK A		LINK B		LINK C	
	ROLL	WT	ROLE	WT	ROLE	WT
Armored Cra. 'thy Crew Seat						
Integrally A ed Crashworthy Crew Seat						
Static Seat Testing						
Dynamic Seat Testing						
Crash Energy-Absorption Technology						
Load-Limited Seat Design						

959-72

This report was prepared by Dynamic Science (The AvSER Facility), a Division of Marshall Industries, under the terms of Contract DAAJ02-69-C-0030.

The primary objective of this effort was to design, fabricate, and test a prototype armored pilot/copilot seat system which (1) will be suitable for mounting in rotary-wing and light fixed-wing aircraft following design refinement, (2) will incorporate armor protection against small-arms fire and shrapnel, and (3) will conform to the performance requirements of the draft proposed military specification, entitled "Seats, Crew, Adjustable, Aircraft, Types I and II." A secondary objective was to expand and improve technology relative to crashworthy seat design.

This report contains a description of the seat design concept tradeoff study, seat/occupant dynamic response analysis, prototype seat test articles, static and dynamic tests and program results.

The conclusions and recommendations submitted by the contractor are considered to be valid. Based on the results of this effort, the proposed military specification was revised and published on 27 August 1971 as MIL-S-58095(AV), "Seat System: Crashworthy, Nonejection, Aircrew, General Specification For."

The program was conducted under the technical management of Mr. G. T. Singley, III, Safety and Survivability Division.

Project 1F162203A529
Contract DAAJ02-69-C-0030
USAAMRDL Technical Report 71-54
January 1972

THE DESIGN, FABRICATION, AND TESTING OF
AN INTEGRALLY ARMORED CRASHWORTHY CREW SEAT

Final Report

Dynamic Science 1680-71-24

By

Stanley P. Desjardins
Harold D. Harrison

Prepared by

Dynamic Science Engineering Operations
A Division of Marshall Industries
Phoenix, Arizona

For

EUSTIS DIRECTORATE
U. S. ARMY AIR MOBILITY RESEARCH AND DEVELOPMENT LABORATORY
FORT EUSTIS, VIRGINIA

ABSTRACT

A program was conducted to develop design technology for integrally armored crashworthy crew seats. The effort included theoretical analysis, design, fabrication, and testing.

Dynamic analysis of an occupant seated in an integrally armored crew seat was conducted. Then a seat concept trade-off was performed, a concept was selected and designed, and prototype seats were fabricated. The seats were subjected to a combined static loading test including simultaneous longitudinal, lateral, and vertical components while mounted in a test fixture simulating warped floor conditions typical of crashing aircraft. The seats were then subjected to a series of 10 dynamic tests to investigate and to verify the seat integrity and performance when subjected to dynamic loading conditions up to and including the 95th percentile survivable crash as defined for present-day aircraft. Empirical data were gathered which enabled determination of the decelerative load factor for use in sizing the energy-absorbing limit load to produce tolerable loads on the occupant. Conclusions were drawn and recommendations made for the design of crashworthy integrally armored crew seats for use in improving the survivability of both future and existing aircraft.

CONTENTS

CONTENTS (CONT'D)

ILLUSTRATIONS

ILLUSTRATIONS (CONT'D)

ILLUSTRATIONS (CONT'D)

ILLUSTRATIONS (CONT'D)

ILLUSTRATIONS (CONT'D)

ILLUSTRATIONS (CONT'D)

xii

ILLUSTRATIONS (CONT'D)

ILLUSTRATIONS (CONT'D)

ILLUSTRATIONS (CONT'D)

ILLUSTRATIONS (CONT'D)

ILLUSTRATIONS (CONT'D)

xvii

ILLUSTRATIONS (CONT'D)

ILLUSTRATIONS (CONT'D)

ILLUSTRATIONS (CONT'D)

TABLES

CHAPTER 1

INTRODUCTION

1.1 GENERAL

This report documents a two-year program (1969-1970) conducted by Dynamic Science to design, fabricate, and test a crashworthy armored crew seat.

The program included a review of background information and existing design criteria, concept trade-offs, detailed design and analysis, prototype fabrication, static and dynamic testing, data analysis, and establishment of design criteria in technical support of a proposed Military Specification entitled "Seat System; Crashworthy, Non-Ejection, Aircrew, General Specification For", for the Eustis Directorate, U. S. Army Air Mobility Research and Development Laboratory (USAAMRDL), Fort Eustis, Virginia.

1.2 BACKGROUND

Early in the 1960s, comprehensive efforts were initiated to analyze the problem of crash safety with particular emphasis on seating and restraint systems. Studies[1] showed that occupant injury was being sustained because of inadequate strength and inadequate design practices in existing seats and restraint systems. Since these seats were designed to meet the requirements of then-current specifications, it was apparent that the specifications were inadequate. Analyses resulted in establishment of the need for increased seat retention strength coupled with energy-absorption capacity to lower decelerative loads. Design criteria were established and, in 1967, documented in the "Crash Survival Design Guide".[2]

Although the seat design criteria seemed adequate for seats of light movable section weight, the advent of integrally armored crew seats to protect the occupant from ballistic ground fire in combat situations complicated the development of a successful energy-absorbing or crashworthy seat. Development programs resulted in seats with heavy movable sections which did not perform as predicted. Dynamic tests showed that seat occupants were subjected to much higher decelerative loading than expected and that seat stroking was not predictable or adequate.[3,4] Several different prototype crashworthy integrally armored crew seats were developed in compliance with the design criteria established. However, most of the seats were inadequate due to structural defects or improper functioning of the load-limiting system and/or the occupant restraint systems.[3,4]

1

In 1968, the Eustis Directorate developed a proposed Military Specification defining the requirements for crashworthy crew seats, the most recent version of which is Reference 5. The program reported herein was initiated in early 1969 to design, fabricate, and performance test a crashworthy armored crew seat to meet and verify the requirements of the specification. The seats were to conform to the performance and strength requirements of the specification or to comply with new technology developed during the program. The purpose of the program was to verify the feasibility of integrally armored crashworthy crew seats and to develop new technology, where needed, to update the established criteria. If possible, the seat was to provide protection for occupants exposed to the 95th percentile survivable crash pulse as defined in Reference 2. If this proved not to be feasible in a practical configuration, then the survivable crash pulse for which protection could be provided in a practical integrally armored crew seat design was to be established. Design efforts were not restricted to retrofit requirements of an existing aircraft but, rather, were directed toward eventual application to future aircraft in which the seat and fuselage could be designed simultaneously.

Advanced features of the resulting seat design included increased ballistic coverage for the 95th percentile occupant with sufficient clearance to permit the use of heavy arctic clothing, freedom of movement, and room for the increased size of future generations of crew members. Another advanced feature was the special floor mounts designed to permit floor buckling and warping while minimizing the forced racking of the seat structure. The vertical stroke length established as a practical limit for crew seats was considerably increased over previous established lengths, and an energy absorber with a tri-level limit load was provided to reduce the decelerative loading on the 5th through the 95th percentile range of occupants. The seat design also included rolling guidance suspension to permit a predictable energy-absorbing stroke.

In conducting the program, previous technology was first reviewed and a seat concept trade-off was conducted to establish the overall configuration of the seat to be designed. A prototype seat was designed and fabricated. The design was supported by dynamic analysis to establish performance requirements for the energy-absorbing systems in the seat. The resultant seat was then subjected to a combined static test which included longitudinal and lateral loading simultaneously with vertical energy-absorber stroking. The floor was warped during the test to simulate what might occur during an aircraft crash.

After successfully passing the static testing, the seat was subjected to a series of 10 dynamic tests to verify: (1) the vertical stroke distance required to provide occupant protection, (2) the limit load of the energy-absorbing system required to provide protection to the occupant in the vertical direction, and (3) the structural integrity of the seat design.

The results of the program are presented in Chapters 2 through 6 of this report.

CHAPTER 2

SEAT DEVELOPMENT

2.1 INTRODUCTION

This chapter presents the design criteria and a detailed description of the experimental seat.

2.2 DESIGN CRITERIA AND CONCEPT DEVELOPMENT

2.2.1 DESIGN CRITERIA

Seat design criteria were developed in the form of requisites to guide the design effort from concept inception through final design. These requisites were:

1. Overall: The seat design should incorporate those features and characteristics representative of an end-item seat. However, the design should contain the flexibility required to permit its test evaluation in a variety of environments necessary to establish performance trends as a function of the selected system variables. Components should be designed from flight-type materials; however, substitutes in both materials and configuration may be used to reduce price. Factors affecting performance of the seat such as mass and center-of-gravity location should be duplicated; however, operational refinements such as hinged panels for ingress and egress need not be duplicated.

2. Energy Absorption: The design should permit sufficient energy-absorbing vertical stroke to limit the loads on the 5th through 95th percentile occupants to tolerable levels, and it should make maximum use of the stroke distance between the seat pan and the floor of the aircraft in any adjustment position. In addition, the seat design should be flexible enough to permit quick and easy changes of the energy-absorber limit load during the test program if desirable.

3. Application: The basic configuration and size of the seat should be designed for application to future aircraft, not for retrofit into existing vehicles. This criterion should apply both to the evolutionary increase in size projected for Army aviators and to the interfacing aircraft structure. It should be assumed

4

that the seat and aircraft attachment provisions
would be designed as a system and, consequently, pro-
vide compatibility.

4. State of the Art: The seat design should make maxi-
mum use of previously developed hardware and tech-
nology.

5. Configuration: The configuration of the seat should
conform to the occupant physical characteristics
falling between the 5th and the 95th percentiles in
accordance with Technical Report EP-150, "Anthropom-
etry of Army Aviators".[6]

6. Composition/Comfort: The seat should consist of a
movable and fixed section. The movable portion
should support the occupant comfortably, permitting
easy access to controls while constraining him
against forces resulting from crashes classified as
survivable. This requires seat adjustment in the
longitudinal and vertical directions, contact sur-
faces that conform to the body, and a restraint sys-
tem that distributes the loads and does not locate
adjustments or metal fittings, etc., over bony sec-
tions of the body. In addition to the mechanical
comfort aspects, the seat and restraint system should
not cause excessive thermal discomfort of the occu-
pant.

7. Ballistic Protection: The seat should be of an inte-
gral armored design, i.e., the movable bucket should
be formed of ballistic armor. The armor should be of
a design capable of providing protection from a 30-
caliber armor-piercing threat. Protection should be
provided for projectiles approaching from the bottom,
sides, and back. Frontal protection will be provided
by an armored vest. For this investigative and demon-
strative program, the armor may be simulated by a co
figuration duplicating the areal density and center
of gravity of the armored bucket. Ballistic protec-
tion should generally comply with Reference 7.

8. Crash Protection: The seat should restrain the occu-
pant against applied loads up to and including the
95th percentile survivable crash as defined in Refer-
ences 2 and 5. The seat should provide protection
from as severe a crash pulse as possible with a mini-
mum energy-absorbing stroke distance of 12 inches in
the vertical direction.

9. **Seat Load Limiting:** The seat should be designed to maintain occupant restraint during a warped floor condition typical in aircraft crashes and as defined in Reference 2. The seat design should therefore have provisions which permit floor deflection and rotation while not imposing excessive loads on the seat structure and armored bucket or on the floor attachments that could result in failure of either of these components.

10. **Occupant Load Limiting:** The seat should be designed to limit the acceleration of the occupant to within human tolerance levels as specified in References 2 and 5. Although desirable, energy-absorption strokes in the lateral and longitudinal directions are not required; however, the vertical energy-absorption features of the seat must be designed to limit vertical acceleration. Protection should be evaluated considering duration at G level using the curve presented in Figure 12 in Reference 5 as judgment criteria. Provisions in the design should be made for protection of the lighter seat occupants to a comparable value afforded the heavier occupants.

11. **Weight:** The experimental seats to be fabricated should incorporate flight-type structure and joining techniques and should be as light as possible consistent with investigative and concept proof type hardware. Investigative hardware should contain the flexibility required to conduct matrix type testing covering wide variations in input pulse and energy-absorption parameters.

12. **Simplicity:** The seat should be as simple as possible for meeting the other specified requirements.

13. **Degree of Design Refinement:** The experimental seats fabricated in the program should be technology development test models. No special effort or cost should be expended to conform to those sections of the seat specification dealing with production hardware such as finish, color, dimensional tolerances, etc., except as they affect the performance of the seat for testing purposes. Mass and volume associated with movable portions of the seat system must be representative of the conceptual end item to provide meaningful operational test data and proof of the feasibility and performance of the seat concept.

2.2.2 CONCEPT DEVELOPMENT

Preceding preliminary designs of the experimental seat configuration, a concept trade-off was conducted. The goal was to develop a variety of concepts which could be compared through a weighted trade-off of several important parameters and thus guide the selection of a near-optimum concept. It was decided initially to concentrate on occupant protection against vertical decelerative loads as, because of low human tolerance in this direction, load limiting is absolutely required. Although load limiting in the longitudinal and lateral directions is desirable, it is not considered mandatory, as human tolerance limits would not be exceeded by the environments resulting from 95th percentile survivable accidents with no intentional load limiting.

A brief discussion of the candidate concepts which were developed and evaluated is presented in the following paragraphs. All concepts presented use essentially the same contoured integral armored bucket. Modifications to this basic configuration are minor and involve only the energy-absorbing or support systems. A weighted trade-off of the concepts is presented following the concept discussion.

2.2.2.1 Crushable Seat Cushion (Fixed Seat) - Concept 1:

This seat concept (Figure 1) attaches the major portion of the bucket rigidly to the aircraft floor. The bottom of the seat pan is a separate section and is placed on crushable material. The comfort cushion positioned on top of this panel provides the interface with the occupant. Upon loading, the armored seat pan serves a second purpose by spreading the decelerative load of the occupant evenly over the crushable material, thus providing a predictable limit load for the energy-absorbing crushable material.

Advantages of the system include a reduction in movable mass; i.e., the entire weight of the armored bucket is not required to stroke with the occupant. This reduces the degree of interaction between the occupant and the heavy seat, thus lowering loads originating from this cause. The system would be relatively light and simple to maintain, and would require a minimum volume.

Disadvantages include the properties associated with typical crushable energy-absorbing material. Normal crushable materials such as honeycomb can be crushed only about 70 percent of their original height; consequently, the system makes inefficient use of the space available for stroking. Another. disadvantage of the system is that the lap belt would have to

7
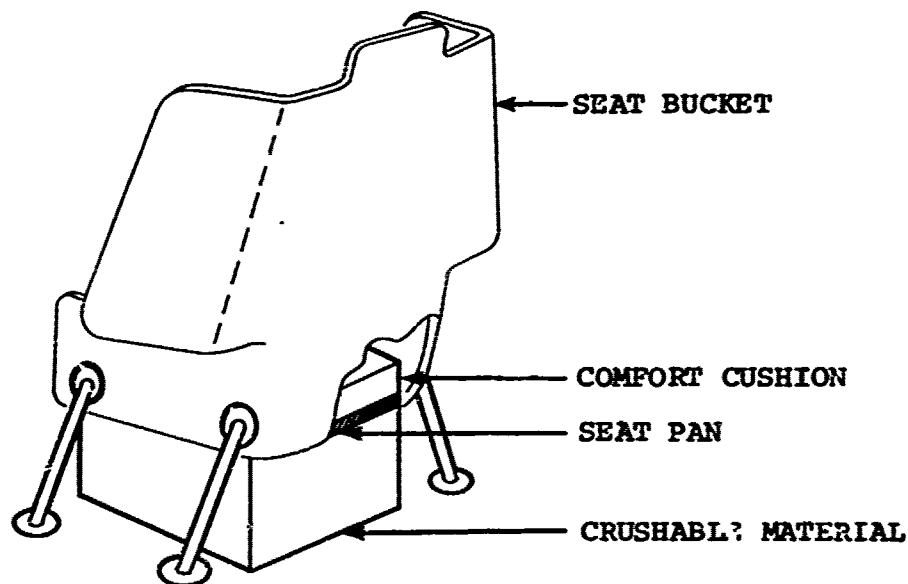
Figure 1. Crushable Seat Cushion (Fixed Seat) - Concept 1.

be attached to the floor through a ratchet arrangement (which would keep slack from forming) to provide the necessary restraint to the occupant. Still another disadvantage is that, in its simplest form, the system does not provide stable or predictable restraint when loaded in the biaxial or triaxial direction. One side or one corner of the seat pan could displace more than the remaining portion and result in tipping and only partial crushing of the energy-absorbing material.

2.2.2.2 <u>Crushable Seat Base (Honeycomb) - Concept 2</u>: This concept (Figure 2) is identical to the first one except that the design of the crushable material under the seat pan was modified to eliminate the stability problem discussed in the previous paragraph. The modified design uses a honeycomb type material sandwiched between two cover plates which are tied together by energy-absorbing cables passing through the cover plates and the honeycomb material. The sandwich is maintained by swaged end fittings on the ends of the cables.

When loaded in the vertical direction, the honeycomb would crush at the design load and the cables would tend to buckle and offer no resistance to movement. When loaded in the longitudinal or lateral direction, however, the sandwich would be loaded in shear. Resistance would be supplied by the honeycomb material, shearing the cables through the honeycomb core

8
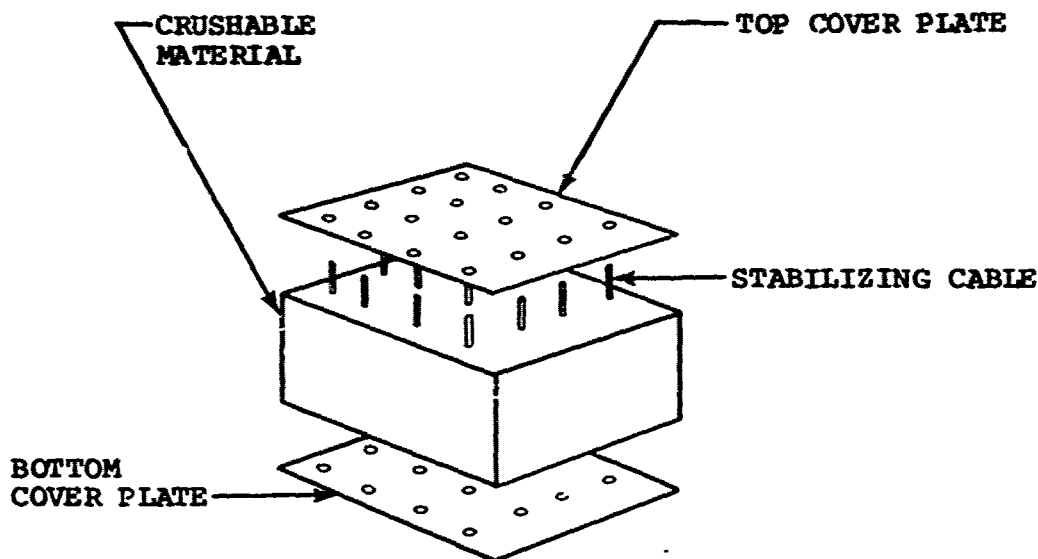
Figure 2. Crushable Seat Base (Modified Honeycomb) - Concept 2.

material, and through the compressive loads applied by the plates to the honeycomb material as the cables rotated about their fixed length.

This innovation could be used equall, well on Concepts 1, 3, and 4. It would solve the stability problems; however, it would not solve the inefficient use of stroking space resulting from the compressed height of the honeycomb material. In its present configuration, this concept would not solve the lap belt restraint problem; however, if the belt were attached to the seat bucket and the bucket were mounted on the crushable base, the lap belt problem would be solved.

2.2.2.3 Crushable Seat Base (Corrugated Sheet) - Concept 3: The armored bucket is placed upon a crushable material made up of corrugated sheet metal in this concept (Figure 3). Decelerative loads would crush the base, permitting energy-absorbing stroking during decelerative loading. As in Concept 2, cables could be used to provide directional stability to the energy-absorbing base of this seat.

The system would be extremely ꞏ, simple, economical, and easy to maintain. Further, it would be relatively insensitive
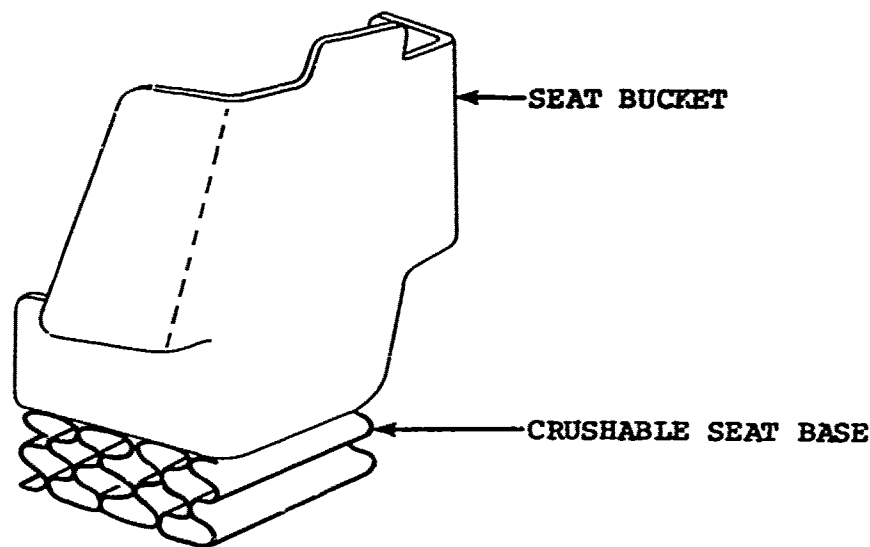
Figure 3. Crushable Seat Base (Corrugated Sheet) -
Concept 3.

to warped floor configurations and would present no problems
from binding during a symmetrical loading. Although this con-
cept has a potential for making much more efficient use of the
stroke distance available under the seat than does the crusha-
ble honeycomb concept, the efficiency is still low, as part of
the distance must be reserved for compacted material.

2.2.2.4 Crushable Armrest - Concept 4: In this concept
(Figure 4), the seat bucket is placed upon crushable material
columns which are located on the sides of the armored bucket,
removing them from the critical area beneath the seat pan.
When the seat is loaded vertically, it could stroke (deform-
ing the crushable material) until the seat pan actually
bottomed out on the floor of the aircraft, thus eliminating
the lack of efficiency inherent in the other concepts of this
general type. Again, the cable technique could be used to
provide stability to the columns of crushable material; how-
ever, additional lateral support would be required to provide
the stability necessary when loaded in the lateral direction.
Also, the relatively wide spread between energy-absorbing
columns would tend to decrease the effects of a symmetrical
loading.

Disadvantages include the requirement for increased lateral
floor space within the aircraft. This disadvantage could

10
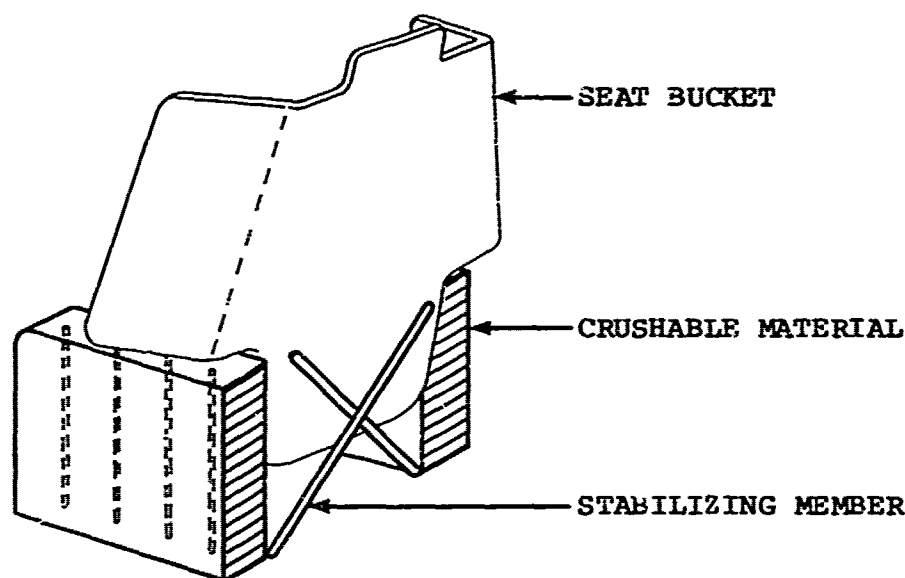
Figure 4. Crushable Armrest - Concept 4.

totally eliminate this concept from contention, as lateral
space in cockpits is normally extremely limited.

2.2.2.5 Tensile Cable - Concept 5: In this concept, the
movable seat bucket is suspended on energy-absorbing cables
(Figure 5). Additional restraint is provided to increase the
stability of the system. The system uses 100 percent of the
available stroking distance, but provides no rebound capa-
bility without the use of special components that tend to
eliminate the initial simplicity of the concept. There could
be a cable fatigue problem also, which would tend to reduce
the service life of this seat concept.

2.2.2.6 Extruding Sheave - Concept 6: This concept (Figure
6) is somewhat like Concept 5, as the armored bucket is sus-
pended from a structural support through extruding sheave-
type energy absorbers. These energy absorbers operate by re-
quiring the metal sheath around the pulley to be plastically
deformed as a cable is sheared out through the lip. These de-
vices have been used successfully in the past; however, in
this application additional structure would be required to
provide rotational, longitudinal, and lateral stability. In
addition, the concept has no rebound capability.

11
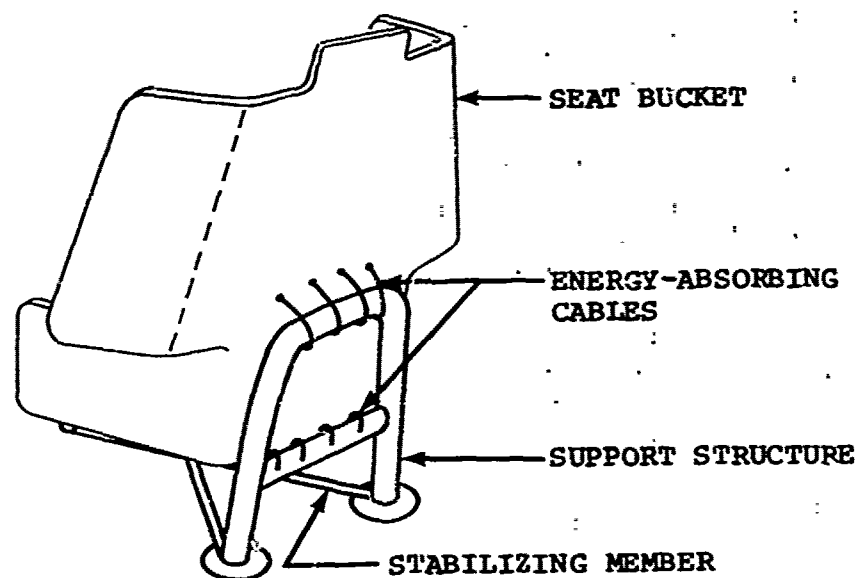
Figure 5.   Tensile Cable - Concept 5.
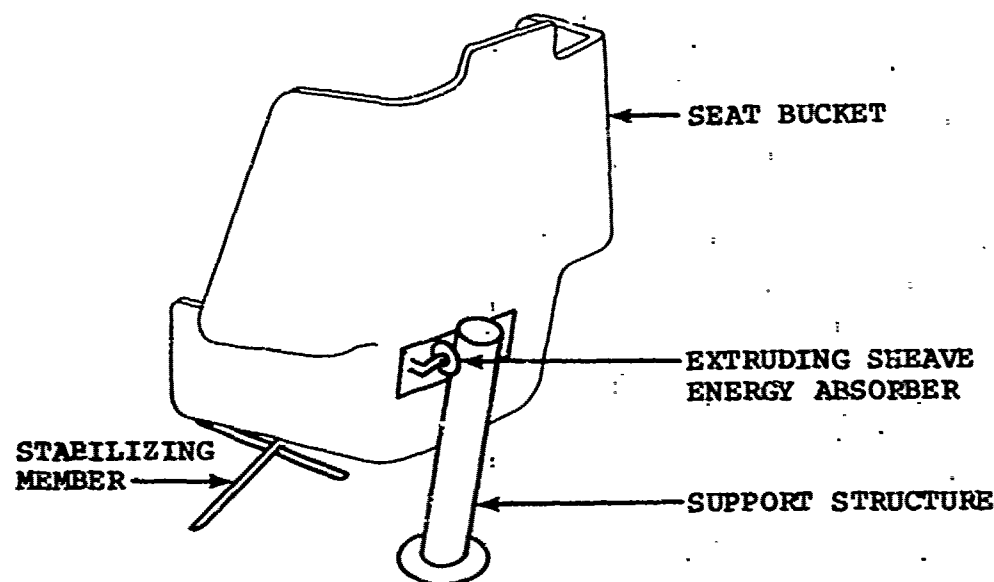
Figure 6.   Extruding Sheave - Concept 6.

2.2.2.7 Rolling Torus Cantilevered Tube - Concept 7:   In this
concept (Figure 7), the armored bucket is attached to a tubular
guide through a rolling-torus-type energy absorber.   Vertical
decelerative loads are attenuated through concentric movement
of the outer tube down the inner tube.   Energy absorption is
accomplished by cyclic deformation of the tori which are inter-
ference fitted between the tubes.
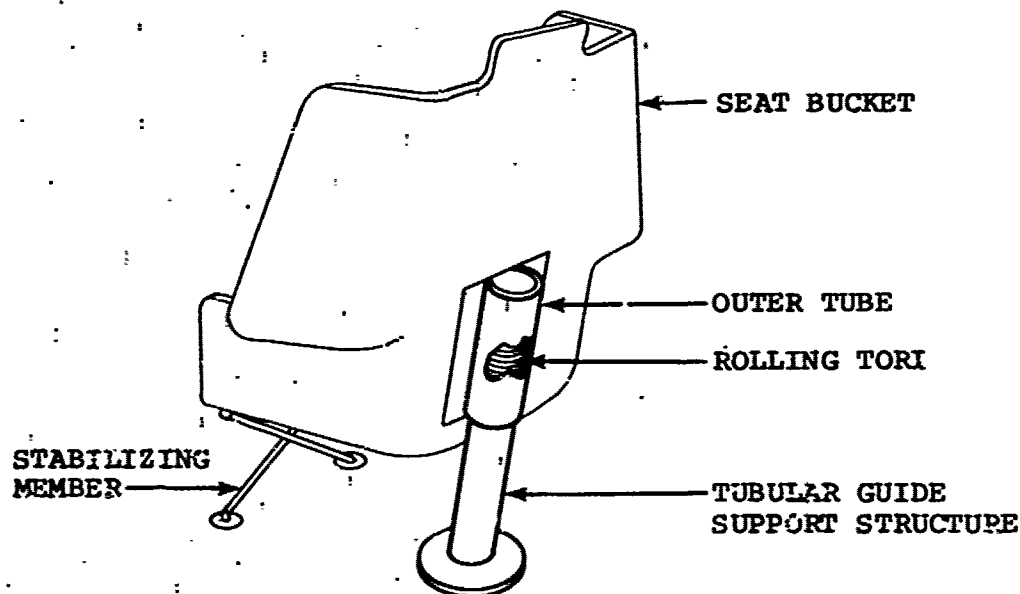
Figure 7.   Rolling Torus Cantilevered Tube -
Concept 7.

This system has the advantage of providing rebound energy-
absorbing capability, as the rolling-torus-type energy ab-
sorber is capable of repeated strokes in either direction.
In addition, it combines the support structure and the energy
absorber, thus reducing the number of components.   However,
since the system is cantilevered from the pedestal, large
moment loads are imposed on the floor of the aircraft, re-
quiring major structural strengths to be designed into this
area of the airframe.   In addition, rotational motion around
the tube would have to be restrained by the use of separate
devices.

2.2.2.8 Cantilevered Panel - Concept 8: In this concept (Figure 8), the armored bucket is cantilevered from a more or less flat panel reinforced with a gusset. Needle bearings are located between the interfacing surfaces to provide freedom of movement up and down the panel guide. An energy absorber is connected between the panel guide and the movable seat bucket. Under decelerative loading in the vertical direction, the box section strokes down the guide panel, compressing the energy-absorber tube.
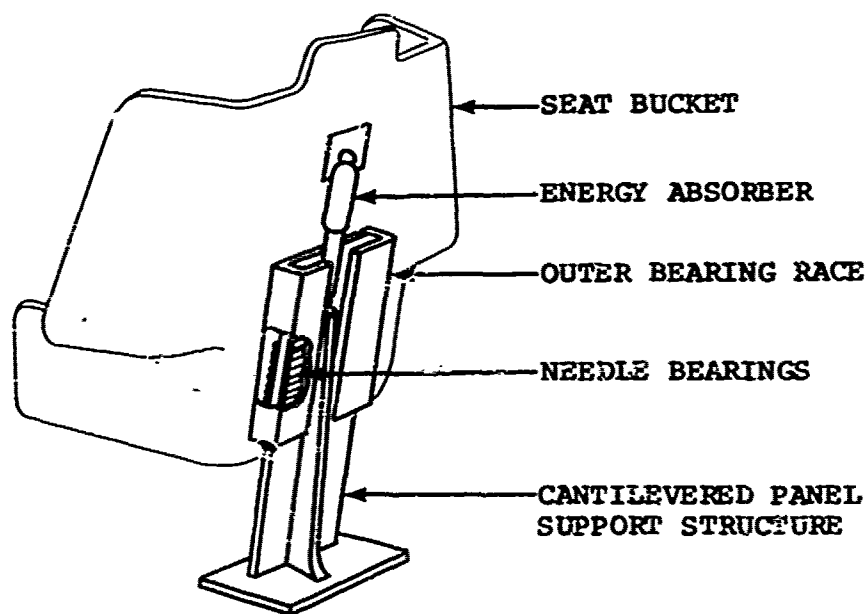
Figure 8. Cantilevered Panel - Concept 8.

This concept provides rotational resistance through the shape of the panel support member. However, it requires separation of the energy absorber from the stroking mechanism, requiring an extra component. The load requirement imposed on the air-craft floor is essentially identical to that of Concept 7.

2.2.2.9 Cantilevered Box - Concept 9: This concept (Figure 9) is essentially identical to the previous concept except that, through use of the rectangular-shaped support structure, needle bearings can be located to resist binding and permit freedom of movement under all loading directions. Further, the shape of the tubular support member is a more stable

SEAT BUCKET

ENERGY ABSORBER

NEEDLE BEARINGS

OUTER BEARING RACE

CANTILEVERED BOX
SUPPORT STRUCTURE
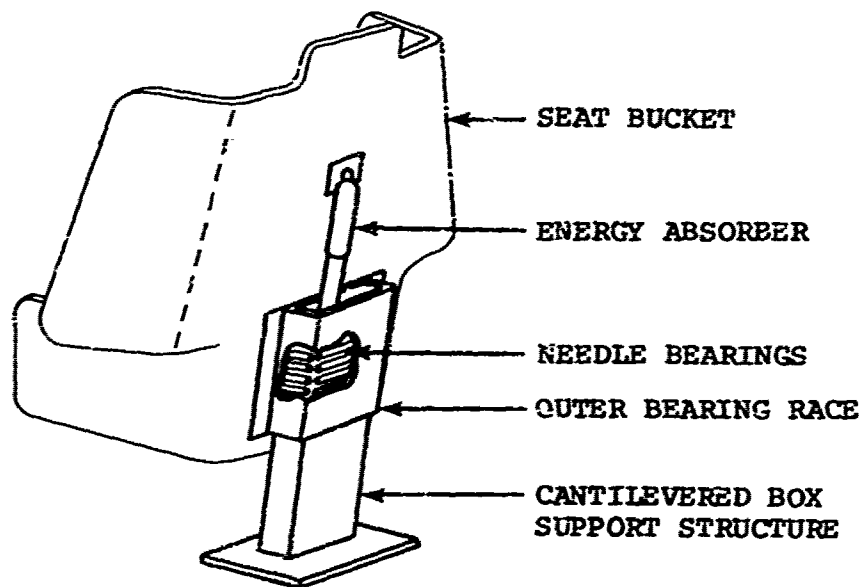
Figure 9.   Cantilevered Box - Concept 9.

structure and would result in a decrease in weight over Concept 8.

2.2.2.10 Overhead Suspension - Concept 10: In this concept
(Figure 10), the armored bucket is suspended from the roof of
the aircraft through an energy-absorber device. Additional
members are added to provide the rotational, lateral, and
longitudinal stability required of the system.

The primary advantage of this system is that the seat is supported from the roof of the aircraft which, through fuselage
deformation, is subjected to less severe decelerative loading
than the floor of the aircraft. In addition, being restrained
near the top of the seat, moments resulting from longitudinal
or lateral loading are not developed, thus reducing the floor
strength requirements.

The primary disadvantage of the system is that many aircraft
do not contain sufficient strength in the roof structure to
support the decelerative loads of the seat. Future aircraft,
however, could be designed specifically for this application
and could result in an efficient system.

15
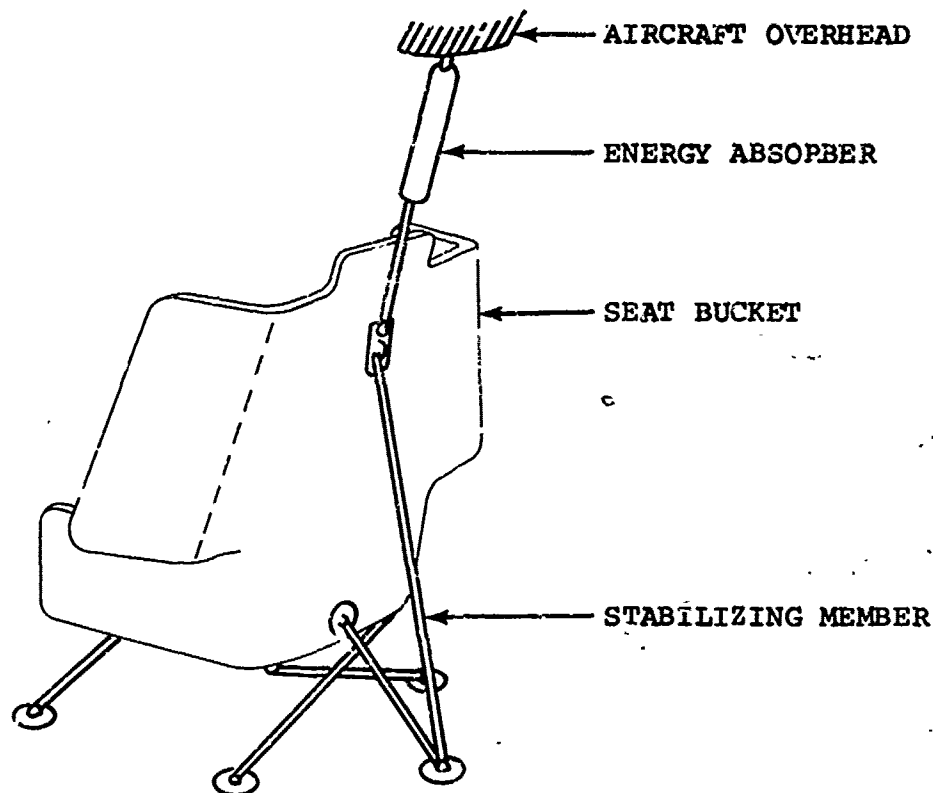
Figure 10.   Overhead Suspension - Concept 10.

2.2.2.11 Compression Tube - Concept 11: In this concept (Figure 11), the armored bucket is supported on four legs made of compression-type energy absorbers. This system also makes efficient use of the available stroking distance. However, the kinematics of the system are again also difficult to control. This concept would require additional s ructure to maintain a predictable respo.se to specific decelerative loading. Again, asymmetric loading could result in the load's being applied over one or two of the devices, thus resulting in bottoming of part of the energy-absorbing system.

2.2.2.12 Tensile/Compression Tubes - Concept 12: The armored bucket in this concept (Figure 12) is supported at the front edge by two legs made from compressible energy absorbers. The aft section of the seat is supported on an energy-absorbing device which is normally loaded in tension. Again, additional structures are required to provide stable and predictable performance during combined decelerative loading; however, the system's stability is an improvement over that of Concept 11.

16
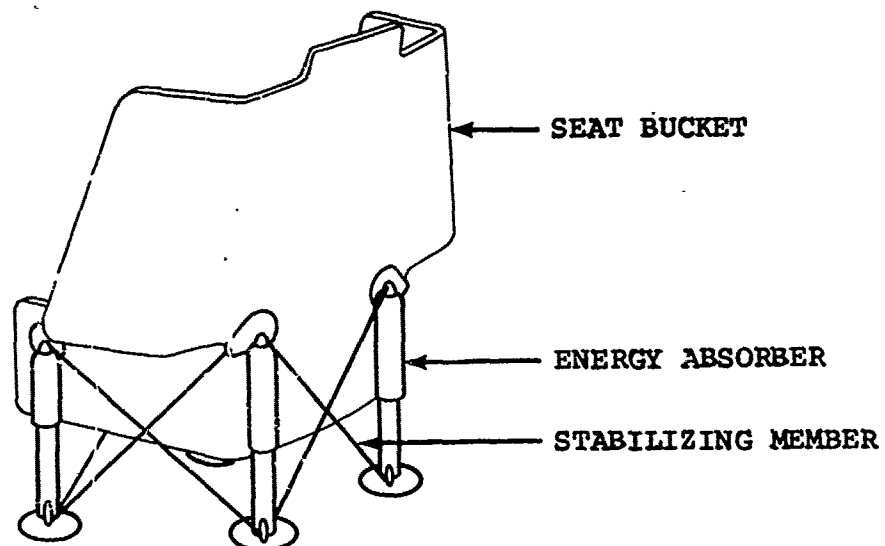
Figure 11.   Compression Tube - Concept 11.
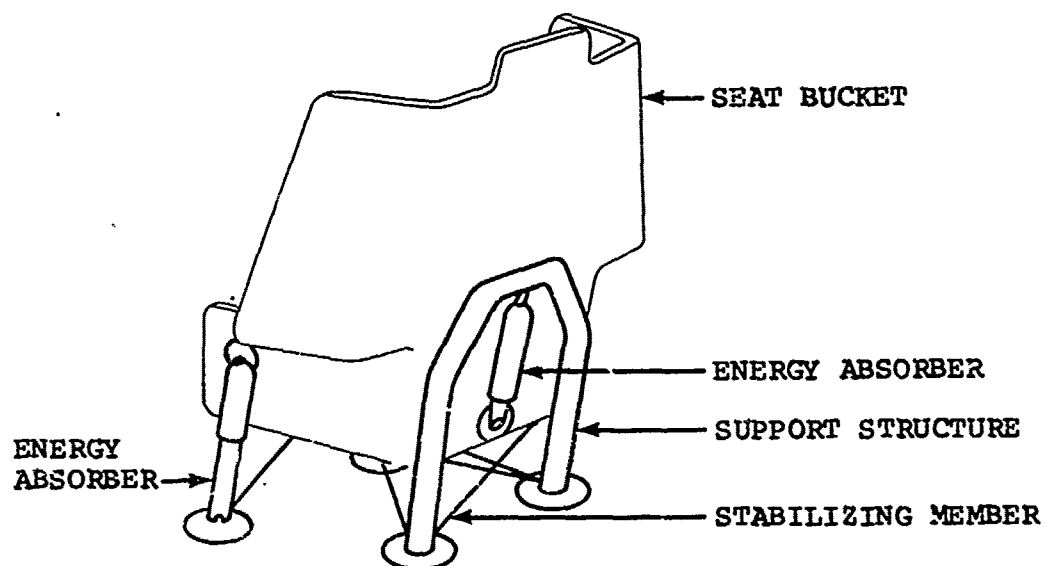
Figure 12.   Tensile/Compression Tubes - Concept 12.

2.2.2.13 Collapsing Frame - Concept 13: In this concept
(Figure 13), the armored bucket is guided by the available
stroking arc of a four-bar mechanism under the seat. Motion
is restrained by reaction of two energy-absorbing devices, one
located on each side of the seat. The advantage of this sys-
tem is that the limit load of the energy absorber is pre-
dictable; the motion envelope is prescribed by the guidance
mechanism. Disadvantages of the system include an initial
high resistance to vertical loading as the mechanism parallelo-
grams from its initial position. A vertical pulse requires a
forward longitudinal acceleration of the system which can re-
sult in additional unnecessary loading of the seat and the
occupant.
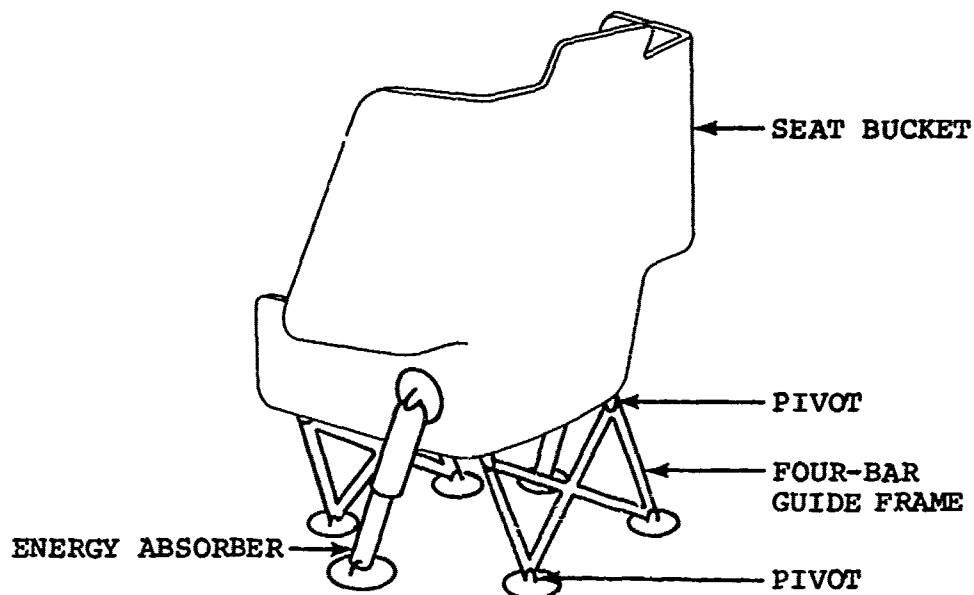
Figure 13. Collapsing Frame - Concept 13.

Although the angles of the guide mechanism and the energy-
absorbing members could be optimized to provide acceptable
force versus deformation characteristics, increased lengths of
the parallelogram support members would be required to reduce
the initial guidance member angles and thus decrease the longi-
tudinal acceleration imposed by a vertical stroke. The system
would therefore increase in volume and weight.

18

2.2.2.14 Rear Leg Pivot - Concept 14: In this concept
(Figure 14), the seat is hinged to the floor through its back
leg attachments. Movement is resisted by two compressive
energy-absorber devices positioned between the front of the
bucket and the floor. Advantages of this system include its
extreme simplicity; however, unless the hinge points are lo-
cated a considerable distance aft of the seat, a wide varia-
tion of load distribution between the back legs and on the
energy-absorbing devices can exist, depending on the input
load vector. The result is an overall variation in resis-
tance to movement.

Another disadvantage of this concept is that, as the seat
strokes, it rotates forward and the lower front lip of the
seat pan makes first contact with the floor. This leaves the
back of the seat suspended a few inches above the floor, thus
decreasing the efficiency of the system by not using the
available stroke distance beneath the seat. This disadvantage
could be alleviated by providing a one-way plastic hinge in
the leg at the rear corner of the seat pan (Figure 14B). A
cable or other control system that senses the stroking of the
front edge of the pan then could be used to force the rear
edge of the seat to follow the front, thereby providing a
predictable stroke. The main disadvantage of the modified
concept is its complexity; the basic simplicity of the origi-
nal concept has been eliminated.

2.2.2.15 Medium Direction Guided - Concept 15: In this con-
cept (Figure 15), the armored bucket is guided down structural
tubes at a predetermined angle. Bearings are provided between
the attachments and the guide tubes to permit ease of stroking.
Movement is restrained by a rolling-torus-type energy absorber
attached t the seat bucket and to the support frame but inde-
pendent of the guidance mechanism.

This system is totally predictable; the direction of movement
is fixed by the guidance mechanism. It is, however, subject
to racking and binding as a function of asymmetric loading.
Again, the vertical pulse cannot be attenuated without a longi-
tudinal acceleration of the seat and occupant, thus reducing
the efficiency of the system in the primary vertical direction.

2.2.2.16 Vertical Direction Guided - Concept 16: This con-
cept (Figure 16) is similar to Concept 15 except that guidance
is provided in the vertical direction only. Again, the
movable seat bucket is attached to the guide tubes through
bearings to permit ease of movement.

SEAT BUCKET

ENERGY
ABSORBER

REAR LEG

PIVOT

A.   BASIC CONCEPT

FREE-STANDING
SHEAVE SUPPORT

PLASTIC HINGE

CABLE

SHEAVE
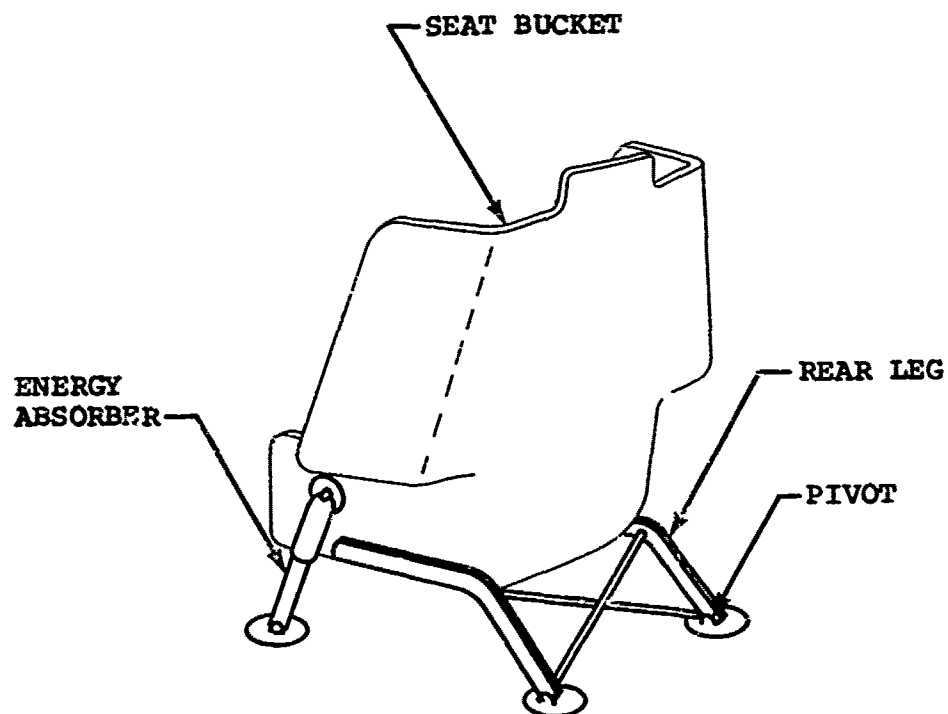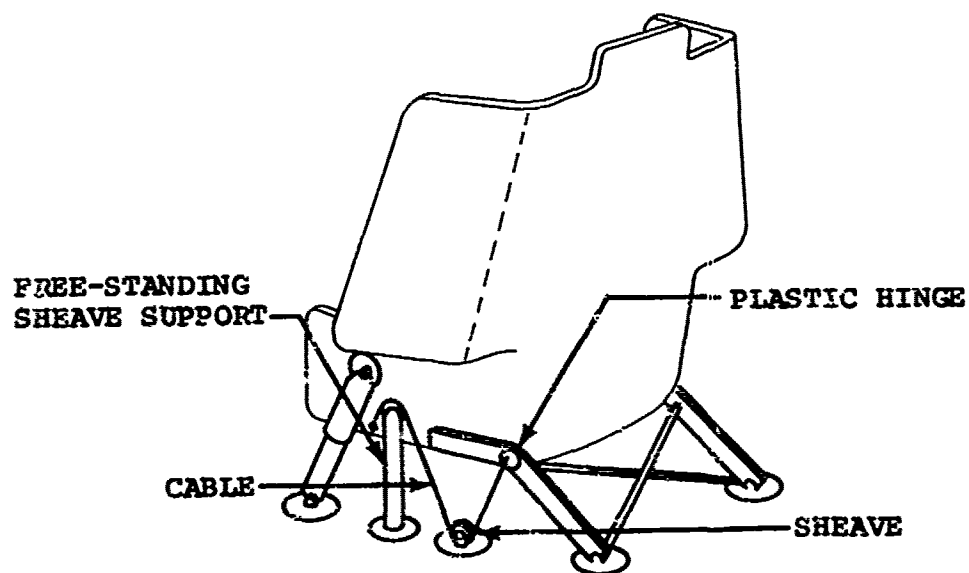
B.   MODIFIED CONCEPT

Figure 14.   Rear Leg Pivot - Concept 14.

20
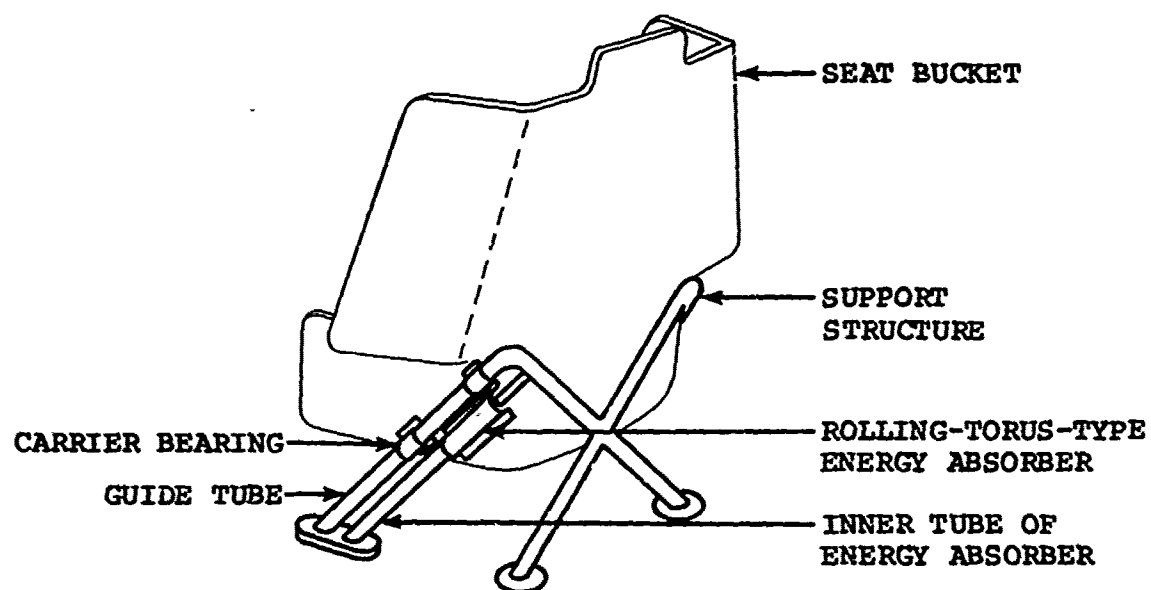
Figure 15.   Medium Direction Guided - Concept 15.
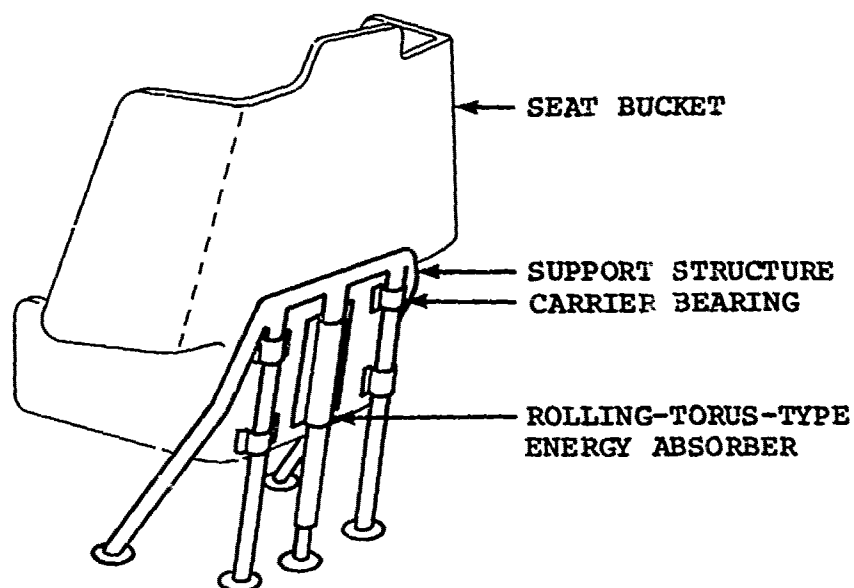
Figure 16.   Vertical Direction Guided - Concept 16.

Predictability of this system is the best of all systems discussed because the guidance is sup lied at four locations (providing resistance to racking) and because only one energy absorber resists movement. This one energy absorber is located towards the center of the seat and, consequently, is nearest to the center of gravity of the system, regardless of input load direction. The weight of this system would be relatively high; however, the development risk would be relatively low. It would provide an extremely efficient energy-absorbing stroke in the vertical direction.

2.2.3 CONCEPT TRADE-OFF

As stated in the introduction, a weighted trade-off was accomplished to help select the system having the best potential for further design effort. The technique used permitted a quantitative comparison of both the variables which could be evaluated quantitatively and the parameters which were abstract. In this analysis, each parameter considered to be important was listed across the top of a table and given a relative weight which was a percentage of unity. Next, each concept to be evaluated was listed in a column down the left-hand side of the table.

The trade-off was conducted by relatively rating each concept for a particular parameter. The ratings were then multiplied by the weighting factors and summed in the right-hand table column. The total value appearing in the right-hand column was therefore the total weighted rating of the system.

The results of this trade-off are shown in Table I. The seat concepts receiving the four highest ratings were:

Ranking	Description	Rating
1	Crushable Armrests (Concept 4)	.925
2	Overhead Suspension (Concept 10)	.923
3	Crushable Seat Base (Corrugated Sheet) (Concept 3)	.906
4	Vertical Direction Guided (Concept 16)	.885

Additional analyses were conducted on the concepts receiving the highest ratings, and Concept 16 (vertical direction guided) was selected for inclusion in the experimental test seat design. This selection included a decision that the design should be based upon demonstrated and existing technology

22

TABLE I. SEAT CONCEPT TRADE-OFF															
Description	Cost	.05	Maintainability	.10	Weight	.15	Volume	.05	Development Risk	.15	Vertical Performance	.30	Lateral and Longitudinal Performance	.15	Total
Crushable Seat Cushion (Fixed Seat)	.75	.038	.85	.128	.90	.135	.95	.048	.85	.128	.70	.210	.70	.105	.792
Crushable Seat Base (Honeycomb)	.95	.048	.95	.143	.95	.143	.98	.049	.90	.135	.75	.225	.88	.132	.875
Crushable Seat Base (Corrugated Sheet)	.90	.045	.98	.147	.95	.143	.98	.043	.80	.120	.90	.270	.88	.132	.906
Crushable Armrest	.80	.040	.98	.143	.98	.143	.75	.038	.90	.135	.98	.294	.88	.132	.925
Tensile Cable	.75	.038	.90	.128	.75	.120	.92	.046	.95	.135	.95	270	.85	.132	.906
Extruding Sheave	.80	.040	.85	.128	.75	.113	.92	.046	.70	.105	.90	.270	.70	.105	.807
Rolling Torus Cantilevered Tube	.80	.040	.80	.120	.75	.113	.90	.045	.85	.128	.90	.270	.70	.105	.821
Cantilevered Panel	.70	.035	.80	.120	.75	.113	.92	.046	.75	.113	.90	.270	.70	.105	.802
Cantilevered Box	.80	.040	.80	.120	.75	.113	.90	.044	.85	.120	.90	.270	.70	.105	.812
Overhead Suspension	.75	.038	.90	.135	.90	.135	.85	.043	.95	.143	.98	.294	.90	.135	.923
Compression Tube	.70	.035	.90	.135	.80	.120	.95	.048	.85	.128	.92	.276	.82	.123	.865
Tensile Tube	.70	.035	.90	.135	.75	.113	.92	.046	.95	.143	.95	.285	.85	.128	.885
Collapsing Frame	.75	.038	.85	.128	.90	.135	.85	.043	.85	.128	.85	.255	.90	.135	.862
Rear Leg Pivot	.85	.043	.95	.143	.05	.143	.05	.048	.98	.147	.70	.210	.70	.105	.839
Median Direction Guided	.75	.039	.85	.128	.75	.113	.95	.048	.95	.143	.90	.270	.90	.135	.875
Vertical Direction Guided	.85	.043	.85	.128	.80	.120	.95	.048	.98	.147	.98	.294	.70	.105	.885

and not require the development of entirely new components and materials. This decision was justifiable on the basis that many components and systems were available which had previously been developed to the point that would permit application into a system. Consequently, the development risk could be minimized by the selection of a concept using these devices.

Other factors which influenced the final decision are summarized as follows: (1) the crushable armrest concept was eliminated because of its requirement for the development of the energy-absorbing columns, inherent lack of stability, and potential difficulty in providing adjustment; (2) the overhead suspension concept was eliminated because the imposition of high support strengths in the roof of the aircraft was outside the scope of the objectives of the program; and (3) the crushable seat base (corrugated sheet) concept required development of the crushable material, introduced an unknown with respect to the degree of solution of the stability problem, and provided a potential problem in providing adjustment.

The vertical direction guided concept, however, represented a highly predictable concept which required the development of very few new items, relative to the other concepts. Because of this and, of prime importance, because it possessed the greatest potential for providing the desired vertical crash protection, it was selected.

2.3 DESIGN DESCRIPTION

2.3.1 OVERALL CONFIGURATION AND OPERATION

The experimental seat configuration consisted of a simulated armored bucket, a vertical energy-absorbing system, a support structure including a guide frame subassembly, and floor attachments and is illustrated in Figures 17 and 18.

Figure 17 is an oblique, frontal view of the seat which shows the configuration of the simulated armored bucket with cushions and restraint harness in place and a partial view of the guide frame assembly and support structure of the seat.

The seat bucket was attached to the guide tubes through four roller bearing subassemblies and the energy-absorbing mechanism. The energy-absorbing mechanism was connected to the seat bucket at the lower bearing cross member and to the vertical adjustment bracket located on the top of the guide frame structure.

The guide frame was attached to the floor on the bottom end and was restrained from overturning moments resulting from flight or crash loads by the rear supporting structure. This structure attached to the guide frame assembly in four primary locations and extended aft from the guide frame assembly, converging at a single floor tie-down point. Floor attachments were located on the bottom of each guide tube and on the bottom of the single rear tie-down point. Thus the seat was

24

Figure 17.   Frontal View of Experimental Seat.

supported on a three-point mount which permitted floor buck-
ling and rotation without imposing deflection on the seat
structure.

Spherical rod ends were used on the floor attachment end of
the structure to allow angular misalignment without imposing
bending on the members.

The three floor attachments were equipped with slides retained
in a box section rail. Longitudinal seat adjustment was accom-
plished by removal of pins locking the slides in the two
front rails.

The movable seat bucket, by virtue of its four carrier bear-
ings, was free to roll up and down the guide frame for either
vertical adjustment or energy-absorbing stroke.

25

The energy-absorbing system consisted of a stainless steel
tube and two stainless steel cables. The two stainless steel
cables were designed for selective engagement to provide vari-
ations in the energy-absorber limit load as a function of
occupant weight, thus lowering the deceleration to be ex-
perienced by lighter seat occupants. The stainless steel tube
device was selected for its predictability, economy, and fast
turnaround. The device provided the flexibility needed for
incorporating variations during dynamic testing of the system.

The energy-absorbing mechanism was connected to the top of the
guide frame by a quick-release pin locking device. A pair of
tension coil springs were connected to the outer tube surround-
ing the energy-absorbing mechanism and to the bottom of the
bracket on the upper yoke cross member. The springs were de-
signed to lift the weight of the movable portion of the seat
when unloaded.

Adjustment was accomplished by removing the pin which locked
the upper end fitting of the energy absorber into the bracket
attached to the upper guide frame cross member which permitted
the movable seat weight to be carried by the spring. Vertical
adjustment could then be made and the pin replaced to lock the
seat in the desired position.

During the energy-absorbing stroke, the inertial load of the
seat bucket and occupant drove the bucket downward. Since the
bucket was restrained in its vertical location by only the
energy absorber, the energy absorber stroked, providing the
resistance desired for deceleration. The seat adjustment
springs were not deflected during stroking, as they were
attached to the end of the energy absorber, remaining fixed
with respect to the upper attachment bracket.

The back leg on the seat was not locked in position with re-
spect to longitudinal travel. Since it was not locked, it was
free to move aft and forward in its rail during crash loading
while performing its primary function of restraining the seat
from an overturning moment. It therefore permitted longi-
tudinal changes in floor dimension between the rear and the
front leg tie-down points without loading the seat support
structure.

The design of the structural support assembly provided for
load transfer from each seat carrier bearing through the guide
tube and into the back floor attachment.

A structural X was located diagonally in the plane of the
guide tubes between the lower structure cross member and the
support structure attachments located between the upper and
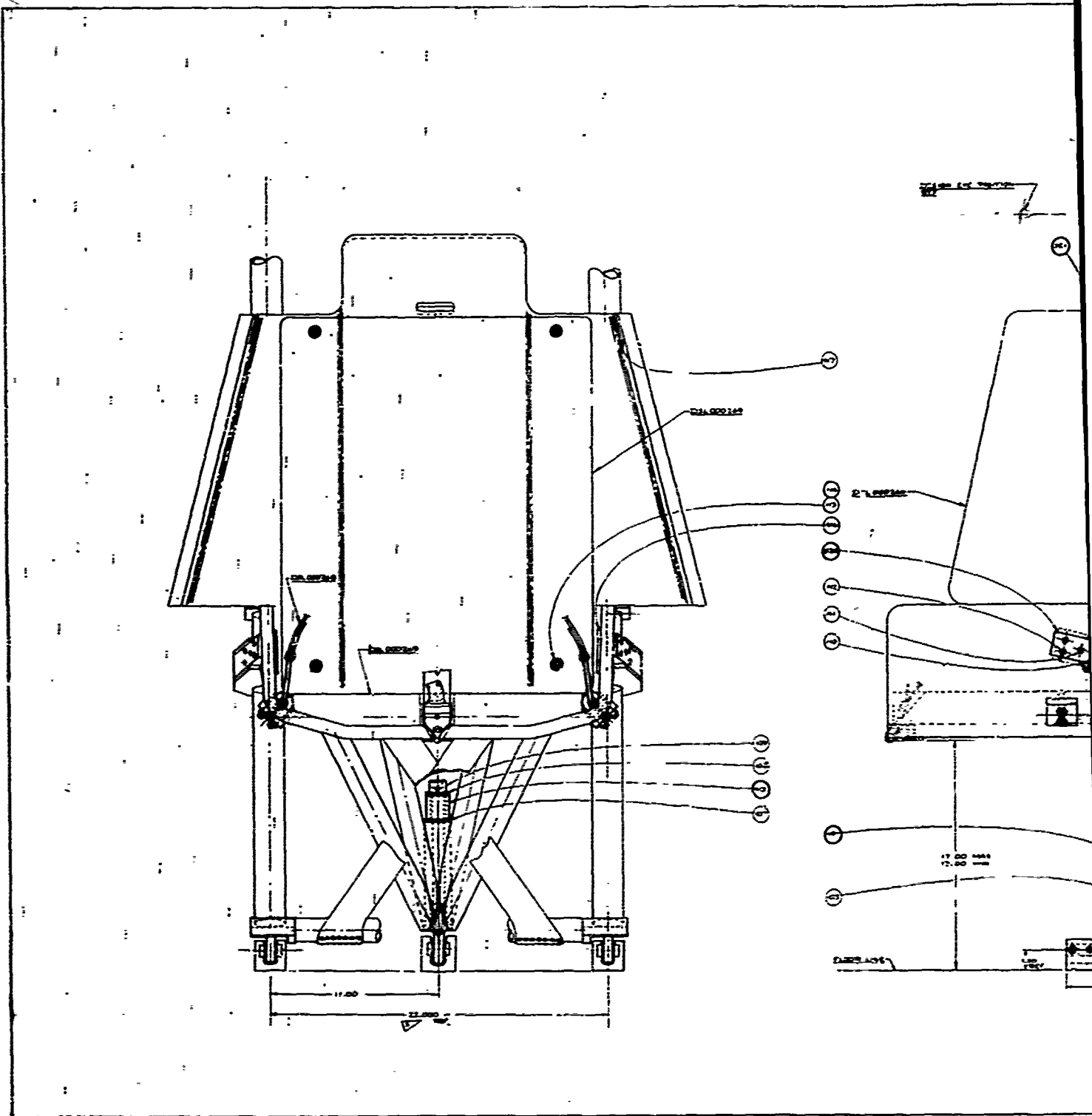
Figure 18. Experimental Seat Configuration Top Assembly.

27

B
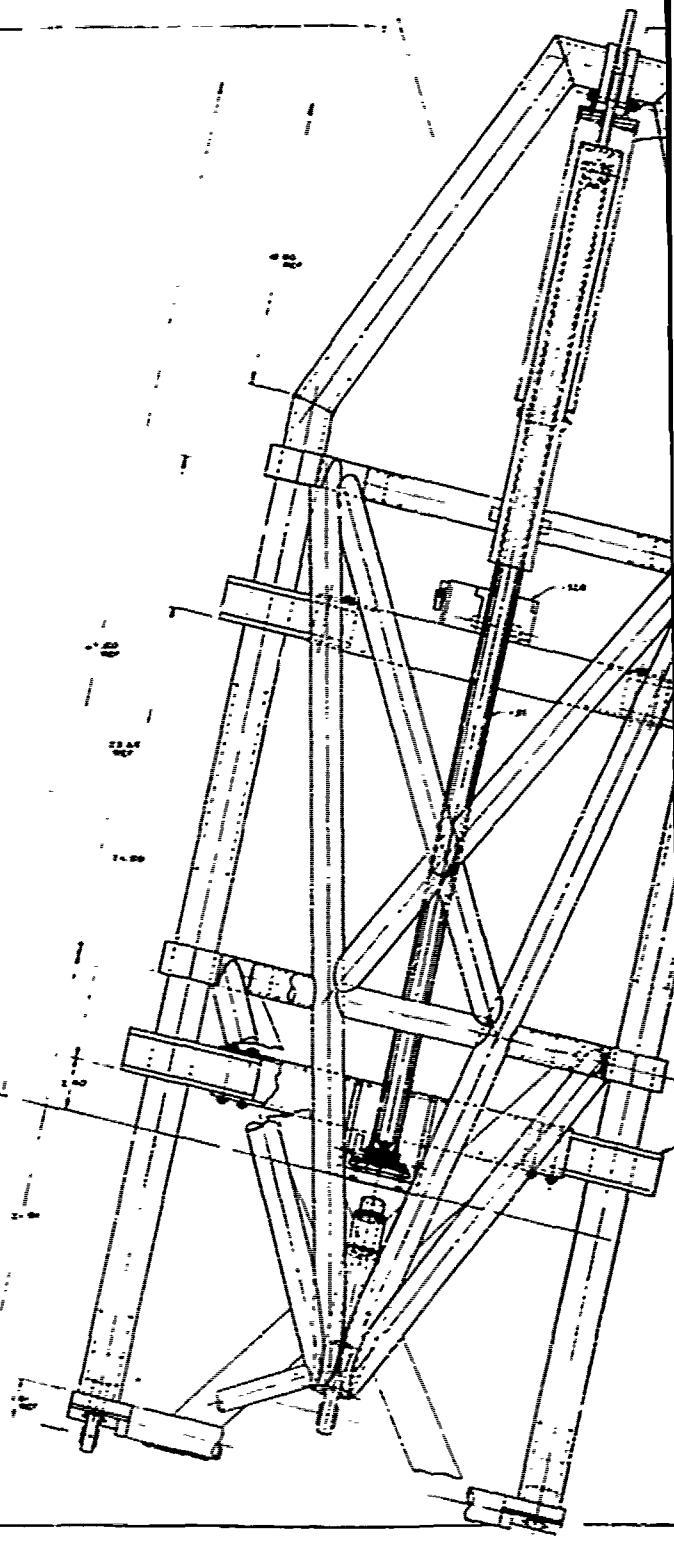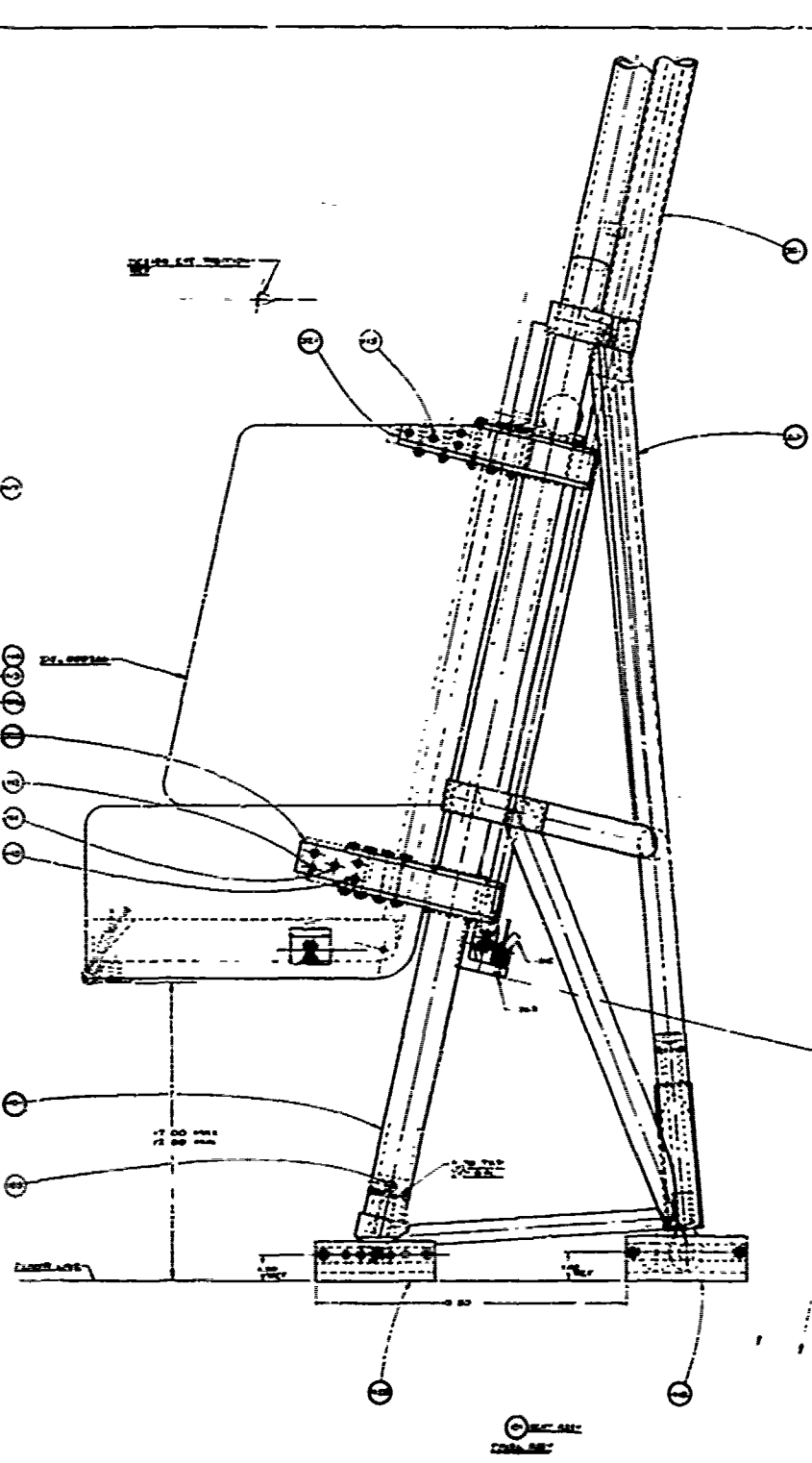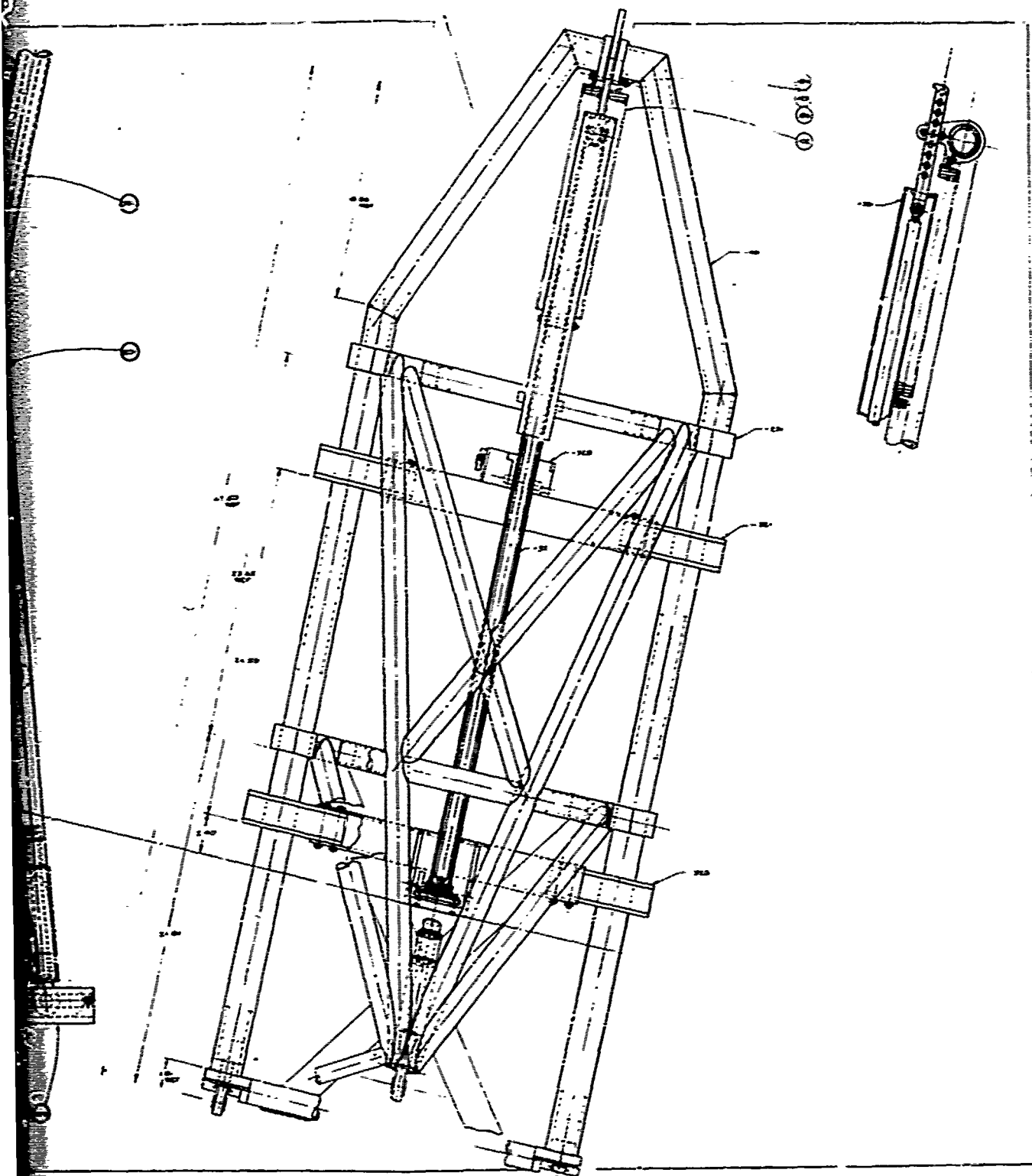
lower bearings on the guide tubes. This X resisted in-plane racking of the guide frame assembly. In addition, the design of the entire structure provided a reinforced frame capable of resisting all of the imposed loads, including fore and aft racking from combined loading.

The weight, areal density, center of gravity, and general configuration of the ceramic-type armored seat bucket was simulated by a solid, glass-cloth composite. The armored seat bucket was simulated to expedite the economical development and demonstration of the energy-absorbing mechanism of the seat. Although the general configuration was representative of an operational design, modifications such as hinged side protection panels would be required to adapt it to a specific use.

The restraint harness was essentially a standard military crewman type (MS22033 lap belt and MS16068 shoulder harness) modified to meet the requirements of References 2 and 5. The system used Dacron webbing throughout and included a negative G strap.

The cushions were custom fabricated from a newly developed, low-rate-of-return, loading-rate-sensitive foam material.

The experimental seat design is defined in Dynamic Science Drawing DSL 000267. This drawing consists of four sheets, the first of which was the top assembly, with the remaining sheets defining the component details and subassemblies. The top assembly is shown in Figure 18. The simulated armored bucket, cushions, and restraint system are defined on separate drawings, which are referenced in the discussion of specific components. The excessive height of the support structure was provided to permit the desired degree of energy-absorber flexibility for the matrix type dynamic testing. It would not be included on an operational flight-weight seat of identical conceptual design. Figure 19 is a view of the seat fitted with a rolling-torus-type energy absorber and is more typical of the operational configuration.

2.3.2 ANTHROPOMETRY BALLISTIC COVERAGE

Anthropometry, a prime consideration in the design of the experimental seat, was considered from several aspects including comfort, freedom of movement, and ballistic coverage. Figure 20 presents the general anthropometric considerations of interest. Two dimensions are listed for each dimensional callout. The top figure (or smaller number) presents the dimension for a 5th percentile occupant, while the bottom figure (or larger number) presents the same dimension for the
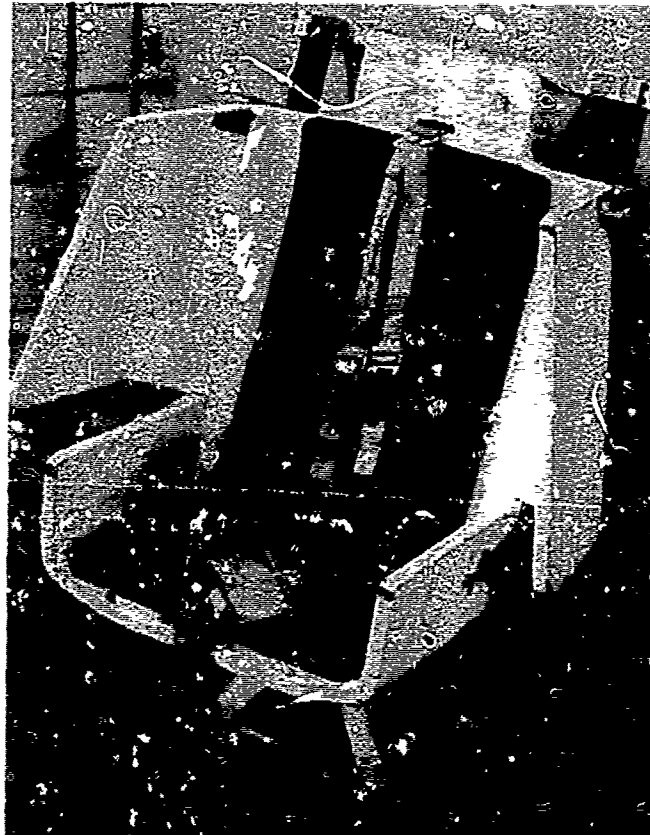
Figure 19.   Frontal View of Modified Seat
Configuration Using Operational
Type Energy Absorber.

95th percentile occupant. These data were primarily taken
from Reference 6; however, where dimensions were not listed,
additional data were obtained from References 8, 9, 10, and 11.
All of the dimensions shown in Figure 20 are for the nude body
except the helmet sitting height, which is 2 inches larger
than the nude dimension. Increments must be added to the nude
dimensions to allow for clothing. Since the clothing varies
appreciably, it was not added to the base dimensions included
in Figure 20.

Figure 21 shows the front view of the armored bucket with the
5th and 95th percentile head, shoulders, elbows, and hips
dashed in. It can be seen that adequate clearance is provided
in all areas for heavy winter clothing, or to allow for the
increased size of humans projected for the next several years.
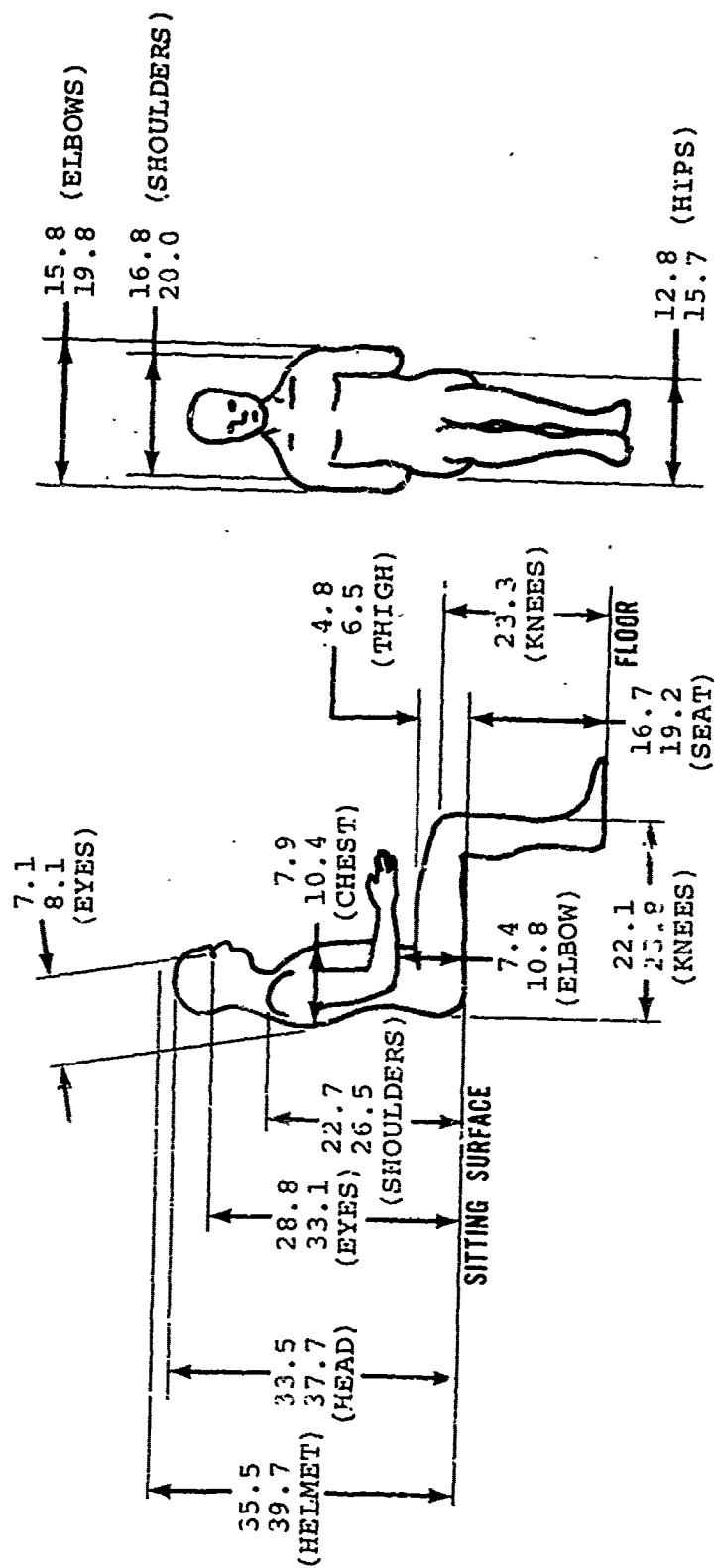
Figure 20. Representative Nude Static Anthropometric Dimensions - 5th and 95th Percentile Males.

15.8 (ELBOWS)
19.8

16.8 (SHOULDERS)
20.0

12.8 (HIPS)
15.7

4.8 (THIGH)
6.5

23.3 (KNEES)

FLOOR

16.7 (SEAT)
19.2

7.1 (EYES)
8.1

7.9 (CHEST)
10.4

7.4 (ELBOW)
10.8

22.1 (KNEES)
25.8

28.8 (EYES)
33.1
22.7 (SHOULDERS)
26.5

SITTING SURFACE

33.5 (HEAD)
37.7

35.5 (HELMET)
39.7

LEGEND

TOP DIMENSION 5TH PERCENTILE
BOTTOM DIMENSION 95TH PERCENTILE
ALL DIMENSIONS IN INCHES

23.74 IN.

21.00 IN.

33.44 IN.
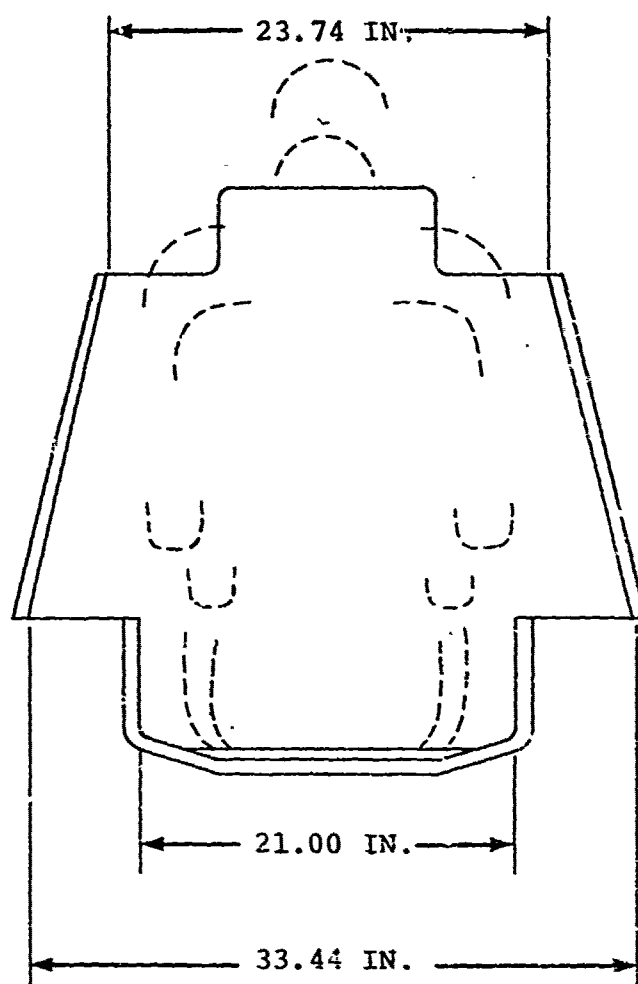
LEGEND

DOTTED LINES SHOW APPROXIMATE LOCATION OF NUDE 5TH AND
95TH PERCENTILE AVIATORS' HEAD, SHOULDERS, ELBOWS, AND
HIPS. ADDITIONAL INCREMENTS ARE REQUIRED TO ACCOUNT
FOR CLOTHES.

Figure 21. Front View of Ballistic Armor Coverage
and Clearance for Aviator.

It can also be seen that adequate ballistic coverage is pro-
vided from the aft direction when allowance is made for the
slump of the normal seated position of the 95th percentile
occupant. Controls such as the collective stick can be
reached easily through the slot between the seat pan and the
side armor panels.

Figure 22 shows the seat bucket from the side with the 5th and 95th percentile chest and legs dashed in. Again, it can be seen that adequate ballistic coverage for the critical members of the body except the head has been provided. Protection for the head cannot be provided by opaque armor because of visibility requirements for the crew member's operational functions. This protection could be provided by transparent armor panels if desired. Frontal body protection is provided by armored vests.
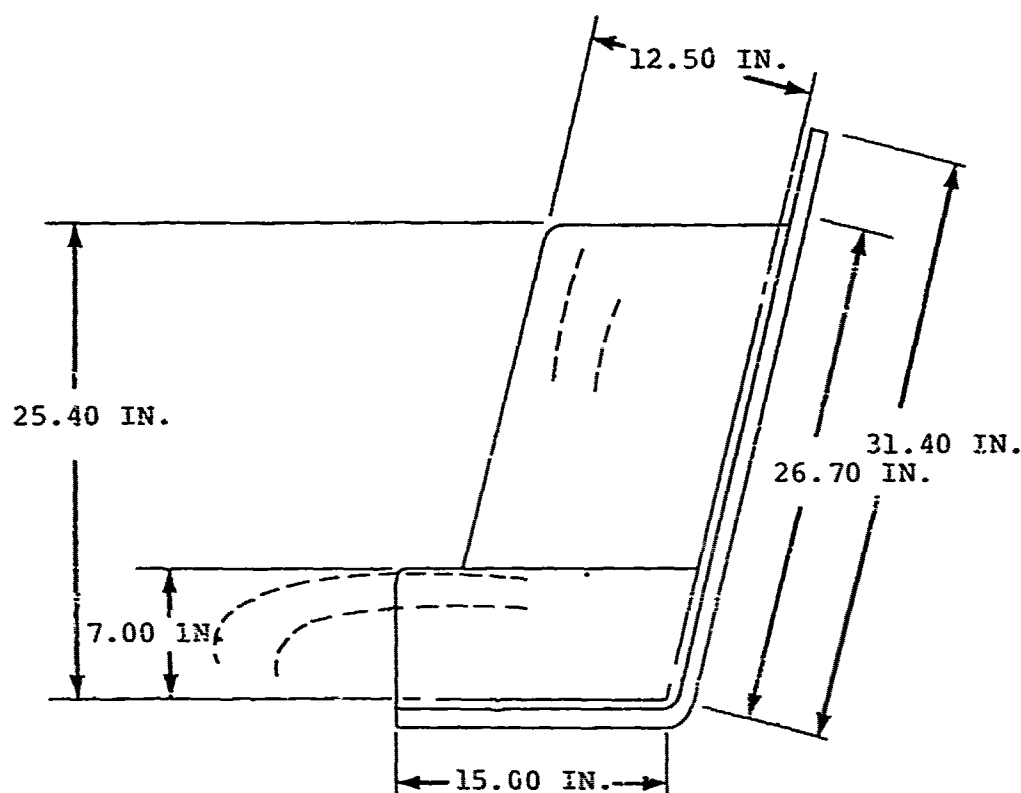
LEGEND

DOTTED LINES SHOW APPROXIMATE LOCATION OF NUDE 5TH AND 95TH PERCENTILE AVIATORS' CHEST AND LEGS. ADDITIONAL INCREMENTS ARE REQUIRED TO ACCOUNT FOR CLOTHES.

Figure 22. Side View of Ballistic Armor Coverage.

The lowest seat reference point (seat in bottom adjustment position) places the bottom of the seat pan 12 inches above the floor of the aircraft. A 0.55-inch compressed cushion thickness and a 2.50-inch vertical adjustment to the neutral location positions the neutral seat reference point 15.88 inches above the floor. This height provides a comfortable working level and is the approximate height used for design of office furniture and other seats in which people are required to remain seated for long periods of time.

The seat back tangent line was sloped back 13 degrees from vertical. This is the dimension recommended in human engineering handbooks as the optimum for comfort in working positions. It is also specified in Military Standard 1333, Aircrew Station Geometry for Military Aircraft.[12]

Table II shows typical increments to be added to nude body dimensions to account for winter flying clothes. These dimensions were taken from Reference 9 and may vary with the particular armed service; however, they are representative of the clearances required. It can be seen that the seemingly excessive coverage of the bucket is required to permit freedom of movement when these increments are added to the nude occupant.

TABLE II. TYPICAL INCREMENTS TO BE ADDED TO NUDE BODY DIMENSIONS TO ACCOUNT FOR WINTER FLYING CLOTHES	
Dimension	Additive Increment (In.)
Body Height, Sitting	1.6
Eye Height, Sitting	0.4
Shoulder Height, Sitting	0.6
Shoulder-to-Elbow Length	0.3
Shoulder Breadth	1.3
Chest Depth	1.4
Elbow-to-Elbow Breadth	4.4
Hip Breadth, Sitting	1.7
Buttock-to-Knee Length	0.5
Knee Height, Sitting	1.8

These figures show that a 95th percentile crewman would be adequately protected from ballistic fire from the side, bottom, and back from mid-thigh to shoulder. They also show that the crew member would have access to the controls located in the normal positions on present aircraft and visibility through more than a 180-degree arc measured through the design eye position.

2.3.3 WEIGHT AND CENTER OF GRAVITY

The total seat weight including restraint system, cushions, floor tracks, and inertia reel was 211.5 pounds. This included 101 pounds of armor and 50 pounds of movable seat structure. The 50 pounds included the restraint system, cushions, and inertia reel, in addition to the movable guidance mechanism.

The 211.5 pounds represents the weight of this experimental seat design and is therefore somewhat excessive. Subsequent studies indicate that an operational seat having these same general characteristics could be designed to weigh on the order of 170 to 180 pounds. This weight would be competitive with the weight of some armored crew seats in use today. For example, the heavy-weight armored seat configuration used in the UH-1D and H helicopters weighs approximately 170 pounds and contains no crash force attenuating features.[13]

The center of gravity of the completed seat assembly was 25.61 inches above the floor and 3.33 inches aft of a vertical plane passing through the longitudinal seat adjustment locking pin centerline as shown in the following sketch.

35
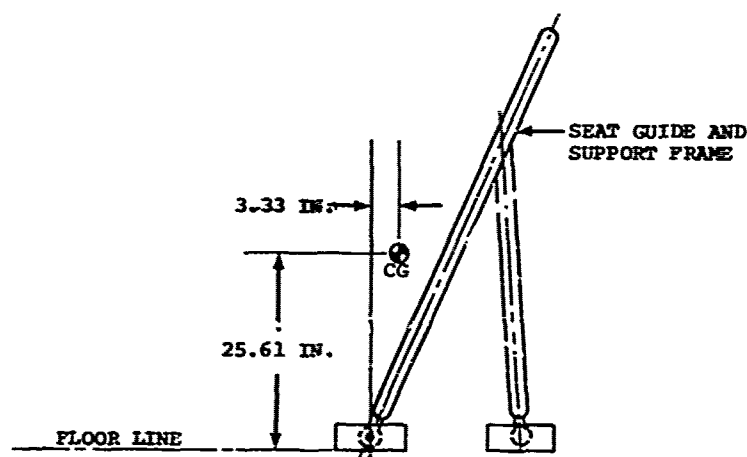
2.3.4 MAJOR COMPONENTS

2.3.4.1 Bucket: The seat bucket was designed as a fiberglass laminate, duplicating the weight, armor coverage, and center of gravity of an equivalent armored bucket. The design was detailed on Dynamic Science Drawing Number DSL-000266. The total armor coverage amounted to 13 square feet and weighed 101 pounds. The standard UH-1 armored seat provides about 10 square feet of coverage. Figure 23 is a frontal view of the armored bucket. The fixed-wing side panel design allows access to side controls such as collective pitch, while providing full side coverage for the upper torso and the upper arms of the crewman. The sides of the lower portion of the bucket were high enough to give side protection to the top of the crewman's thighs. A 95th percentile crewman would be protected from the back of his head to below his knees. Figure 24 is a side view of the bucket and shows the ballistic coverage provided for a 99th percentile occupant. Figure 25 shows a 1st percentile occupant with corresponding ballistic coverage. Attachment points for the lap belt and front tie-down portions of the restraint harness were integral with the bucket.
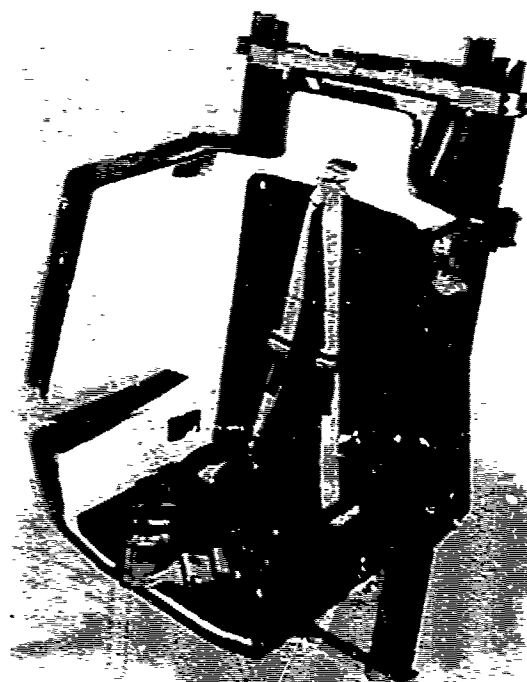
Figure 23. Frontal View of Armored Bucket.

Figure 24. Ballistic Coverage for 99th
Percentile Occupant.

Figure 25. Ballistic Coverage for 1st
Percentile Occupant.

37

2.3.4.2 <u>Restraint Harness</u>: After a survey was made of the available restraint systems on the market, it was determined that none of them were suitable for this application that would comply with the requirements specified in References 2 and 5. Therefore, a system was developed for this particular application that used conventional components where possible but provided a harness that met all the primary requirements. Figure 26 shows the full restraint system installed in the crew seat.
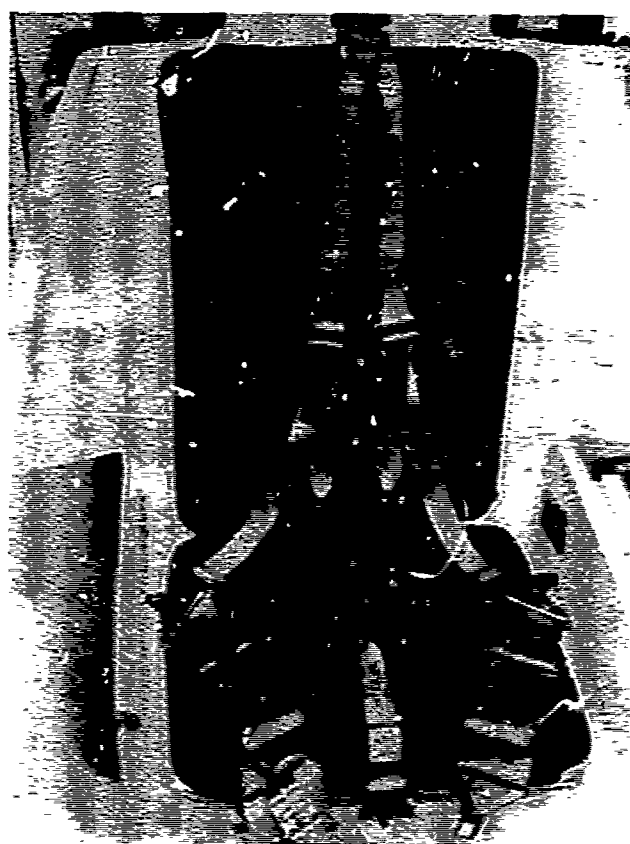
Figure 26. Full Restraint System
Installed in Crew Seat.

An existing Dacron webbing type was chosen for the entire harness. The webbing was designated MIL-W-25361A(USAF) and was available in 1-3/4-inch (Type III) and 3-inch (Type IV) widths.

The lap belt was 3 inches wide, with the overall length at maximum adjustment designated to be 40 inches between centers of the end fitting ferrules. By using short-length stitch patterns of the WW type as called out in References 2 and 5 and paralleling the adjuster with an extra piece of webbing, there was only one stitch pattern per side necessary, each being 2 inches long. Figure 27 shows the stitch pattern and also the special load cell developed by Dynamic Science to measure the harness loads. Paralleling the adjuster also alleviated half of the load that would otherwise be applied to the adjuster, thereby assisting the weakest part of the standard hardware. The hardware used was standard military hardware including MS22010-1 end fittings, MS22004-1 adjusters, and MS22003-1 and MS22013 buckle assemblies.

Figure 27. Lap Belt Stitch Pattern and Load
Cell for Measuring Harness Loads.

The shoulder harness was basically an MS16068 type with a substitution of the MIL-W-25361A Type III Dacron webbing and the incorporation of the WW type stitch patterns as specified in References 2 and 5. The vee at the back of the harness was defined to be a 60-degree included angle. Figure 28 shows the
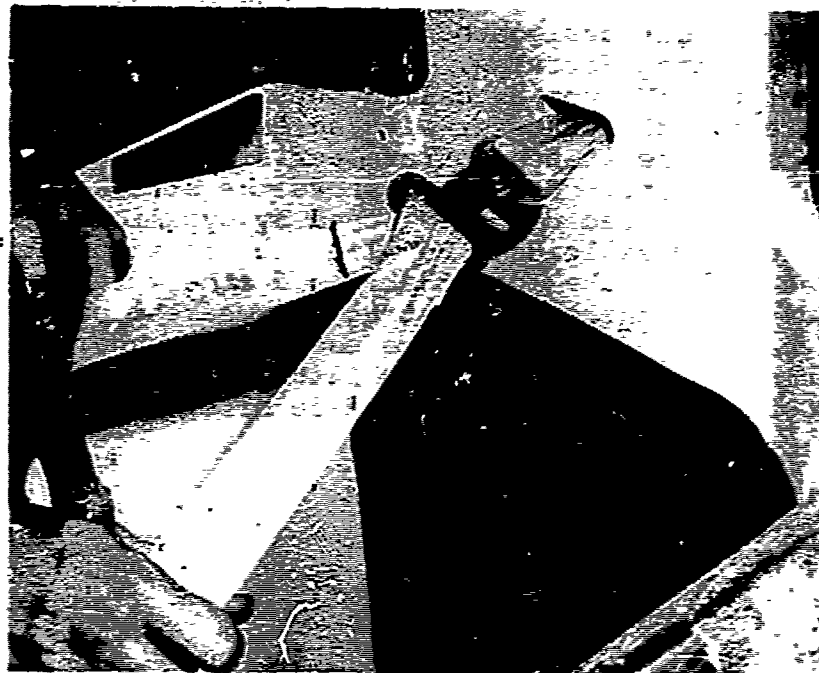
Figure 28. Vee Shoulder Harness Installation
and Load Cell for Measuring
Harness Loads.

vee portion of the shoulder harness installed on the seat and
the load link developed for that location.

An MA-6 inertia reel was used in conjunction with the shoulder
harness. The inertia reel was fastened to the top bearing
crossmember immediately behind the upper portion of the seat
bucket. The inertia reel strap passed through the slot in the
back of the bucket and attached to the shoulder harness at the
vee.

The front tie-down (negative G) strap was of similar construc-
tion to the shoulder harness in that it used the same 1-3/4-
inch Dacron webbing. The buckle attachment end fitting was an
NAS312817, which was the same as those used on the shoulder
harness. The adjuster was equivalent to those used on the
shoulder harness and was used to interface between the tie-
down strap and the piece of hardware used to attach the load
cell. This load cell was then anchored to the forward edge of
the seat pan. The anchor attachment on the bucket was formed
from a small plate attached to the under side of the seat pan
which exposed a slot extending beyond a cutout in the seat

40

pan. This configuration spread the tension load in the tie-down strap over a wide area on the under side of the seat pan, thus reducing the stress applied to the seat pan.

During the seat bucket stroke, the entire restraint system traveled as an integral part of the moving bucket, producing no change in the relative position or length of any portion of the restraint system with respect to the bucket.

2.3.4.3 Cushions: The seat cushions were made of a newly developed 5-pound-per-cubic-foot, load-rate-sensitive foam, designated X-3 by the manufacturer. The bottom or seat pan cushion was a 2-inch-thick slab of this material and covered the entire bottom of the seat bucket. The cushion was restrained by strips of Velcro fasteners and a metal lip along the front edge of the bucket. The metal lip provided added support to the cushion from a severe longitudinal crash pulse. The back cushion was a 1-inch-thick slab of the X-3 material and extended from just beneath the inertia reel strap slot in the bucket back down to the rear edge of the seat cushion. This back cushion was also retained with the Velcro fasteners.

The hook side of the Velcro was stitched onto the cover of both cushions, and the mating pile was bonded to the interior surface of the seat bucket. The cushion covers simulated Nomex-type materials to provide equivalent texture, strength, and appearance. Figure 26 also shows the seat cushions installed in the bucket.

2.3.4.4 Guide Frame and Support Structure: The guide frame consisted of two hard-anodized aluminum tubes (7076-T6), 2 inches in diameter, and an upper yoke assembly which fitted into the upper ends of the two guide tubes. This guide frame was held in position by a heat-treated aluminum support structure which maintained a fixed, parallel support for the guide frame. The support structure was a tube space frame consisting primarily of 1-1/2-inch-diameter tubing with a 1/8-inch wall. Figure 29 shows an oblique rear view of the support structure, carrier bearing assemblies, and the guide tubes without the upper yoke assembly.

2.3.4.5 Carrier Bearings: The carrier bearings consisted of sets of four needle roller bearings retained in bearing block assemblies as shown in Figure 30. Special sleeve bushings with a concave outer cross section allowing curvilinear contact with a large sector of the guide tube were pressed onto the outer faces of the rollers. One set of four bearings completely circled one region of the guide tube. A mating set on the other guide tube directly opposite was connected through a

41
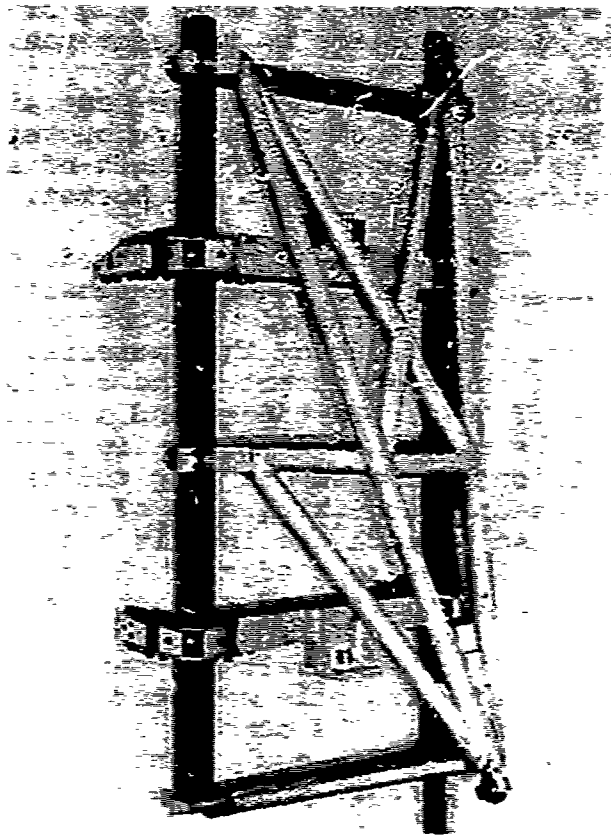
Figure 29. View of Support Structure,
Carrier Bearing Assemblies,
and Guide Tubes.

square tubular crossmember. A complete assembly for one seat
included four bearing assemblies and two crossmembers, one at
the top of the bucket and one near the bottom just beneath the
lower edge of the side panels of the bucket.

The upper crossmember carried a platform to which the inertia
reel was mounted. The lower crossmember carried an attachment
bracket for the lower end of the energy-absorber system.
Figure 31 presents a front view of these carrier bearings and
the associated hardware mounted on the guide tubes.

2.3.4.6 Energy Absorber: An energy-absorbing system with a
tri-level limit load was designed for use on the crew seat.
The primary energy-absorber device was an annealed, stainless
steel, tensile tube which was backed up by two small stainless

42

CROSSMEMBER

GUIDE
TUBE

SPACER
BLOCK

BEARING SHAFT

COVER PLATE

NEEDLE
BEARINGS

CONTOURED 4130
ROLLER

BUCKET CONTOUR
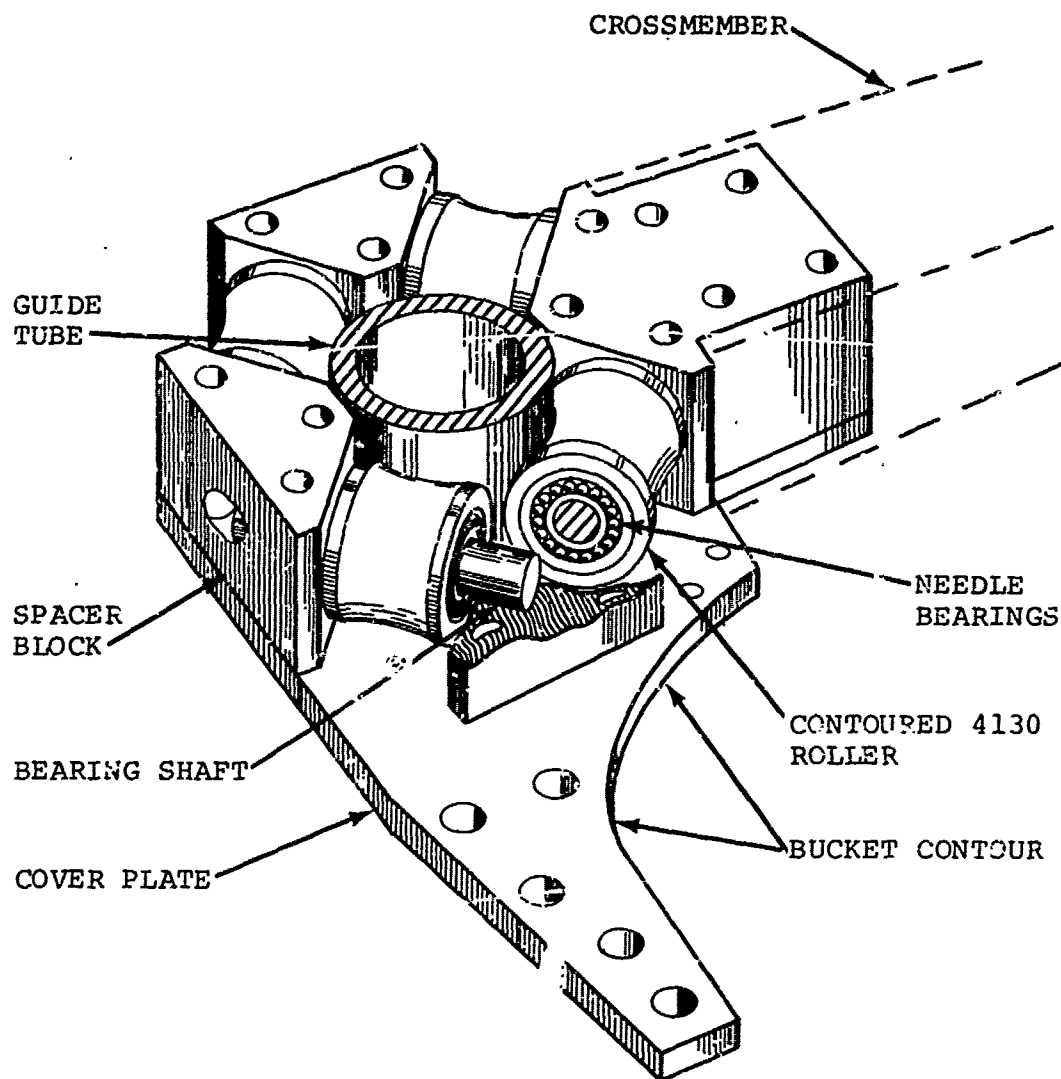
Figure 30. Bearing Assembly With 7 . Cover Plate Removed.

steel cables which provided the necessary load limit changes
required for adjustment to a particular crewman's weight. The
lower end of the energy-absorbing system was attached to the
lower crossmember discussed in the preceding paragraph. The
upper end was attached to the seat adjuster which provided an
overall height adjustment for the seat bucket. Figure 32
shows the vertical adjuster with a special section designed
for strain gaging. Static support tests of candidate stain-
less tubing were conducted during the design effort. These
tests are summarized in Appendix I.
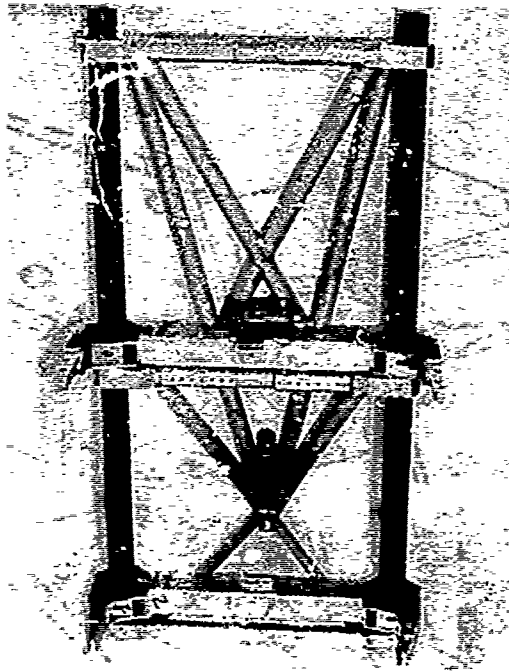
Figure 31.   Front View of Support Structure,
             Carrier Bearing Assemblies, and
             Guide Tubes.
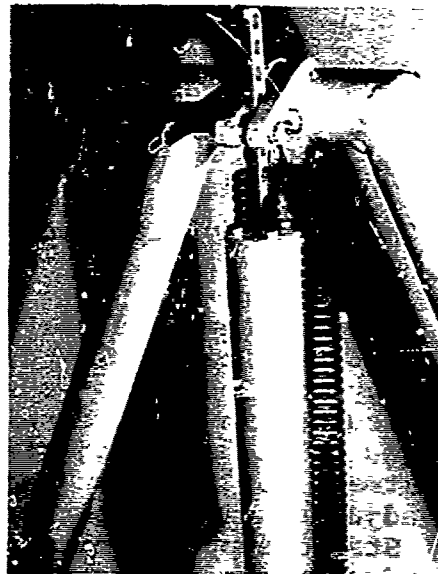
Figure 32.   Vertical Adjuster.

Another energy absorber was designed to limit the loads on the aft structural seat mount. It consisted of a small aluminum column positioned beneath the head of the rear support structure bolt. The wall thickness of this column was sized to establish the limit load of this energy absorber. Figure 33 shows the primary energy absorber before and after a test. Figure 34 shows the short-column energy absorber at the back of the support structure and also the lower end of the primary energy absorber.
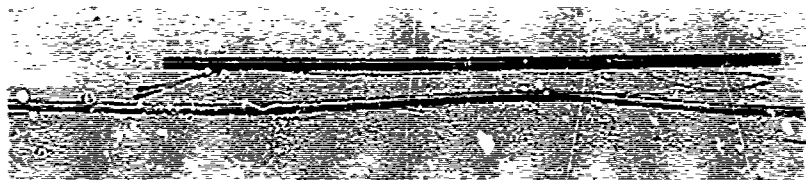
Figure 33. Primary Energy Absorber Before and After Test.
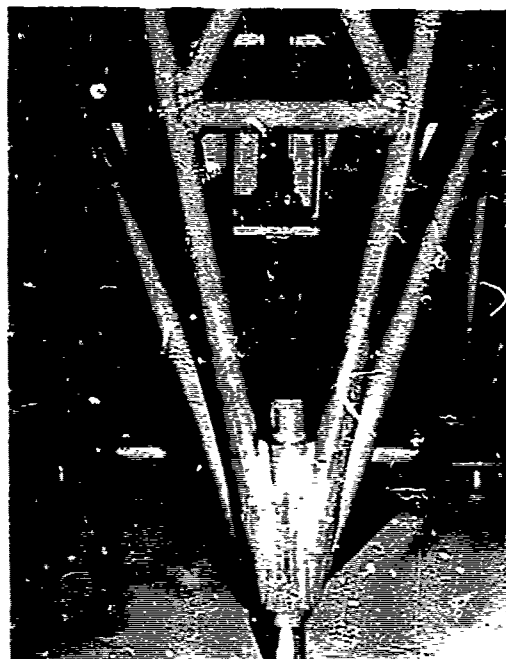
Figure 34. Short-Column Energy Absorber and Lower End of Primary Energy Absorber.

45

2.3.4.7 **Floor Attachments:** Three mounting points at the lower end of the seat support structure were provided with attachments to connect the seat to the floor. These attachments consisted of spherical bearing rod-ends. A small T-shaped steel slider slipped through the hole in the rod-end and extended into grooves in the sides of the floor track. The two forward rod-ends could be fixed in position by two quick-release pins, thus providing longitudinal adjustment locks. Figure ?. shows one of the forward floor attachments as it was orien .. for the static test.
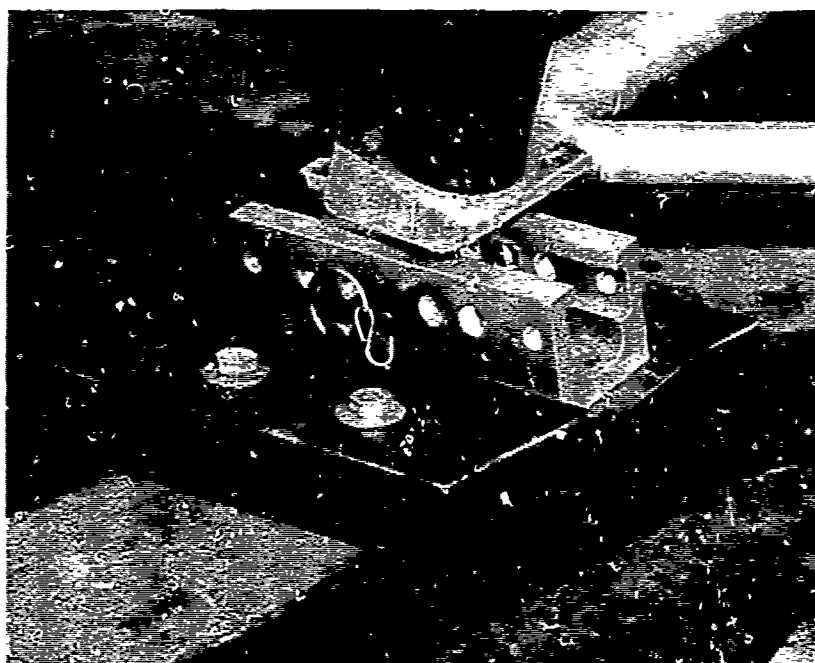
Figure 35. Forward Floor Attachment
Oriented for Static Test.

CHAPTER 3

THEORETICAL ANALYSIS

3.1 INTRODUCTION

Of the many theoretical analyses conducted during the program, the most significant ones were those conducted to establish the performance requirements for the energy-absorbing system. This chapter presents three of these analyses in the following order:

1. Rigid-body energy-absorber analysis.

2. Dynamic response as a function of movable seat weight.

3. Dynamic response as a function of percentile crash pulse and limit load.

3.2 RIGID-BODY ENERGY-ABSORBER ANALYSIS

3.2.1 PURPOSE OF ANALYSIS

A rigid-body parametric analysis was accomplished to establish relationships between variables for the following three problems:

Problem No. 1: Determine the relationship between seat pan deceleration and available stroke length for the following test conditions:

1. Maximum Occupant Weight Range

   Lower Limit - 5th percentile occupant with minimum clothing and equipment

   Upper Limit - 95th percentile occupant with maximum clothing and equipment

2. Limit Load Setting

   Fixed at one limit load setting and limit load based on the upper limit of occupant weight range

Problem No. 2: Determine the relationship between seat pan deceleration and available stroke length for the following test conditions:

47

1. **Occupant Weight Range - Normalized Clothing and Equipment**

   Lower Limit - 5th percentile occupant with minimum clothing and equipment

   Upper Limit - 95th percentile occupant with minimum clothing and equipment

2. **Limit Load Setting**

   Fixed at one limit load setting and limit load based on the upper limit of occupant weight range

Problem No. 3: Determine the relationship between seat pan deceleration and the weight of the load-limited mass for the following test conditions:

1. **Occupant Weight Range - Normalized Clothing and Equipment**

   Lower Limit - 5th percentile occupant with minimum clothing and equipment

   Upper Limit - 95th percentile occupant with minimum clothing and equipment

2. **Limit Load Setting**

   Adjustable to three limiting load levels with the limiting load level selected to provide equal increases in deceleration G level over the occupant weight range covered by a particular setting

3.2.2 RIGID-BODY ANALYSIS TECHNIQUE

The analysis technique used is explained in Reference 2. The relationship developed is

$$s = 12gG_m t_m^2 \left(\frac{-K^3}{24} + \frac{K}{2} + \frac{1}{2K} - 1\right) \tag{1}$$

where s = stroke length, in.

   G_m = maximum input deceleration, G

   t_m = one-half input pulse duration, sec

   g = acceleration due to gravity, 32.2 ft/sec^2

48

$$K = G_L/G_m$$

$$G_L = \text{limit deceleration, G}$$

$$12 = \text{constant, in./ft}$$

3.2.3 OCCUPANT PROPERTIES

The nude weights of the 5th percentile and 95th percentile Army aviators were determined from Reference 6 as 135.9 pounds and 199.7 pounds, respectively.

The equipment weights, determined from Reference 12, were as shown in Table III.

TABLE III. NUDE WEIGHTS OF 5TH AND 95TH PERCENTILE ARMY AVIATORS		
	Weight (lb)	
Item	5th Percentile	95th Percentile
Gloves	.28	.28
Revolver	2.05	2.05
Ammunition	1.60	1.60
Survival Kit	4.50	4.50
Radio	2.00	2.00
Clipboard	.87	.87
Chest Armor	14.56	14.56
Pen Light	.10	.10
Flight Clothes	2.10	3.10
Helmet	3.50	4.00
TOTAL EQUIPMENT	31.56	33.06

The weight of the aviators' boots was not included in the anal-
ysis as they and the lower legs were assumed to be supported
by the floor of the aircraft during vertical loading.

For the calculation of the effective weight of the lightly
equipped 5th percentile aviator, only the weight of the light
clothes and helmet was included. Therefore,

$$Wt_{eff} = (135.9 + 2.1) \ .8 + 3.5 = 114 \text{ pounds} \tag{2}$$

For the calculation of the effective weight of the heavily
equipped 95th percentile aviator, the weight of all equipment
was included. One-hundred percent of all equipment weight
carried by the seat and 80 percent of the weight of all items
carried partially by the seat and partially by the floor was
used:

$$Wt_{eff} = (199.7 + 3.1 + .87) \ .80 + 28.10 = 192 \text{ pounds} \tag{3}$$

In like fashion, the effective weight of the lightly equipped
95th percentile aviator was calculated to be 166 pounds. For
convenience, a curve of the effective weight of the lightly
equipped Army aviator was calculated and plotted versus cumu-
lative frequency of occurrence (Figure 36).

3.2.4 ENVIRONMENT

The crash environment chosen for analysis was the 95th percen-
tile vertical survivable accident as defined in Reference 2.
The conditions used were as follows:

Velocity change = 42 ft/sec

Peak deceleration = 48G

Pulse duration = 0.054 sec

Pulse shaps = isosceles triangle

3.2.5 RESULTS

3.2.5.1 Problem No. 1: The results of the computed basic re-
lationship between stroke and deceleration are presented in
Figure 37. The curve shows that the seat stroke decreases at
a diminishing rate with deceleration level. The curve in-
cludes only the stroke achieved through seat deformation and
does not represent the total decelerative stroke of the seat
and occupant during a crash. The stroke provided by fuselage
deformation is implicit in the definition of the input pulse.

50
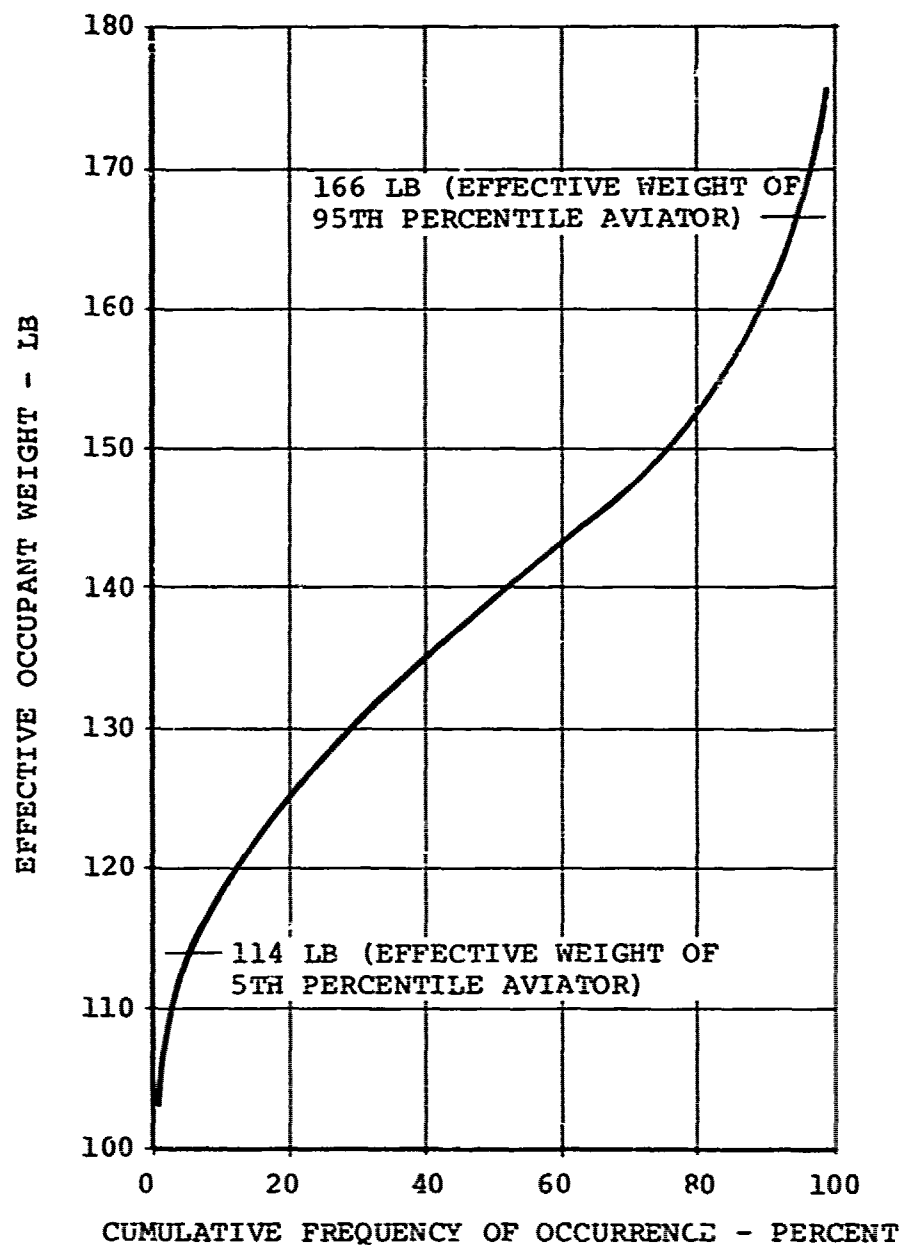
Figure 36.   Effective Weight of Lightly Clothed
Army Aviator as a Function of
Cumulative Frequency of Occurrence.
(Basic Frequency Data Taken From
Reference 6.)

51
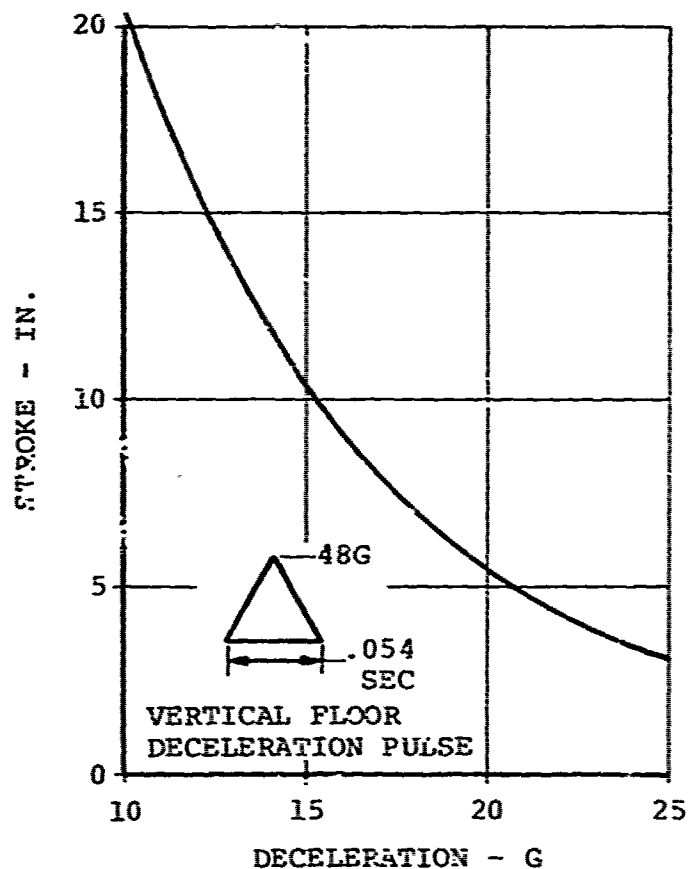
Figure 37. Seat Stroke Versus Deformation.

The relationship between deceleration and stroke length for
the 5th and 95th percentile occupant with the load limit set
for the 95th percentile occupant was determined for an assumed
movable seat weight of 30 pounds. The load limit was calcu-
lated as follows:

$$L_L = (Wt_{eff} + W_{ms}) \, (G_L) \tag{4}$$

where L_L = limit load, lb

Wt_{eff} = effective weig `· of heavily equipped 95th per-
centile occupant, lb

W_{ms} = weight of the movable portion of the seat, lb

G_L = limit deceleration level, G

52

Assuming that the energy absorber was set to provide this resistive force, the limit deceleration level was then computed for the 5th percentile occupant representative of the lighter possible seat occupants. The calculations were made again assuming a rigid mass consisting of the effective weight of the occupant plus the weight of the movable or stroking portion of the seat.

$$G_L = \frac{L_L}{Wt_{(eff)} + W_{ms}} \tag{5}$$

where G_L represented the deceleration level of the lighter or 5th percentile man, $Wt_{(eff)}$ was the effective weight of the lightly clad occupant, W_{ms} was the movable seat weight, and L_L the limit load as calculated for the 95th percentile occupant.

Calculations were made and the resulting relationships are shown in Figure 38. It can be seen that, for an available 8-inch stroke length, established with criteria previously contained in Reference 2, a 17G deceleration level was predicted for the 95th percentile occupant. When the load required to stroke the energy absorber was sized for the 95th percentile occupant with the heavy clothes and equipment, the lightly clad and equipped 5th percentile occupant was expected to be decelerated at a 26G level. This deceleration exceeds the human tolerance level and shows that when the limit load of an energy-absorption system is set for the large and heavily equipped occupant, the small, lightly equipped occupant could receive a 9G higher deceleration and would not use the entire available stroke.

3.2.5.2 Problem No. 2: The relationships between deceleration and available stroke distance for 5th and 95th percentile occupants dressed and equipped alike are shown in Figure 39. Figure 39 shows that a system designed for an 8-inch stroke, a 17G deceleration level, and a 95th percentile occupant would decelerate a 5th percentile occupant at a 23G level. Although this was an improvement over the situation described in the previous problem (6G versus 9G), the 23G level is approaching the limit of human tolerance in the vertical direction. This level is considered excessive, since dynamic response was not considered in these calculations.

The effect on deceleration of the 5th percentile occupant was included as a secondary analysis relative to the weight of the movable section of the seat. The relationships are shown in Figures 40 and 41 for both occupant weight range conditions already discussed. Increasing the weight of the movable section of the seat tended to decrease the deceleration level of

53
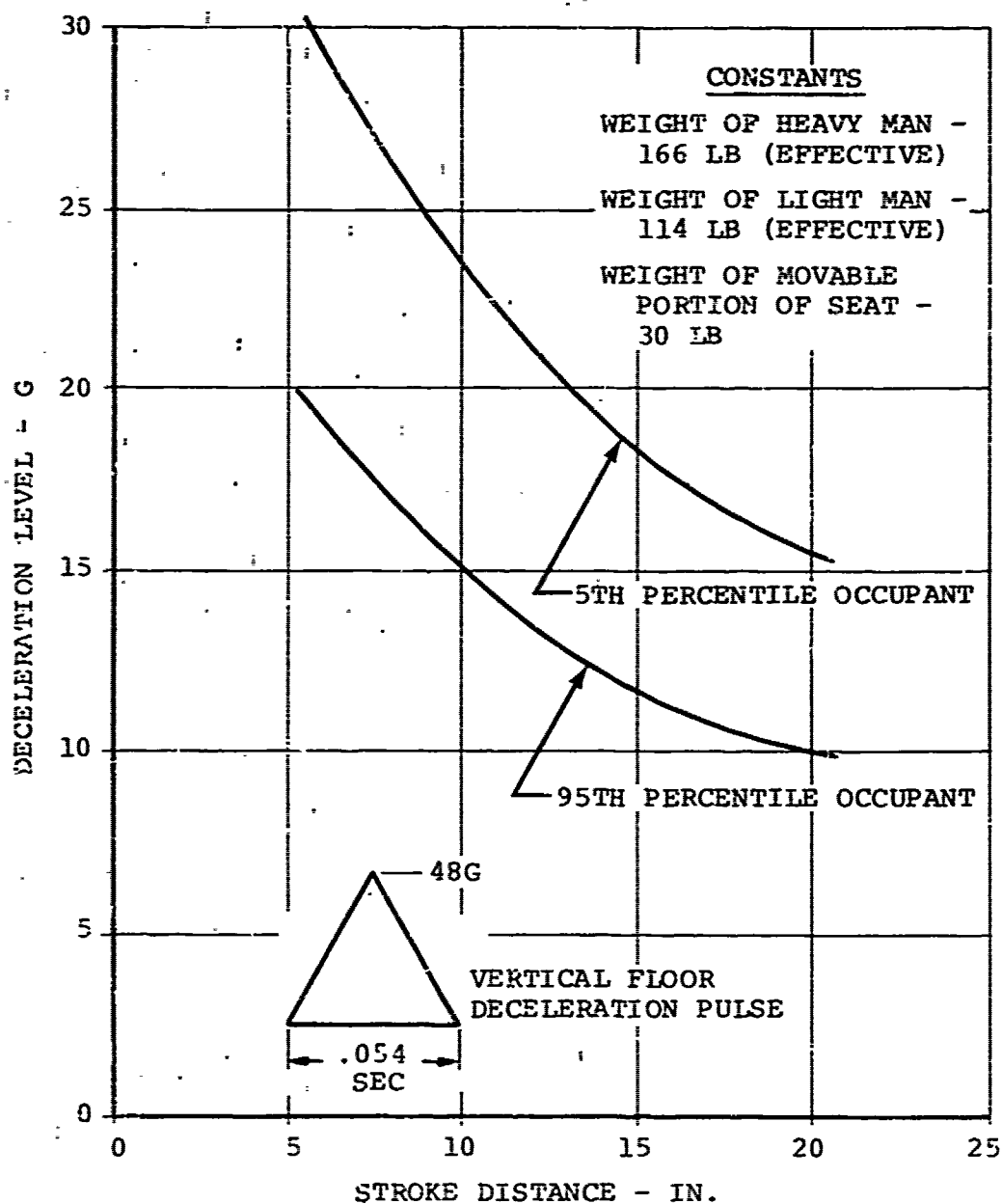
Figure 38. Deceleration Level Versus Available Stroke
Distance (Lightly Dressed 5th Percentile
and Heavily Dressed and Equipped 95th
Percentile Occupants).

54
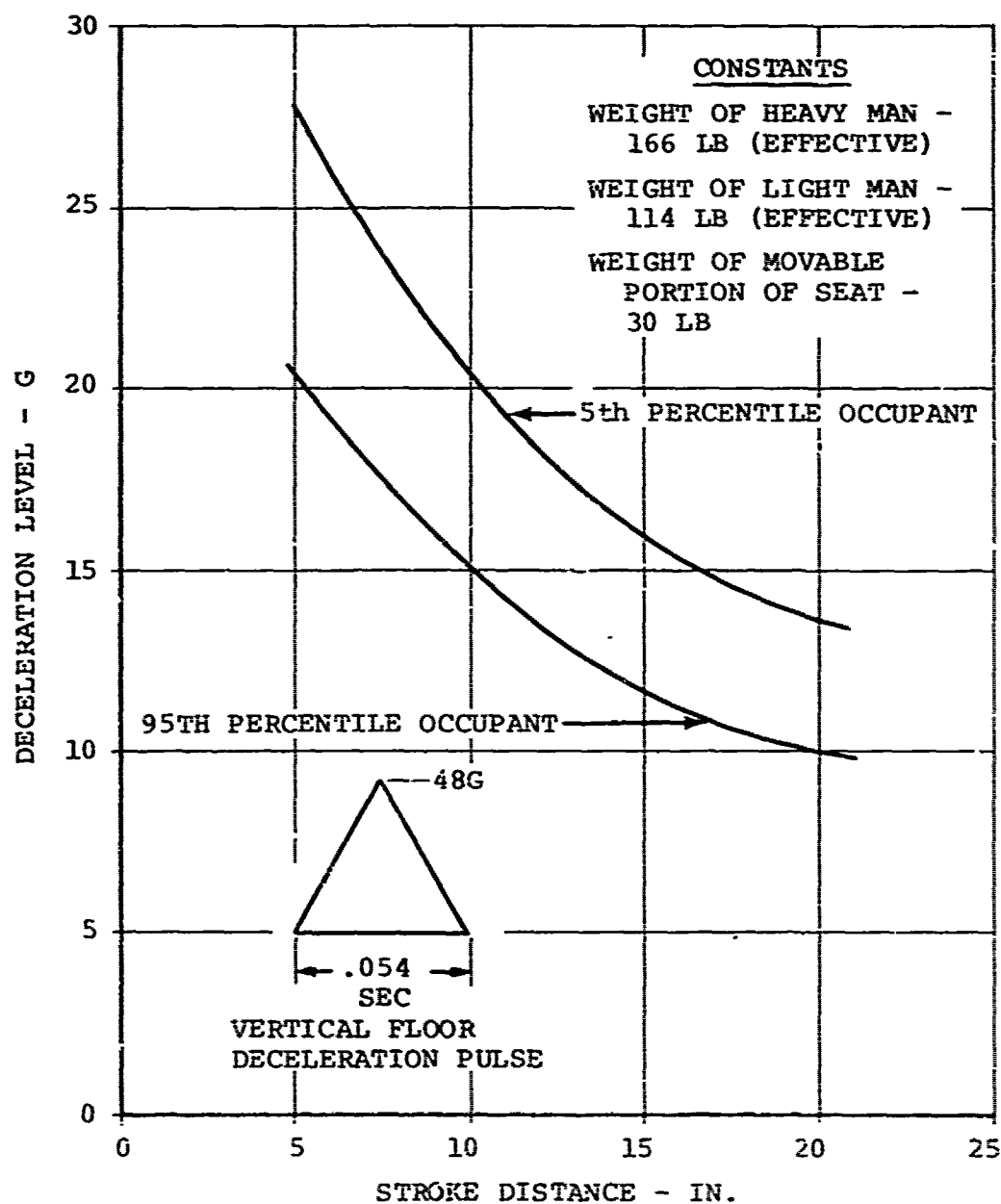
Figure 39. Deceleration Level Versus Available
Stroke Distance (Seat Occupants
Dressed and Equipped Alike).
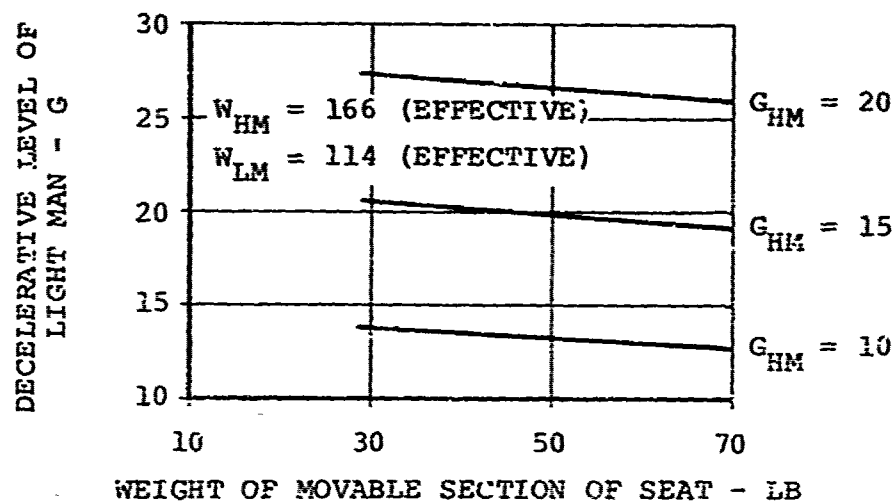
Figure 40. Deceleration Level of Light Man Versus
Weight of Movable Section of Seat (As
a Function of Heavy Man Design
Deceleration G_{HM}, With Occupants
Dressed Alike).
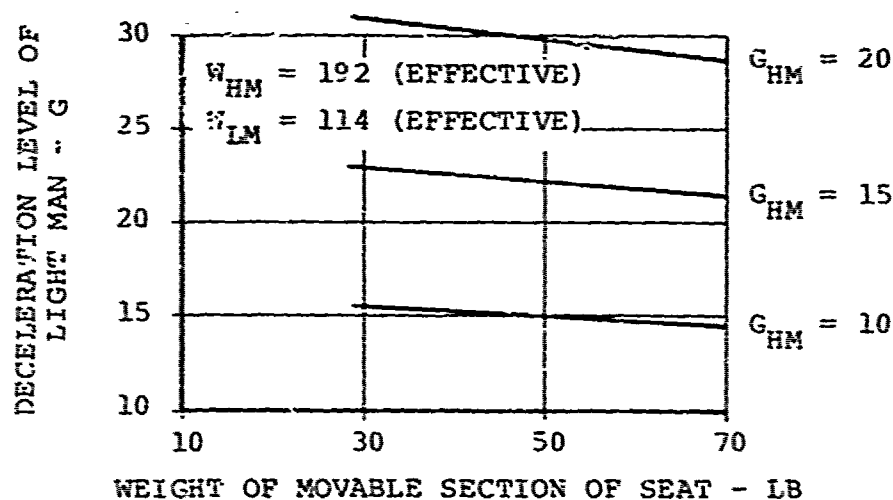
Figure 41. Deceleration Level of Light Man Versus
Weight of Movable Section of Seat (As
a Function of Heavy Man Design Limit
Deceleration G_{HM}, With Maximum
Clothing and Equipment Weight
Difference).

the light man because the body weight was a smaller percentage of the total weight decelerated. Increasing the weight of the r   . section of the seat from 30 to 70 pounds decreased the ·˙. ι tion level of the light man by about 1G when clothes . . ;u.pment types were alike. In actual practice, this de-˙˙use in average deceleration would tend to occur, but because of the dynamics of the spring-mass system of the body and the seat, high deceleration spikes could result from interaction between the occupant and the heavy seat bucket.

3.2.5.3 Problem No. 3: In the analysis of this problem, a minimum available stroke length of 8 inches was used to protect the 5th through the 95th percentile occupants dressed in light clothes from the environment associated with the 95th percentile accident.

The energy-absorbing system was assumed to be capable of three different limit load settings, which would permit an occupant to select a limit load based on his particular weight, thus providing him with a custom-designed energy absorber. The limit load settings would be designed to provide equal increases in deceleration G level over the occupant weight range covered by a particular load setting. Since it would be undesirable to have any occupant bottom out or exceed a stroke length for the conditions specified, the load settings were established to provide usage of a full 8-inch stroke for the heaviest effective weight to be decelerated by any load setting.

The deceleration G levels as a function of effective weight of the occupant plus a presumed 30-pound weight for the movable section of the seat are shown in Figure 42. It can be seen that the heaviest weight would be decelerated at a 17G level by any one load setting. The lightest weight to be decelerated by any one setting would produce an 18.8G level. The dotted line on Figure 42 shows the relationship between deceleration and effective weight if the limit load was not adjustable and was designed for the 95th percentile occupant. It can be seen that this curve agrees with that shown in Figure 39, and that use of the multiple-limit load energy absorber decreased the deceleration variation from 6 to 1.8G over the range of effective occupant weight used in the analysis.

3.2.6 GENERAL COMMENTS

It is apparent that a rigid-body analysis cannot account for the dynamic response of the human occupant interfaced to the seat through cushions. Therefore, dynamic analyses were made

CONDITIONS UPON WHICH FIGURE IS BASED

- STROKE LENGTH = 8 IN.
- WEIGHT OF MOVABLE SECTION OF SEAT = 30 LB
- LIMIT LOAD ADJUSTABLE TO THREE LEVELS
- 95TH PERCENTILE SURVIVABLE ACCIDENT
- PROTECTION SHOWN COVERS 5TH TO 95TH PERCENTILE OCCUPANTS CLOTHED AND EQUIPPED ALIKE
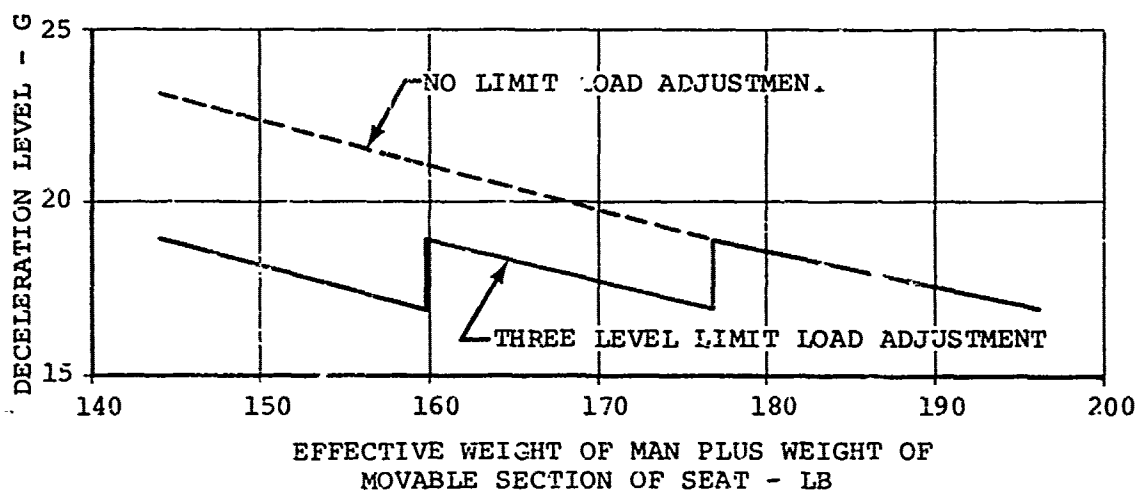
Figure 42. Deceleration Level Versus Effective Movable
Weight of Occupant and Seat.

to establish actual load-limiter design criteria and are discussed in the following text. The results of these analyses were used to assist in seat concept selection.

3.3 DYNAMIC RESPONSE AS A FUNCTION OF MOVABLE SEAT WEIGHT

3.3.1 PURPOSE OF ANALYSIS

A dynamic analysis was conducted to provide insight into the effect of movable seat weight on system response and the resultant effect on decelerative loading of the occupant. The lightly clad 95th percentile Army aviator was used as the seat occupant.

3.3.2 FIVE-DEGREE-OF-FREEDOM DYNAMIC ANALYSIS TECHNIQUE

The analytical model used for the analysis discussed in the previous section is correct for rigid masses; however, this model does not provide adequate simulation of human seat occupants. The dynamic response of seat and occupant in the vertical direction has been analyzed in depth by several models, the most rigorous of which is a Dynamic Science 5-degree-of-freedom digital computer program. [14] In this model, a 3-degree-of-freedom system is used to represent the head, chest, and pelvis of the body. This system is coupled with the cushion and seat to form a 5-degree-of-freedom lumped parameter dynamic model representing the seat, seat cushion, and seat occupant.

The occupant is assumed to be seated in an upright position so that the spinal column is vertical and motion is translational in the vertical direction only. The equations of motion for this model are solved to determine the dynamic response of the body both with or without the cushion and seat.

The model used is illustrated in Figure 43. Masses M_5, M_4, and M_3 represent the head, chest, and pelvis, respectively, of the seated occupant, and masses M_2 and M_1 represent the cushion and seat, respectively. Springs K_5, K_4, and K_3 represent the neck, spinal column, and fleshy area around the buttocks, respectively. Springs K_2 and K_1 possess the load deflection characteristics of the cushion and the seat, respectively. Viscous dampers C_5, C_4, C_3, C_2, and C_1 are provided between each of the masses and between the floor of the seat mass.

The floor in Figure 43 represents the cockpit floor of an aircraft to which the acceleration-time history of the crash pulse under analysis is applied.

The equations of motion for each mass in the system were formulated using Newton's second law of motion:

Force (F) $= \dfrac{d(Mv)}{dt}$ [time rate of change of linear momentum], or, since each mass remains constant,

$$F = M \frac{dv}{dt} = Ma \qquad (6)$$

Thus, considering the general case for any mass in the system, the equations of motion were derived with the aid of the free-body diagram that follows.

59
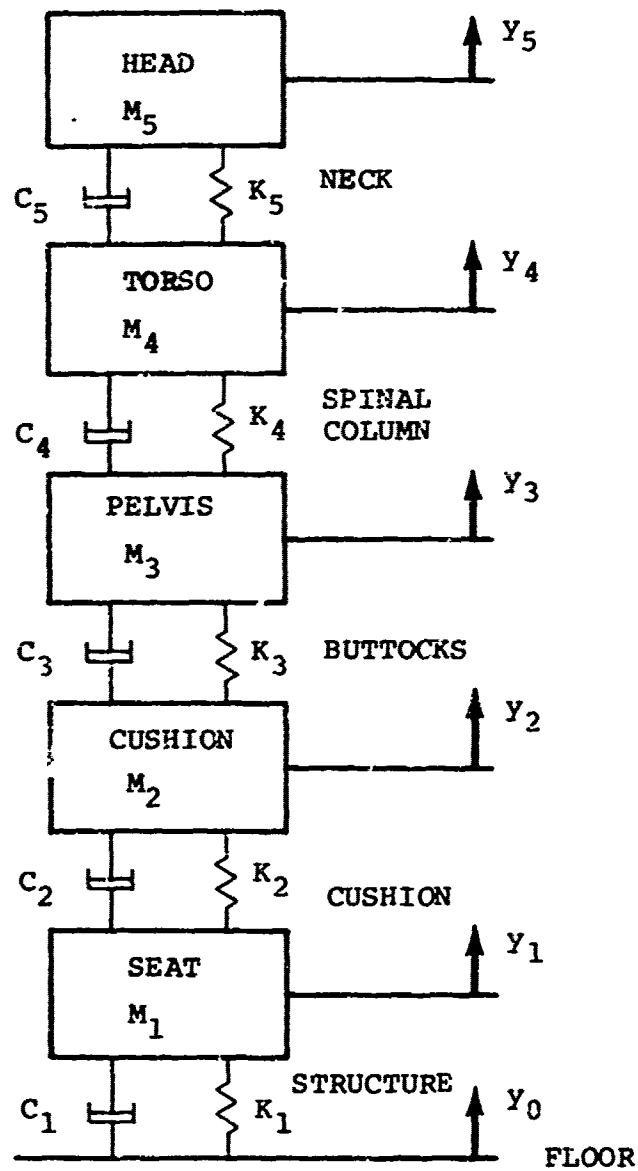
Figure 43.   Lumped Parameter Model Representing a Seat,
             Seat Cushion, and Seat Occupant.[14]

$$C_{i+1}(\dot{y}_{i+1}-\dot{y}_i) \qquad K_{i+1}(y_{i+1}-y_i)$$

$$+Y_i$$

$$M_i$$

$$(i = 1,2,3,4,5)$$
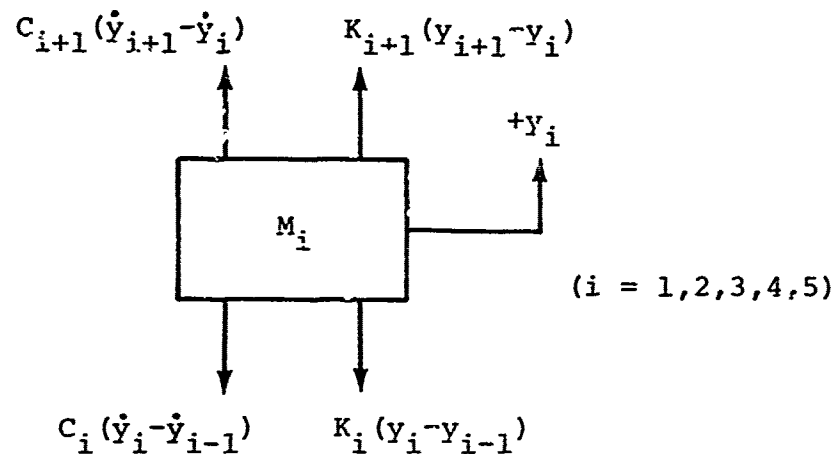
$$C_i(\dot{y}_i-\dot{y}_{i-1}) \qquad K_i(y_i-y_{i-1})$$

$$M_i\ddot{y}_i + C_i(\dot{y}_i-\dot{y}_{i-1}) + K_i(y_i-y_{i-1})$$
$$- C_{i+1}(\dot{y}_{i+1}-\dot{y}_i) - K_{i+1}(y_{i+1}-y_1) = 0 \qquad (7)$$

As can be seen from the equations of motion, a number of co-efficients are required to define the system which consists of three major components (body, cushion, and seat). Each component requires individual definition prior to its integration into the complete system.

An example of the output generated by this program is shown in Figure 44. The response curves for the seat structure, occu-pant pelvis, and chest are shown as a function of time for the input excitation also shown. The seat model used was an energy-absorbing model with a deceleration limit setting of 18G. It can be seen that the dynamic response of the seat and segments of the body are interrelated and vary as the various model springs load and unload.

Initially, the seat bucket deceleration lags the input pulse as the springs constituting the flesh and the cushion and the rather stiff elastic spring of the seat structure are loading up. Since the limit load of the energy absorber was designed for an 18G deceleration of a particular mass, and since the effective mass is not yet being applied to the seat structure because of the degree of compression of springs, the seat de-celeration exceeds the design deceleration to produce the force necessary to stroke the energy absorber. The seat pan deceleration therefore exceeds 18G and reaches approximately 43G before the cushion and flesh springs compress to the point that significant deceleration of the pelvis is achieved. As
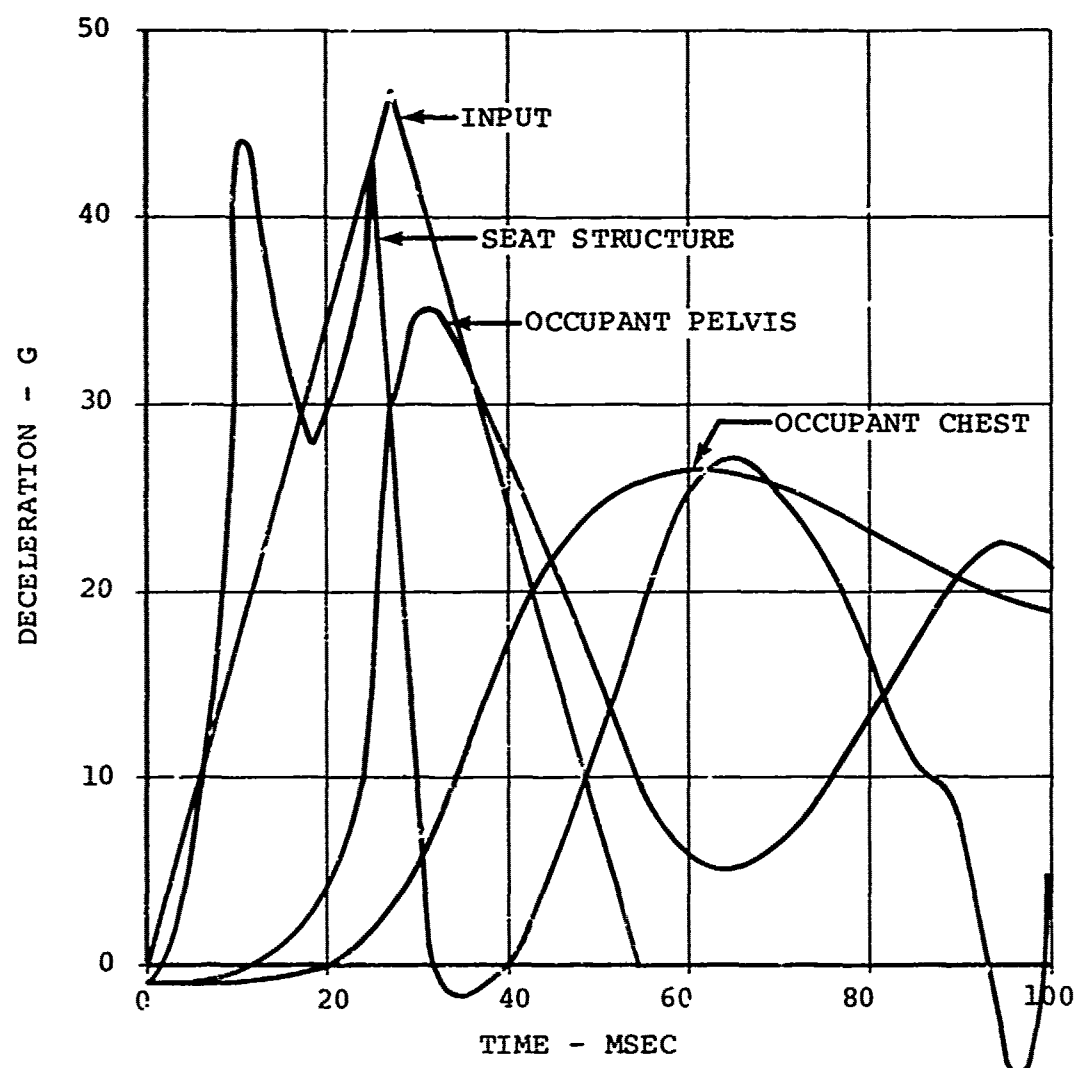
Figure 44. Deceleration Versus Time for Various
Components of Seat and Occupant
(Standard Net Cushion).

deceleration of the pelvic mass builds up, increasing force in
the downward direction on the seat pan is applied, which then
reduces the deceleration of the seat pan. The deceleration
drops from 43G to around 27G as the effective mass being de-
celerated is increased.

Since the input G loading is still increasing, and the chest
mass has not yet been applied to the system because the spring
representing the spine between the pelvis and chest has not

yet been compressed and loaded, both the seat pan and the pelvic deceleration increase. As the spring representing the flesh on the buttocks and the cushion compresses, the pelvic deceleration continues to increase, further loading the seat pan and decreasing its deceleration. It can be seen that the deceleration of the seat pan actually reverses sign and becomes a slight acceleration under the combined loading of the peak pelvis deceleration together with initiation of the occupant chest deceleration.

As the chest deceleration builds up, the deceleration of the seat pan and the pelvis tends to normalize around the G level corresponding to the energy-absorber limit load.

The foregoing discussion presents the analytical explanation for the fact that, in order to hold the decelerative loading within human tolerance, the design limit load must be reduced over that calculated for a rigid mass.

Further analyses have been conducted in a Navy-sponsored program.[15] Results show that the force-versus-deformation characteristic of the particular energy-absorbing system can be shaped to provide more or less efficient use of the stroke distance available.

3.3.3 BODY PROPERTIES

Table IV presents the characteristic body properties used for the analysis.

TABLE IV. OCCUPANT NUDE BODY PROPERTIES			
Portion of Body	Weight (lb)	Spring Constant (lb/in.)	Damping Coefficient (lb/sec/in.)
Pelvis	84.8	2685	13.5
Chest	56.0	347	4.1
Head	15.7	523	2.8

These properties were obtained from Reference 14 and adjusted to represent occupant effective weight as defined in Reference 2. Much of the basic data used in arriving at the properties listed were obtained from References 16, 17, 18, 19, 20, 21, 22, and 23. For the dynamic analysis, one-half the thigh weight and the weight of the lower legs, feet, lower arms, and

63

hands were excluded from the active body weights used as lump masses.

3.3.4 CUSHION PROPERTIES

The cushion selected for the analysis consisted of a 1.56-inch-thick layer of a typical polyethylene slow-rebound foam. A typical stress versus strain curve is shown in Figure 45.
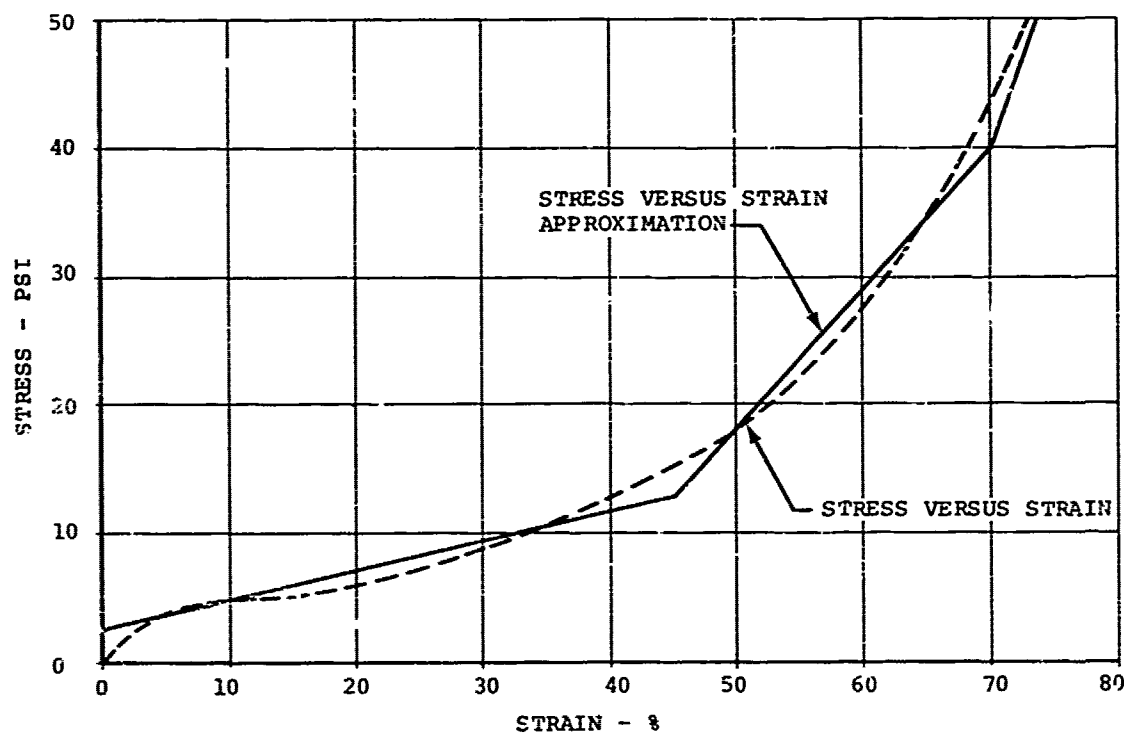
Figure 45. Stress-Strain Data for a Commercially Available Slow-Rebound Foam.

The force versus deformation characteristic for the cushion was calculated by assuming projected buttock contact areas as a function of cushion deflection and calculating the load versus cushion deflection through use of the curve in Figure 45. Unloading rates were assumed. The cushion properties used are given in Table V.

TABLE V. CUSHION PROPERTIES					
Strain (%)	Deflection (in.)	Stress (psi)	Area (in.^{2})	Load (lb)	Unloading Rate (lb/in.)
6.5	.10	2.5	32	89	800
45.0	.70	12.5	50	625	800
70.0	1.10	39.5	58	2280	1000
80.0	1.25	70.0	63	4400	2000

For analytical purposes, the curve was approximated by straight line segments as shown in Figure 45.

3.3.5 SEAT PROPERTIES

The seat spring properties were varied with movable seat weight as shown in Figure 46. The figure shows that the load deformation characteristics used were similar, containing a 0.10-inch elastic deformation prior to reaching the limit load.
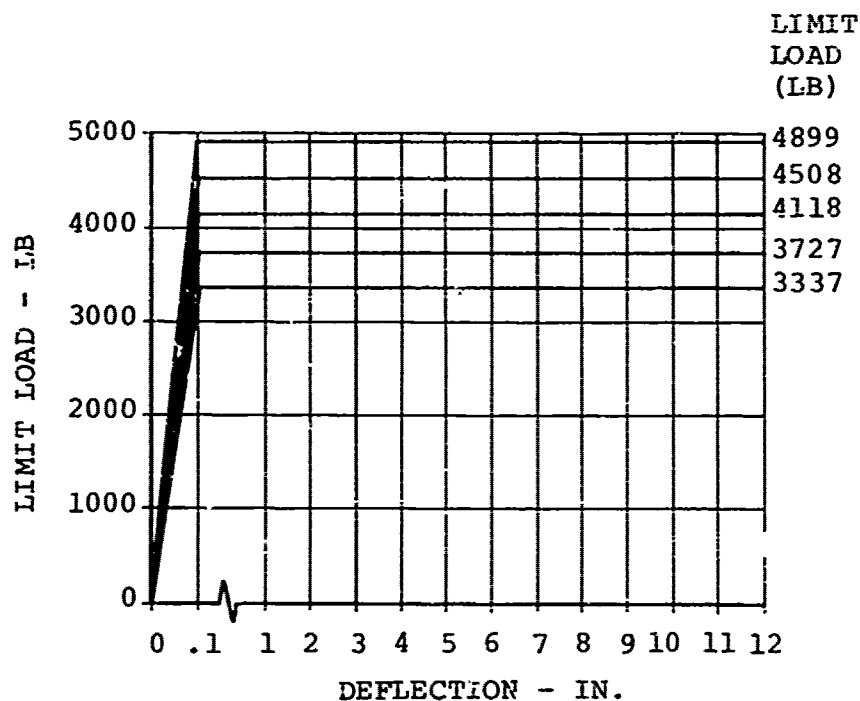
Figure 46. Load Versus Deformation of Seat.

65

The data plotted in Figure 46 were obtained by establishing a
basic seat weight of 28.9 pounds and then increasing it in
increments of 21.7 pounds. The limit load was obtained by
multiplying the summation of the effective occupant weight and
movable portion of the seat by the load factor of 18G. Un-
loading rates again were assumed. The results are given in
Table VI.

TABLE VI. SEAT PROPERTIES					
Effective Occupant Weight (lb)	Movable Seat Weight (lb)	Total Effective Weight (lb)	G_L	Limit Load (lb)	Unloading Rate (lb/in.)
156.5	28.9	185.4	18	3337	16685
156.5	50.6*	207.1	18	3727	18635
156.5	72.3	228.8	18	4118	20590
156.5	94.0	250.5	18	4508	22540
156.5	115.7	272.2	18	4899	24495

*Seat weight of 40.6 pounds was actually used in place of 50.6
pounds by error.

3.3.6 ENVIRONMENT

The input deceleration crash pulses were assumed to be tri-
angular in shape. The most severe pulse was assumed to be the
95th percentile survivable crash pulse as defined in Reference
2. The pulses were then varied in equal velocity increments
while maintaining the peak deceleration of 48G and again at
36G as shown in Figures 47 and 48. The resultant environment
therefore included variations in rate of onset.

3.3.7 RESULTS

Computer values of peak deceleration were plotted as a func-
tion of movable seat weight and as a function of the environ-
mental variations of velocity change and peak input decelera-
tion. Force generated in the spring representing the spinal
column was also plotted as a parameter of interest with re-
spect to spinal column loading and eventual fracture. Cross
plots of some of the data were also prepared to show the
trends of pertinent variables with rate of onset, although it
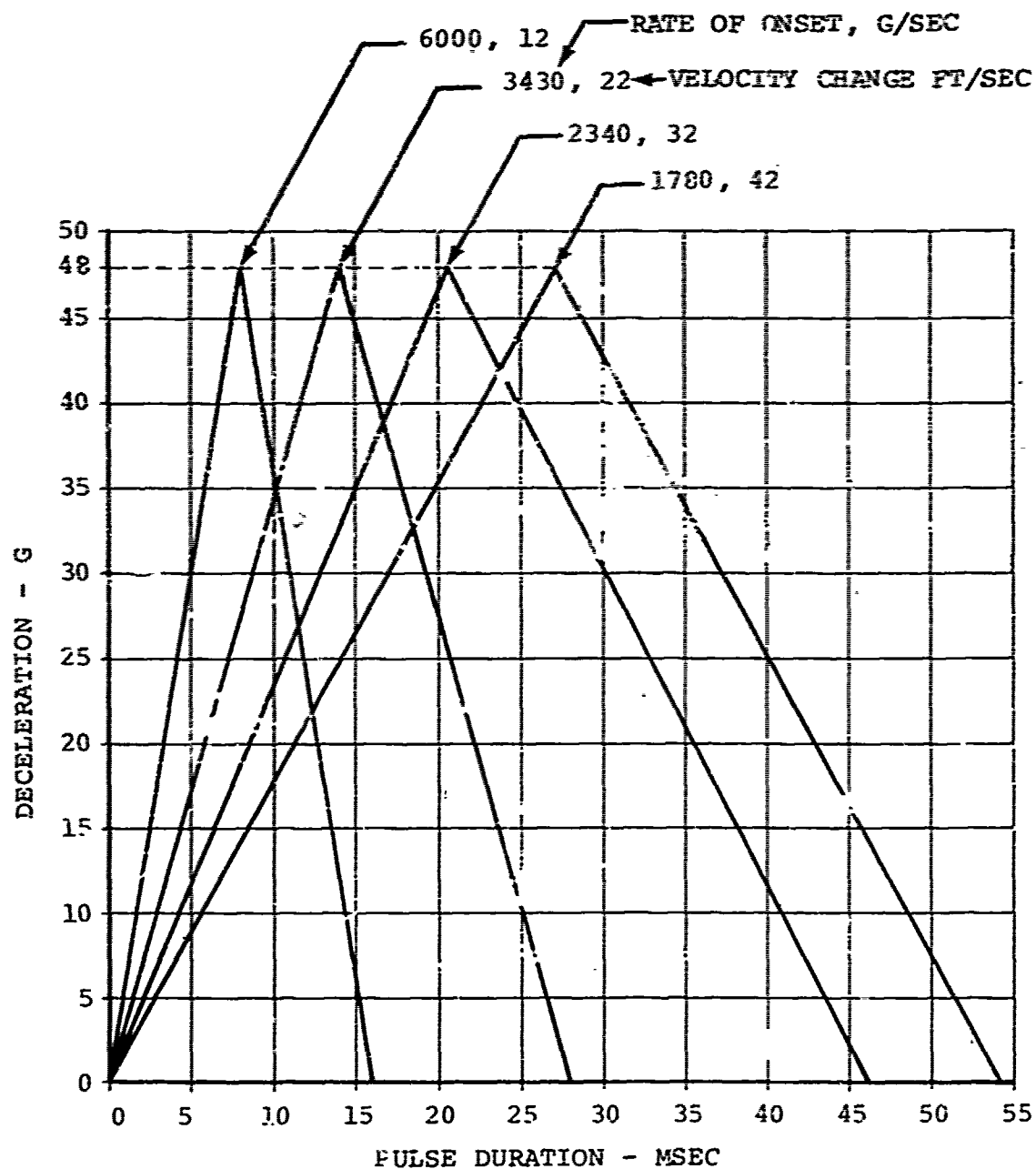
Figure 47. Input Crash Pulses (Peak Deceleration = 48G).

must be remembered that the rate of onset was not an independent variable in this analysis.
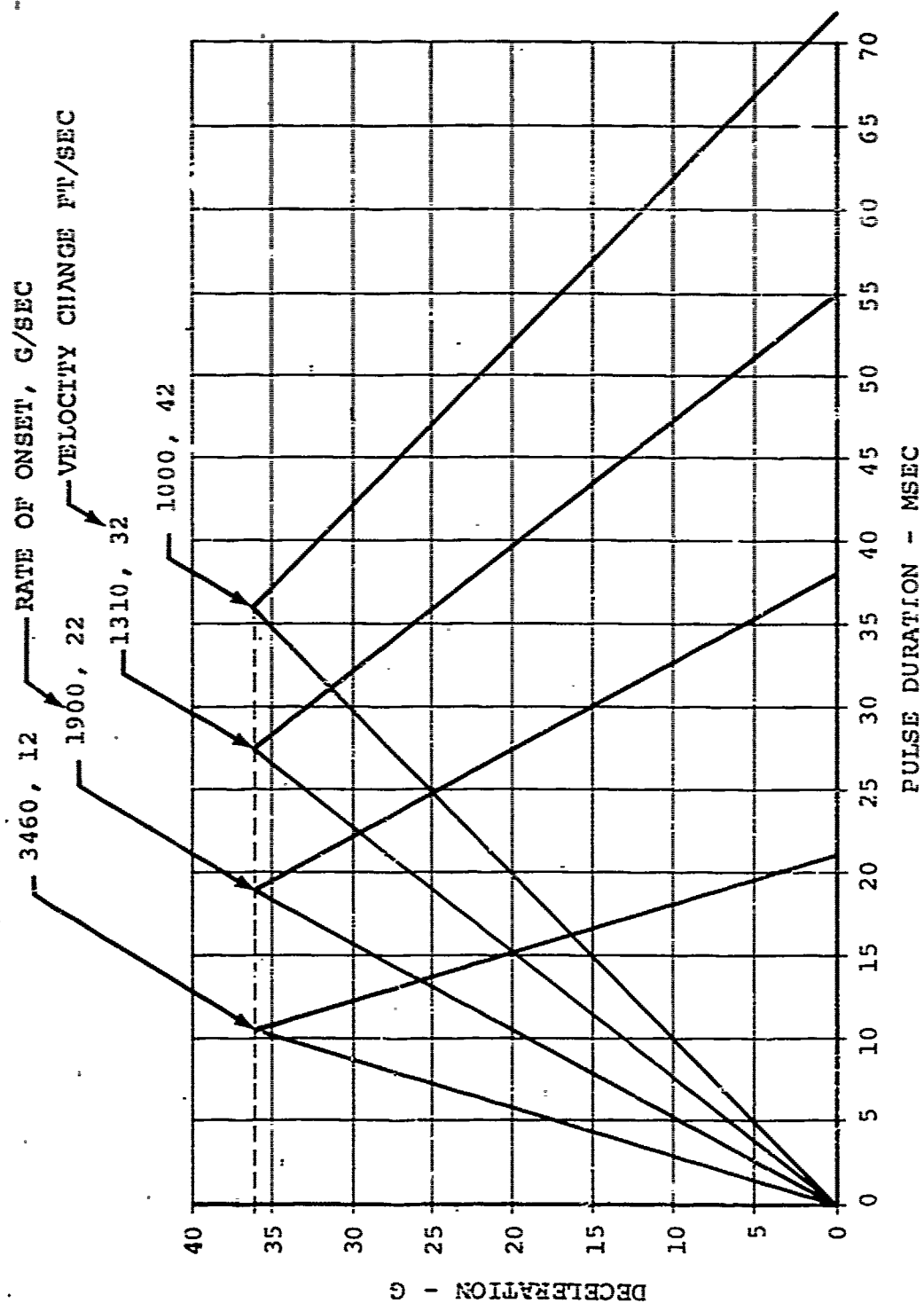
Figure 48. Input Crash Pulses (Peak Deceleration = 36G).

68

3.3.7.1 Input Deceleration of 48G: Figure 49 shows the peak seat deceleration plotted as a function of movable seat weight for the four velocity changes input and a peak input deceleration of 48G (Figure 47). The curves show that the peak deceleration decreases with increased seat weight. They also show a decreased peak deceleration with increased energy content of the crash pulse; however, it must also be remembered that increasing velocity changes are representative of decreased rate of onset.

Figure 50 shows the peak pelvis deceleration as a function of movable seat weight and input velocity change, and a peak input deceleration of 48G. The curves show an increased pelvic deceleration with increased seat weight for all input velocity changes. The increase in pelvic deceleration in going from a 30-pound seat to a 115-pound seat is on the order of 4G.

Figure 51 shows the peak chest deceleration as a function of seat weight and velocity change again for the 48G input pulse. It shows an increase of about 7G as a result of raising movable seat weight from 30 to 115 pounds. It further shows little difference as a function of velocity change between the limits of 22 and 42 ft/sec; however, the lower velocity changes produced the higher chest deceleration values. As in the previous figure, velocity changes on the order of 12 ft/sec produce significantly lower chest deceleration magnitudes than the higher velocities. As a matter of fact, seats weighing on the order of 30 to 50 pounds result in chest deceleration values of around 18G, or that corresponding to the static design limit deceleration.

Figure 52 presents peak chest deceleration as a function of stroke, seat weight, and change in velocity for the 48G input pulse. The curve shows increasing chest deceleration magnitudes as a function of seat weight. The diagonal lines passing through the curves represent the relationship between peak chest deceleration and stroke as a function of seat weight and velocity change. It can be seen that decreased stroke results in increased deceleration magnitudes at a given pulse energy content.

Also included on the curve is a plot of the results of the rigid mass analysis prediction used to perform the analysis in the previous section of the report. The prediction shown was calculated for an input pulse having a peak deceleration of 48G and a velocity change of 42 ft/sec. It therefore corresponds to the curve representing the relationship between deceleration and stroke for the 42 ft/sec velocity change. It can be seen that the peak chest deceleration values as calculated by the dynamic analysis are about double the prediction

Figure 49.   Peak Seat Deceleration Versus Seat Weight and Velocity Change
(Peak Input Deceleration = 48G, Limit Load Factor = 18G).

Figure 50. Peak Pelvis Deceleration Versus Seat Weight and Velocity Change (Peak. Input Deceleration = 48G, Limit Load Factor = 18G).

71

Figure 51. Peak Chest Deceleration Versus Seat Weight and Velocity Change
(Peak Input Deceleration = 48G, Limit Load Factor = 18G).

Figure 52. Peak Chest Deceleration Versus Seat Stroke, Change in Velocity, and Seat Weight (Peak Input Deceleration = 48G, Limit Load Factor = 18G).

of the rigid mass analysis. This is not unexpected, as the rigid mass analysis does not account for the dynamic response of the spring mass system. The average deceleration predicted by the dynamic analysis would more nearly correspond to that of the rigid mass analysis and, consequently, provides an indication of its use limitations.

Figure 53 shows the peak spinal load plotted with respect to movable seat weight and velocity change for a peak input deceleration of 48G. It is apparent that the load in the spinal column follows the chest deceleration trend as would be expected. This curve is of primary eventual interest as the load in the spinal column is the ultimate measure of injury probability. At this time, correlations have not been made between the spinal load prediction of the analysis technique and actual spinal strength. Of course, the strength of the spine varies from top to bottom or as a function of the particular vertebra; however, correlation could be made between the strength of those vertebrae which most frequently fracture and the spinal load prediction. Correlations could also be made between input pulse computed load in the spine, and actual injuries much as one today using the DRI. An analysis of this nature is recommended for future effort.

Figure 54 shows the peak spinal load as a function of rate of onset, velocity change, and seat weight for an input deceleration pulse with a peak of 48G. The curve shows that the spinal load increases with increased movable seat weight, and that it decreases with decreased velocity change. It also shows that the spinal load increases with increased rate of onset for the heavier seats until the effect of reduced energy content of the pulse becomes dominant, resulting in the overall decrease with decreased velocity change.

3.3.7.2 **Input Deceleration of 36G:** Figure 55 shows a plot of peak seat deceleration versus seat weight and velocity change. As was true for the 48G pulses, the peak seat deceleration plots are not continuous and the higher deceleration values occurred during the lowest velocity change pulses. Again, the highest velocity change (42 ft/sec) produced a continuous curve, reducing from around 44G for the lighter seat weight to around 29G for the 115-pound seat.

Figure 56 shows the peak pelvic deceleration as a function of seat weight and velocity change for a peak input deceleration of 36G. This curve shows that the pelvic deceleration increases approximately 2 to 4G with an increase in seat weight from 30 to 115 pounds. Again, except for the lowest velocity input pulse, peak pelvic deceleration magnitude varies inversely with velocity change.

74
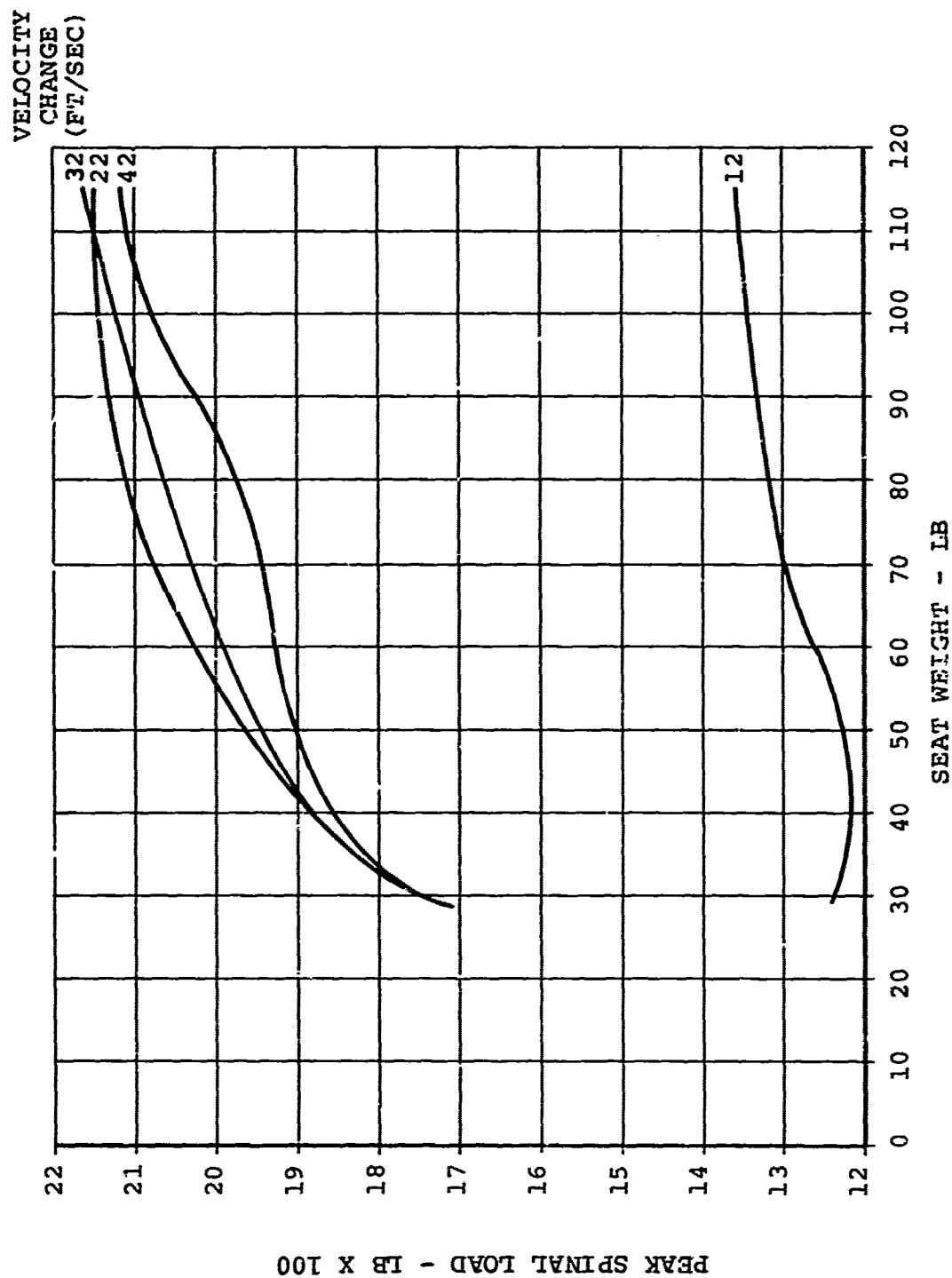
Figure 53. Peak Spinal Load Versus Seat Weight and Velocity Change (Peak Input Deceleration = 48G, Limit Load Factor = 18G).
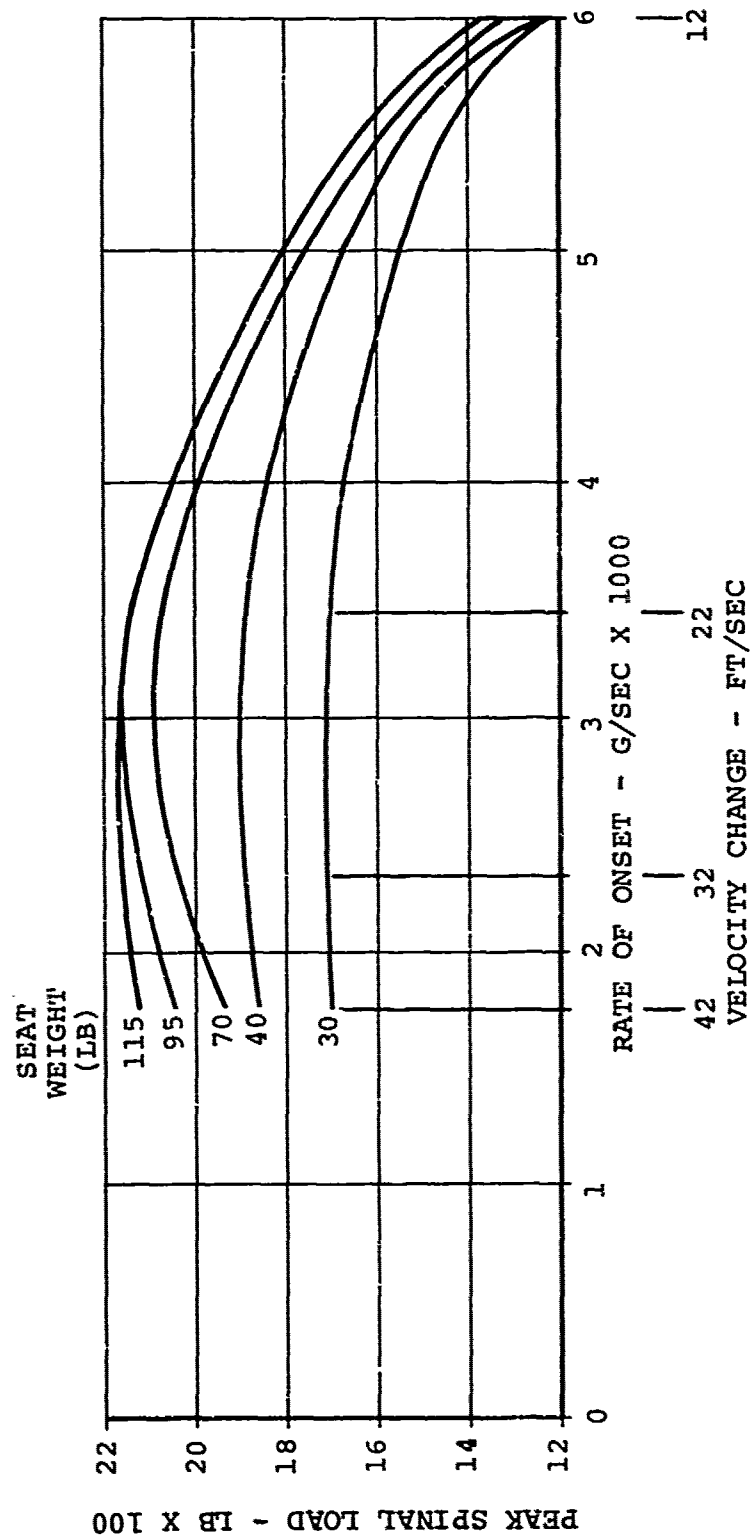
Figure 54. Spinal Load Versus Rate of Onset, Seat Weight, and Velocity Change (Peak Input Deceleration = 48G, Limit Load Factor = 18G).
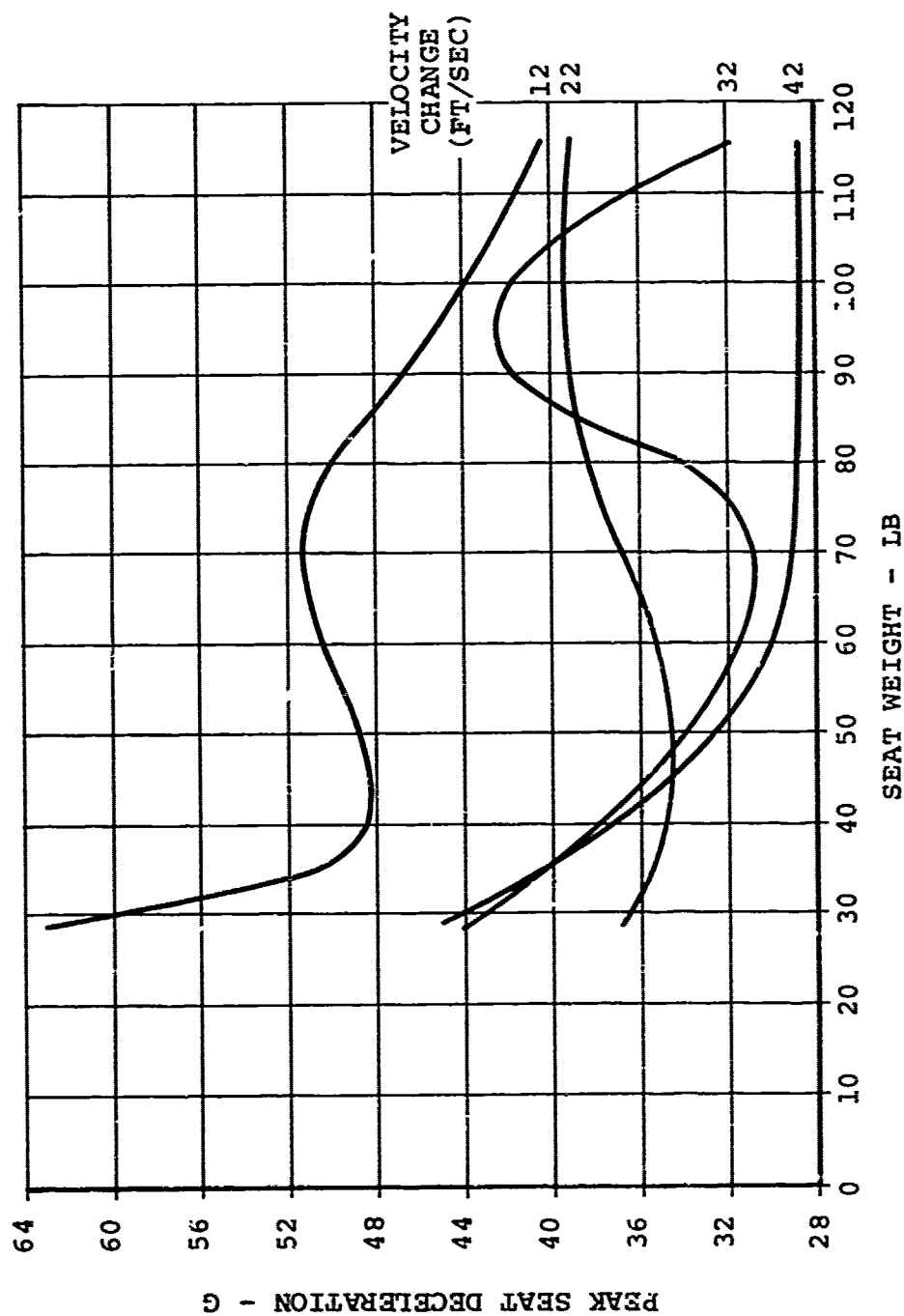
Figure 55.   Peak Seat Deceleration Versus Seat Weight and Velocity Change
(Peak Input Deceleration = 36G, Limit Load Factor = 18G).

77
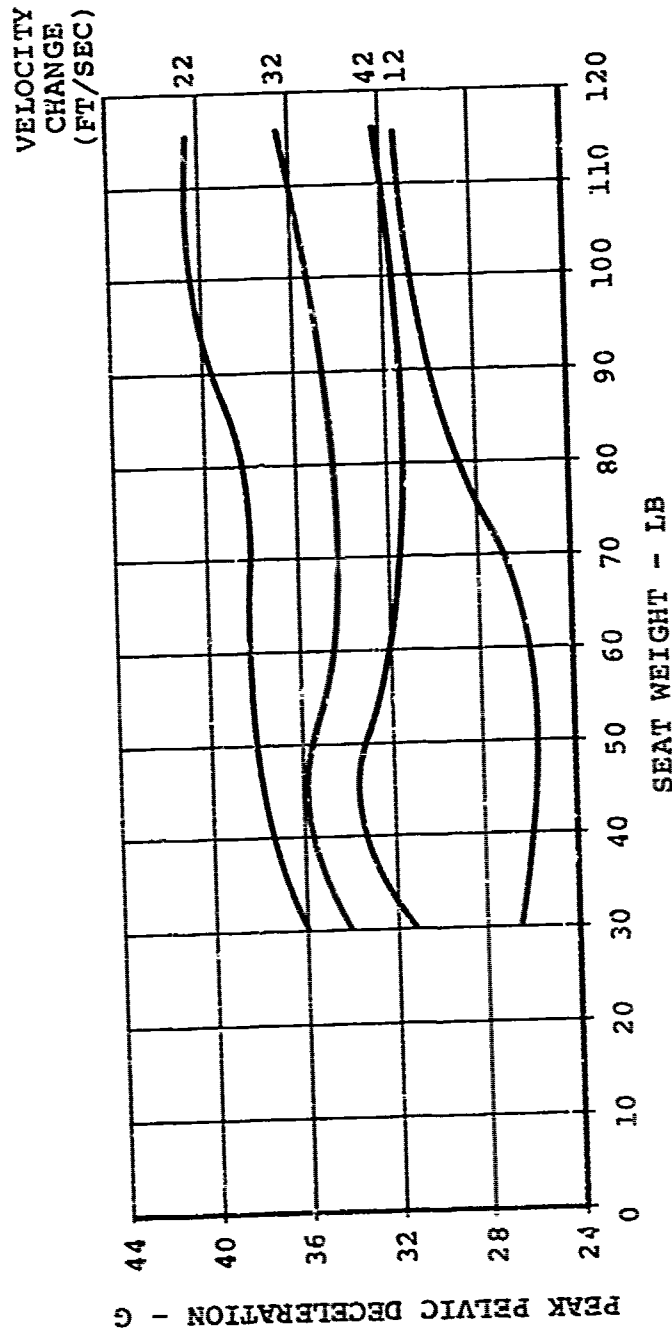
Figure 56. Peak Pelvic Deceleration Versus Seat Weight and Velocity Change (Peak Input Deceleration = 36G, Limit Load Factor = 18G).

78

Figure 57 shows peak chest deceleration as a function of movable seat weight and velocity change for a peak input deceleration of 36G. Again, the curves are similar to those predicted for the 48G pulses and show about a 4 to 6G increase for the chest when the seat weight increases from 30 to 115 pounds.

Figure 58 shows the peak chest deceleration as a function of stroke, seat weight, and velocity change for a peak input deceleration of 36G. This curve shows essentially the same trends as the similar curve for 48G. It shows that peak chest deceleration increases with increased seat weight and decreased stroke.

3.3.8 GENERAL COMMENTS

This analysis indicated that increased peak G loading could be expected on the various body components with increased seat weight. It also indicated that a stroking distance of approximately 12 inches would be required to maintain the peak deceleration of the various members of the body within the human tolerance regime. Another observation can be extracted from the analysis - the crash pulses of lesser magnitude can provide more severe loading on the occupant than more severe crash pulses.

The analysis indicated that: (1) a systems study should be made to arrive at the percentile crash pulse for which protection could be provided within a maximum, reasonable stroke length and (2) an analysis should be made to establish the limit load at which the energy-absorbing mechanisms within the seat should be set to provide the maximum degree of protection within the prescribed minimum stroke and for the crash pulse established as the survivable limit for the integral armored crew seat. These two studies were conducted and are described in the following discussion.

3.4 DYNAMIC RESPONSE AS A FUNCTION OF PERCENTILE CRASH PULSE AND LIMIT LOAD

3.4.1 PURPOSE OF ANALYSIS

The primary purpose of this analysis was to analytically establish the percentile crash pulse for which protection could be provided to the occupant of an integrally armored crew seat. In addition, the analysis was conducted to determine the energy-absorber limit load required to provide the degree of protection necessary within the minimum realistic stroke length, chosen as 12 inches. Secondary objectives were to provide a comparison between two different kinds of load
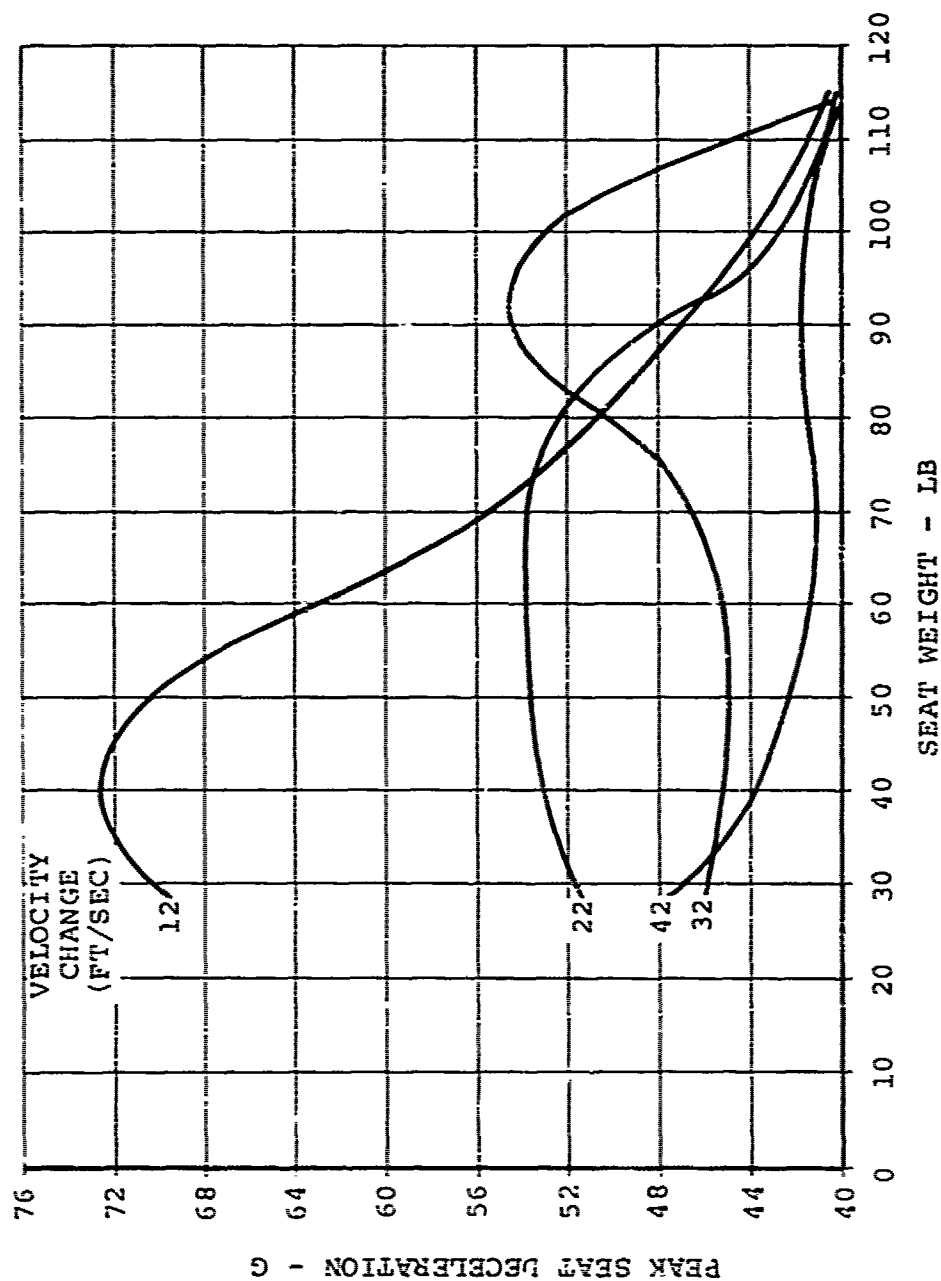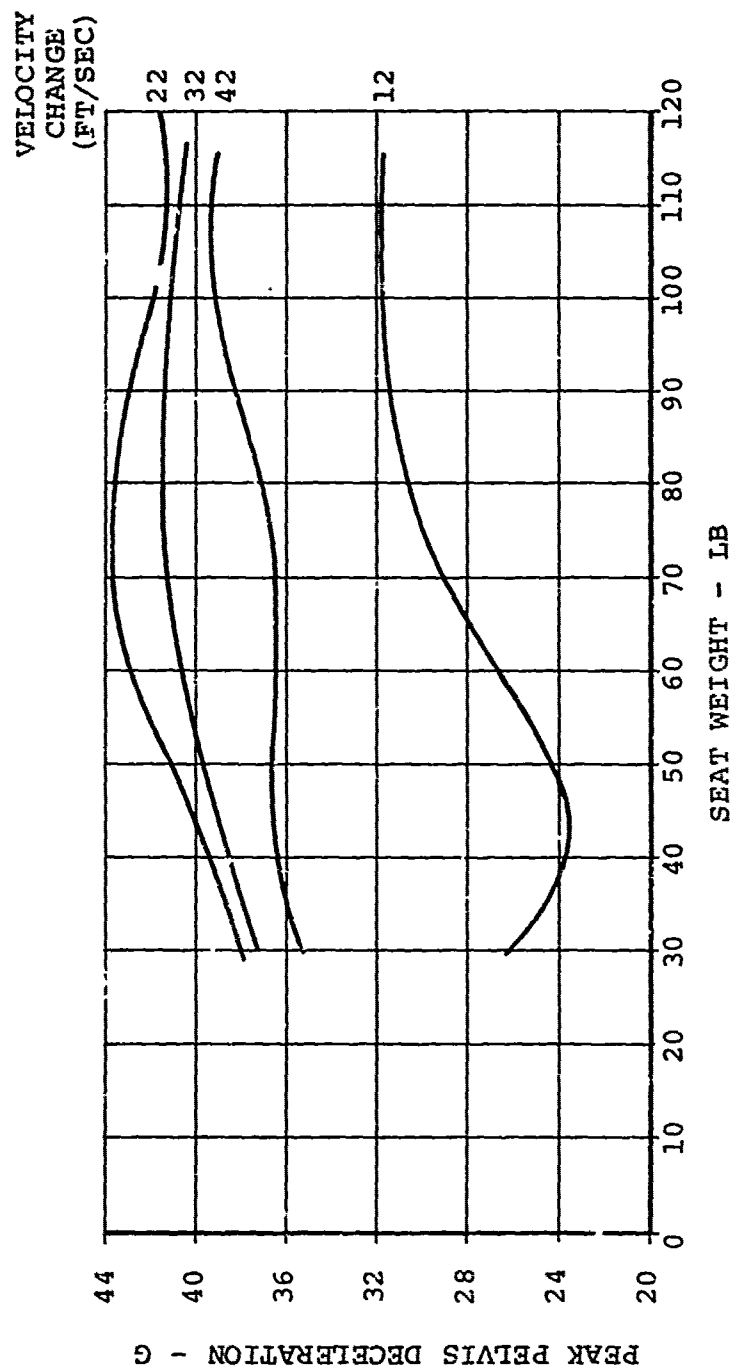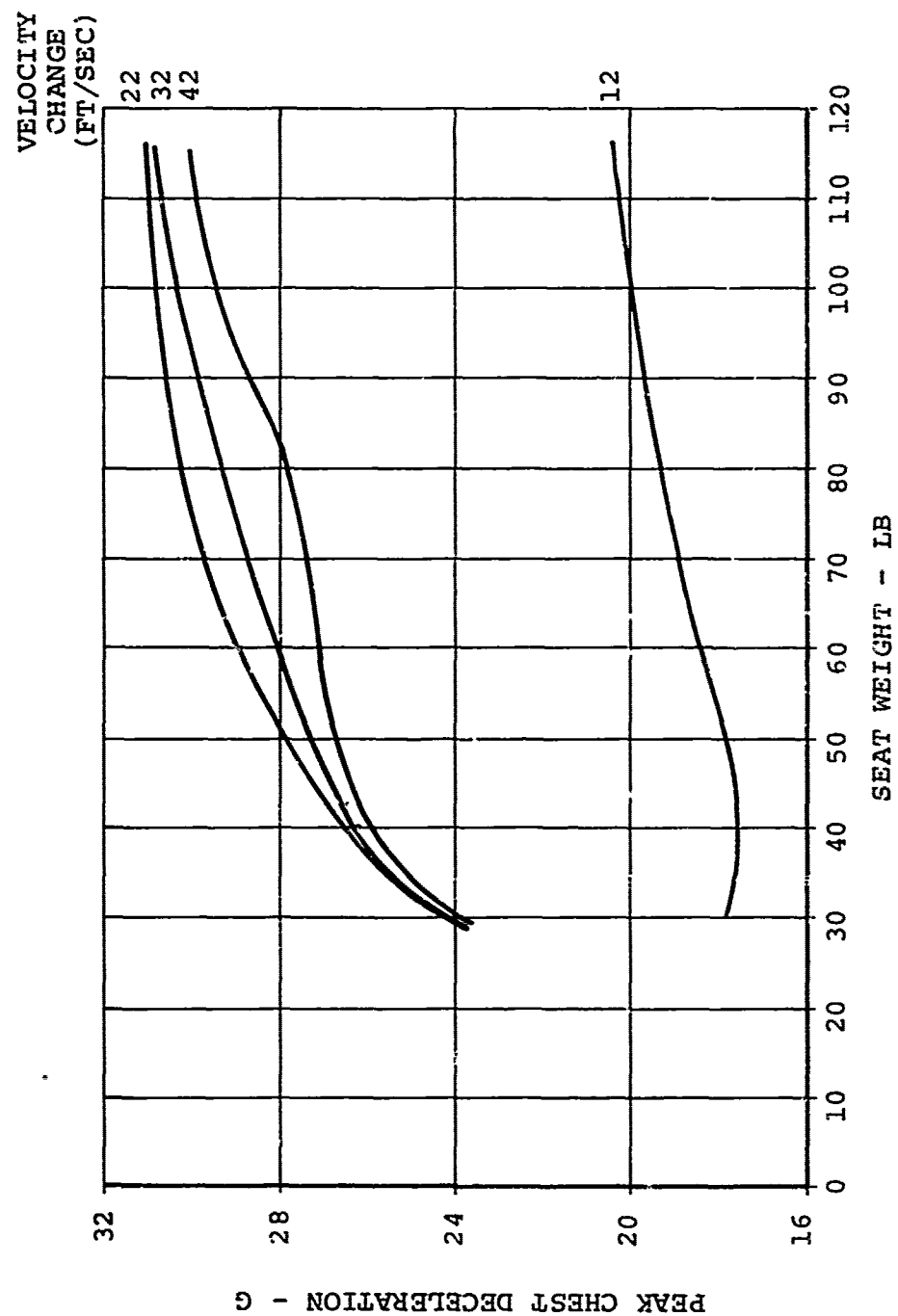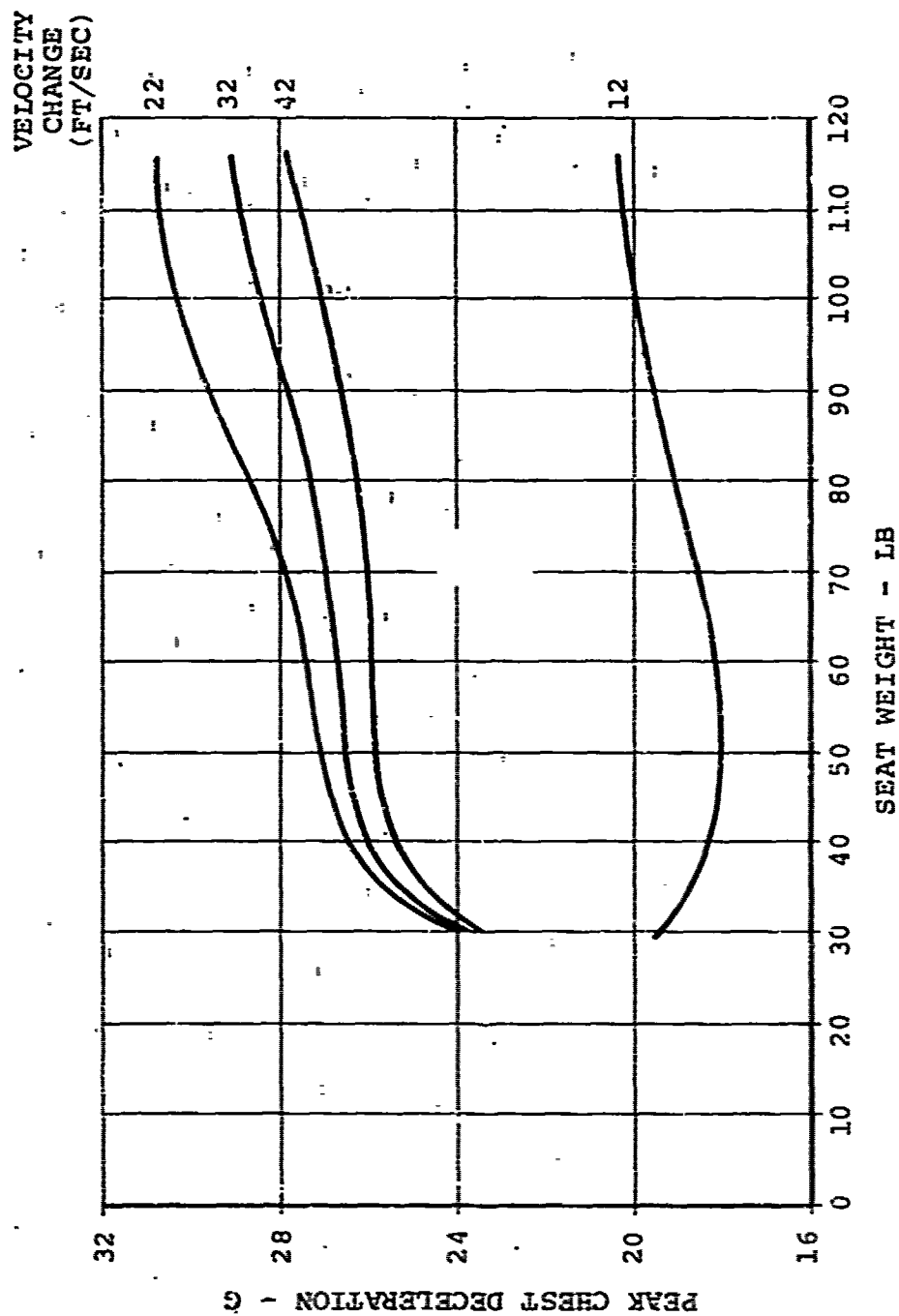
Figure 57. Peak Chest Deceleration Versus Seat Weight and Velocity Change (Peak Input Deceleration = 36G, Limit Load Factor = 18G).
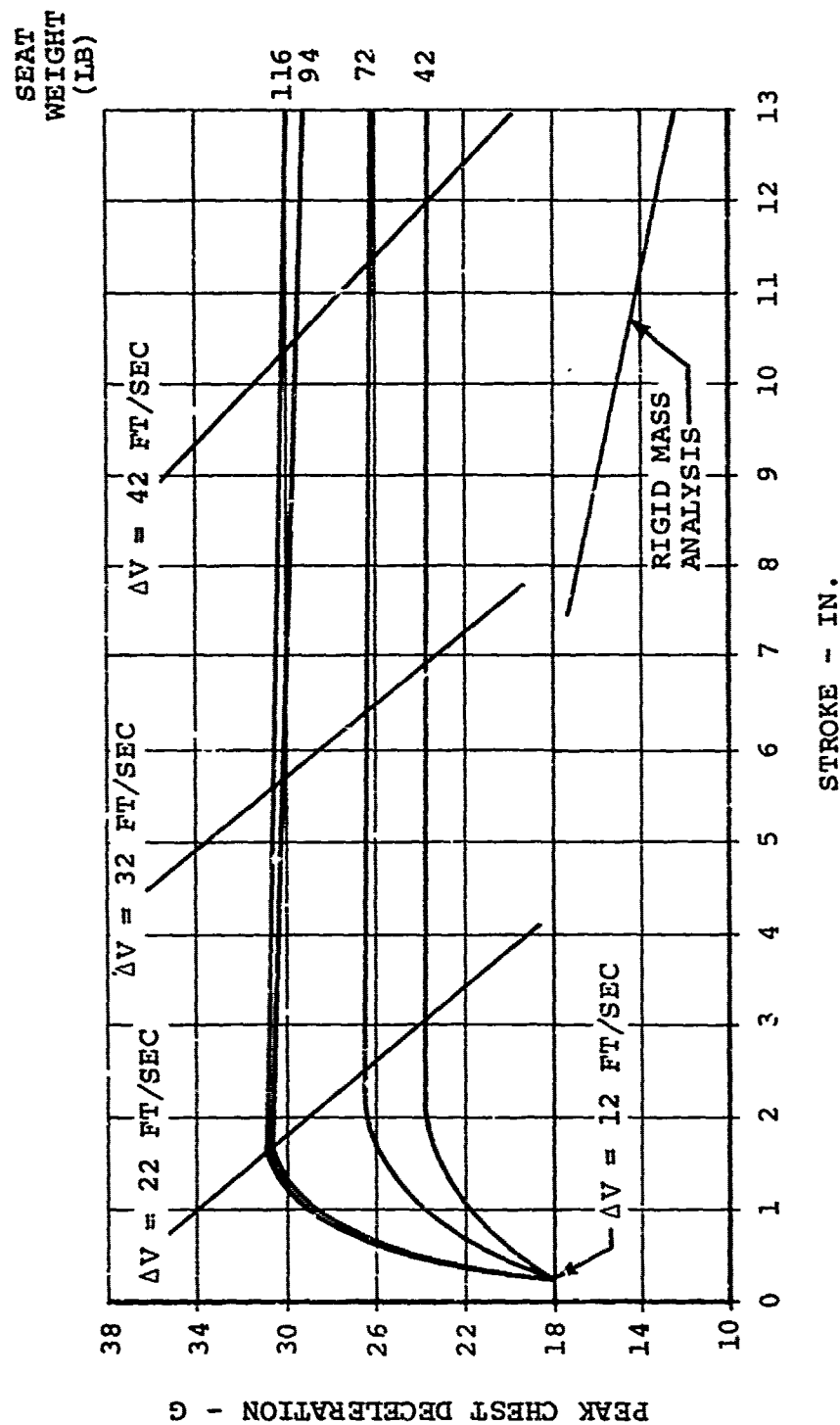
80
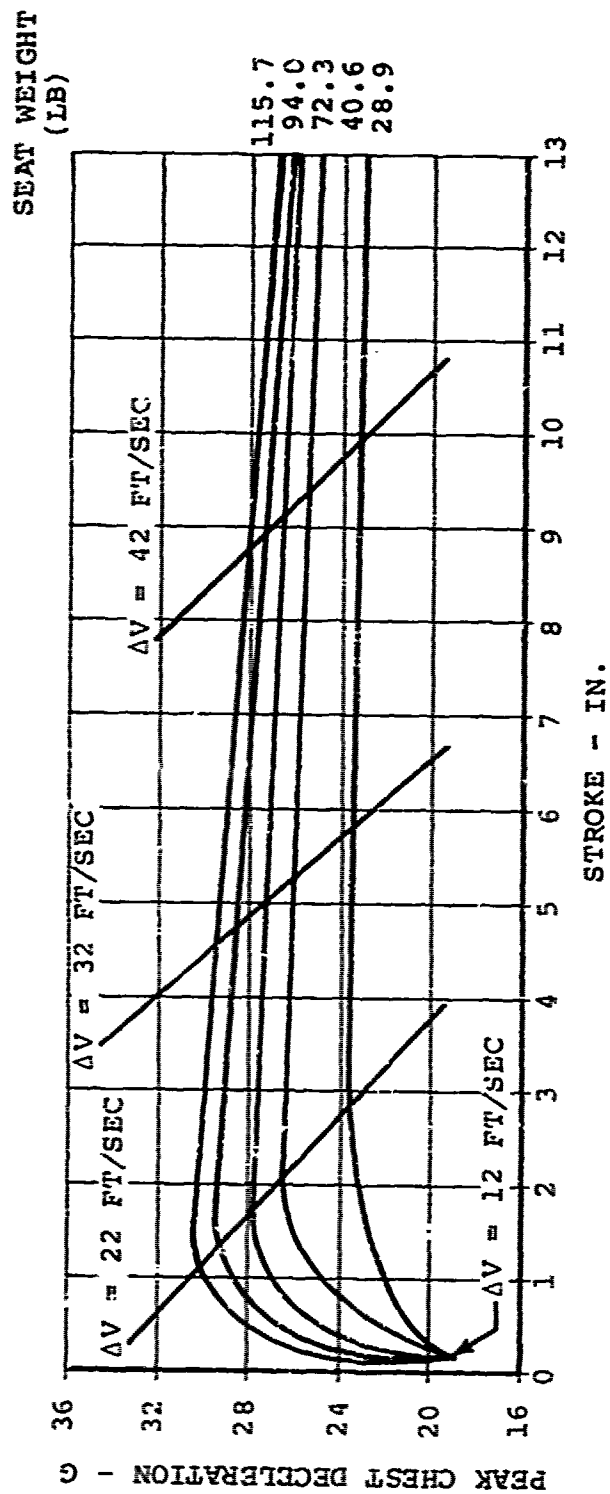
Figure 58. Peak Chest Deceleration Versus Seat Stroke, Change in Velocity, and Seat Weight (Peak Input Deceleration = 36G, Limit Load Factor = 18G).

81

limiters -- the type that produces a trapezoidal pulse shape
such as a crushable honeycomb material, and a type that pro-
duces a curvilinear characteristic such as a stainless steel
tube work-hardening during tensile elongation -- and to make a
dynamic check on the tri-level energy absorber technique for
reducing the influence of occupant weight on deceleration.

3.4.2 FIVE-DEGREE-OF-FREEDOM DYNAMIC ANALYSIS TECHNIQUE

The same five-degree-of-freedom model summarized in the pre-
ceding section was used for this analysis. Input properties
such as percentile crash pulse in terms of velocity change and
peak input deceleration were varied as well as the load-limiter
force versus deformation characteristics. The results were
cross plotted to obtain the final desired results.

3.4.3 OCCUPANT PROPERTIES

The analysis was again conducted for the 95th percentile Army
aviator. Basic body properties used for this analysis were
taken from Reference 14 and adjusted only for clothes. The
properties are given in Table VII.

TABLE VII. OCCUPANT NUDE BODY PROPERTIES			
Portion of Body	Weight (lb)	Spring Constant (lb/in.)	Damping Coefficient (lb/sec/in.)
Pelvis	73.9	2685	13.5
Chest	53.8	347	4.1
Head	19.8*	523	2.8
*Includes Helmet			

Since one of the objectives of this analysis was to determine
the limit-load setting for the energy absorber, various effec-
tive occupant weights were determined and summed with the
weight of the movable portion of the seat. These weights were
then used to develop the specific limit loads for which the
analysis was made.

Observation of dynamic tests indicated that the response of
the arms was usually greatly out of phase with the remaining
portion of the occupant. Consequently, they were probably of
minor influence on seat response during the primary impact.

82

As a result, the weight of the lower arms was omitted from the effective weight calculations for the seat occupant. Various weight combinations were selected to provide a range of limit loads for analyses. These were computed and are tabulated below:

Base	Weight (lb)
95th percentile clothed and with helmet	147.8
5th percentile clothed and with helmet	101.5
95th percentile pelvis and upper thighs only, clothed	74.0

3.4.4 CUSHION PROPERTIES

The cushion was assumed to be fabricat d from two layers of material: 1 inch of polyurethane over 1/4 inch of polyvinyl chloride (recommended as the optimum passive cushion in Reference 24). The load versus deformation data presented in Figure 59 was measured using an indenter that simulated a human buttocks and was therefore usable with no modification. The unloading rates were again assumed. The data used are given in Table VIII.

3.4.5 SEAT PROPERTIES

Two separate limit-load versus deformation curve shapes were chosen for analysis. One was the trapezoidal shape for which the load increases linearly with elastic deformation until the member or system yields. The load-limiting system then deforms with a constant load until the available energy is absorbed as shown below:
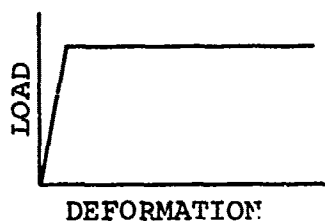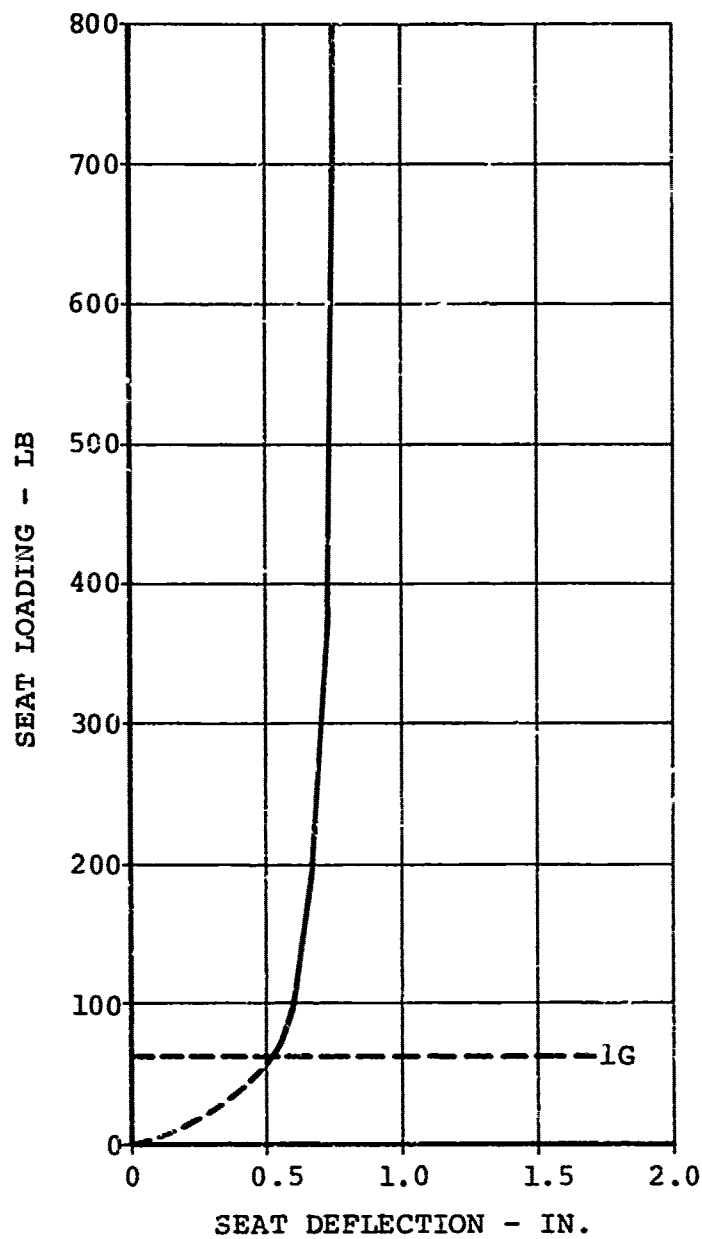
DEFORMATION

Figure 59.   Load Deflection for 1/4 Inch of Ensolite
Covered by 1.6 Lb/Ft^3 Polyurethane Foam
(Taken from Reference 24).

TABLE VIII. CUSHION PROPERTIES		
Load (lb)	Deformation (in.)	Unloading Rate (lb/in.)
0	0	
25	.40	63
93	.63	296
380	.73	2,870
10,000	.78	19,240

The other shape chosen was one in which the load increases linearly with elastic deformation to the yield point. The load then continues to rise in a curvilinear shape as the member plastically deforms as shown below:
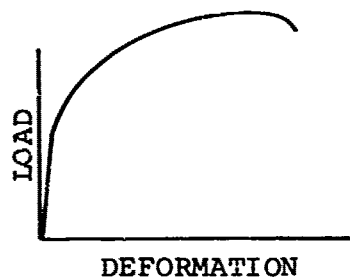
The first type is typical of crushable honeycomb material, or any member designed to deform under constant load once its yield load is exceeded. The second is typical of a ductile material such as annealed stainless steel that work-hardens as it is plastically deformed.

Limit loads were determined for the energy-absorbing portion of the seat by summing the weight of the movable portion of the seat and the effective weight of the occupant, and then multiplying the summation by the limit load factor of 18G as shown in Table IX.

Effective Weight of Occupant (lb)	Movable Weight of Seat (lb)	Total Effective Weight (lb)	G_L	L_L (lb)
147.8	151.2	299	18	5382
101.5	151.2	253	18	4554
74.0	151.2	225	18	4050

TABLE IX. SEAT PROPERTIES

It was assumed that the elastic deflection of the trapezoidal shaped curve reached 0.10 inch. The curves described by the lower limit loads were assumed to follow the same elastic curve to the yield point. The limit load versus deformation curves used in the analysis of the trapezoidal curve system are shown in Figure 60.
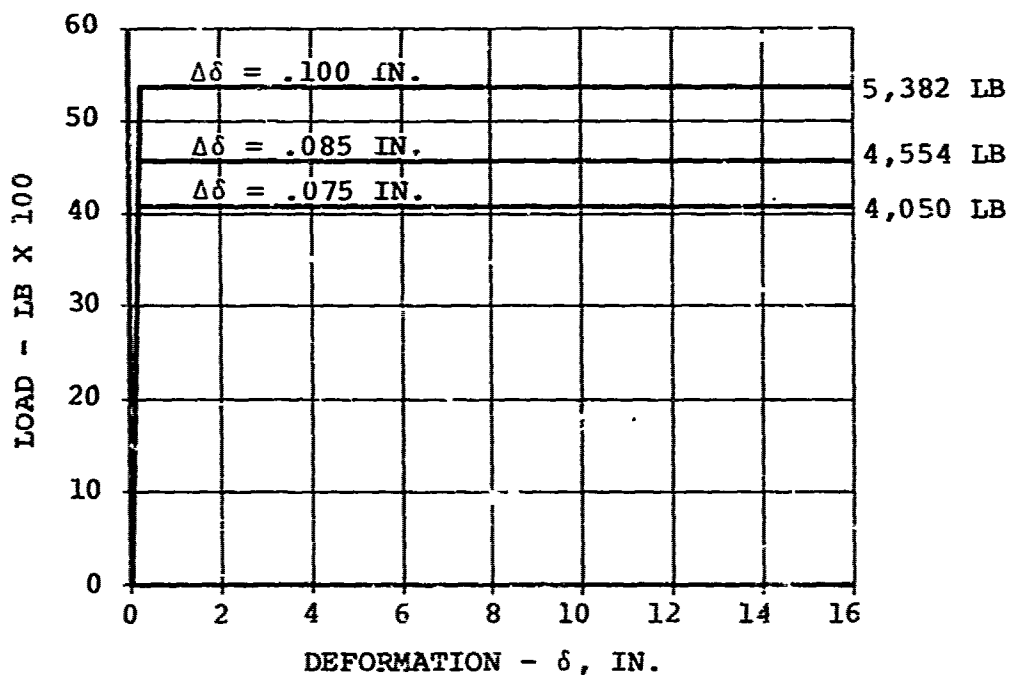
Figure 60. Load Versus Deformation, Trapezoidal Curve Shape.

The curvilinear load versus deformation curves were determined
with test data measured from prior testing of stainless steel
tensile tubes.[25] Observation of the load versus deformation
curves presented in this document revealed that the curves
could be approximated by three straight lines defined in terms
of percentage of ultimate load and percentage of ultimate elon-
gation. Since the minimum stroke had been chosen as 12 inches,
elongation was expressed in inches rather than percent. Defi-
nition of the curve was as shown in Figure 61.
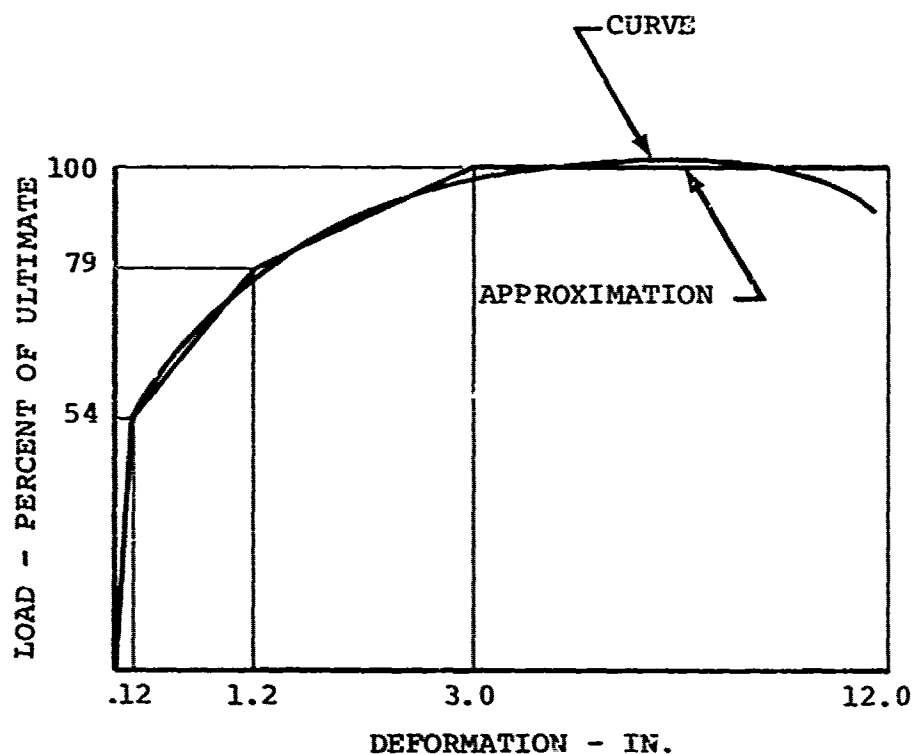
Figure 61.   General Load Versus Deformation,
             Curvilinear Curve Shape.

Two of the three different limit load curves were then deter-
mined by simply multiplying the desired ultimate loads by the
percentages shown in Figure 61; however, one curve was derived
to contain the same energy as its comparable trapezoidal curve
for the indicated 12-inch strokes. This was accomplished by
writing the equations for the energy under the two geometri-
cally different curves, setting them equal, and solving for

87

the ultimate load required for the curvilinear curve as shown
below.
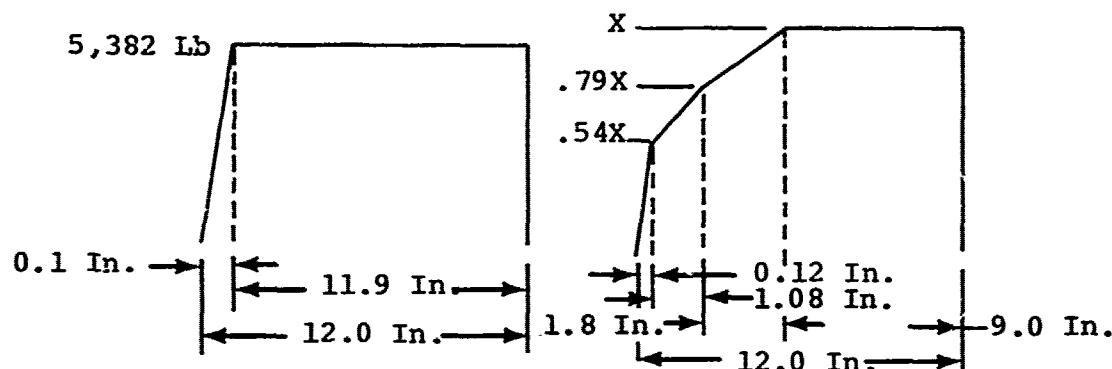
The energy contained in the systems is the area under the
curves. Therefore, $A_T = A_C$, where A_T is the area under the
trapezoidal curves and A_C is the area under the curvilinear
curve.

Then,

$$A_T = \frac{(5382)\ (.1)}{2} + (5382)(11.9) = 64,315 \text{ inch-pounds} \tag{8}$$

$$A_C = \frac{(.54X)\ (.12)}{2} + (\frac{.54X + 79X}{2})\ (1.08) +$$

$$(\frac{.79X + X}{2})\ (1.8) + 9X = 64,315 \text{ inch-pounds} \tag{9}$$

Solving for X, X = 5,661 pounds.

The resultant seat load versus deformation characteristics
were then computed and are shown in Table X.

The unloading slopes were presumed to be constant at 60,000
lb/in.

3.4.6 ENVIRONMENT

Four different crash pulses were defined for analyses. Curves
of velocity change and average deceleration imposed in surviv-
able crashes of today's aircraft contained in Chapter 1 of the

TABLE X. LOAD VERSUS DEFORMATION CHARACTERISTICS OF SEATS

Curve Shape	Load (lb)	Deformation (in.)	Load (lb)	Deformation (in.)	Load (lb)	Deformation (in.)	Load (lb)	Deformation (in.)
Trapezoidal	5382	0.100	5382	-	5382	-	5382	12.0
Trapezoidal	4554	0.085	4554	-	4554	-	4554	12.0
Trapezoidal	4050	0.075	4050	-	4050	-	4050	12.0
Curvilinear	3057	0.120	4472	1.20	5661	3.00	5661	12.0
Curvilinear	2906	0.120	4252	1.20	5382	3.00	5382	12.0
Curvilinear	2459	0.120	3598	1.20	4554	3.00	4554	12.0

Crash Survival Design Guide[2] were used. Since the pulses were assumed to be triangular in shape, peak G values were obtained by multiplying average values by 2. Time duration of the pulses was calculated from

$$T = \frac{(2)\ (\Delta V)}{g\ G_p}$$

(10)

where T = duration, sec

         ΔV = velocity change in major impact, ft/sec

         g = acceleration due to gravity, ft/sec^2

         G_p = maximum deceleration felt at floor level of aircraft, G

The pulses chosen for analysis were defined as shown in Table XI.

TABLE XI. CRASH PULSES			
Percentile Accident	Peak G (G)	ΔV (ft/sec)	T (sec)
85	24	33.5	0.087
90	30	36.0	0.075
92	34	38.0	0.069
95	48	42.0	0.054

3.4.7 RESULTS

3.4.7.1 Limit Load and Percentile Accident: The matrix of cases was run, and the data were then plotted for use in determining the percentile crash pulse for which protection could be provided to the occupant of an integral armored crew seat for both the trapezoidal and the curvilinear limit versus deformation shaped curves, and the limit load which the energy absorber should be designed to provide.

Figures 62, 63, and 64 show peak deceleration versus energy-absorbing system stroke as a function of percentile accidents for the chest and the pelvis of the seat occupant and the movable section of the seat for the trapezoidal-shaped load

90
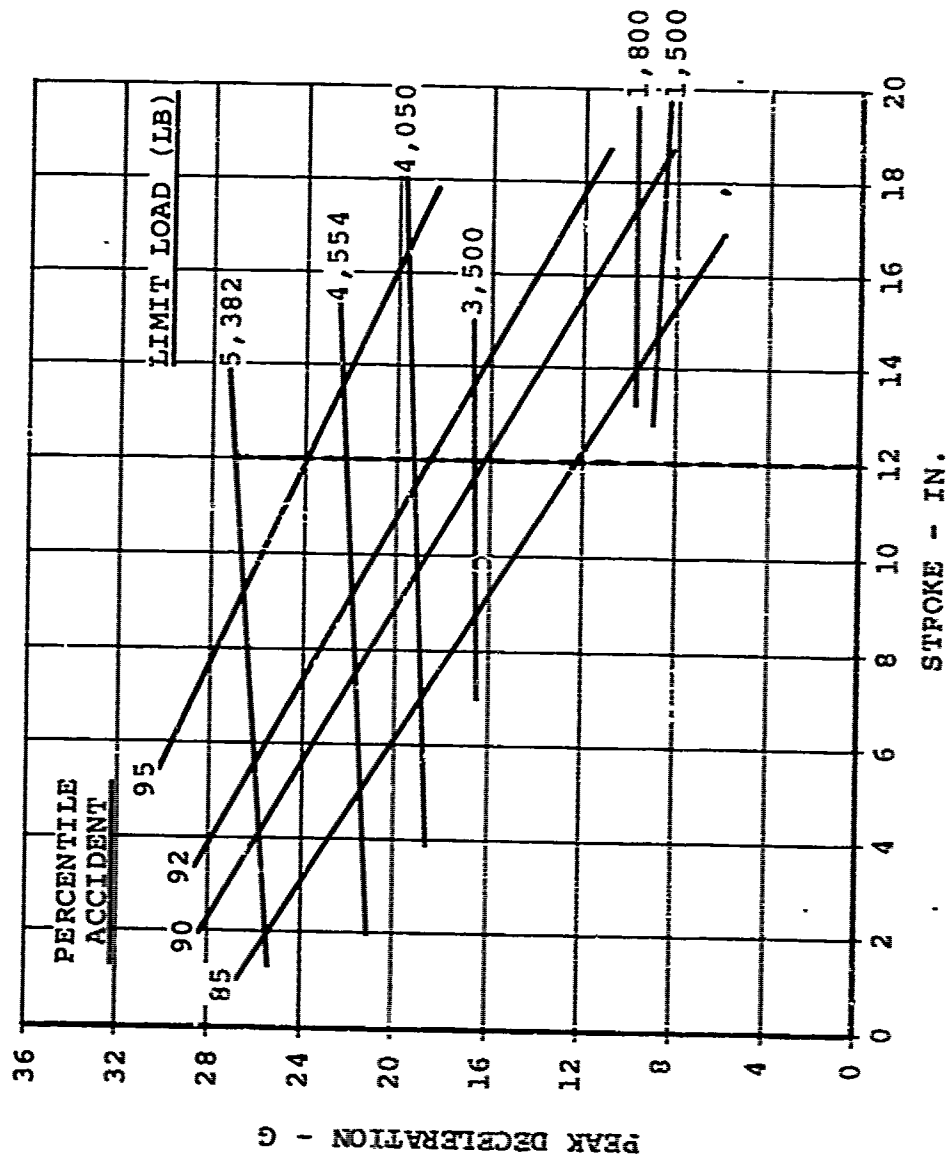
Figure 62. Peak Chest Deceleration Versus Stroke (Trapezoidal-Shaped Limit Load Versus Deformation Curve).

91
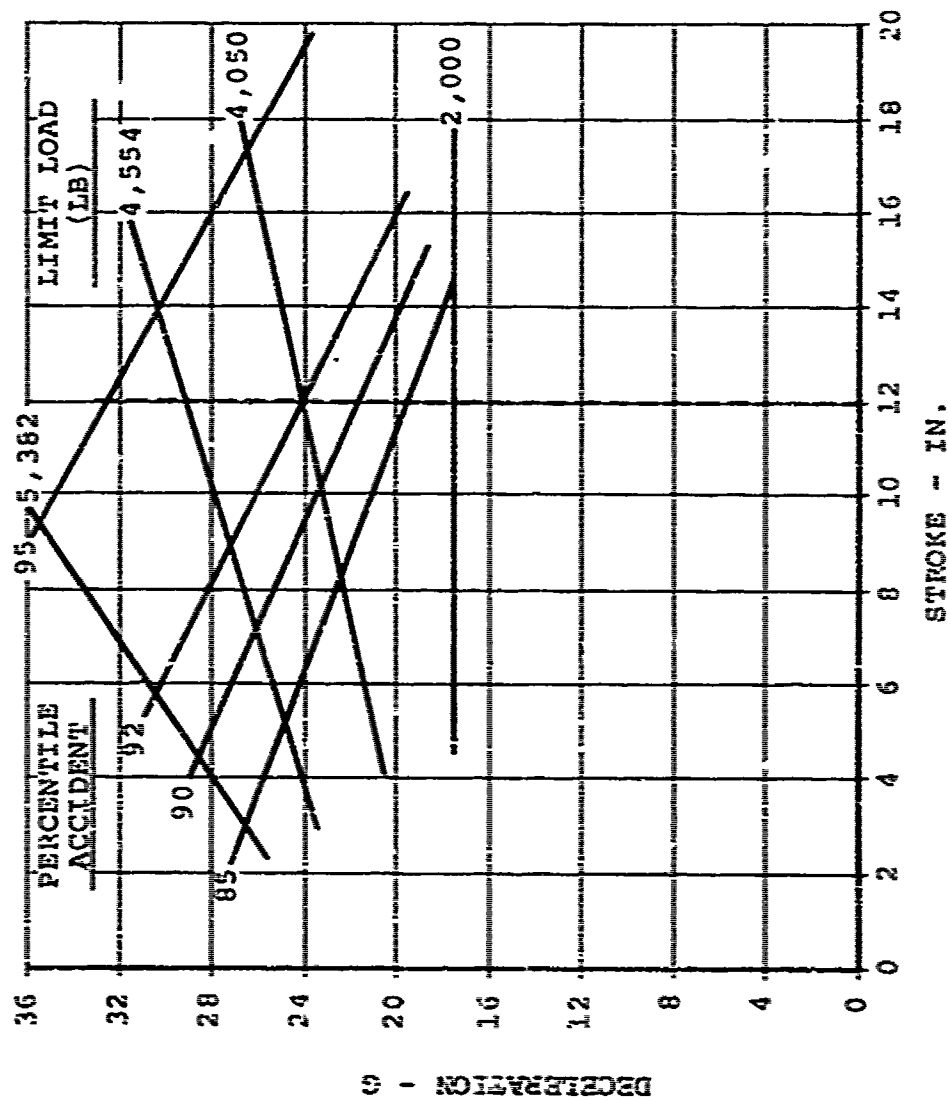
Figure 63. Peak Pelvis Deceleration Versus Stroke (Trapezoidal-Shaped Limit Load Versus Deformation Curve).

92
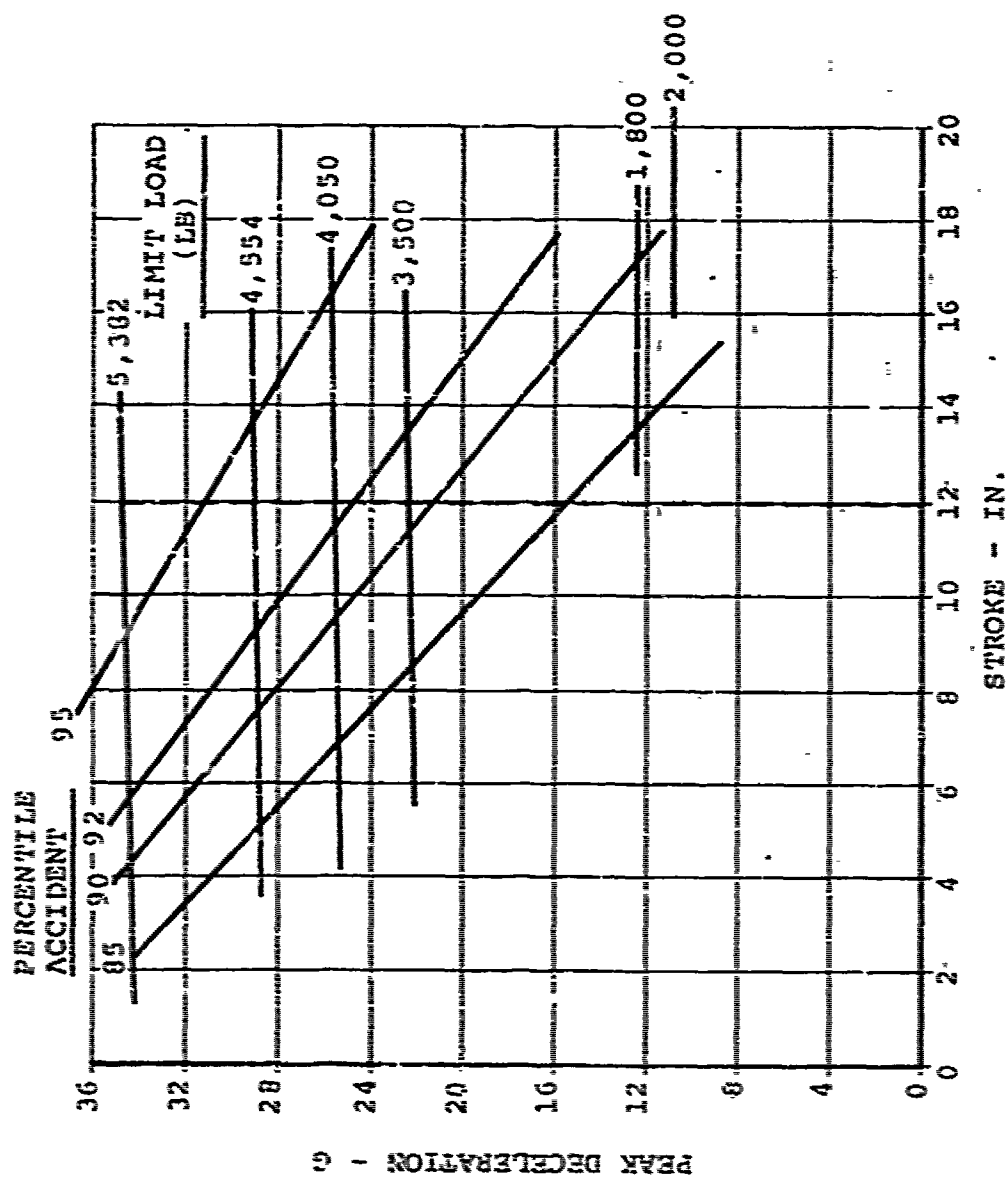
Figure 64. Peak Seat Deceleration Versus Stroke (Trapezoidal-Shaped Limit-Load Versus Deformation Curve).

93.

versus deformation curve. Cross plots of limit loads are
superimposed on the curves. The dotted line extended through
the curves at a stroke length of 12 inches defines both prop-
erties of interest, as a 12-inch stroke was established as the
maximum practical seat stroke for analysis.

Figures 65, 66, and 67 show peak deceleration of the chest,
pelvic, and seat as a function of limit load and percentile
crash pulse for the trapezoidal-shaped load versus deformation
curve. It can be seen from these curves that peak decelera-
tion of the seat and chest are very strong functions of limit
load and relatively insensitive to percentile crash pulse. It
can be seen in Figure 66, however, that the deceleration of
the pelvis, although being a strong function of limit load, is
a stronger function of percentile crash pulse. This is par-
tially a result of interaction with the heavy integral armored
bucket and simply shows considerable data dispersion.

Figures 68, 69, and 70 show peak deceleration plotted as a
function of energy absorber stroke and percentile crash pulse
for the curvilinear-shaped limit load versus deformation
curve. Again, limit load was superimposed on the curves.

Figures 71, 72, and 73 show peak chest, pelvic, and seat de-
celeration as a function of limit load. These curves show
that, although the chest is relatively insensitive to percen-
tile crash pulse, both the pelvis and the seat are stronger
functions for the curvilinear-shaped curve than for the trape-
zoidal.

A summary of the data presented in the previous curves is
shown in Table XII. Peak chest, pelvic, and seat decelera-
tions are tabulated as a function of percentile accident for
both the trapezoidal and the curvilinear-shaped limit load
versus deformation curves. Also shown is a summary of the
limit loads extrapolated from the curves at the intersection
of the percentile crash pulse with 12 inches of stroke.
Figures 74 and 75 graphically portray the data tabulated in
Table XII. Figure 74 shows the peak deceleration for the
pelvis, seat, and chest as a function of percentile accident
for the trapezoidal-shaped load versus deformation curve.
Figure 75 shows the same data for the curvilinear-shaped
curve.

Since this analysis was made with a 95th percentile occupant,
a limit load factor of 18G was selected for use as the param-
eter against which choice of a percentile accident would be
selected. In other words, the percentile accident for which
protection could be provided for a 95th percentile occupant
would be indicated by the intersection of the pelvis, seat,
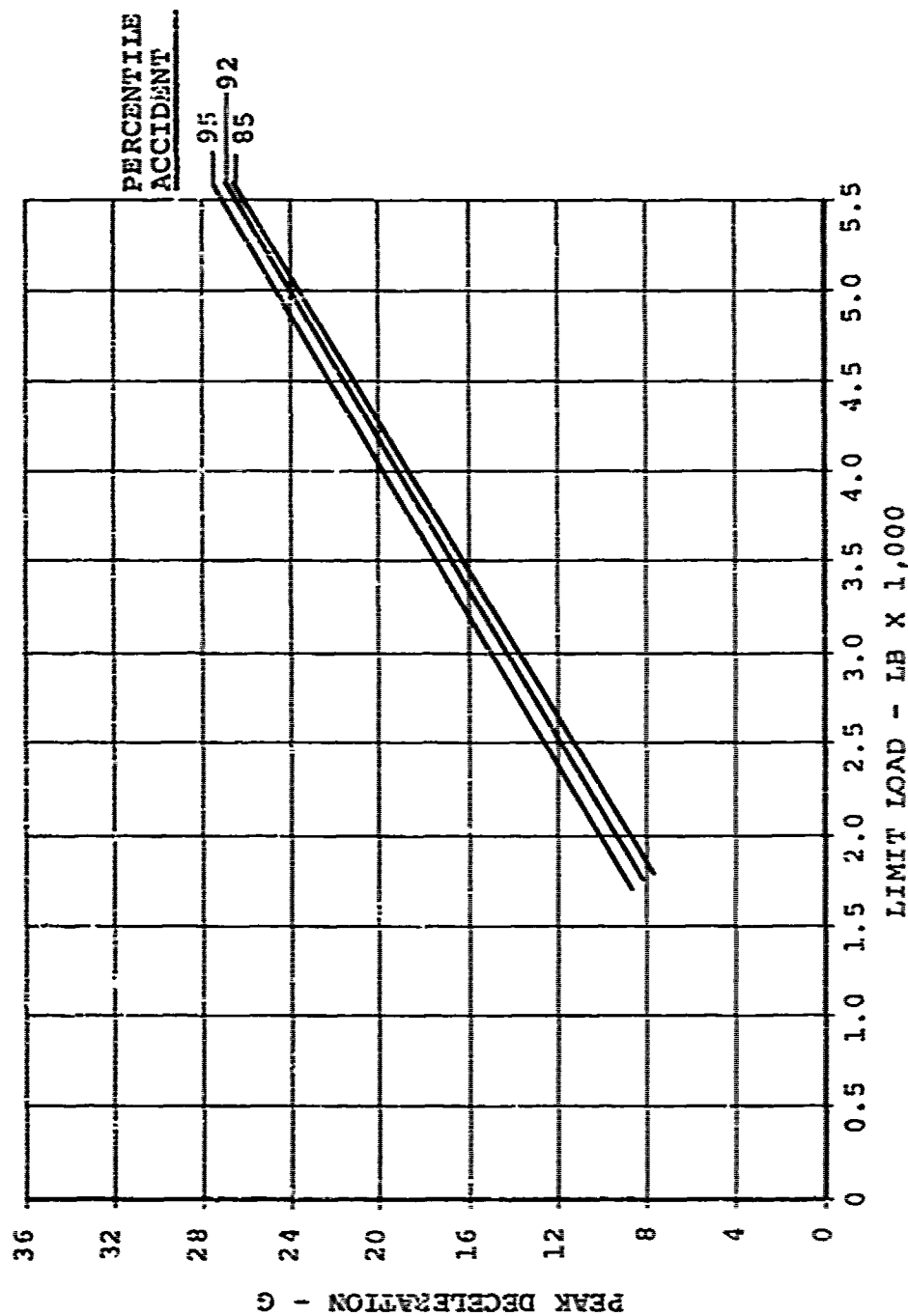
Figure 65. Peak Chest Deceleration Versus Limit Load (Trapezoidal-Shaped Limit Load Versus Deformation Curve).

95
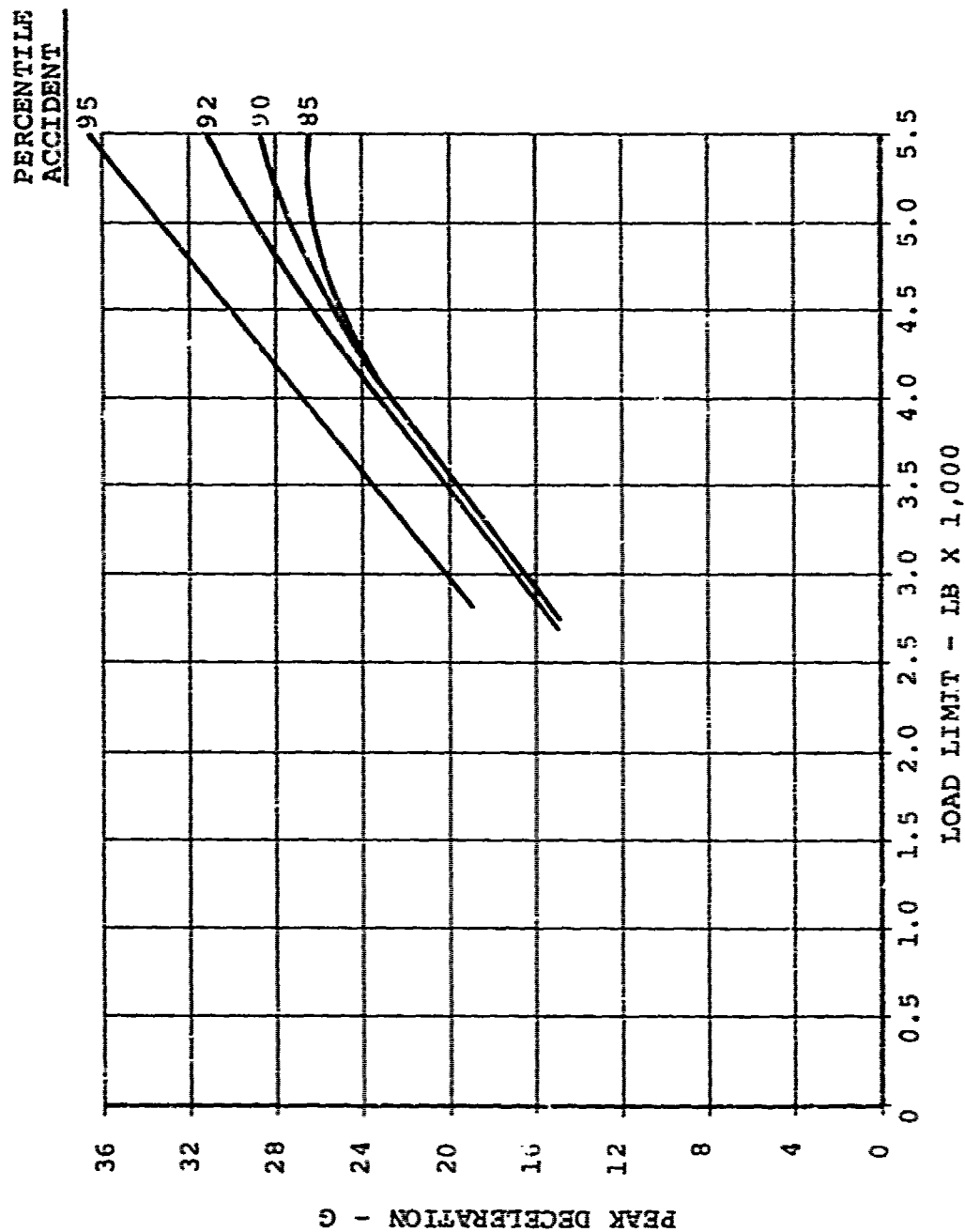
Figure 66. Peak Pelvic Deceleration Versus Limit Load (Trapezoidal-Shaped Limit Load Versus Deformation Curve).

96
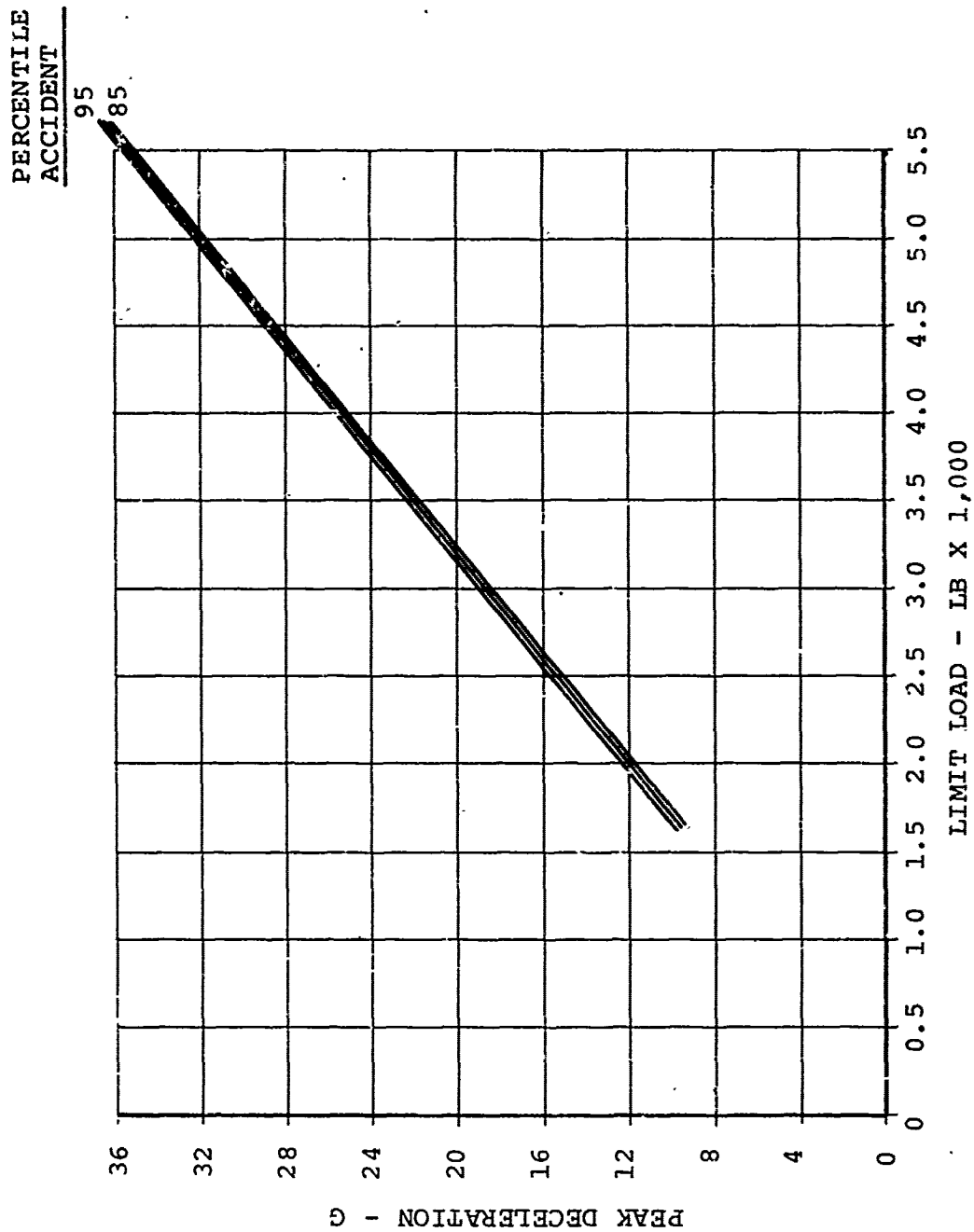
Figure 67. Peak Seat Deceleration Versus Limit Load (Trapezoidal-Shaped Limit Load Versus Deformation Curve).

97
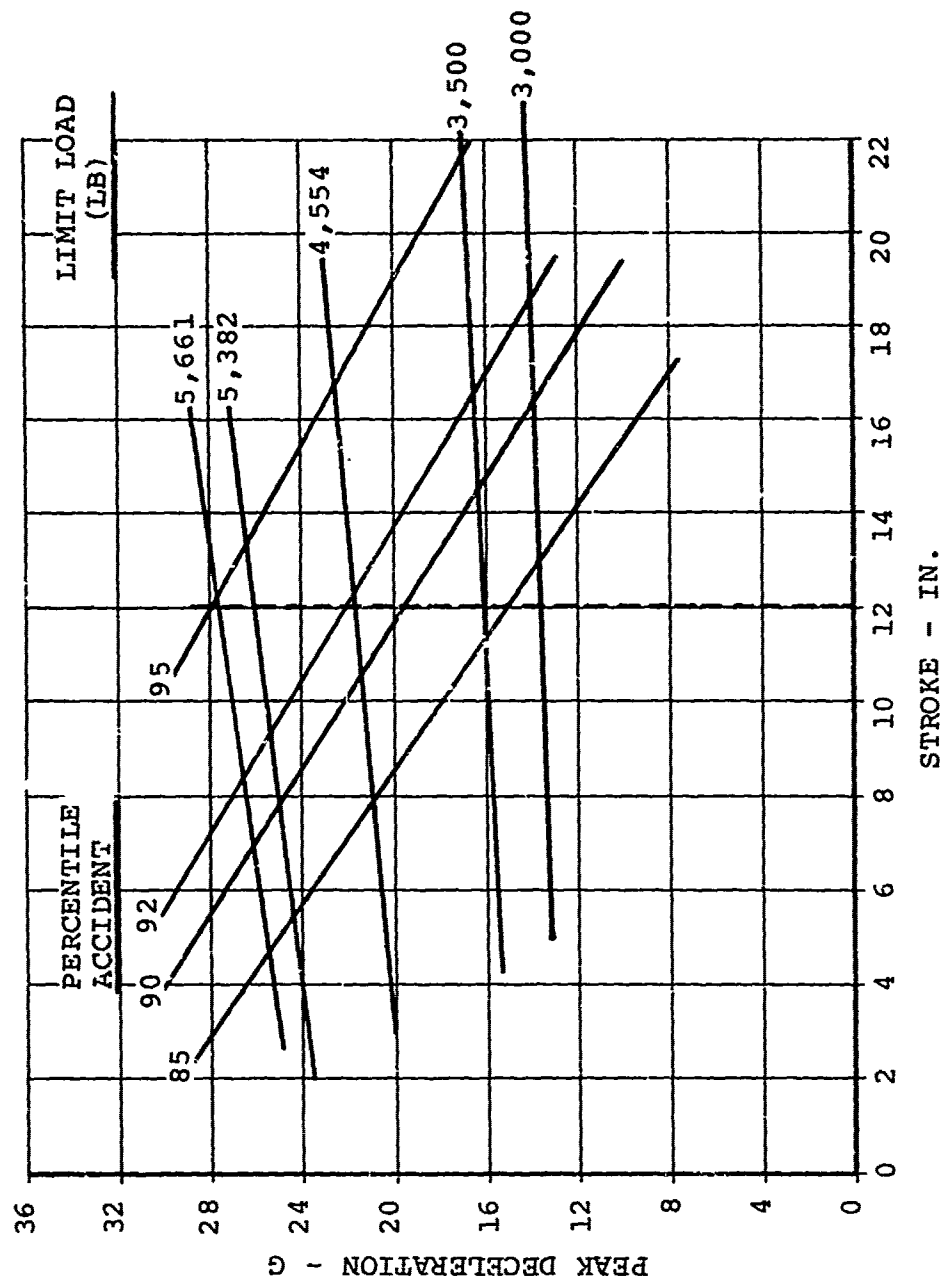
Figure 68. Peak Chest Deceleration Versus Stroke (Curvilinear-Shaped Limit Load Versus Deformation Curve).

98
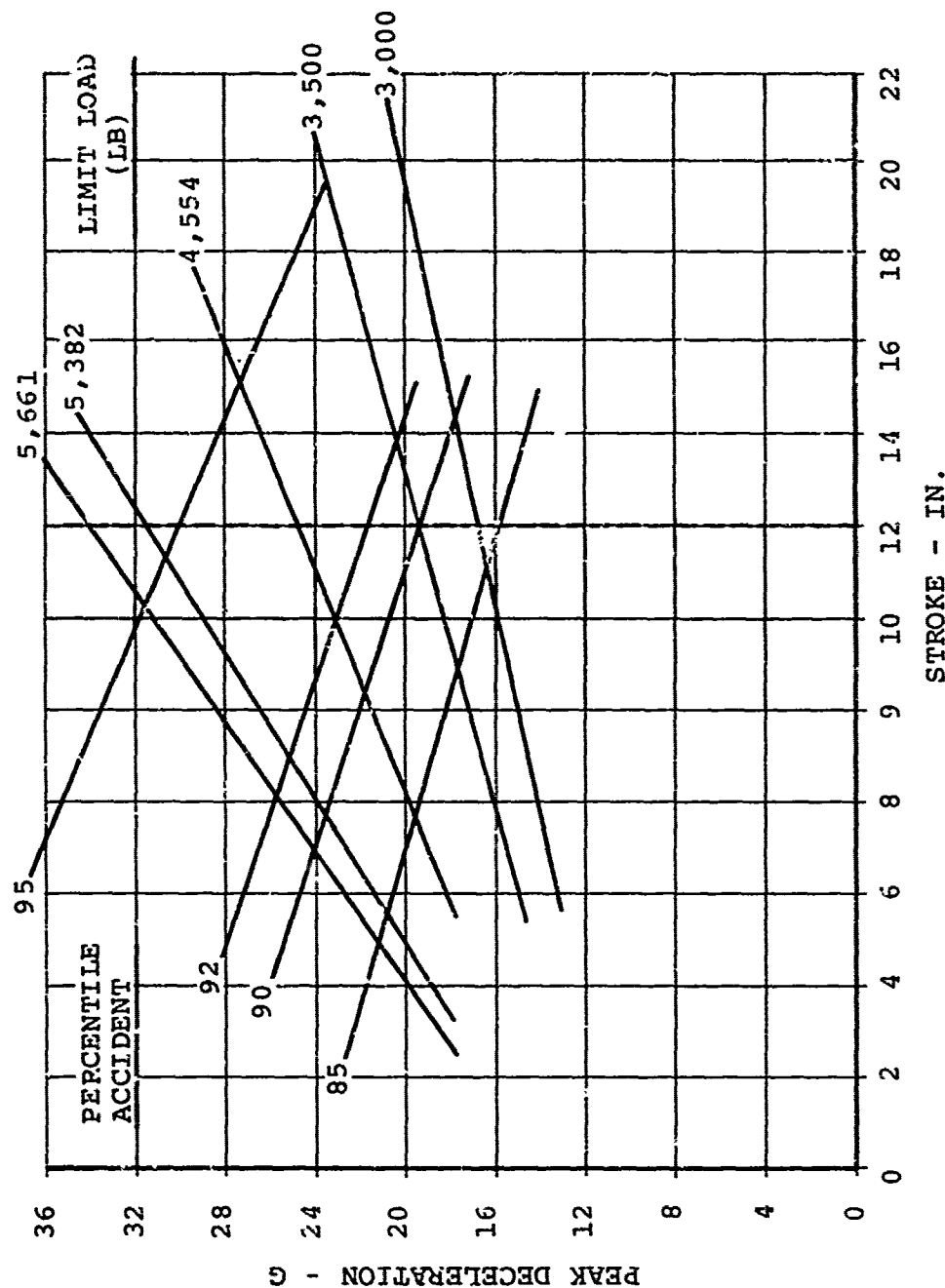
Figure 69. Peak Pelvic Deceleration Versus Stroke (Curvilinear-Shaped Limit Load Versus Deformation Curve).

99
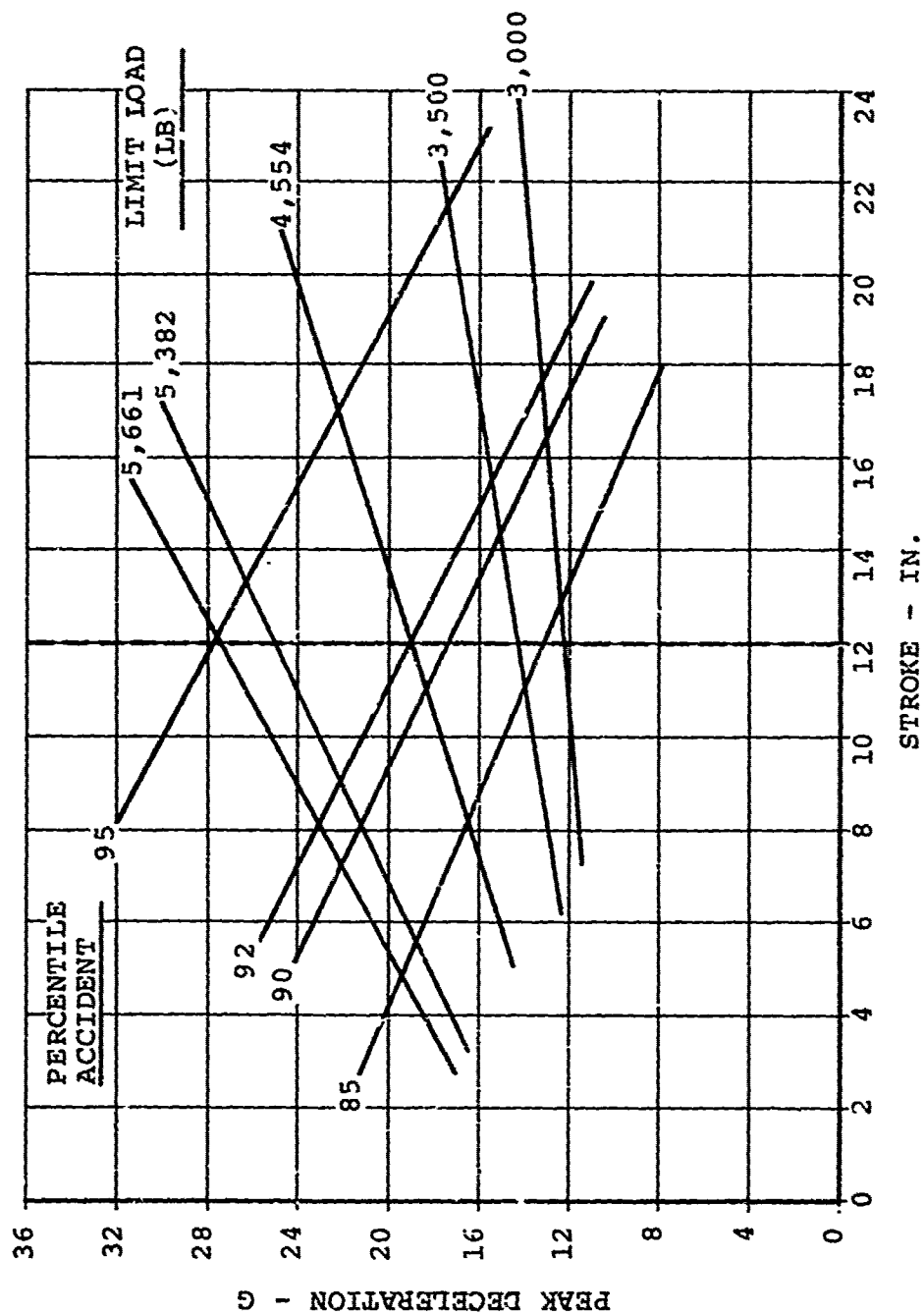
Figure 70.   Peak Seat Deceleration Versus Stroke (Curvilinear-Shaped Limit Load Versus Deformation Curve).

100
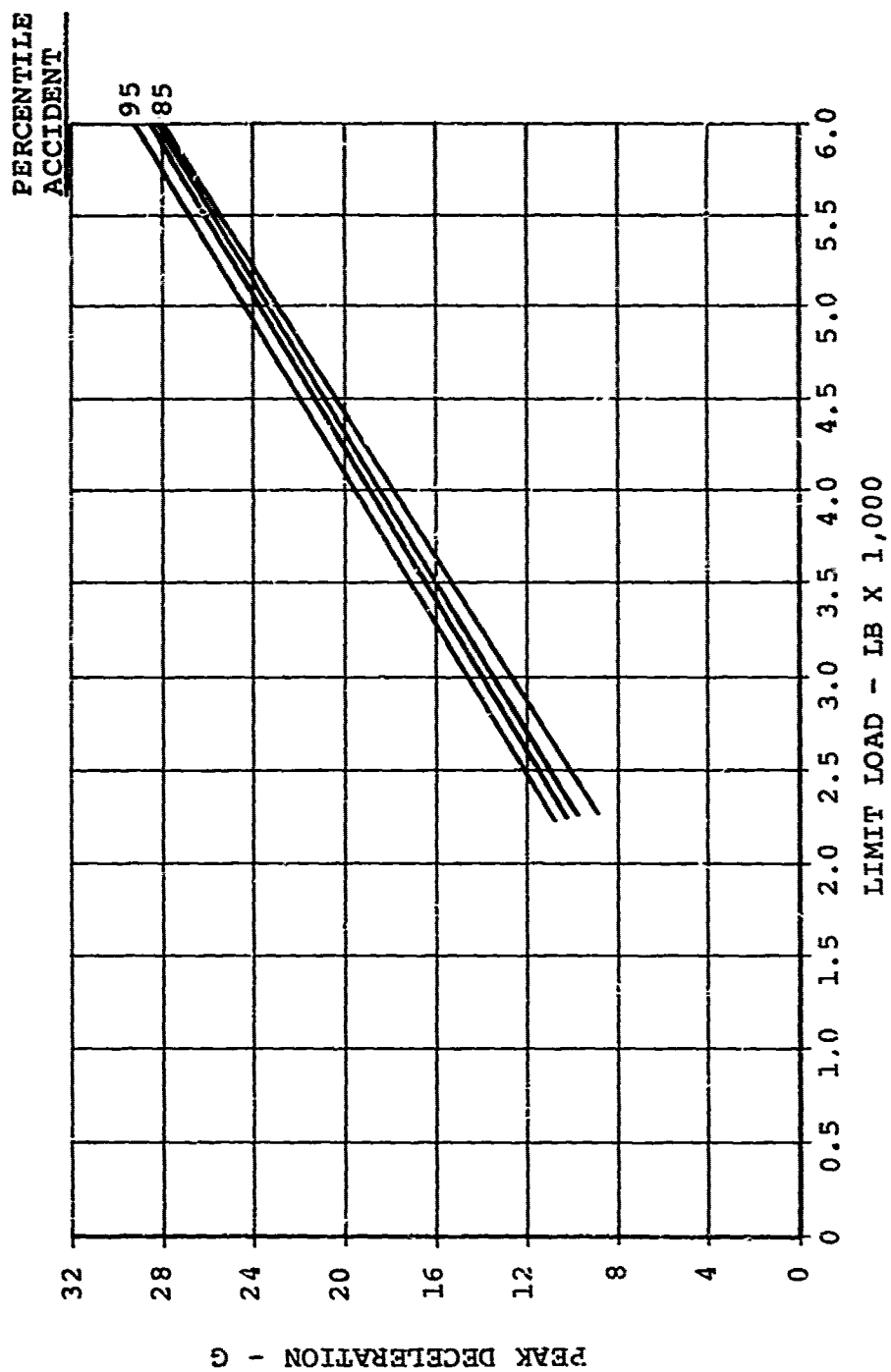
Figure 71. Peak Chest Deceleration Versus Limit Load (Curvilinear-Shaped Limit Load Versus Deformation Curve).

101
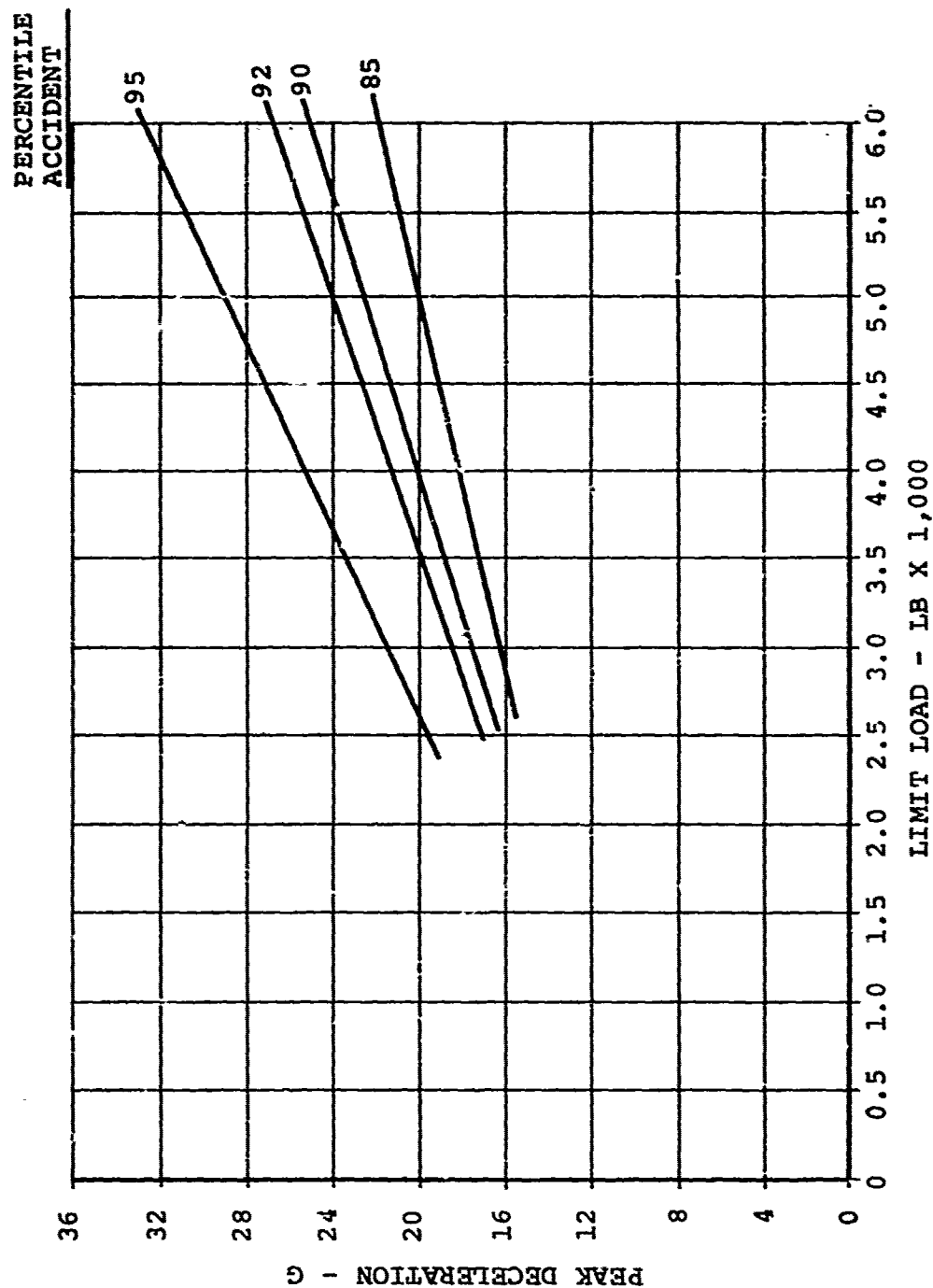
Figure 72. Peak Pelvic Deceleration Versus Limit Load (Curvilinear-Shaped Limit Load Versus Deformation Curve).

102
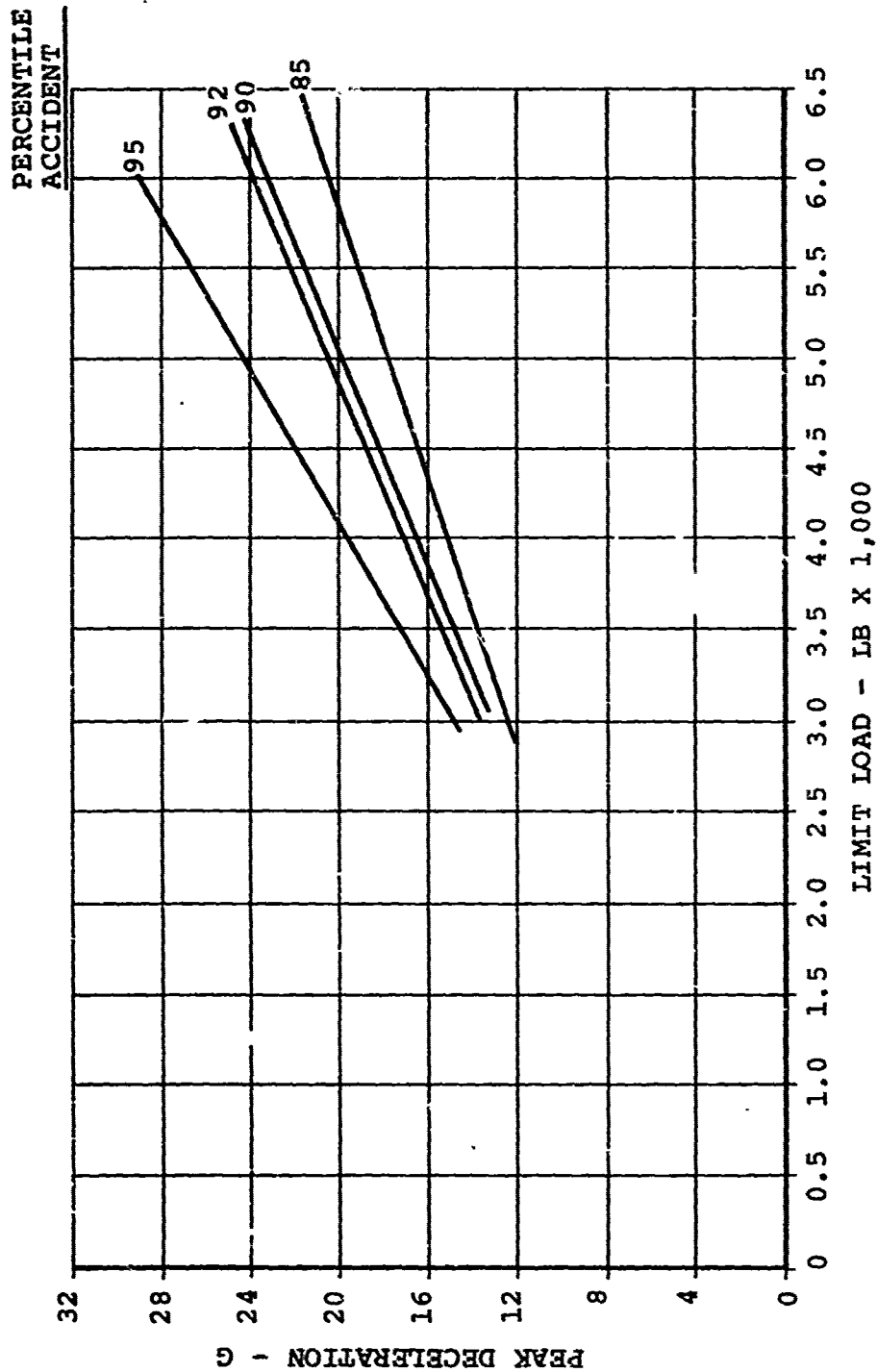
Figure 73. Peak Seat Deceleration Versus Limit Load (Curvilinear-Shaped Limit Load Versus Deformation Curve).

103

TABLE XII.	PEAK DECELERATION OF CHEST, PELVIS, AND SEAT AND ASSOCIATED LIMIT LOADS AS A FUNCTION OF PERCENTILE ACCIDENT FOR 95TH PERCENTILE OCCUPANT*

Trapezoidal-Shaped Limit Load Versus Deformation Curve

Percentile Accident	Peak Deceleration (G)			Limit Load (lb)		
	Chest	Pelvis	Seat	Chest	Pelvis	Seat
85	12.3	19.5	15.5	2,750	3,500	2,550
90	16.2	21.6	21.2	3,500	3,825	3,425
92	18.8	24.0	24.8	3,950	4,125	3,930
95	24.0	32.6	31.0	4,900	4,900	4,850

Curvilinear-Shaped Limit Load Versus Deformation Curve

Percentile Accident	Peak Deceleration (G)			Limit Load (lb)		
	Chest	Pelvis	Seat	Chest	Pelvis	Seat
85	15.1	17.0	13.2	3,480	3,450	3,350
90	19.7	20.7	17.4	4,250	4,250	4,300
92	22.2	23.0	19.1	4,680	4,650	4,630
95	28.1	31.8	27.9	5,750	5,750	5,750

*All values relate to 12.0 inches of stroke as read from previous figures.

and chest curves with the 18G deceleration level. Although 23G was taken as the human tolerance limit for durations longer than 0.006 second, 18G was selected as the limit load factor for use with the 95th percentile weight to size the limit load to permit use of the seat by lighter occupants without forcing their deceleration out of acceptable human tolerance. Inspection of Figures 74 and 75 shows that the curvilinear-shaped limit load curve provides protection from a higher percentile accident than does the trapezoidal shape.
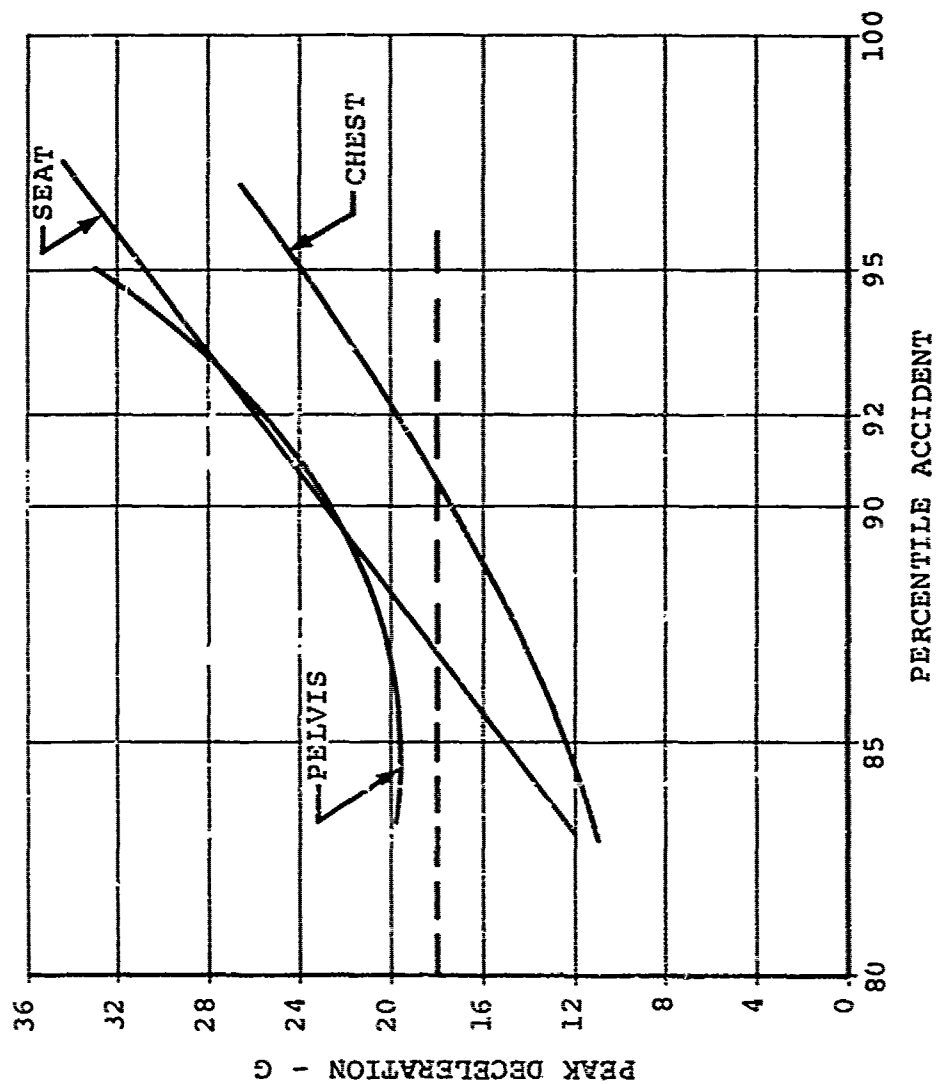
Figure 74. Peak Deceleration Versus Percentile Accident (Trapezoidal-Shaped Limit Load Versus Deformation Curve With 12 Inches of Stroke).

105
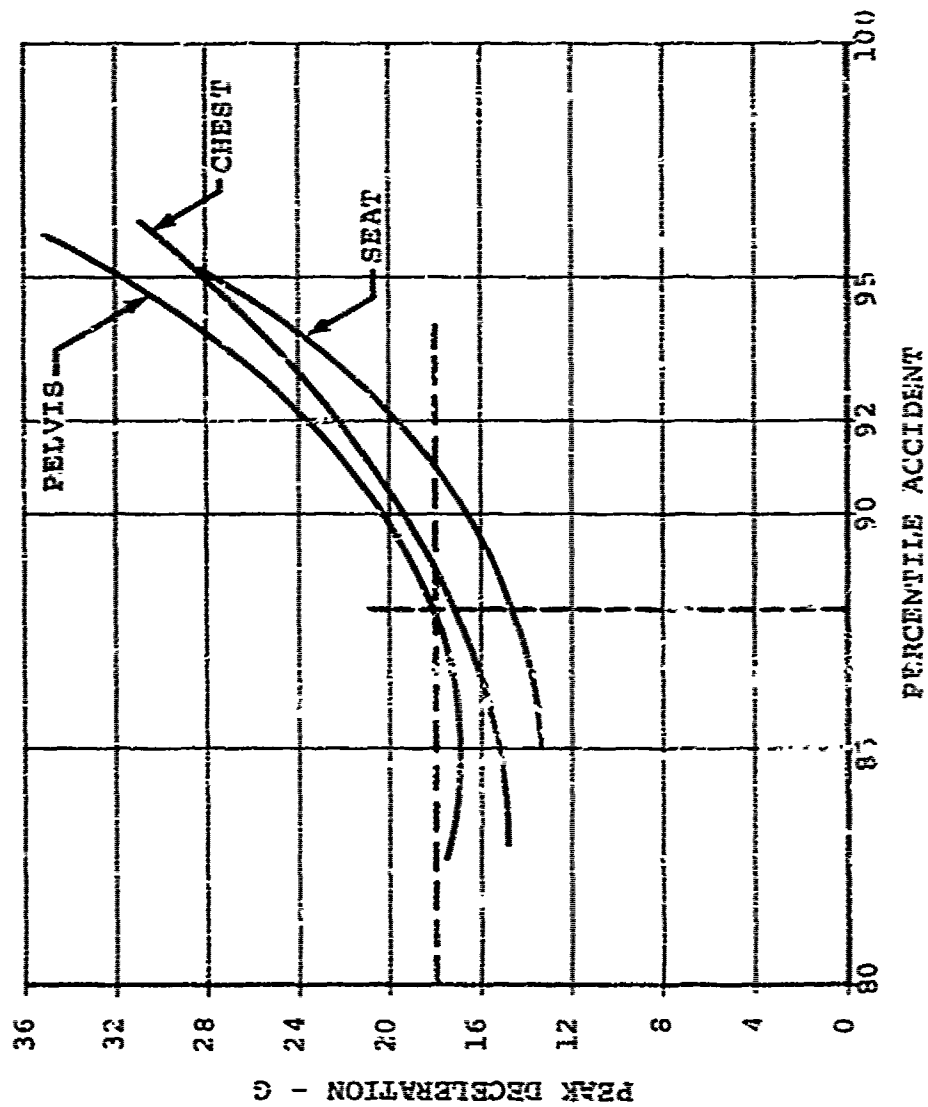
Figure 75. Peak Deceleration Versus Percentile Accident (Curvilinear-Shaped Limit Load Versus Deformation Curve With 12 inches of stroke).

In spite of the prediction, little real difference is expected between the two curve shapes.

All of the data contained in Table XII and Figures 74 and 75 were taken from the previous figures at a constant stroke length of 12 inches. They therefore represent an analytical prediction of the indicated trend for the 95th percentile occupant seated in an integral armored bucket subjected to the various percentile accident environments and stroking 12 inches for each environment.

Figures 76 and 77 show limit load as a function of percentile accident for 12 inches of stroke for both the rectangular and curvilinear, load-limiting curve. Figure 77 shows that a 3,800-pound limit load is required to provide protection to a 95th percentile occupant seated in an integral armored crew seat with a curvilinear-shaped limit load versus deformation energy-absorption system and subjected to the 88th percentile survivable crash pulse.

3.4.7.2 Limit Load for Tri-Level Limit Load: A straight linear ratio technique was used to establish the limit loads for the various occupant weight ranges. The technique was based on the presumption that three limit loads should be provided to permit an occupant to select the limit load best suiting his particular weight. The basis of the determination was that the force setting should span the 5th through the 95th percentile occupant weight ranges and that the decelerative loads imposed on the lightest occupant using any of the three ranges would be equivalent. This provision would nearly eliminate the increased decelerative loading of light occupants using seats with limit loads designed for the 95th percentile occupant.

The basis for establishment of the ratios used to calculate the various load settings was that $18/G_x$ be constant. The calculations were as follows:

107
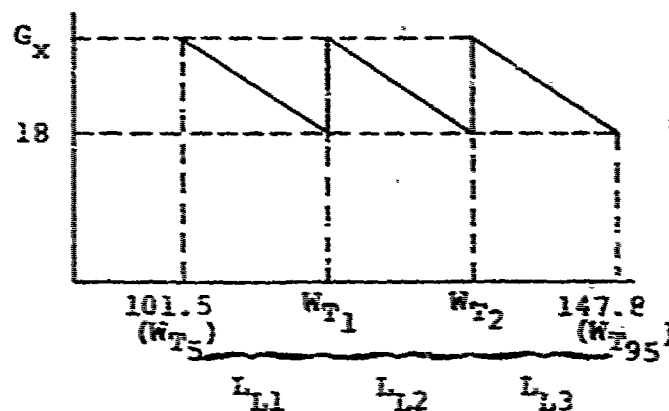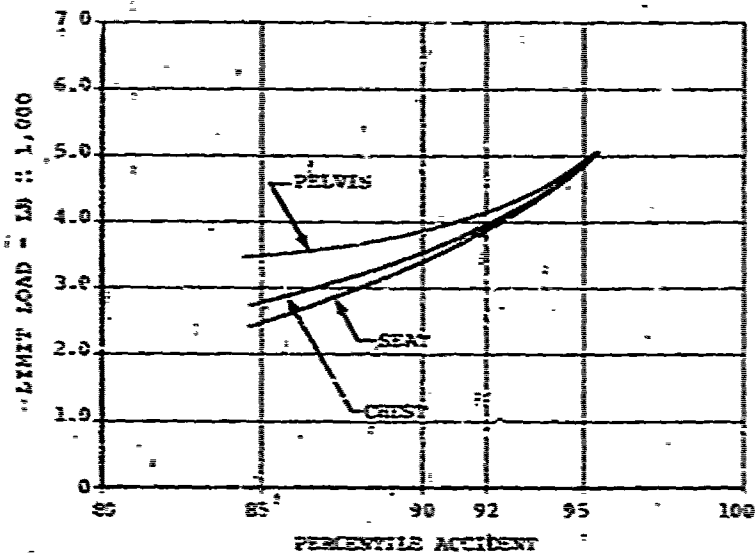
Figure 76. Limit Load Versus Percentile Accident for Chest,
Pelvis, and Seat (Trapezoidal-Shaped Limit Load
Versus Deformation Curve With 12 Inches of
Stroke).
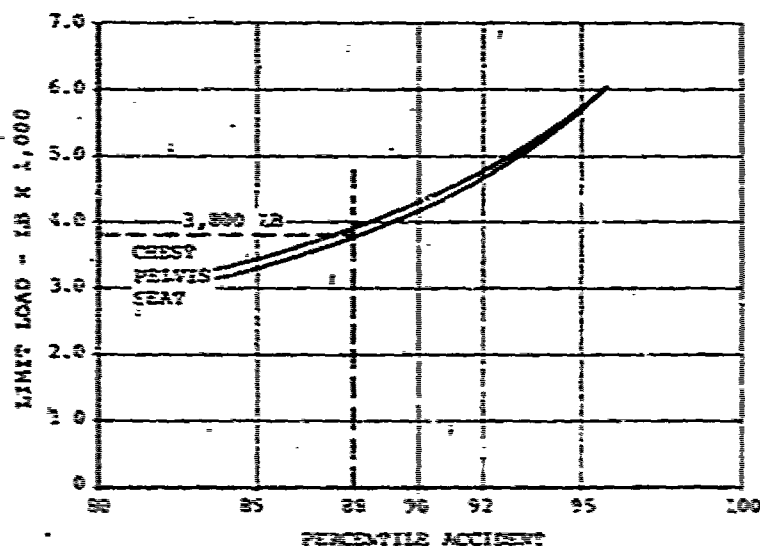
Figure 77. Limit Load Versus Percentile Accident for Chest,
Pelvis, and Seat (Curvilinear-Shaped Limit Loa⁻
Versus Deformation Curve With 12 Inches of
Stroke).

$$\frac{(18)(W_{T_{95}} + 151.2)}{(G_x)(W_{T_2} + 151.2)} = \frac{18(W_{T_2} + 151.2)}{G_x(W_{T_1} + 151.2)} = \frac{18(W_{T_1} + 151.2)}{G_x(W_{T_5} + 151.2)}$$

$$\frac{299}{W_{T_2} + 151.2} = \frac{W_{T_2} + 151.2}{W_{T_1} + 151.2} = \frac{W_{T_1} + 151.2}{252.7} \tag{11}$$

where $W_{T_{95}}$ = effective weight of the 95th percentile occupant, lb

W_{T_5} = effective weight of the 5th percentile occupant, lb

W_{T_1} = effective weight of the heaviest occupant to use the lowest limit load (L_{L1}) and the lightest occupant to use the intermediate limit load (L_{L2}), lb

W_{T_2} = effective weight of the heaviest occupant to use the intermediate limit load (L_{L2}) and the lightest occupant to use the highest limit load (L_{L3}), lb

151.2 = weight of the movable section of the seat, lb

18 = load factor, G

G_x = deceleration imposed on the lightest occupant within a load limit range, G

Solution of the ratios produced the following results:

W_{T_2} = 131.5 pounds

W_{T_1} = 116.1 pounds

Limit load settings were calculated for the three ranges as shown in Table XIII.

TABLE XIII. CALCULATION OF LIMIT LOADS				
Effective Occupant Weight (lb)	+ Seat Weight (lb)	= Total Weight (lb)	x G =	Limit-Load Settings (lb)
147.8	151.2	299.0	18	5,382
131.5	151.2	282.7	18	5,089
116.1	151.2	267.3	18	4,811

Ratioing the loads down by the ratio of the selected 88th percentile crash pulse limit load (L_{L3}) of 3,800 pounds to the 95th percentile crash pulse limit load of 5,382 pounds yields

$$L_{L2} = \frac{3,800}{5,382} (5,089) = 3,593 \text{ pounds} \tag{12}$$

$$L_{L1} = \frac{3,800}{5,382} (4,811) = 3,397 \text{ pounds} \tag{13}$$

A dynamic analysis was conducted using these three limit loads together with the effective occupant weights listed above. Figure 78 presents the results.

The figure shows that use of a tri-level load limiter limits the increase in deceleration due to weight variations of the occupant to about 1G. There was a slight increase in deceleration with decreased occupant weight, which indicates that the ratio technique used for establishing the limit loads is not optimum or overly accurate. It is apparent, however, that the tri-level energy absorber can be used effectively to eliminate significant affects of occupant weight variations.

Figure 78 shows peak deceleration plotted against total occupant weight and includes light clothes, helmet, and boots. Consequently, a potential seat occupant weighing less than 166 pounds would select the lowest limit load before occupying the seat. An occupant weighing more than 191 pounds would select the highest limit load. Those of intermediate weight would select the intermediate limit load.

3.4.8 GENERAL COMMENTS

This analysis indicated that to provide protection to integral armored seat occupants, a considerably lower limit load than calculated by standard practice could be required. The dynamic
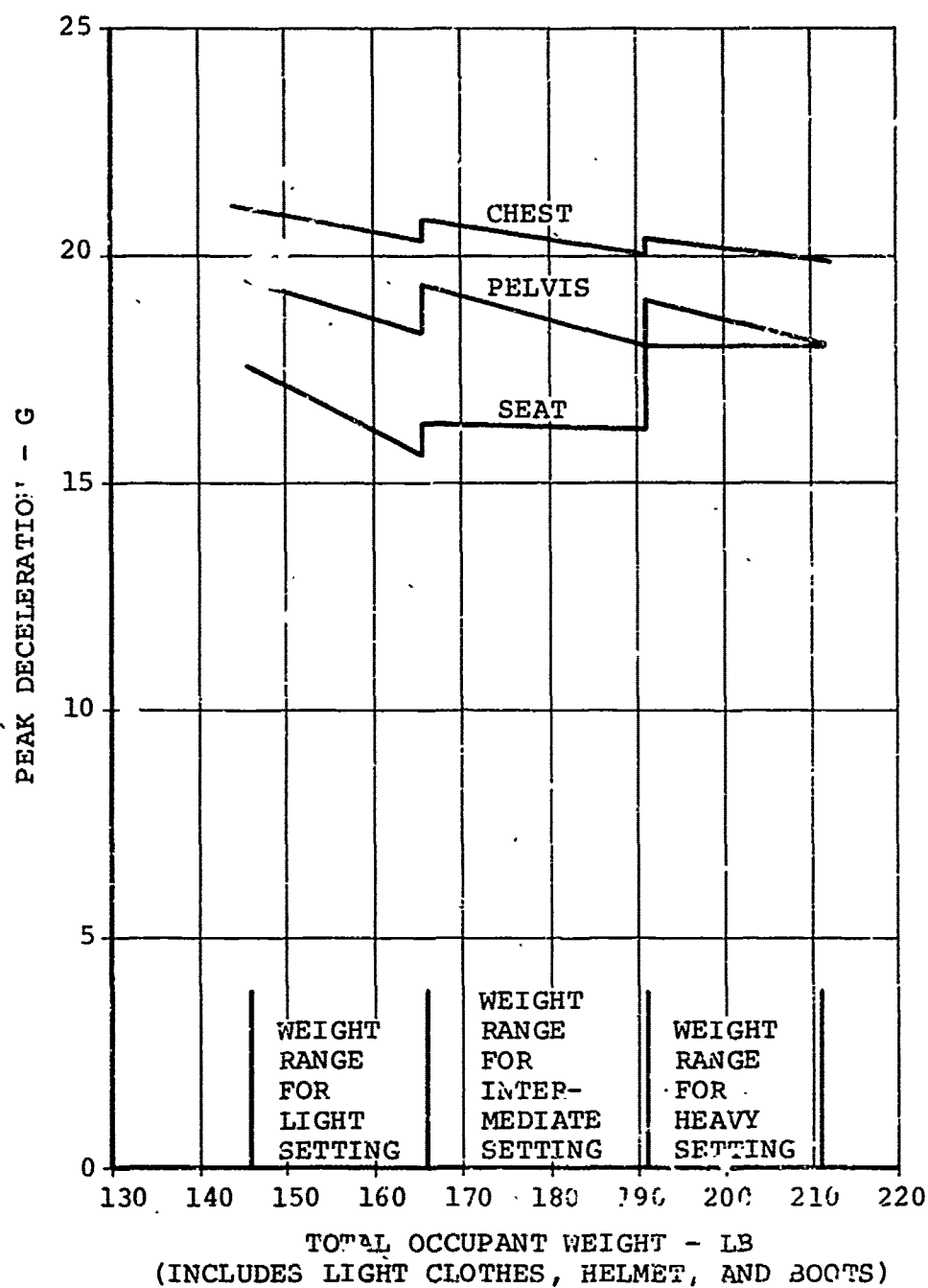
Figure 78. Deceleration Versus Total Seat Occupant
Weight With Tri-Level Load Limiter
(151.2-Pound Movable Seat Weight).

111

test matrix was therefore established to provide empirical data with varying percentile crash pulses, varying seat orientations, and varying limit loads. The variation in limit load with percentile crash pulse resulted in the requirement for flexibility in the energy-absorbing system mentioned previously, which explains why a high yoke was used on the test seat. It was needed to permit a long enough energy-absorber stroke to assure that low-limit loads combined with severe test pulses would not result in seat bottoming. Obviously, with the design criteria established, subsequent seats could be designed for specific energy-absorbing systems, strokes, and limit loads, eliminating the high seat-back feature of the prototype test seat.

The analysis also showed that a multiple, limit-load, energy-absorbing system could be used to advantage to increase occupant protection over the entire seat occupant weight range.

CHAPTER 4

TEST METHODOLOGY AND RESULTS

4.1 INTRODUCTION

The methodology for each test series is discussed first in this chapter. The program test results are then summarized and are presented categorically to simplify evaluation. Only those results that were verifiable and pertinent to the primary efforts of the program are presented. Data traces are presented in Appendix IV. Discussion and interpretation of the results are included in Chapter 5.

4.2 TEST METHODOLOGY

4.2.1 ENERGY-ABSORBER QUALITY ASSURANCE TESTS

4.2.1.1 Purpose: The purpose of this test series was to establish the load-deformation curves of the candidate energy absorbers to determine if they met the design requirements, and to establish a base for comparison of the static and dynamic responses of the energy absorbers.

4.2.1.2 Test Environment: The test conditions under which the tensile tubes were loaded were:

Ambient temperature - 75°F

Load application rate - 1 inch per minute

Deflection-governed system, i.e., deflection rate independent variable

4.2.1.3 Instrumentation: The instrumentation consisted of a direct-write oscillograph, a 4,000-pound load cell, a 10,000-pound load cell, a precision potentiometer, and a reference scale.

4.2.1.4 Calibration: The load cells used were calibrated transducers which are checked for calibration every year and records kept on file. The precision potentiometer was a displacement measuring device used to monitor the travel of the moving portion of a tensile testing machine. This device was calibrated prior to each test. The calibration consisted of displacing the traveling portion of the testing machine a known distance and adjusting the potentiometer to provide a known output over that distance. Each device was coupled into one channel of the direct-write oscillograph. The load cell

113

input was calibrated on the oscillograph by a single shunt calibration that simulated a known input of that load cell.

4.2.1.5 **Test Facility**: The primary instrument used in testing the tensile tube load versus elongation was a 10,000-pound tensile testing machine. This machine was adjusted to drive the operating screw at a maximum rate of 1 inch per minute. Figure 79 shows the test configuration.
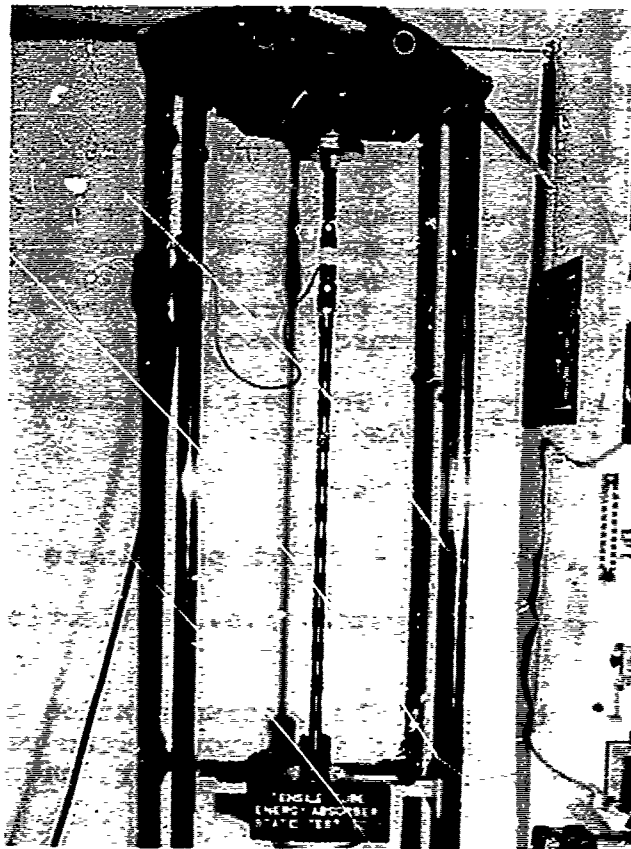
Figure 79. Tensile Tube Test Setup.

4.2.1.6 **Test Procedures**: The test specimens were mounted in the testing machine with special attachment hardware that transmitted the load to the energy absorber through a shear bolt at each end. The lower bolt was not installed until after all pretest calibrations were established. The lower bolt was then inserted into the fixture and the load was

applied to the tensile tube. The load applied to the tensile
tube was visually monitored on a read-out dial on the testing
machine to help detect any anomalies in the test sequence.
The extension of the tube was continued until the tube frac-
tured.

4.2.2 SEAT STATIC TEST

4.2.2.1 Purpose: The primary purpose for the seat static
test was to establish the structural integrity of the seat
with a longitudinal-lateral load imposed on it while having
the simulated floor attachments in a warped mounting condition,
simulating a condition that might occur in a crashing aircraft.
Two additional purposes for the test were (1) to establish
whether the vertical stroking force required was affected by
the longitudinal-lateral load and (2) to establish the struc-
tural integrity of the restraint harness.

4.2.2.2 Seat Occupant: The seat occupant during the static
test was an aluminum body block which simulated the size of
the 95th percentile aviator but was void of the lower portion
of his arms and legs. Figure 80 shows the body block mounted
in the crew seat. Appropriate loads were applied directly to
the body block, thereby making it possible to statically simu-
late the loads that would be imposed by high deceleration
forces on the system.

Figure 80. Body Block Mounted in Crew
Seat for Static Test.

115

4.2.2.3 Test Environment: The static test body block was mounted in the armored crew seat and placed in a drop cage normally used for vertical dynamic tests. The seat was mounted on blocks which simulated the warped floor conditions called out in References 1 and 2.

Figure 81 shows the basic mounting configuration, and Figure 82 shows the seat mounted in the cage in that configuration.
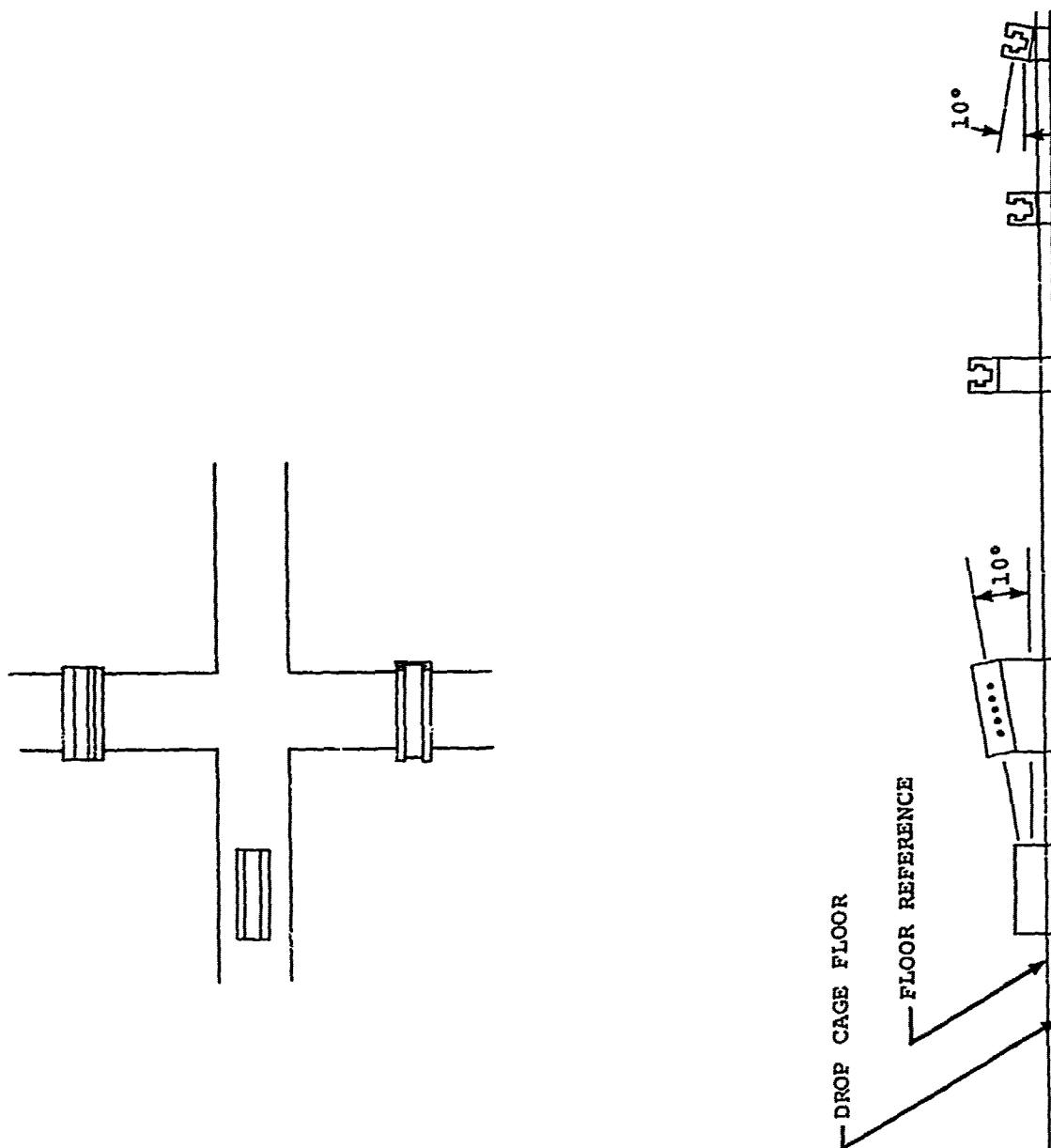
Figure 81. Static Test Floor Mount Configuration.

116
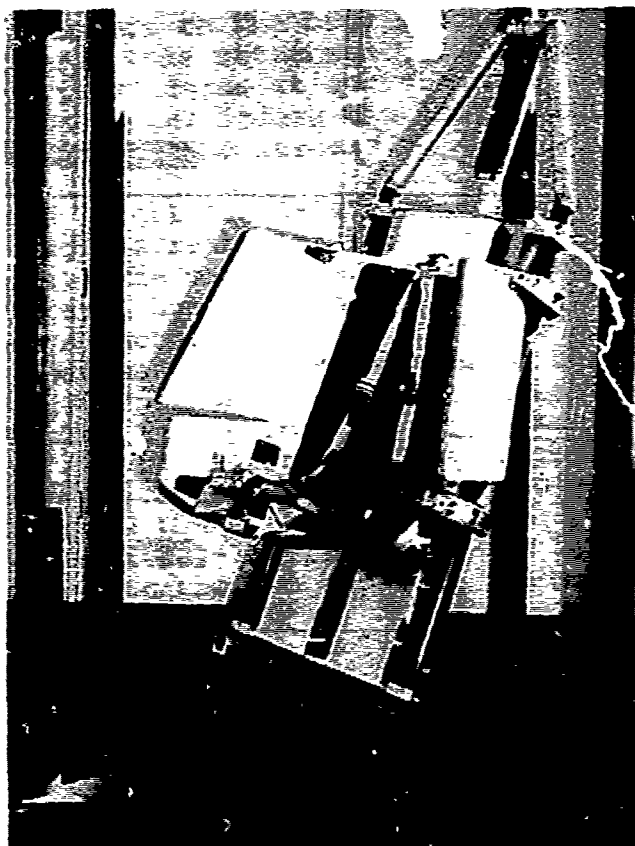
Figure 82.   Seat Mounted in Drop Cage
for Static Test.

The drop cage was located between static test anchor uprights
and the drop tower facility poles as shown in Figure 83.   The
drop cage was secured upside down to simplify the application
of the vertical load.   The cage was rotated 20 degrees as
shown in Figure 84 to orient the resultant longitudinal-
lateral load properly.

The drop cage was restrained in this position against the
longitudinal-lateral resultant force of 11,080 pounds.   The
longitudinal component of force was 10,425 pounds, which repre-
sented 25 times the total weight of 417 pounds.   The lateral
component was 3,753 pounds, which was 9 times 417 pounds.   The
417 pounds consisted of 211 pounds, which was the weight of
the 95th percentile Army aviator equipped in light clothes and
a helmet, a movable seat weight of 151 pounds, and a seat sup-
port structure weight of 55 pounds.

117
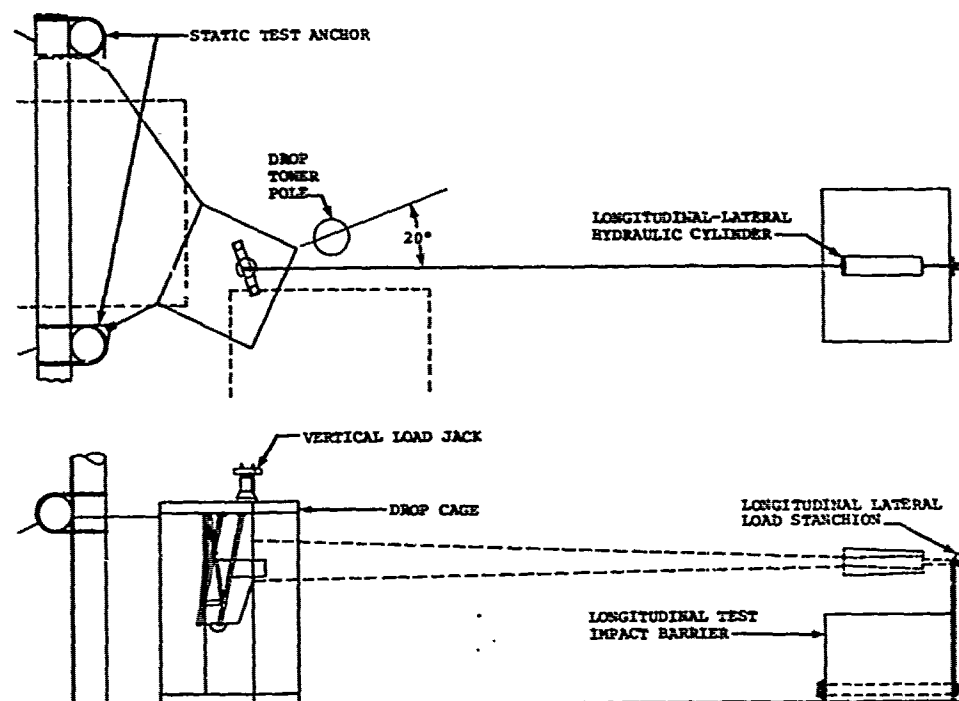
Figure 83. Static Test Setup.
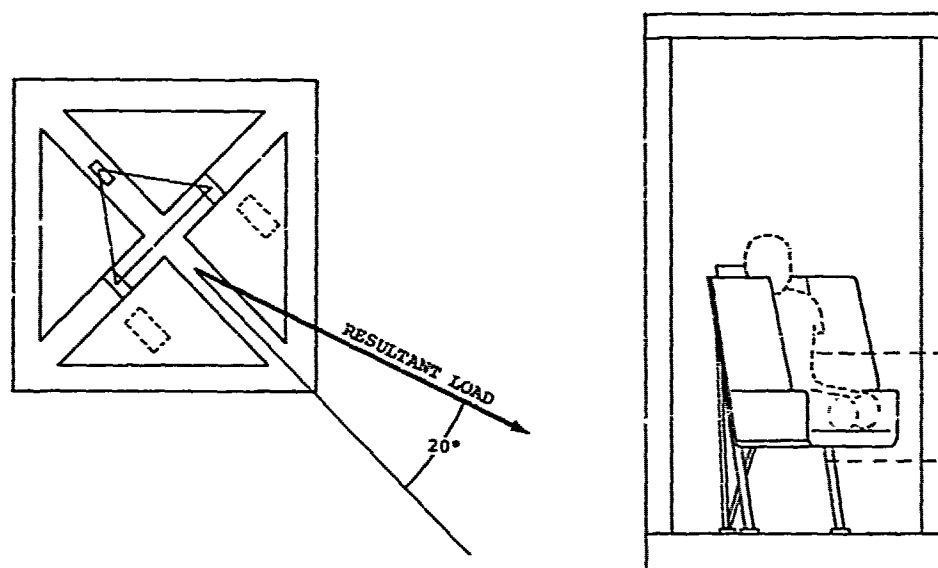
Figure 84. Drop Cage With Seat and Static Test Dummy Installed.

118

The aluminum body block was placed in the seat, and the restraint harness was attached and tightened. A hydraulic jack was positioned on top of the inverted cage and connected to the attachment fixture on the body block through access holes in the cage floor. This attachment fixture was designed to position the vertical force at a distance 6 inches forward of the seat reference point before the longitudinal load pulled the body block against the harness.

To introduce the longitudinal-lateral load into the seat without overstressing the restraint harness, the force was applied at two locations. The major load which corresponded to the longitudinal-lateral acceleration acting on the 211-pound occupant (times a factor of 1.5) equalled a force of 8,410 pounds. This load was applied directly to the body block from two sources: 7,700 pounds applied through the lateral-longitudinal cable, and up to 760 pounds through the horizontal component of the energy-absorber stroking force. The remainder of the 11,080-pound test load was applied through a strap wrapped around the seat bucket. The load applied through the longitudinal-lateral cable and hydraulic cylinder was proportioned into the two separate loads through a lever bar as shown in Figure 85.
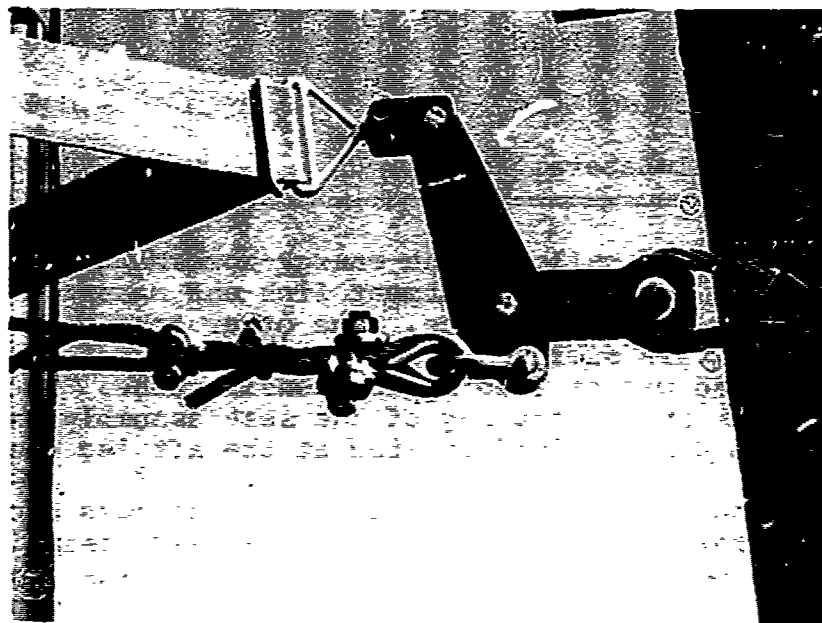
Figure 85.   Lever Bar for Proportioning the
             Longitudinal-Lateral Load.

119

4.2.2.4 Instrumentation: The instrumentation used in the static test consisted of ten load cells, a direct-write oscillograph, a strain indicator, and a marker galvanometer. The size and application of these load cells are tabulated in Table XIV. Their locations are shown in Figure 86.

	TABLE XIV. STATIC TEST INSTRUMENTATION REQUIREMENTS	
	Application	Capacity (lb-tension)
1.	Harness Load Cell	5,000
2.	Harness Load Cel.	5,000
3.	Harness Load Cell	5,000
4.	Harness Load Cell	5,000
5.	Energy Absorber Rod End	5,000
6.	Seat Adjustment Link (Total Energy Absorber Load	5,000
7.	Rear Frame Tie-Down Bolt	30,000
8.	Vertical Jacking Load	4,000
9.	Vertical Jacking Load	4,000
10.	Longitudinal-Lateral Load	15,000

There were two load cells in the energy-absorbing system. One was attached to the seat adjustment link and measured total energy-absorber resistive force. The other load cell was built into the main energy-absorber rod end to determine how much of the load was carried by the tensile tube. The 30,000-pound load link in the aft leg of the seat assembly was used to measure the tensile load applied at the aft leg location.

The 5,000-pound load links attached to the harness anchors provided the force-time history of the harness assembly. As a major portion of the longitudinal-lateral load was applied through the harness, these load links were closely monitored during initial load application to insure against unforeseen catastrophic failure in the harness or seat bucket. The two 4,000-pound load cells in the upper jack assembly revealed the
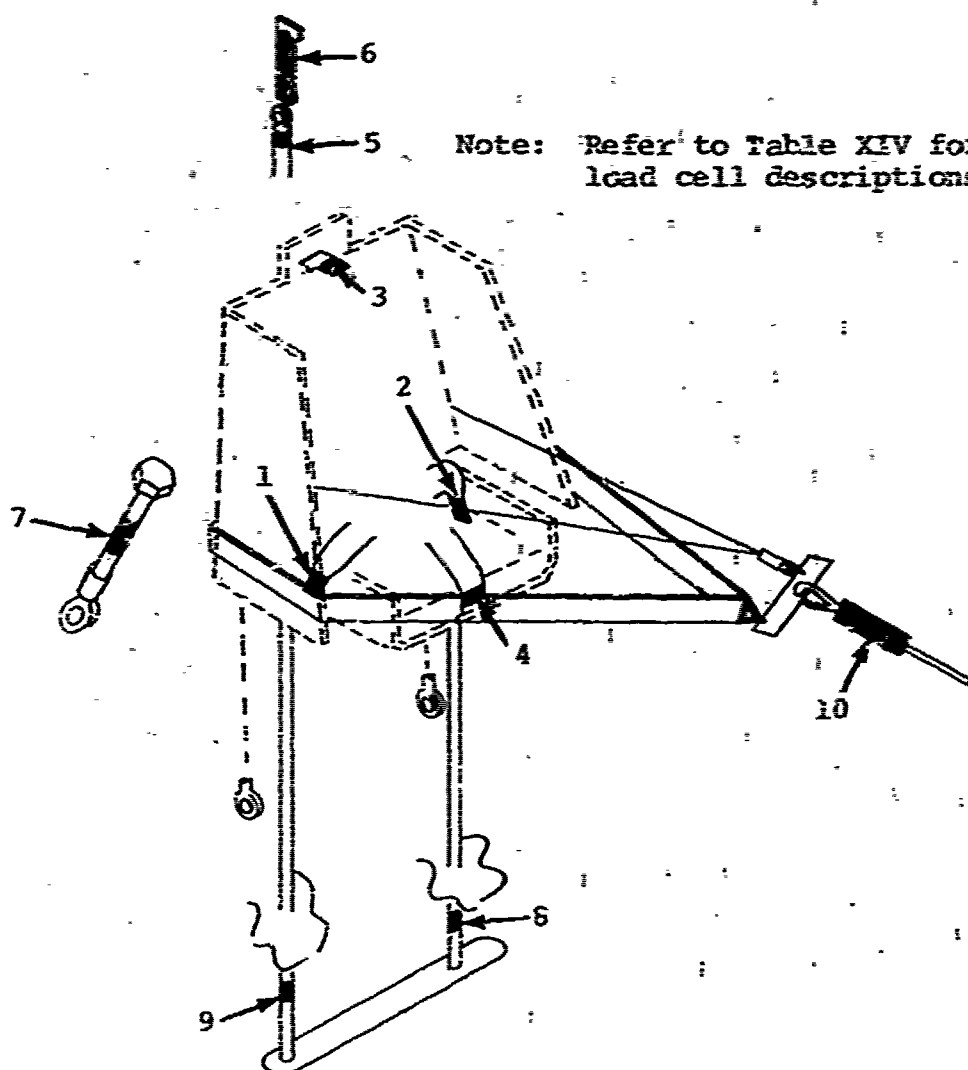
Figure 86. Load Cell Location for Static Test.

required stroking force applied to the movable part of the
seat as a function of stroke distance. The 15,000-pound load
cell in the longitudinal-lateral cable measured the force
being applied by the hydraulic cylinder shown in Figure 87.

The signals from all gages except the load link in the
longitudinal-lateral cable were recorded on the direct-write
oscillograph. The marker galvanometer was installed to allow
manual marking of the oscillograph record. It was used to
mark increments of load application and energy-absorber stroke

121
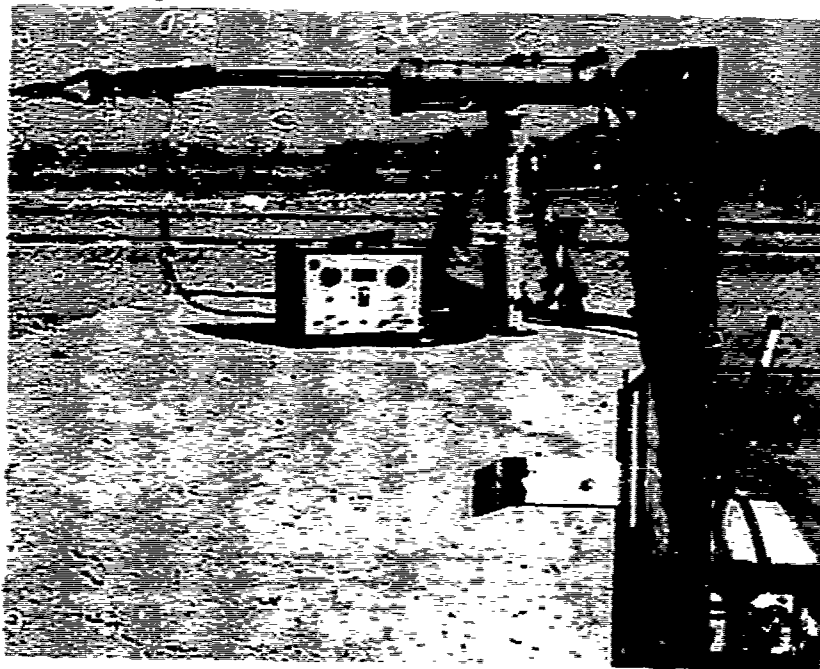
Figure 87. Load Cell Installation for Measuring
Longitudinal-Lateral Loads.

to provide the necessary force-displacement relationships.
The load cell in the longitudinal-lateral cable was connected
to the strain indicator for continuous monitoring of the
longitudinal-lateral load. Figure 87 shows the strain indi-
cator hooked to the longitudinal-lateral load cell.

4.2.2.5 Calibration: All load cells were calibrated prior to
the test. Calibration of the oscillograph was accomplished by
single-shunt calibration of each transducer input. The strain
indicator periodic calibration was current.

4.2.2.6 Test Procedure: The principal effort involved in
performing the static test was in setting up the static test
apparatus. With the cage properly tethered to the static test
anchors and oriented to provide the 20-degree angle desired,
the longitudinal-lateral cable was attached to the load appli-
cation harness link. Then, with the oscillograph running and
monitoring all transducers (with the exception of the main
longitudinal-lateral load, which was monitored by the strain
indicator), the longitudinal-lateral load was applied in
1,000-pound increments. The purpose of loading in steps was
to provide loading plateaus to help establish a relationship

122

between the various loads monitored on the seat and the corresponding input load. The input longitudinal-lateral load then became the independent variable to which all other measurements were referenced.

Once the full longitudinal-lateral load that was applied by the large hydraulic cylinder was reached, the vertical seat stroking load was applied. Due to the 13-degree orientation of the guide tubes, there was an interrelationship between the vertical displacement and the longitudinal-lateral displacements. As the seat stroked down the guide tubes, it moved forward and released some of the longitudinal-lateral load. This was corrected for by monitoring the input load and bringing it back to the nominal value before the seat stroked another increment. This procedure was followed until maximum stroking distance was reached.

4.2.3 DYNAMIC TESTS

4.2.3.1 Purpose: This series of tests was established not only to demonstrate the performance of the energy-absorbing seat but also to provide a minimum of empirical data necessary to establish trends to support crashworthy seat design and optimization. Specific objectives of these tests were as follows:

1. To measure the response of the seat and occupant as a function of crash pulse in the vertical direction.

2. To determine the effect of energy-absorber limit load (resistive force) on response as a function of crash pulse in the vertical direction.

3. To determine the effect on occupant and seat response in the vertical direction with lateral and longitudinal decelerative components imposed.

4. To establish the percentile survivable crash for which protection can be provided by an integral armored crew seat of practical design limitations.

5. To determine the ability of the seat to provide protection to the occupant in the vertical, longitudinal, and lateral directions.

6. To determine the loads imposed on the structural members of the seat.

7. To provide sufficient information to permit the design of a flight-weight, crashworthy, integral armored crew seat.

123

4.2.3.2 Seat Occupant: The seat occupant in this dynamic test series was a 95th percentile dummy that was fully instrumented with triaxial accelerometers in the pelvis, chest, and head. The dummy had a highly developed spinal column and rib cage assembly and a realistic upper pelvic structure including the iliac crests. Its lower pelvic structure, however, did not correspond to a human equivalent, as the dummy was developed primarily for tests with deceleration inputs in the longitudinal direction. The dummy represented a 95th percen-tile civilian occupant in the "as delivered" condition and was modified to correspond to a 95th percentile Army aviator. Its modified nude weight came to 201 pounds. This weight included the internally mounted accelerometers but did not include the connectors on these accelerometers. The dummy was clothed in a lightweight Nomex flight suit and a suitable crew helmet. Figure 88 shows the dummy positioned in the crew seat.

Figure 88. Dummy Installed in Seat for Dynamic Test.

124

4.2.3.3 Test Environment: The test series was divided into three phases. The first phase consisted of five vertical drops in a drop tower. The second phase consisted of three vertical drops with triaxial components induced by reorienting the seat in the drop tower. The third phase consisted of two longitudinal-lateral tests conducted on a test sled. Figures 89, 90, and 91 show the configurations for each of the three phases, and Table XV presents the test conditions.

The drop cage used for the vertical and triaxial drops was a 1,400-pound steel cage with a 150-pound triaxial mount added for the triaxial test series. This cage was suspended in a 65-foot tower and dropped on a stack of paper honeycomb designed and shaped to provide the desired crash pulse when combined with a specific drop height. The two longitudinal-lateral tests made use of an accelerator sled which was propelled down a track by a 5,700-pound weight which was suspended and then released in the drop tower. The sled weighed approximately 2,00⊔ pounds and was guided by two parallel rails. The crash deceleration pulse was shaped in the same manner as the vertical drop tests, i.e., a shaped stack of paper honeycomb.

4.2.3.4 Instrumentation: The data acquisition system used in the tests was a 49-channel FM multiplex system which recorded with full redundancy on a 14-track airborne tape recorder. Up to 32 transducers were used simultaneously in this test series. Table XVI shows the type and application of these transducers for a typical test configuration, as well as the size and location of the nine load cells used.

There were two load cells in the energy-absorbing system. One was attached to the seat adjustment link and measured total energy-absorber resistive force. The other load cell was built into the main energy-absorber rod end to determine how much of the load was carried by the tensile tube. The load link in the aft leg of the seat assembly measured the tensile load applied at that location. It provided information concerning the performance of the aft leg energy absorber as well as the force-time history exerted on this part of the structure. The load links attached to the harness anchors provided the force-time history of the harness assembly. The load cells in the front frame supports and attachment blocks provided information on the axial loads in the seat guide rails. The general location of these load cells is shown in Figure 86.

Twenty-one accelerometers were installed for use throughout the test series. Redundant installations were provided in

125

TESTS 1-5
DOWNWARD LOADS

DUMMY INERTIA LOAD
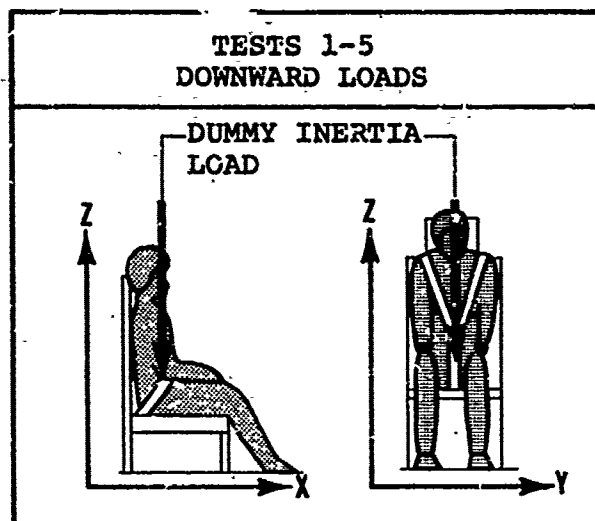
Figure 89. Floor Mount Configuration 1.

TESTS 6-8
DOWNWARD, FORWARD, AND LATERAL LOADS

DUMMY INERTIA LOAD

30°   10°
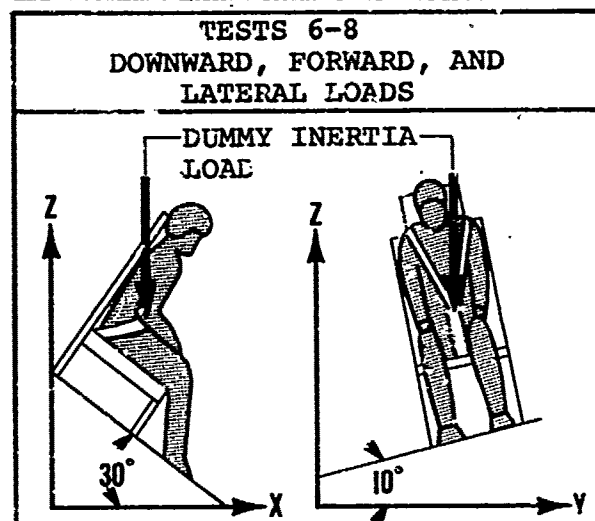
Figure 90. Floor Mount Configuration 2.

TESTS 9-10
FORWARD AND LATERAL LOADS

30°

DUMMY INERTIA LOAD
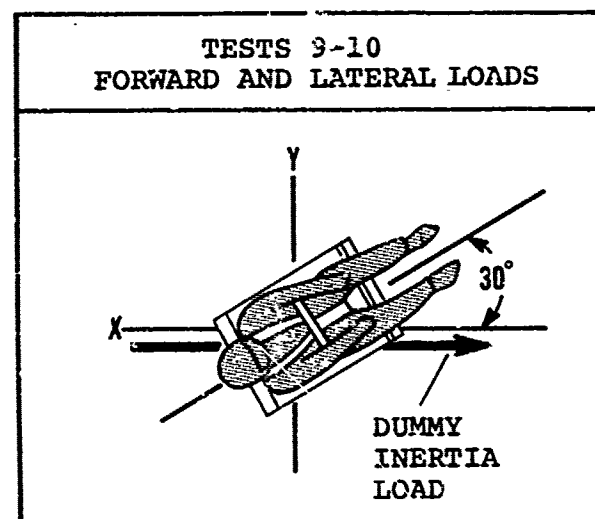
Figure 91. Floor Mount Configuration 3.

126

TABLE XV. TEST CONDITIONS

Test No.	Percentile Crash Pulse	Orientation of Seat	Peak Acceleration (G)	Velocity Change (ft/sec)	Time Duration (sec)
1	88*	See Figure 54	27	35	.081
2	93*	See Figure 54	38	39	.064
3	95*	See Figure 54	48	42	.054
4	93*	See Figure 54	38	39	.064
5	95*	See Figure 54	48	42	.054
6	88*	See Figure 55	32	41	.081
7	93*	See Figure 55	45	46	.064
8	95**	See Figure 55	48	50	.065
9	93	See Figure 56	23	47	.127
10	95***	See Figure 56	30	50	.103

*Vertical crash percentile.
**Test 1, Table 3-III, Crash Survival Design Guide.
***Test 2, Table 3-III, Crash Survival Design Guide.

127

Channel	Type	Capacity	Predicted Peak	Location
1	Load	5,000 lb	5,000 lb	Lap Belt
2	Load	5,000 lb	5,000 lb	Lap Belt
3	Load	5,000 lb	3,000 lb	Shoulder Harness
4	Load	5,000 lb	2,500 lb	Hold-Down Strap
5	Load	5,000 lb	4,600 lb	Energy Absorber Rod End
6	Load	5,000 lb	5,000 lb	Seat Adjust
7	Load	30,000 lb	25,000 lb	Rear Frame Support
8	Load	25,000 lb	20,000 lb	Right Front Frame Support
9	Load	25,000 lb	13,000 lb	Left Front Frame Support
10	Accel	100G	40G	x ⎫
11	Accel	100G	25G	y ⎬ Pelvic
12	Accel	100G	25G	z ⎭
13	Accel	100G	30G	x ⎫
14	Accel	100G	18G	y ⎬ Seat Pan
15	Accel	100G	25G	z ⎭
16	Accel	100G	40G	x ⎫
17	Accel	100G	25G	y ⎬ Torso
18	Accel	100G	25G	z ⎭
19	Accel	100G	30G	x ⎫
20	Accel	100G	18G	y ⎬ Fixture Floor
21	Accel	100G	48G	z ⎭
22	Accel	100G	25G	z Seat Pan (Redundant)
23	Accel	100G	30G	x ⎫ Fixture Floor
24	Accel	100G	18G	y ⎬ (Redundant)
25	Accel	100G	48G	z ⎭
26	Accel	100G	40G	x ⎫
27	Accel	100G	25G	y ⎬ Head
28	Accel	100G	25G	z ⎭

TABLE XVI.   INSTRUMENTATION REQUIREMENTS

critical areas, when space permitted, where loss of information would invalidate the entire test.

4.2.3.5 Calibration: All transducers were calibrated prior
to the test series or within the time limit specified for
periodic calibration. The data acquisition system was cali-
brated by single-shunt calibration resistors that represent
the full-scale outputs of each of the transducers.

4.2.3.6 Test Procedure: In preparation for each dynamic test,
the cage or sled was set up with the proper mounts correspond-
ing to the desired seat orientation and then installed in the
drop tower or on the accelerator sled track. The seat, after
being inspected, was mounted to the floor attachment tracks.
The appropriate energy-absorber system chosen for the test was
then installed in the seat, and the seat height was adjusted
to the uppermost position compatible with the limitation im-
posed by the instrumented portion of the adjuster. This posi-
tion corresponded to two position increments above the null,
which raised the seat pan about 15-3/4 inches above the floor.
The pitch and roll angles of the seat were checked and ad-
justed by use of the rod end at each of the two forward attach-
ment points on the seat support structure. The fore and aft
position of the seat was adjusted to the neutral position,
which centered the seat attachment rod ends in the three
tracks. All bolt torque and preloads were checked, and the
restraint harness and the cushions were prepared for installa-
tion of the dummy.

After transducer installation and inspection, the dummy was
fitted into the seat bucket and the restraint harness was
buckled and tightened (Figure 92). All the instrumentation
leads were patched into the main terminal block to which the
umbilical was attached, and preliminary system check-out was
initiated. All transducers were adjusted for balance and
sensitivity. All load cells were checked for alignment and
freedom of movement. The dummy's posture was adjusted with
its limbs oriented in a natural seated position. After a
check of the camera locations and photographic fields of view,
a system control check-out was run to determine that all
cameras and related equipment would activate and function
properly for the duration of the test interval. Film was then
loaded into the high-speed cameras, and still photographs were
taken of the final test setup. Simultaneously, final calibr-
ation was initiated and pretest calibration was run.

The cage was then raised in the tower (or in the case of the
longitudinal tests, the sled was drawn back on the guide rails
raising the weight in the drop tower) to the point established
during pretest calibration. This height provided the desired
impact velocity for a particular test. The drop height and
the honeycomb stack identification were checked and verified.

129
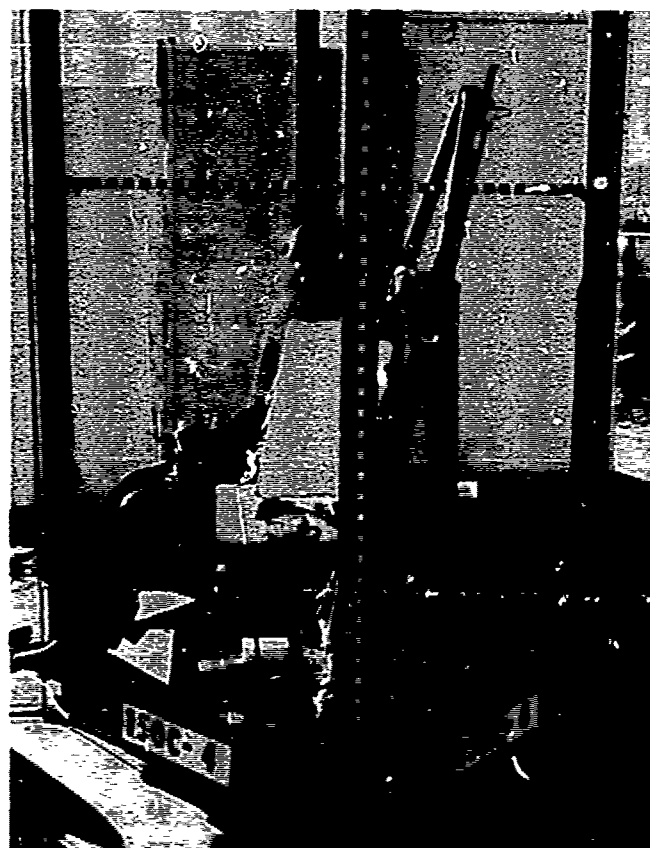
Figure 92.   Side View of Dummy Installed in
Seat for Dynamic Test.

The release hook safety was then fired, thereby arming the re-
lease mechanism and placing the remainder of the test sequence
under the control of the master control sequencer.   The pro-
vision for system abort was reserved up to the point of hook
release.

Immediately after impact (Figure 93), the posttest calibration
was made, during which time posttest still photographs were
taken to document the seat system configuration after the im-
pact.   At this point, close visual observations and measure-
ments were recorded of such items as static displacement of
seat bucket (which was usually an inch less than dynamic
stroke due to buckling of the energy absorber on rebound and
elastic rebound of the tensile tube).   A systems check was
made to determine if any transducers were lost during the test
either through open circuits from severed cables or zero
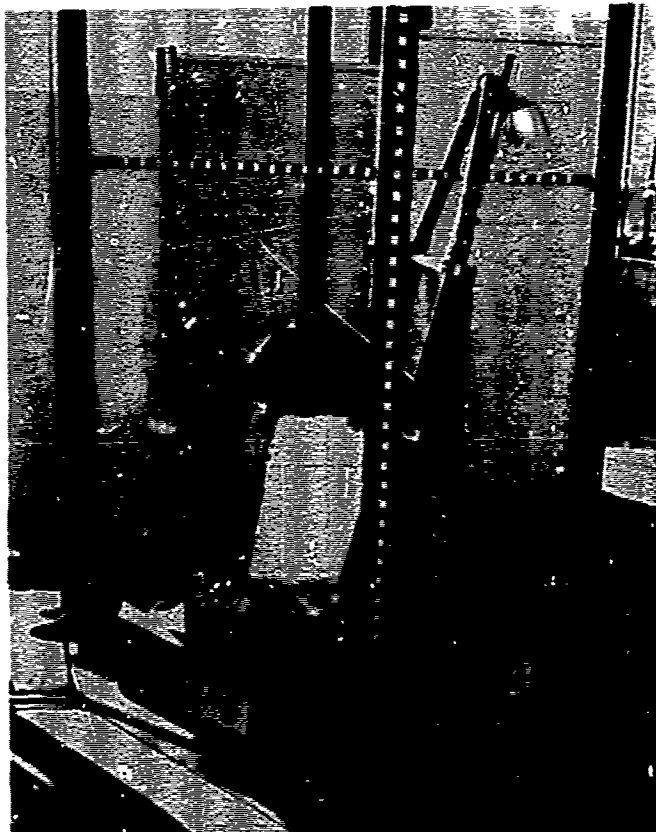
Figure 93.   View of Dummy/Seat After
Dynamic Test.

shifts from damaged transducers. The test tape was then pro-
cessed and "quick look" traces run on all major parameters to
determine test validity.

4.3   TEST RESULTS

4.3.1   ENERGY-ABSORBER QUALITY ASSURANCE TESTS

4.3.1.1 Test Data: Figures 94, 95, and 96 show the results
of the tensile tube load versus elongation tests that were
performed to check the quality and performance of the stain-
less steel tubing used for energy-absorber fabrication. The
percentage of elongation plotted on the abscissa corresponds
to the working length of the test specimen and does not in-
clude the region of the tube around the end fittings, where
no appreciable deformation occurs. Thus, when comparing these
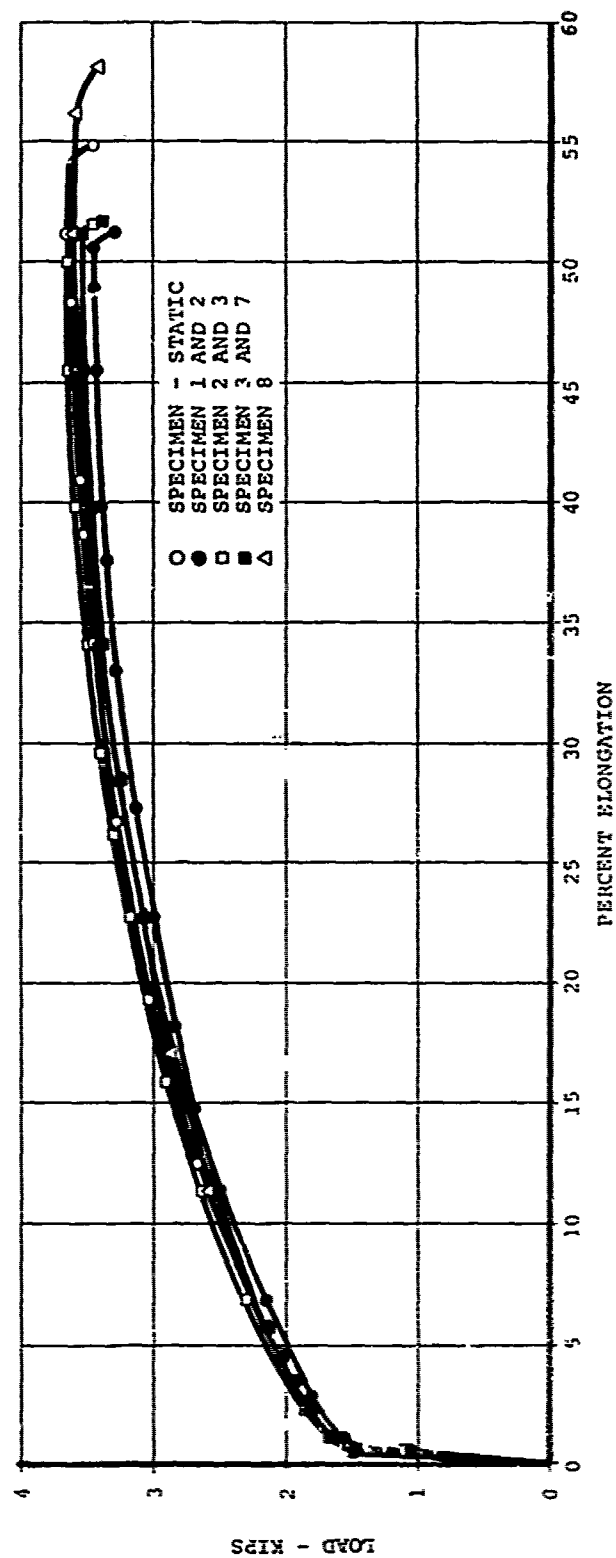
Figure 94. Load Versus Elongation — 0.750 In. x 0.616 In. Stainless Steel Tube.

132
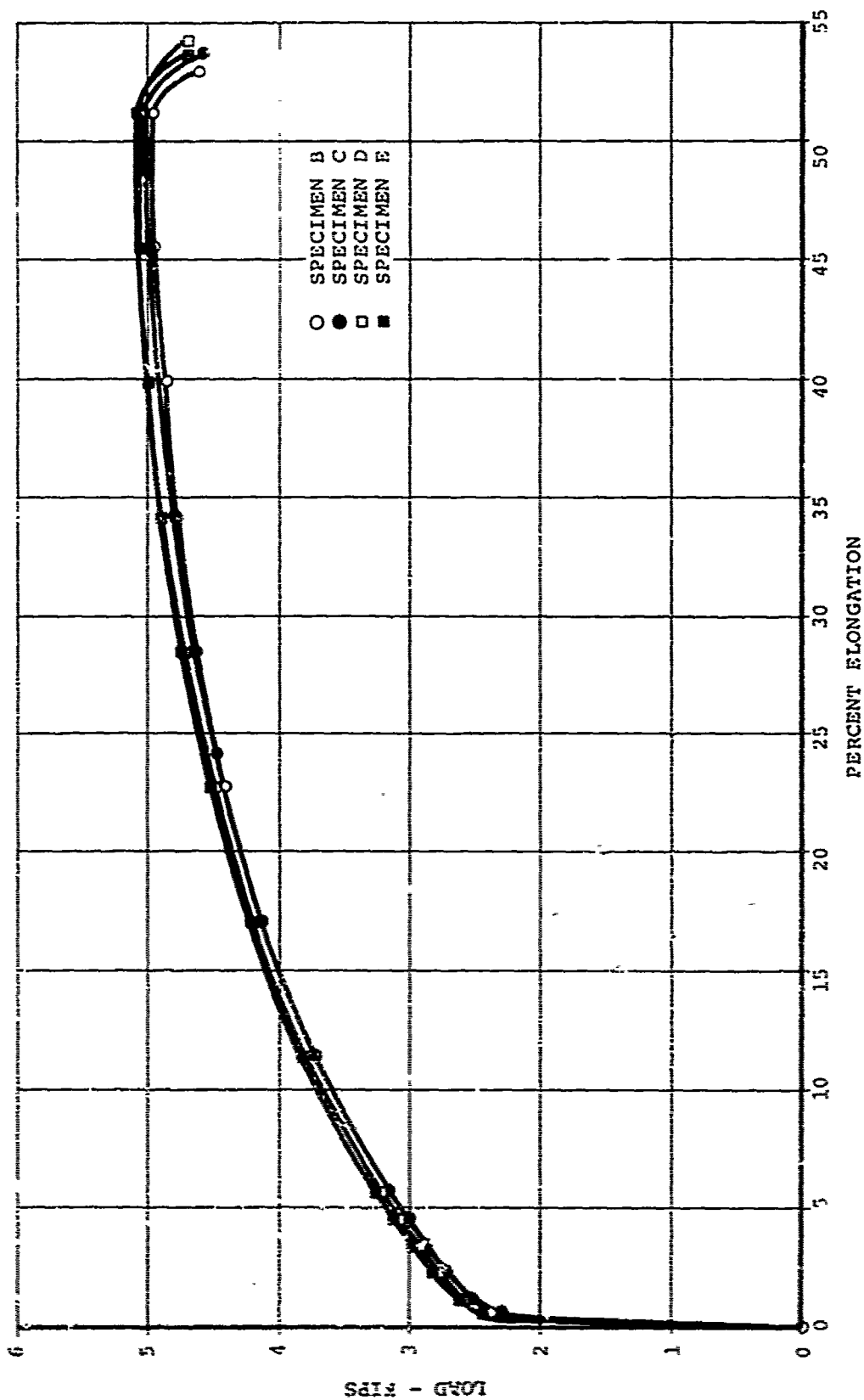
Figure 95. Load Versus Elongation - 0.625 In. x 0.028 In. Stainless Steel Tube.

133
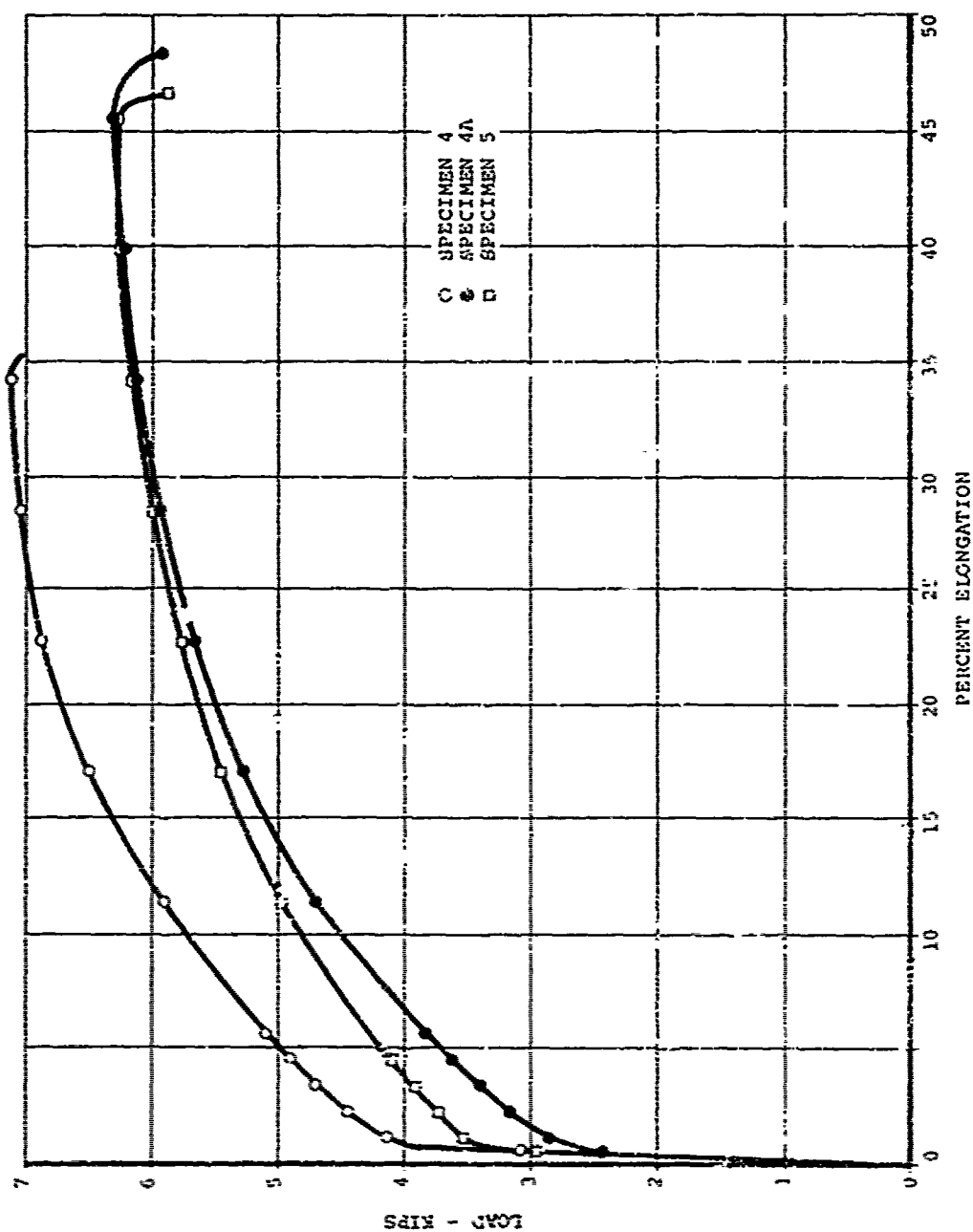
Figure 96. Load Versus Elongation - 0.750 In. x 0.028 In. Stainless Steel Tube.

134

values with those of the energy absorbers used in the dynamic
tests, the percentage elongation values should correspond
directly to the working length, not the overall length.

Figure 94 presents the load-deformation responses of the
sample tensile tubes corresponding to the lowest limit loa '
energy absorber. The intermediate and highest limit load
tensile tube load-deformation responses are shown respectively
in Figures 95 and 96.

4.3.1.2 Summary of Results: The two main lots of materials
tested proved to have consistent properties, which established
confidence in their dynamic performance. A third lot of mate-
rial intended for use for the higher force levels proved to be
totally unsatisfactory for this application. The tensile tube
had been sized for a force level of about 5,100 pounds, where-
as two tubes loaded to over 6,000 pounds and one loaded to
over 7,000 pounds with elongations considerably less than
those necessary for this application. These tubes were there-
fore replaced with tubes providing the desired characteristics.

4.3.2 SEAT STATIC TEST

4.3.2.1 Test Data: As there were three main objectives to
the static tests, there were also three parameters which were
of primary interest. The first of these was the stroking
force versus displacement curve for the energy-absorbing sys-
tem which is shown in Figure 97. The values obtained compare
readily with the results of the quality assurance tests and
represent a cross check of data acquired in the seat test con-
figuration with that acquired in the controlled conditions of
the laboratory.

The second parameter of interest was the rear frame support
load, which represents the highest reaction load in the struc-
ture of the seat. This is shown in Figure 98. The loads mea-
sured correspond to values expected as a result of the system
geometry.

The third parameter of interest was the restraint harness
anchor loads that counteract the load applied to the static
test body block. Anchor loads are illustrated in Figure 99.
The sum of the three loads at any one point on the abscissa
is roughly equal to the applied load.

Since the load was being applied to the seat structure in
1,000-pound increments, data reference points were formed,
enabling the development of the curves illustrated in this
section.

135
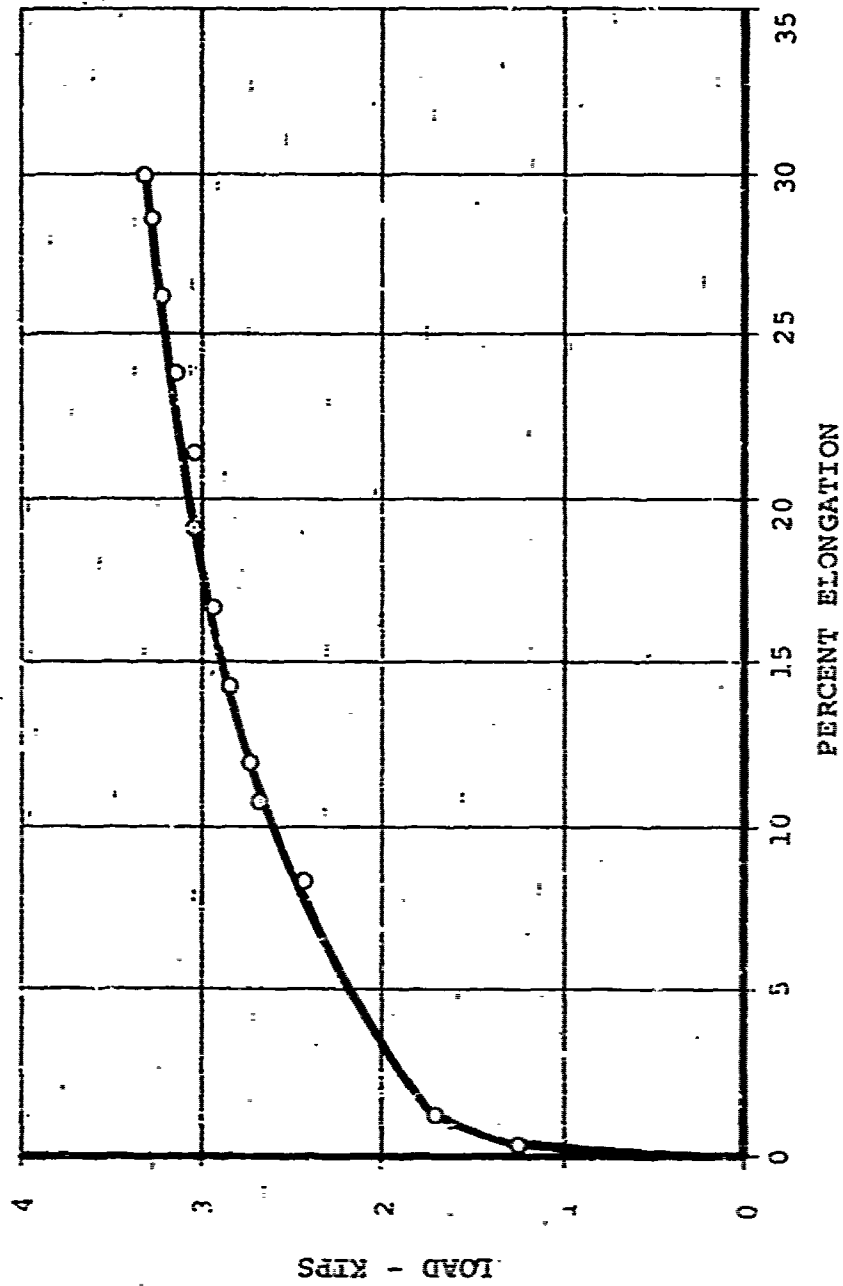
Figure 97. Seat Static Test Energy-Absorber Load Versus Elongation.

136
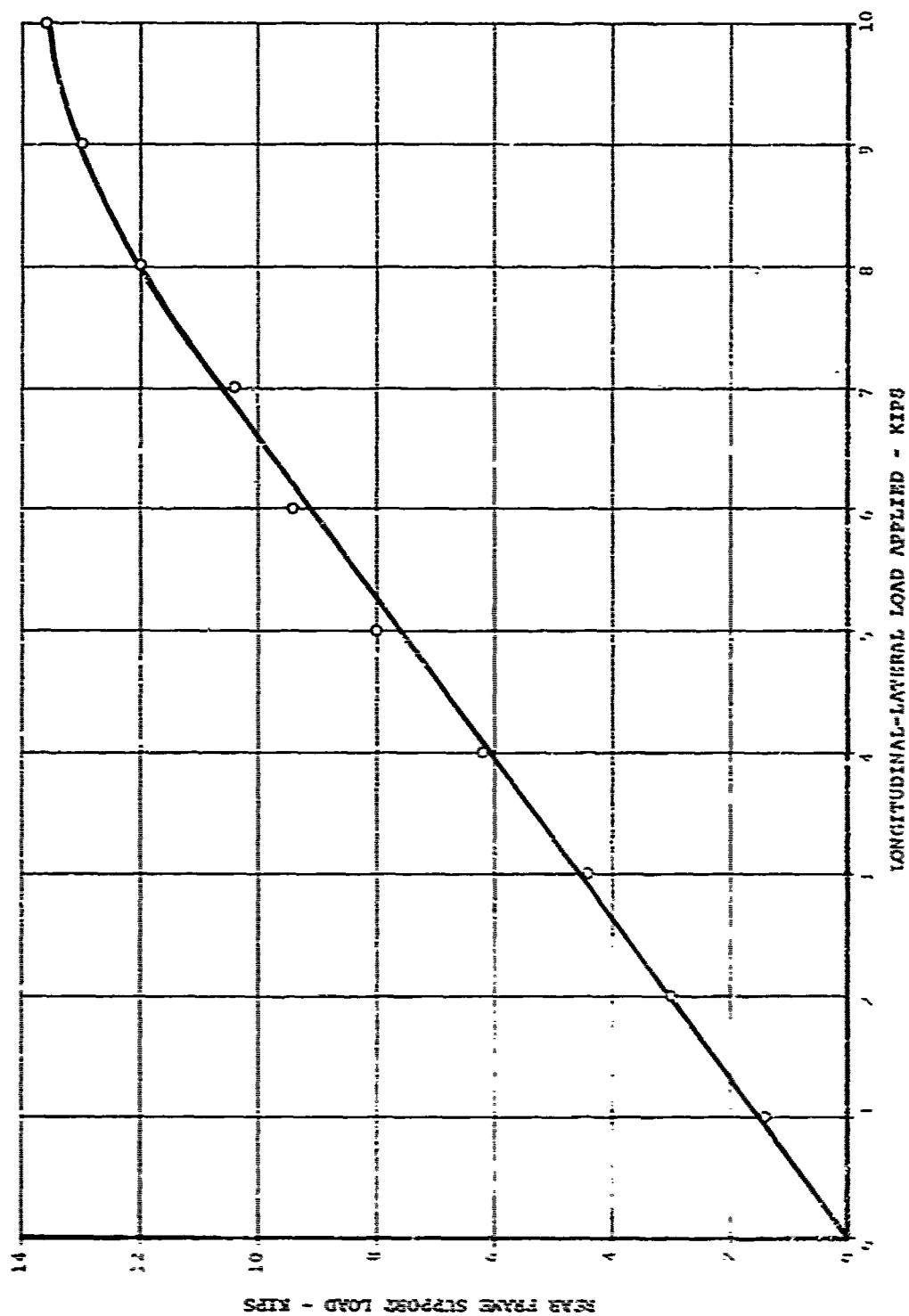
Figure 98. Static Test Rear Frame Support Load.

137
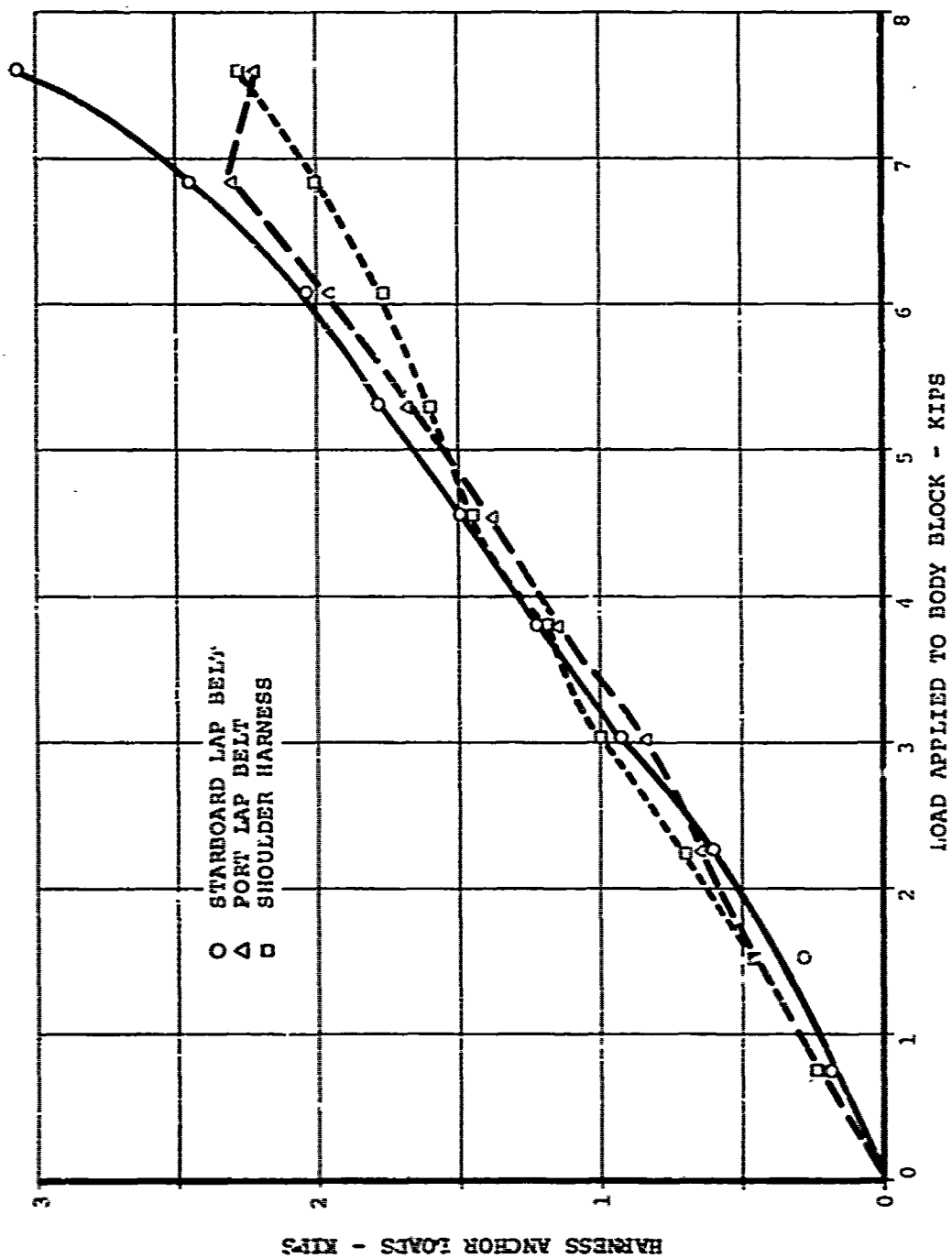
Figure 99. Static Test Restraint Harness Loads.

138

4.3.2.2 <u>Summary of Results</u>: At a point near attainment of the required maximum longitudinal-lateral load, the seat structure racked. The compressive loads exerted on the forward side of the structure caused the thin racking plates to warp and buckle, thereby providing little resistance to the racking forces. The saddle blocks attached to the forward guide tube did not hold tight enough to resist racking at the maximum load condition. This allowed the right-hand side of the support structure to slip down the guide tube 1.73 inches. After the displacement ceased, the load was again increased to the maximum value and the test was continued. As the seat stroked, a standing wave in the racking plate developed and rolled ahead of the lower bearing crossmember. However, only near the bottom of the stroke when the racking plate began to compact at the end of the guide frame was any additional resistance to stroking noted. Figure 100 illustrates the racked condition.

Figure 100.   Seat Support Structure After Racking.

The only other noteworthy observation was the loss of one of the energy-absorbing cables used with the higher percentile occupant. The cable pulled out of the swaged end fitting installed by the cable manufacturer.

4.3.3 SEAT DYNAMIC TESTS

The dynamic tests were run in three phases based on the orientation of the deceleration vector. The first phase consisted of five tests with the deceleration vector in the vertical direction with respect to the seat. The second phase consisted of three triaxial tests with the primary deceleration component in the vertical direction but with longitudinal and lateral components also included. The third phase consisted of two biaxial tests with the primary input in the longitudinal direction. The test results are presented in groups corresponding to the three testing orientations. Due to the quantity of data involved, all graphical results are presented in Appendix IV.

The sign convention used for all deceleration data is shown in Figure 101 and complies with the requirements specified in Reference 2. All load data is presented with tension loads positive (up), as standard convention dictates.

DIRECTION OF DECELERATIVE FORCE

VERTICAL

  Headward - Eyeballs down
  Tailward - Eyeballs up

TRANSVERSE

  Lateral Right - Eyeballs left
  Lateral Left - Eyeballs right
  Back to Chest - Eyeballs in
  Chest to Back - Eyeballs out

Note:

The decelerative force on the body acts in the same direction as the arrows.
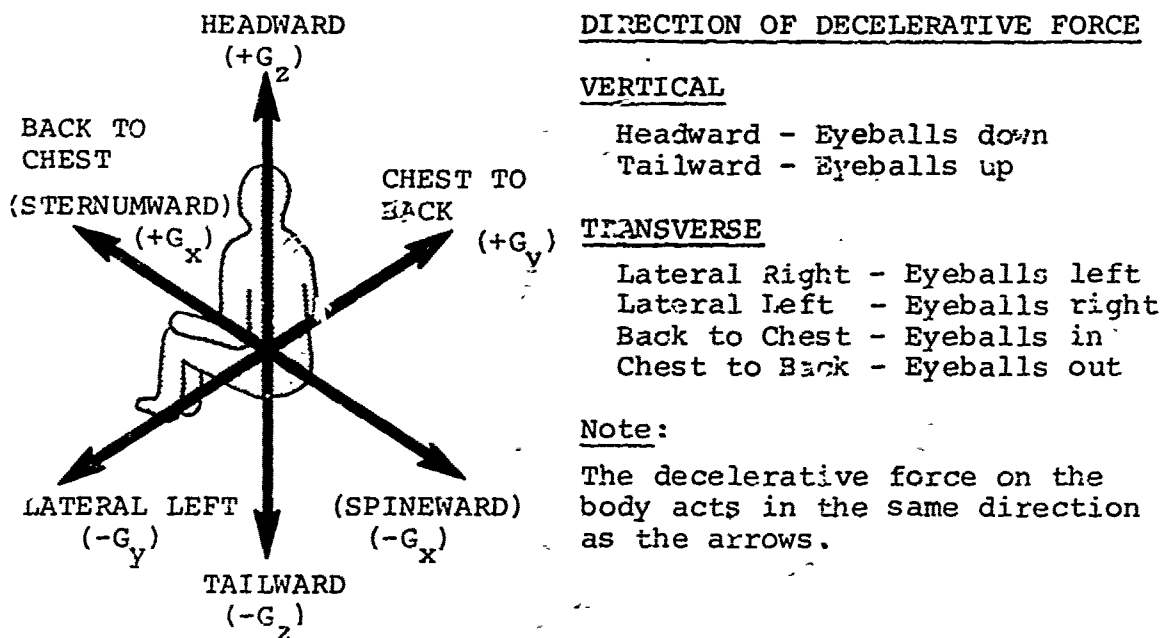
Figure 101. Direction of Decelerative Force on the Human Body.

Figure 102 represents a typical input deceleration pulse and shows the area used to determine the velocity change corresponding to that input pulse. The two smaller regions represent equal areas on opposite sides of the zero G axis which therefore have no effect on the overall velocity change. The entire sequence downstream in time from the primary pulse is caused by the drop cage actually lifting off the crushed honeycomb stack and reimpacting later in the sequence.
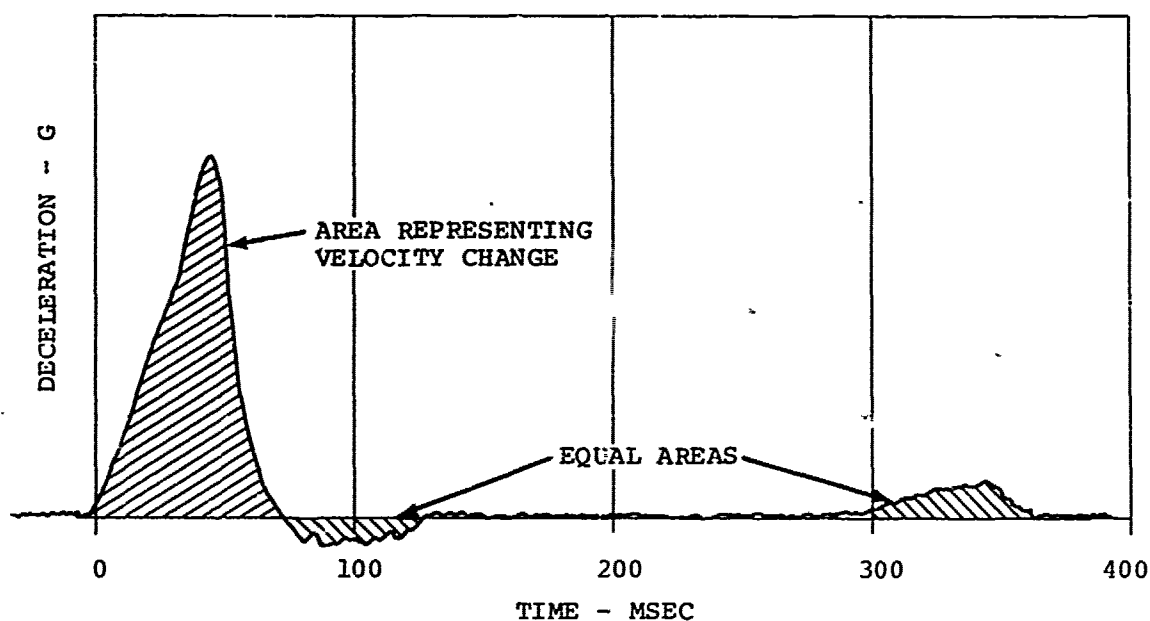
Figure 102. Typical Input Pulse.

The second small area is not shown in the data in Appendix IV, as it is not significant to the seat performance. The longer time span is shown here to clarify the actual configuration of the measured pulses.

4.3.3.1 Vertical Tests: The five vertical tests were all performed in a similar manner with the test installation setup as shown in Figure 103. The seat floor attachment tracks were mounted on the floor of the drop cage. The restraint system was cinched up firmly against the anthropomorphic dummy, and his initial position was duplicated from test to test. As the tests were performed in January 1971, the ambient temperatures ranged from 40° to 60°F, which had its most significant effect

141
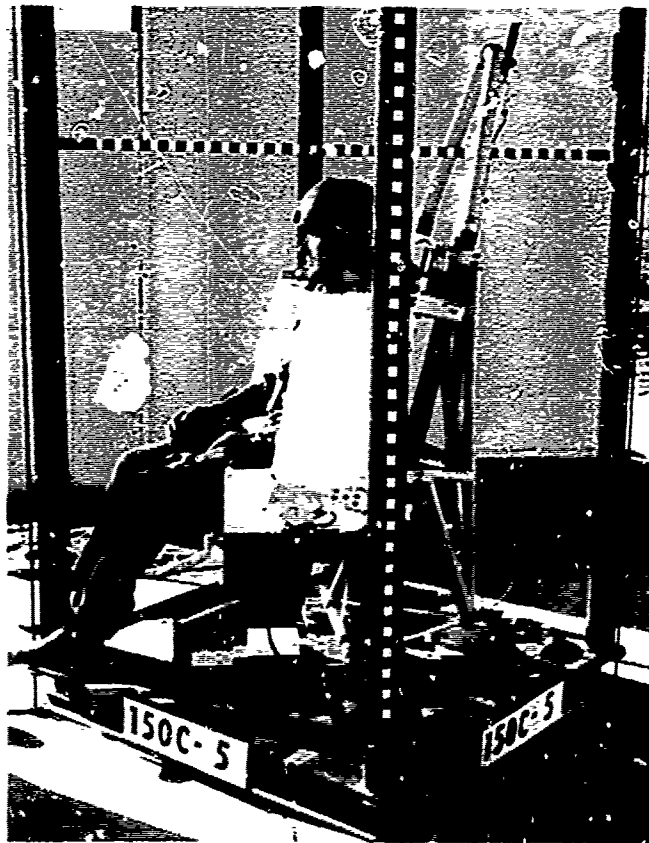
Figure 103. Vertical Test Configuration.

on the rate-sensitive cushions. Those portions of the cushions that were shaded were nearly rigid to the touch, whereas those portions exposed to direct sunlight were quite soft.

4.3.3.1.1 Overall Performance: There were no failures or malfunctions in the seating system, and no measurable deformations were noted in the support structures as revealed by a review of the high-speed photography. Seat bucket rebound was greater than would be tolerated in a production type crew seat because of the limited resistance of the long, slender tensile tube to buckling. This had negligible effect on the performance of the seat, as rebound was easily identifiable during data analysis. Figure 104 represents a posttest configuration typical of the vertical test series. The tensile tube energy absorber can be seen with a large bow and a sharp kink in it, both caused by rebound.

142

Figure 104. Vertical Posttest Configuration.

Due to a faulty transducer in the vertical chest cavity, verifiable data were not collected on any vertical test except Test 4. Longitudinal accelerations in the ches cavity are shown in Appendix IV with the other data. These were caused by the forward motion induced by the slope of the guide rails and the corresponding deceleration into the harness when the seat displacement in the longitudinal direction ceased.

4.3.3.1.2 Test 1A: The input pulse for Test 1A had a peak vertical deceleration of 25G and a velocity change of 38 fps. The seat bucket stroked 10 inches down the guide tubes with a corresponding limit load of 3,600 pounds. This load included the resistive force generated by two stainless steel, energy-absorbing cables. As the load was directed along the plane of the guide tubes, it consequently required correction to represent the vertical component of the load. The seat pan was subjected to a peak deceleration of 16.3G and the pelvis

143

experienced a peak deceleration of 17.8G, which indicates a minor overshoot.

All peak values and the corrections referred to previously are tabulated in Table XVII.

TABLE XVII. TEST DATA SUMMARY										
	Test Number									
Measurement	1	2	3	4	5	6	7	8	9	10
Input										
Resultant ΔV, fps	38.9	38.0	42.0	41.0	47.0	41.3	43.0	49.0	44.5	51.0
Z Axis ΔV, fps	38.0	38.0	42.0	41.0	47.0	36.0	38.5	42.5		
X Axis ΔV, fps						20.0	21.0	24.0		
Y Axis ΔV, fps						5.6	6.8	7.1		
Percentile Vertical Pulse	92.0	91.0	95.0	94.0	97.5	90	92	95.5		
Resultant Gp, G	25.0	37.1	42.8	39.0	51.6	28.5	42.8	43.5	20.0	26.5
Z Axis Gp, G	25.0	37.1	42.8	39.0	51.6	25.3	39.1	39.0		
X Axis Gp, G						14.3	20.0	21.4		
Y Axis.Gp, G						4.6	5.6	6.8		
Percentile Vertical Pulse	86.0	93.0	94.0	93.5	96.0	96.5	93.0	93.0		
Resultant Duration, Sec										
Rate of Onset, G/Sec	433	759	1111	800	1375	458	878	851	168	300
Response										
Seat Pan Gp, Z, G	16.3	22.1	20.8	17.2	24.9	17.6	25.8	25.0	7.0	17.3
Seat Pan Gp, X, G						14.3	20.6	18.6	19.6	30.8
Seat Pan Gp, Y, G						8.6	9.0	10.9	12.4	16.1
Seat Pan Stroke, In.	10.0	10.0	11.4	13.9	13.2	11.5	11.5	12.5		
Corrected Vertical Seat Pan Stroke	9.7	9.7	11.1	13.5	12.9	11.2	11.2	12.2		
Pelvis Gp, Z, G	17.8	19.0	24.4	15.0	23.6			35.0	22.4	27.2
Pelvis Gp, X, G		20.0	23.8	18.4	30.1	14.4	18.7	21.0	19.4	28.3
Pelvis Gp, Y, G						5.8	13.2	14.0	17.0	16.0
Chest Gp, Z, G				21.9		17.4	27.7	40.0	22.8	10.0
Chest Gp, X, G		8.5	12.8	9.7	16.6	17.3	26.0	25.6	23.6	31.0
Chest Gp, Y, G								9.6	15.6	16.8
Loads (Maximum)										
Energy Absorber Designation*	2**	B	C**	3**	D**	6**	A	E**	7**	7**
Energy Absorber Total Limit Load, Lb	3600	4860	5210	4100	5550	3720	4850	5280	1450	1580
Corrected Vertical Limit Load, Lb	3695	4988	5347	4208	5696	3818	4977	5419	1488	1622
Shoulder Strap Load, Lb						380	810	790	1050	2470
Lap Belt Port, Lb						825	790	1240	1990	930
Lap Belt Starboard, Lb							340	560	640	2230
Negative G Strap, Lb						250	410	400	2230	

*Energy-absorber designations correspond to those listed in Figures 94, 95, and 96.
**Includes 2 cables.

144

4.3.3.1.3 Test 2: The input pulse for Test 2 had a peak deceleration of 37.1G and a velocity change of 38 fps. The seat bucket stroked 10 inches down the guide tubes with a corresponding limit load of 4,860 pounds. Vertical seat pan deceleration reached 22.1G, while the pelvis reached only 19.0G.

4.3.3.1.4 Test 3: The peak input deceleration for Test 3 reached 42.8G, and the velocity change was 42 fps. Seat bucket stroke down the guide tubes reached 11.4 inches with a limit load of 5,210 pounds, which included the load from two energy-absorbing cables. Seat pan deceleration peaked at 20.8G, and the pelvis reached 24.4G.

4.3.3.1.5 Test 4: The input pulse for Test 4 had a peak deceleration of 39G and a velocity change of 41 fps. The seat bucket stroked 13.9 inches down the guide tubes with a limit load of 4,100 pounds. The seat pan reached a peak deceleration of 17.2G, and the pelvis reached a peak of 18.4G. Vertical chest deceleration peaked at 21.9G.

4.3.3.1.6 Test 5: Test 5 had the strongest input pulse, with a peak deceleration of 51.6G and a velocity change of 47.0 fps. The seat bucket responded with a 13.2-inch stroke down the guide tubes, and the energy absorber, with the aid of two cables, provided a limit load of 5,550 pounds. With the high limit load, the seat pan experienced a 24.9G peak deceleration but the pelvis reached only 23.6G.

4.3.3.2 Triaxial Tests: The three triaxial tests were all performed in a similar manner with the overall test configuration as shown in Figure 105. The seat was attached to the special triaxial mounting fixture in the drop cage. This mount provided a rigid base to support the seat in a 10-degree lateral (roll) and 30-degree longitudinal (pitch) tilt as established in References 2 and 5. The three triaxial tests were designed to establish the crashworthiness and performance of the seat system in a typical crash orientation involving a large vertical component with lateral and longitudinal loads superimposed. Tests 6 and 7 had the same vertical input decelerations as Tests 1 and 2, respectively, thereby providing a comparison of the seat's vertical performance under purely vertical loading with the effect of triaxial loading on vertical performance.

4.3.3.2.1 Overall Performance: There were no malfunctions or failures in the seat structure during the triaxial tests, and no measurable deformations were noted in the support structures as revealed by a review of the high-speed photography. Figure 106 shows a posttest configuration, typical of the triaxial tests. Unfortunately, there was one malfunction that

145

Figure 105. Triaxial Test Configuration.
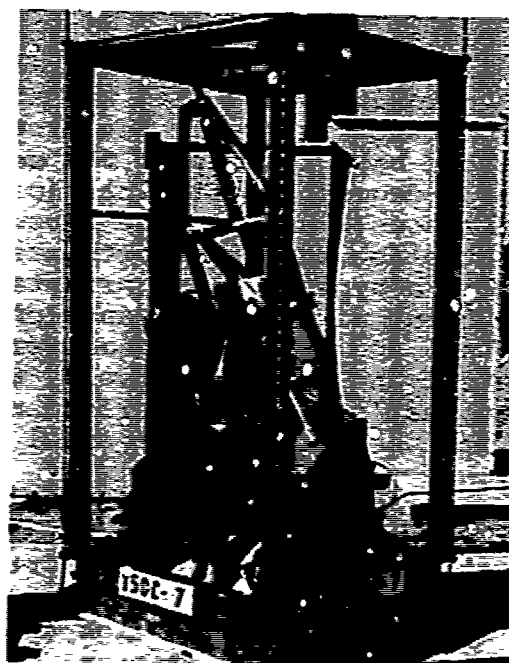
Figure 106. Triaxial Posttest Configuration.

146

eliminated usable information from the vertical accelerometer in the pelvis (due to a limitation of the pelvic structure simulation). The corner of the box section making up the lower pelvic structure of the dummy penetrated the seat cushion and impacted the seat pan. Figure 107 shows how the outline of the box structure was impressed on the cover material without actually puncturing it.
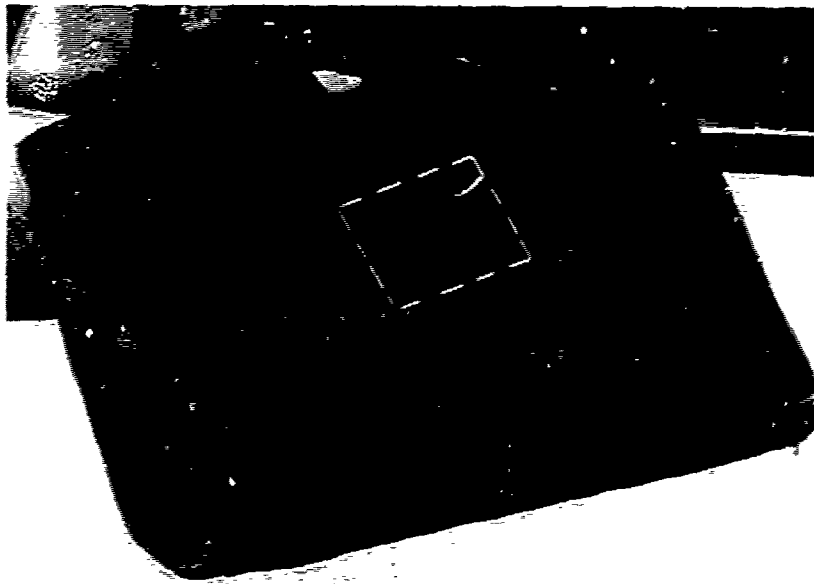
Figure 107. Box Structure Impression on
Cover Material.

Figure 108 shows the break in the cushion material that was generated. The "hammer blow" caused the accelerometer to be overdriven. making the remaining portion of the trace highly suspect.

4.3.3.2.2 Test 6: The triaxial input pulse for Test 6 had a peak deceleration of 28.5G and a velocity change of 41.3 fps. The three component decelerations and corresponding velocity changes oriented in the coordinate system of the seat were:

147
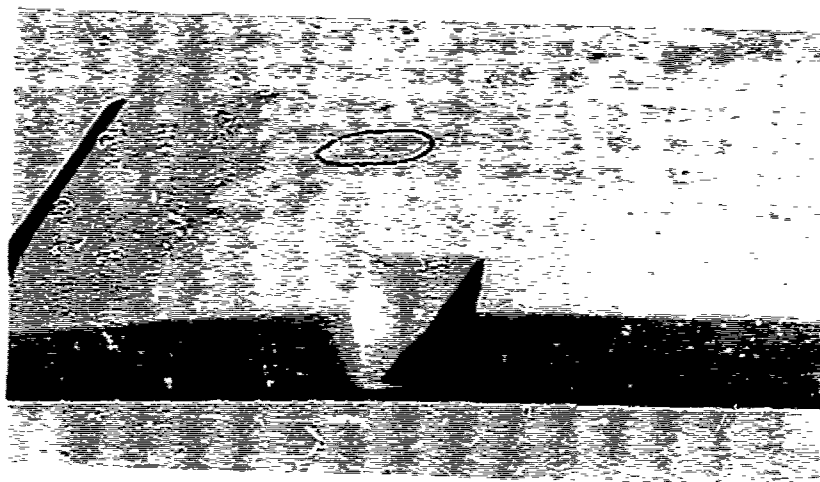
Overall

Closeup

Figure 108. Punctured Cushion Material.

Axis	G Peak	ΔV (fps)
X (longitudinal)	14.3	20.0
Y (lateral)	4.6	5.6
Z (vertical)	25.3	36.0

The seat bucket stroked 11.5 inches down the guide tubes, and the limit load reached 3720 pounds with the aid of two energy-absorbing cables. The vertical component of the seat pan deceleration reached 17.6G. This was close to the vertical chest deceleration peak of 17.4G.

4.3.3.2.3 Test 7: The resultant peak input deceleration for Test 7 was 42.8G, and the velocity change was 43.0 fps. The three component decelerations and velocity changes were:

Axis	G Peak	ΔV (fps)
X	20.0	21.0
Y	5.6	6.8
Z	39.1	38.5

Seat bucket stroke down the guide tubes reached 11.5 inches with a limit load of 4,850 pounds. Vertical seat pan deceleration peaked at 25.8G, and the vertical chest deceleration peaked at 27.7G.

4.3.3.2.4 Test 8: The resultant input pulse for Test 8 had a peak deceleration of 43.5G, and the corresponding velocity change for this pulse was 49.0 fps. The component decelerations and velocity changes in the seat coordinate system were:

Axis	G Peak	ΔV (fps)
X	21.4	24.0
Y	6.8	7.1
Z	39.0	42.5

The seat bucket traveled down the guide tubes 12.5 inches. The limit load reached 5,280 pounds with the aid of two energy-absorbing cables. The peak vertical seat pan deceleration was 25.0G, while the chest peaked at 40.0G in the vertical direction.

149

4.3.3.3 **Biaxial Tests:** The two biaxial tests were performed in a similar manner and provided longitudinal-lateral loading of the seat systems. Figure 109 shows the basic test configuration. The seat was mounted on the acceleration sled with its longitudinal axis 30 degrees off the resultant velocity input vector direction. The two biaxial tests were designed to establish the crashworthiness and performance of the seat system in a typical severe crash orientation involving a large longitudinal component with a lateral component superimposed.
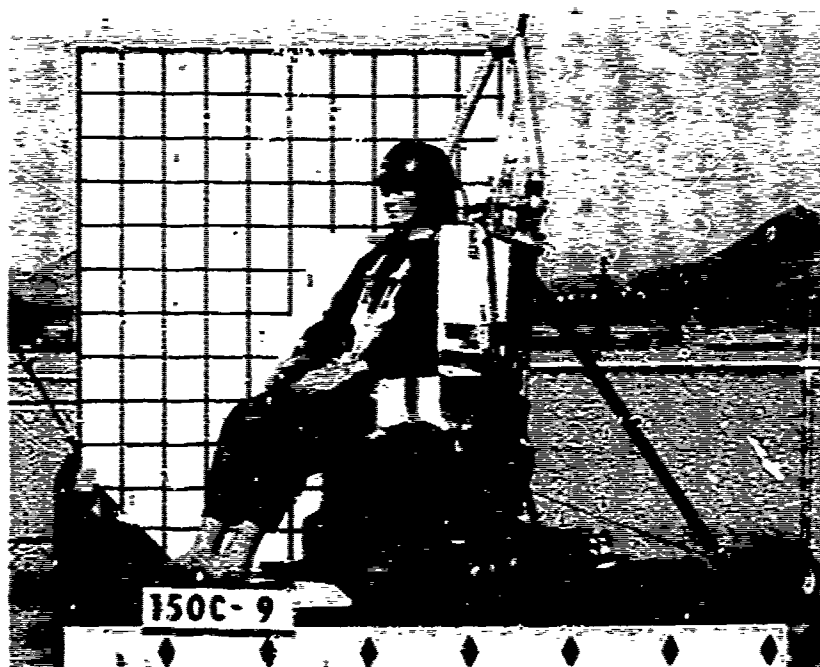
Figure 109. Biaxial Test Configuration.

With the seat in this orientation, the primary energy absorber was not expected to stroke. Seat system performance was therefore confined to surviving the test without catastrophic failure and providing restraint for the seat occupant. However, any deformation resulting from the input pulse would lower the loading by absorbing energy.

4.3.3.3.1 **Overall Performance:** The primary energy absorber did not stroke, although loads approached values near the initial yield point of the low-limit-load energy absorber chosen for these tests. The seat support structure deformed

150

elastically in Test 9, but deformed plastically in Test 10.
Figure 110 shows the deformation of the lower support struc-
ture as a result of the racking motion in Test 10. The perma-
nent deformation was provided by the saddle blocks on the right
side slipping down the guide tube as they had during the com-
bined static test. Primary bending occurred at the lower for-
ward crossmember through a 1.50-inch-diameter solid section
adjacent to each forward support track attachment fitting,
resulting in appreciable energy absorption.

Figure 110.   Plastic Deformation of the Lower
Support Structure Due to Racking.

Observations of the high-speed film indicated that in the
longitudinal-lateral crash, the occupant was endangered by the
fixed side panels on the armored bucket because of the ten-
dency to throw his arms out and back against the side panels
during rebound. When the upper arms contacted the leading
edge of the panels, there appeared to be enough leverage to
break both arms at the elbows or above. Figure 111 illus-
trates the posttest configuration with the endangering arm
position.

151
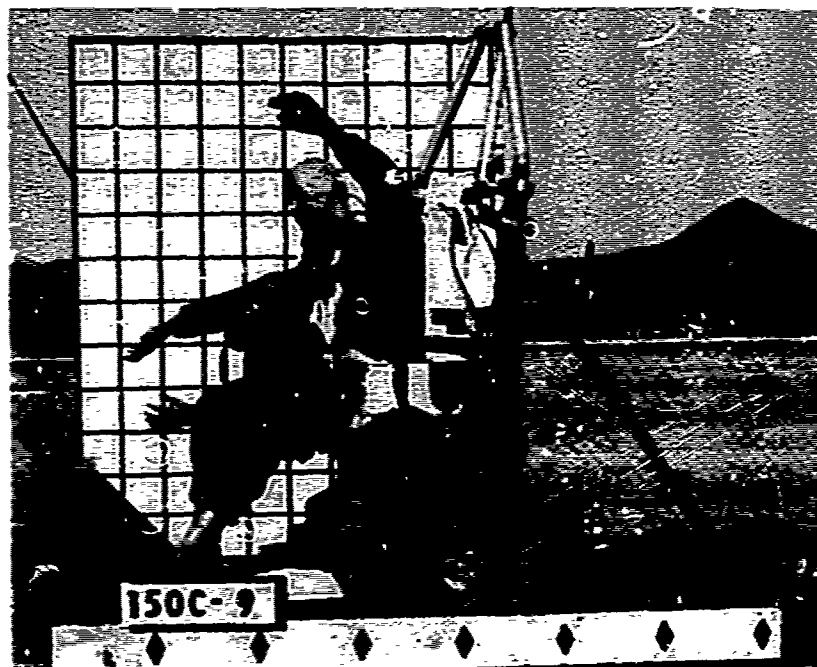
Figure 111. Biaxial Posttest Configuration.

4.3.3.3.2 Test 9: The resultant input pulse peak decelera-
tion for Test 9 was 20.0G, and the velocity change was 44.5
fps. The peak longitudinal seat pan deceleration was 19.6G.
The pelvis reached a peak deceleration of 19.4G in the longi-
tudinal direction but reached 22.4G in the vertical direction.
The fact that there was no measurable displacement in the ver-
tical direction indicated that a significant portion of the
acceleration was due to a rotational motion related to a minor
degree of submarining underneath the lap belt. The chest ex-
perienced a similar phenomenon, with a longitudinal peak de-
celeration of 23.6G and a 22.8G peak in the vertical direction.
This high vertical acceleration was due to an inertia reel
failure. After initially loading to 1,050 pounds, the reel
released and allowed the occupant to rotate forward with mo-
tion limited by the fully extended inertia reel strap, there-
by causing the high peak value. Figure 112 shows the posttest
configuration after rebound. At this point, the strap could
be moved freely in and out of the inertia reel. Section 5.4.4
covers this failure in more detail.

4.3.3.3.3 Test 10: The resultant input pulse in Test 10 had
a peak deceleration of 26.5G and a velocity change of 51.0 fps.
Longitudinal seat pan deceleration reached a peak of 39.8G.

152

Figure 112. Extended Inertia Reel Strap
After Rebound.

Pelvic deceleration reached 28.3G longitudinally and 27.2G
vertically. Chest deceleration reached 21.0G longitudinally
but only 10.0G vertically as a result of the inertia reel's
resisting the upper torso load properly.

4.3.3.4 Summary of Results: Table XVII summarizes the peak
values of interest from the dynamic test series. Also tabu-
lated are the equivalent percentile survivable crash pulses as
defined in Reference 2. Other values tabulated are input
pulse rates of onset and restraint system peak loads. Head
deceleration was measured to complete the data spectrum; how-
ever, it has little relevance to the evaluation of the seat
energy-absorbing mechanism and was therefore not included in
this report.

The characteristic wave shape of the seat pan deceleration
trace was consistent with that produced by the dynamic anal-
ysis. The notch in the trace immediately following the ini-
tial spike was established as being caused by the dynamic
reaction between the dummy and the seat pan. Loading by the
pelvis caused a momentary decrease in deceleration of the seat
pan. This, then, corresponded to a deceleration spike of the

153

dummy pelvis occurring at the same point in time. Comparison of the pelvis and seat pan traces shown in Appendix IV for each test illustrates this.

A close match of the load-deformation responses of the tensile tube energy absorbers between static and dynamic loading conditions was also revealed. By taking the peak limit loads and the corresponding seat pan strokes (measured, not corrected) and converting the stroke length to percentage elongation, the comparison can be made. The working length of the tensile tube was 41.5 inches. Correlation for these tests was made using the tensile tube limit loads and indicates that dynamic limit loads are typically equal to or up to 8 percent greater than corresponding static loads. Peak loads exerted by the complete energy absorbers and the corresponding corrected limit loads in the vertical direction are also shown in Table XVII. Note that the values presented for all tests except 2 and 7 include the resistive force of two stainless steel cables, which typically contribute about 300 pounds at these stroke lengths.

The paper honeycomb pad shown in Figure 113, which was used to keep the dummy's feet from being damaged during impact, reveals the effect of dissipating the energy stored in the lower legs.

Figure 113. Effect of Energy Dissipation of Lower Legs.

154

Roping of the lap belt webbing and gouging of the buckle into
the dummy's inner thighs were common problems throughout the
dynamic test series, as illustrated in Figure 114. This prob-
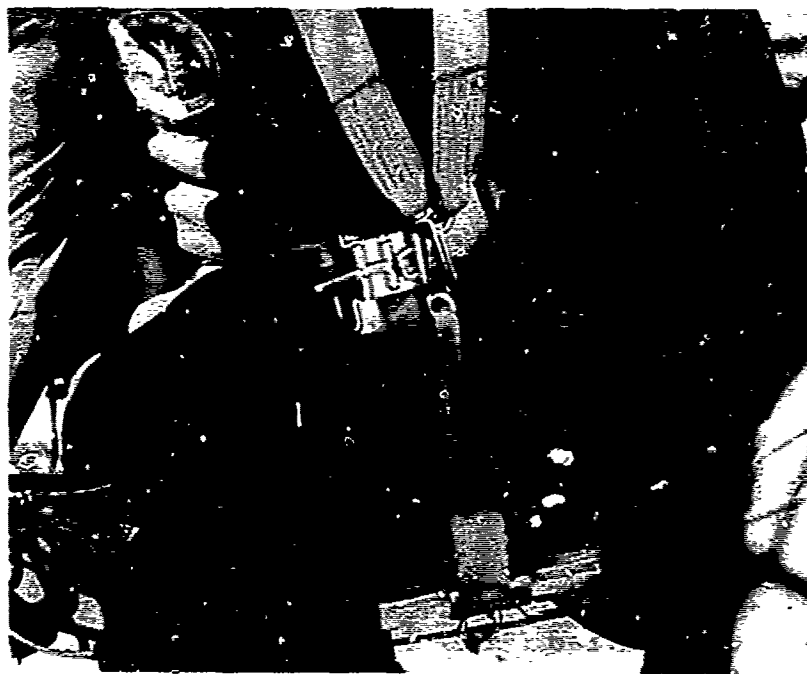lem is discussed further in Section 5.4.4.

Figure 114. Example of Lap Belt Roping and
Buckle Gouging.

CHAPTER 5

DISCUSSION OF RESULTS

5.1 INTRODUCTION

This section includes a discussion of the experimental seat performance together with the analysis and implications of the data measured. The information is presented under four major headings:

1. Overall Experimental Seat Performance

2. Vertical Crash Protection

3. Component Performance

4. Projected Production Seat Design

5.2 OVERALL EXPERIMENTAL SEAT PERFORMANCE

The experimental seat performed exceptionally well. The seat withstood the dynamic crash environments involving vertical, triaxial, and biaxial dynamic loading up to and including the 95th percentile survivable crash. Only a few minor component failures occurred during testing, enabling the full matrix of dynamic testing to be conducted. The lateral, longitudinal, and combined strength of the seat were verified. The desired vertical energy management data needed to establish design criteria were acquired, thus fulfilling the primary objectives of the program.

5.3 VERTICAL CRASH PROTECTION

5.3.1 ACHIEVEMENT OF PROTECTION IN TESTS

The technique described in the following paragraphs was estab-lished to check whether or not the seat maintained tolerable loads on the occupant during the dynamic tests. First, the human tolerance curve presented in Reference 5 and shown in Figure 115 was accepted as the criterion against which judge-ments would be made. Next, the equation for the part of the tolerance curve having a negative slope was written as

$$\ln G_t = m \ln t + \ln a \qquad\qquad (14)$$

where G_t = tolerable deceleration, G

t = time duration, sec

156
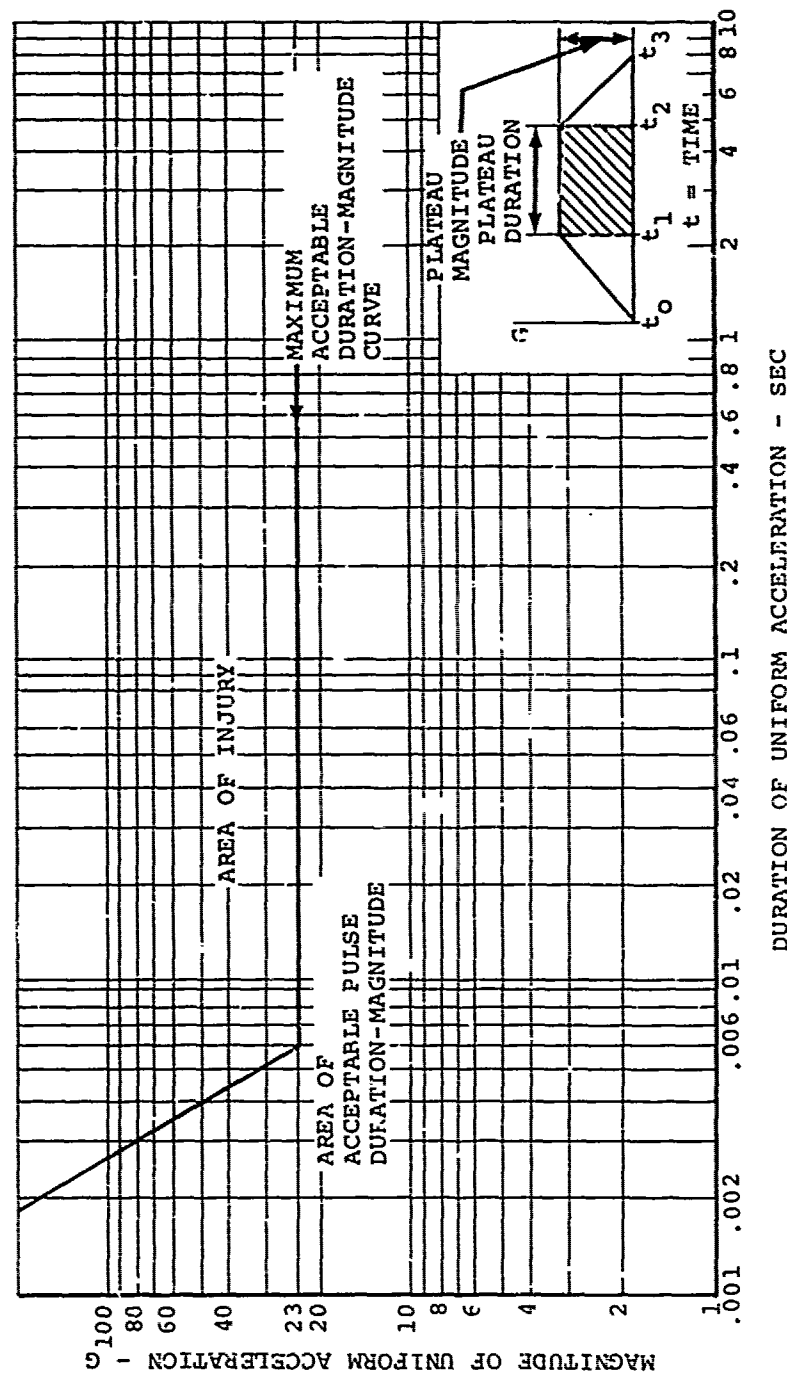
Figure 115. Maximum Acceptable Vertical Pulse Acceleration and Duration
Values (Reference 5).

m = slope of the ln-ln curve

a = constant

and, specifically,

$$\ln G_t = -1.71 \ln t + \ln 0.00345 \tag{15}$$

The curve of tolerable deceleration in G versus time in seconds
was computed and plotted in Figure 116. Since the human toler-
ance curve used as criterion was developed from seat decelera-
tion data, the tolerance check was conducted for the measured
seat deceleration data.
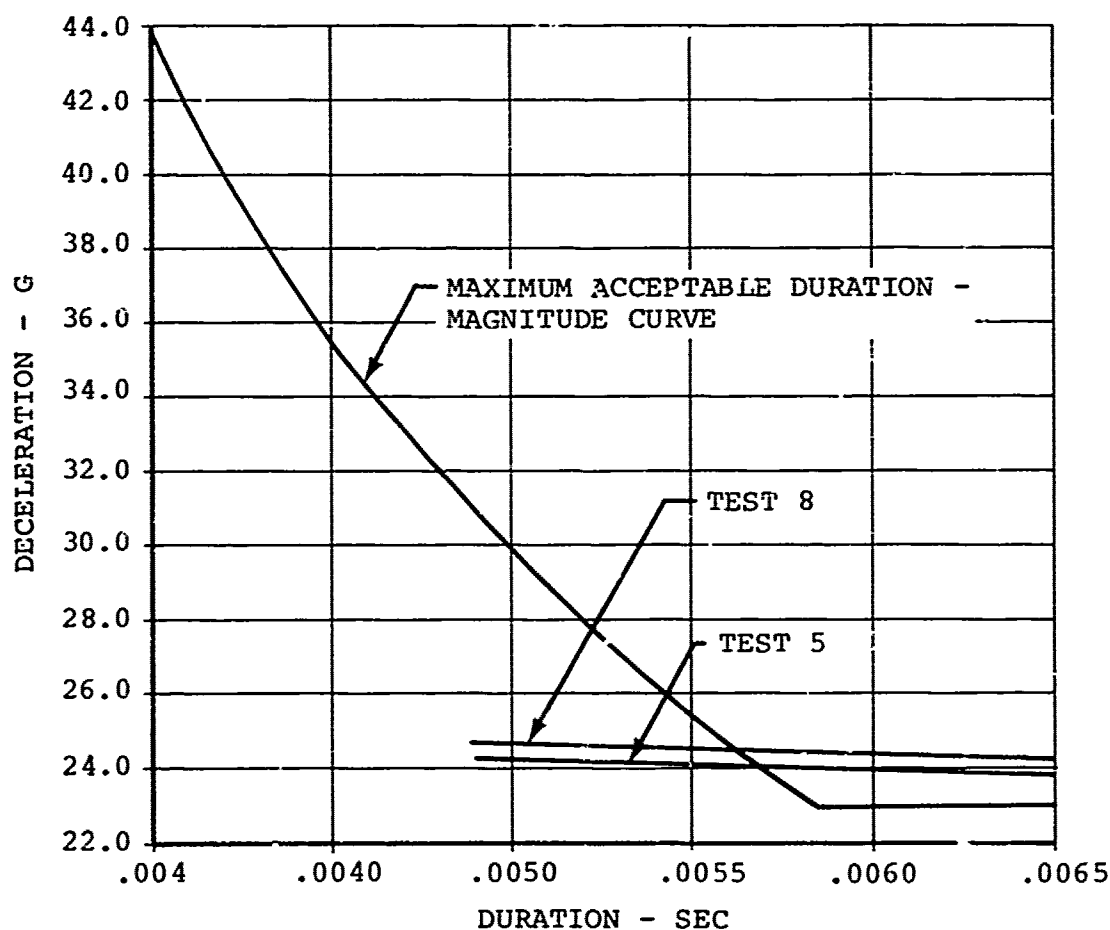
Figure 116. Control Curve, Human Tolerance to Decelerative
Loading Versus Duration.

158

The tolerance check was made by progressively measuring the
duration of the deceleration trace at a specific G level as
shown below and plotting the results on the control curve of
Figure 116.
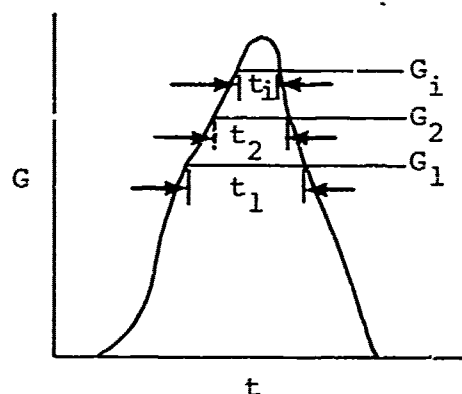
Only tests 5 and 8 exceeded the human tolerance limits, and
then only by about 1G. Both of these pulses exceeded the 95th
percentile vertical velocity change pulse: 97.5 and 95.5 per-
centile, respectively. Both seats had energy absorbers whose
resultant limit loads exceeded the recommended value of 4,550
(explained in the next section), 5,696, and 5,419 pounds, re-
spectively. Both seats stroked slightly in excess of 12
inches: 12.9 and 12.2 inches, respectively.

5.3.2 ENERGY-ABSORBING STROKE

Table XVIII presents the amount of seat stroke measured during
each test. Since the seat stroke was measured with respect to
distance down the guide tubes which were at an angle of 13
degrees to the vertical, the strokes were decreased by the
cosine of the angle to attain the purely vertical stroke dis-
tance. The corrected vertical strokes are tabulated in the
last column in Table XVIII.

Also included in the table is a tabulation of the percentile
survivable crash achieved during the test.

It is apparent from the curves shown in Chapter 1 of Reference
2 that the percentile survivable crash can be determined in
two ways: maximum deceleration (or peak G) and change in
velocity.

159

TABLE XVIII. SEAT STROKE AS A FUNCTION OF TEST NUMBER				
Test No.	Corrected Vertical Limit Load (lb)	Measured Stroke (in.)	Vertical Stroke (in.)	Percentile Vertical Pulse*
1	3,695	10.0	9.7	92.0
2	4,988	10.0	9.7	92.0
3	5,347	11.4	11.1	95.0
4	4,208	13.9	13.5	94.0
5	5,696	13.2	12.9	97.5
6	3,818	11.5	11.2	90.0
7	4,977	11.5	11.2	92.0
8	5,419	12.5	12.2	95.5

*Based on change in velocity.

Since seat stroke is a function of energy content, once the limit load of the energy-absorbing system has been exceeded, percentile pulse based on velocity change was used in this analysis.

Figure 117 shows curves of predicted and measured stroke plotted as a function of percentile survivable pulse based on velocity change. The dashed lines represent predictions for various limit loads. Points represent measured data and are identified by both limit load and test number. Data from tests 2, 4, and 7 (data produced by tests with limit loads in the range of 4,208 to 4,988 pounds) are shown within the shaded band. The shaded band is representative of the resolution of the data and indicates the data trend for limit loads in this range.

The data indicate that the test pulses exceeding the 93rd percentile required more than 12 inches of stroke when equipped with energy absorbers of limit loads in the range of 4,200 to 5,000 pounds. They also showed that if the seat were designed so that energy-absorbing stroke length were added when the seat was adjusted up, then sufficient stroke length would be available from the neutral position (14-1/2 inches) to absorb the energy of a 95th percentile pulse.
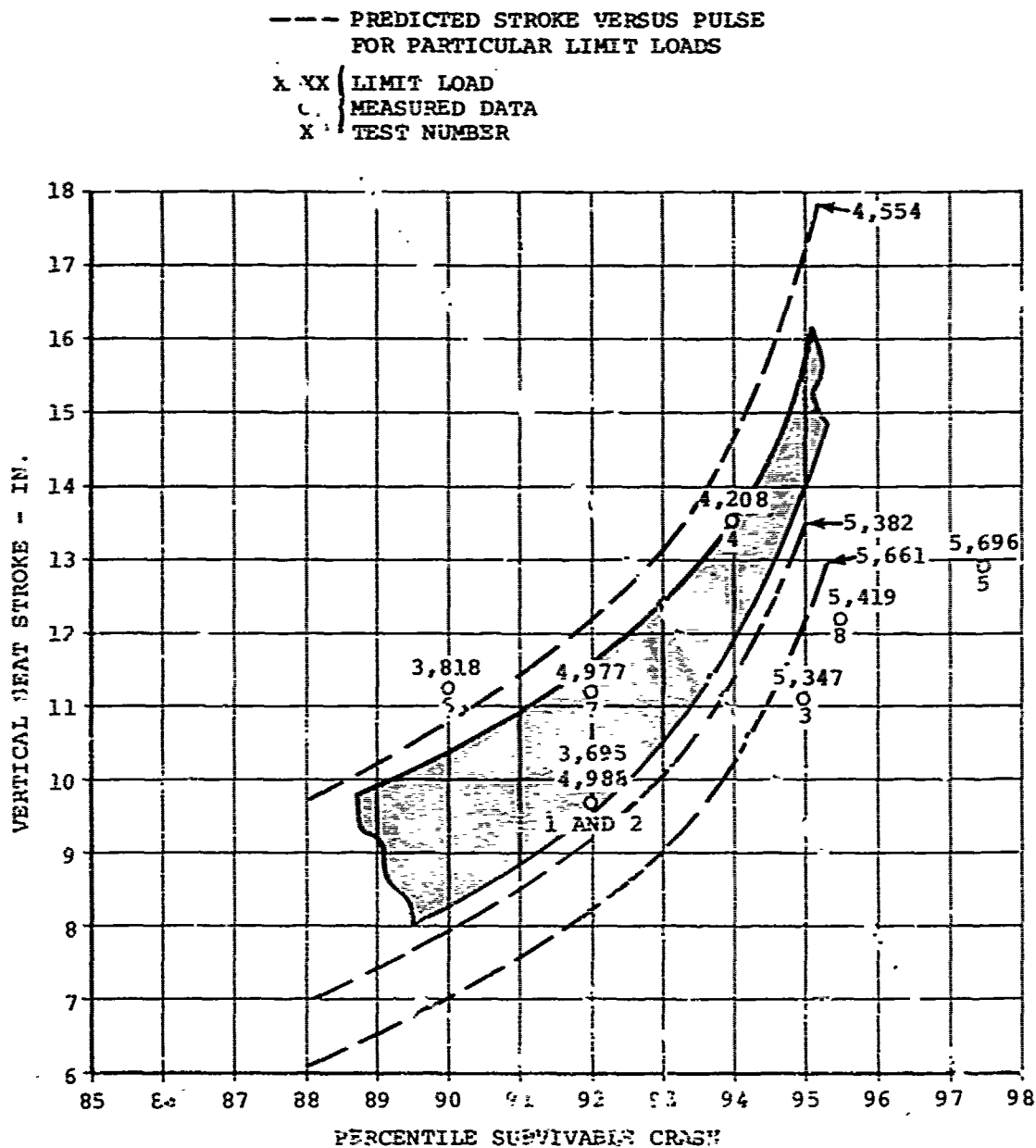
Figure 117. Predicted and Measured Vertical Seat Stroke Versus Percentile Survivable Crash (Based on Velocity Change).

5.3.3 LIMIT LOAD AND OCCUPANT PROTECTION

The force resisting the vertical movement of the seat was re-
quired to accomplish this analysis. Since the guide tubes
angled backward at a 13-degree angle from vertical and since
the energy-absorbing device was essentially parallel to these
guide tubes, the energy-absorbing force was applied at an
angle to the vertical. Consequently, the vertical movement of
the seat was resisted by a load in excess of the energy-
absorber limit load. In order to determine the correction
factor, the equations of equilibrium were written and solved.
Friction was ignored in the analysis as the system was essen-
tially friction free. The movable part of the seat rode on
rollers down the guide tubes and, since no deformation of the
hard, anodized, coated guide tube surface was noted, rolling
friction could be assumed to be insignificant. Further, since
the rollers rotated on needle bearings which have very low
friction, bearing friction was assumed to be insignificant.
No racking was noticed in the frame during the vertical or
triaxial pulses and, consequently, it was assumed safe to con-
sider friction as being insignificant in the analysis to de-
termine a resistive force to vertical movement.
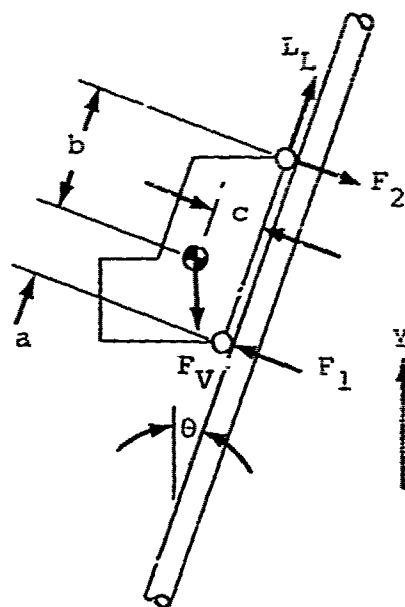
LEGEND

L_L = ENERGY ABSORBER LIMIT
LOAD

F_V = VERTICAL INERTIAL
FORCE

F_2 = TOTAL TOP BEARING
FORCE

F_1 = TOTAL BOTTOM BEARING
FORCE

θ = GUIDE TUBE ANGLE

a, b, c = DIMENSIONS

Referring to the sketch above and summing forces in the Y
direction yielded

$$\sum F_Y = 0 \tag{16}$$

$$-F_Y + F_1 \sin\theta + L_L \cos\theta - F_2 \sin\theta = 0 \tag{17}$$

Summing forces in the X direction yielded

$$\sum F_X = 0 \tag{18}$$

$$-F_1 \cos\theta + L_L \sin\theta + F_2 \cos\theta = 0 \tag{19}$$

Summing moments about the center of gravity yielded

$$\sum M_{CG} = 0 \tag{20}$$

$$F_2 b - L_L c + F_1 a = 0 \tag{21}$$

Simultaneous solution and simplification yielded

$$F_Y = \frac{L_L}{\cos\theta} \tag{22}$$

which indicated that the force resisting vertical movement of
the seat exceeded the limit load of the energy-absorbing de-
vice by the reciprocal of the cosine of the guide tube orien-
tation. The peak force resisting the vertical movement of the
seat was computed for each test and tabulated in Table XIX.

Figure 118 shows peak deceleration data for chest, pelvis, and
seat bucket plotted as a function of the peak limit load for
both vertical and triaxial loading. The circles represent the
deceleration of the movable seat bucket; the open circles
represent the data for the purely vertical pulses, while the
solid circles represent the data from the triaxial tests. The
solid line represents the correlation of peak measured decel-
eration of the seat bucket with peak limit loads. It can be
seen that this curve also correlated quite well with the
pelvic data.

A dashed line was plotted through the solid circles and repre-
sents the correlation of seat bucket deceleration during the
triaxial test pulses. It can be seen that this line lies
about 3G above the data measured for the purely vertical direc-
tion. A trend line made up of long, continuous sections inter-
spread with two dashes has also been plotted on the curve. It
represents the theoretical vertical prediction presented pre-
viously in Chapter 3. It correlates extremely well with the
vertical data measured in the triaxial test pulses.

163

TABLE XIX.	FORCE RESISTING VERTICAL STROKING OF SEAT AS A FUNCTION OF TEST NUMBER	
Test No.	Measured Limit Load (lb)	Force Resisting Vertical Movement (lb)
1	3,600	3,695
2	4,860	4,988
3	5,210	5,347
4	4,100	4,208
5	5,550	5,696
6	3,720	3,818
7	4,850	4,977
8	5,280	5,419

Assuming 23G as the maximum tolerable human deceleration limit in the vertical direction and further assuming that vertical protection should be provided for the combined loading pulse, the curve was used to establish the limit load to provide this protection. Extending a horizontal line from 23G on the ordinate of Figure 113 to the correlation line representing the triaxial test data and then dropping a vertical line to the abscissa produced intersection at a 4,650-pound peak limit load.

The foregoing analysis indicated that the peak deceleration of a 95th percentile occupant of this integral armored crew seat could be maintained below 23G if the limit load, including influences of energy absorber, friction, binding, racking, etc., was on the order of 4,650 pounds.

Using the effective weight of the occupant and the weight of the movable section of this particular seat, a limit load factor was computed from which other adequate options of load limiters and crashworthy crew seats may be extrapolated. Using the effective weight of a 95th percentile occupant, normally computed as 80 percent of the body weight plus clothes that are evenly distributed over the body plus 100 percent of all items carried by the upper body, yielded an effective
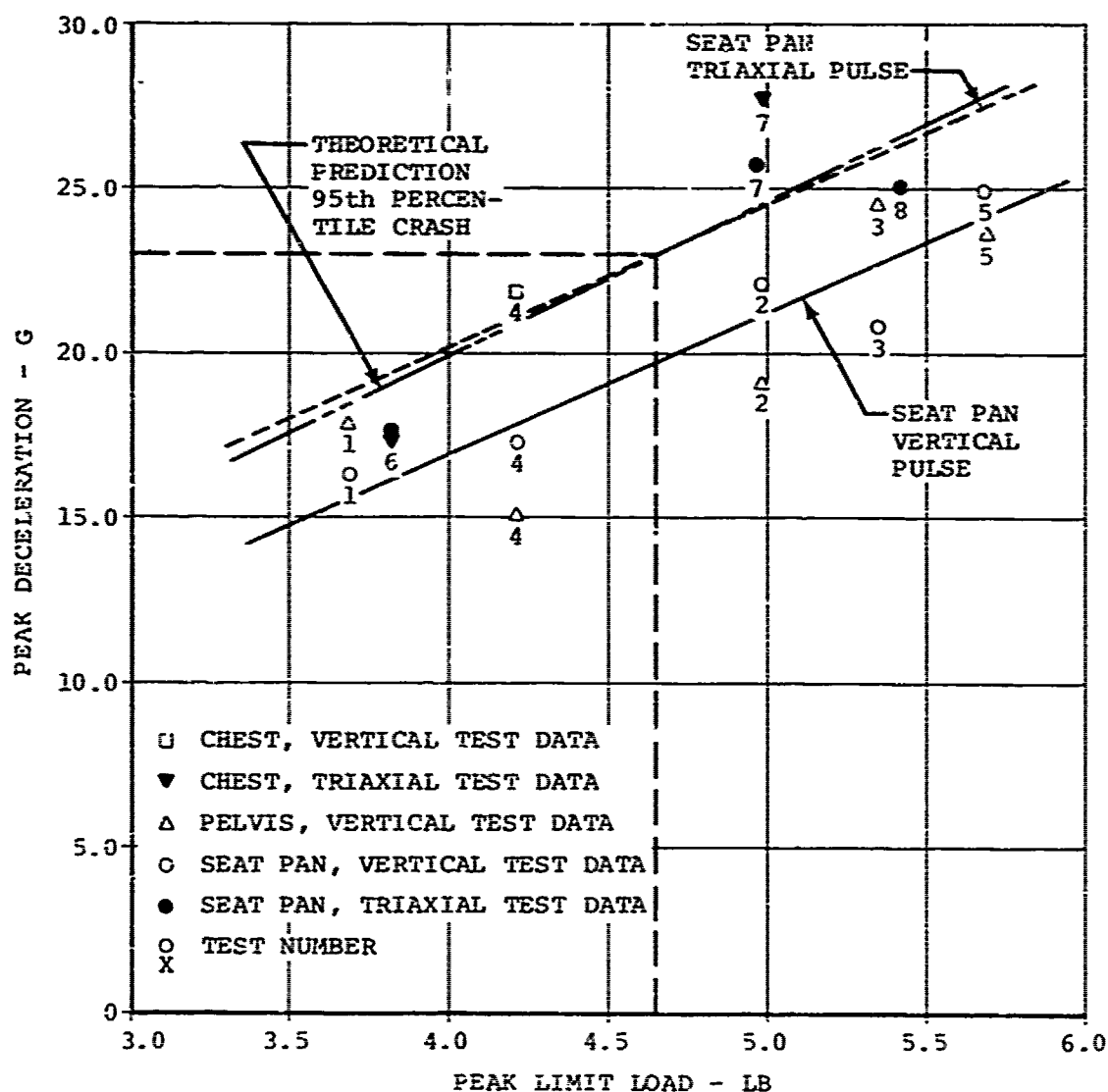
Figure 118. Peak Vertical Deceleration of Chest, Pelvis, and Seat Versus Corrected Peak Limit Load.

weight of 166 pounds. The movable portion of the experimental seat weighed 152 pounds, so the total effective weight was 318 pounds. Dividing this number into the limit load of 4,650 pounds yielded a limit load factor of 14.62G.

Since the deceleration G values measured and used in the data analysis were total (including 1G for static weight), 1G was

165

subtracted from the limit load factor to arrive at deceleration-producing input velocity change. Using this value of 13.62G and calculating the stroke required for a 95th percentile crash pulse using the rigid-body analysis explained in Reference 2 and Chapter 3 of this report, yielded a predicted stroke of slightly more than 12 inches. Whether this agreement will be consistent for all cases is not known; however, it is felt that, based on this data, the rigid-body analysis can be used for calculation of approximate stroke lengths. Again, the limit deceleration used will not reflect peak values to be imposed on the occupant, but rather limit values required to keep the peaks below tolerance values. This approach is consistent with the derivation of the rigid-body analysis, which uses a trapezoidal or flat limit deceleration representative of an average value.

5.3.4 RATE OF ONSET

Figure 119 presents the peak deceleration of the seat pan for both the vertical and the triaxial pulses plotted as a function of rate of onset. It can be seen that the correlation curve for the triaxial tests has a steeper slope than does the correlation curve for the purely vertical tests. Good correlation is shown, however, and it must be remembered that the rate of onset is not an independent variable. Additional analysis would be required to separate the influence of the rate of onset from the other variables incorporated in this plot.

The curve appears to be logical in that increased rates of onset in the triaxial tests produced increased deceleration magnitudes on the seat. This could be explained by the fact that during the triaxial tests the occupant shifts forward in the seat, thus delaying the vertical deceleration of the body weight (reducing effective weight) and resulting in a phase shift between the response of the occupant and the seat.

5.3.5 EFFICIENCY

Deceleration efficiencies of the various components in the seating system were calculated and tabulated for review. For the purposes of this analysis, efficiency (η) was defined as the average value of a parameter divided by the maximum measured value of the same parameter. Average values and η were determined as follows:
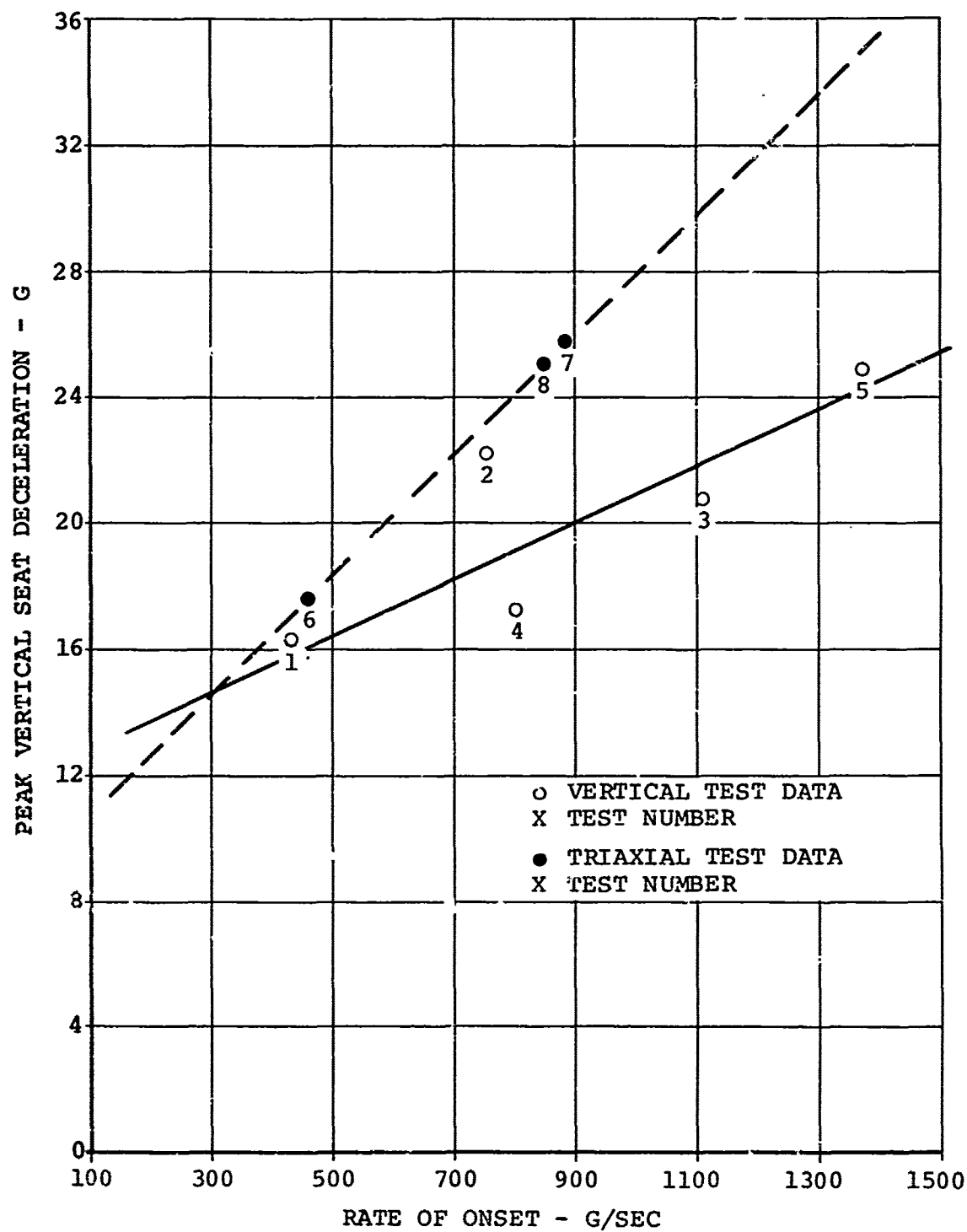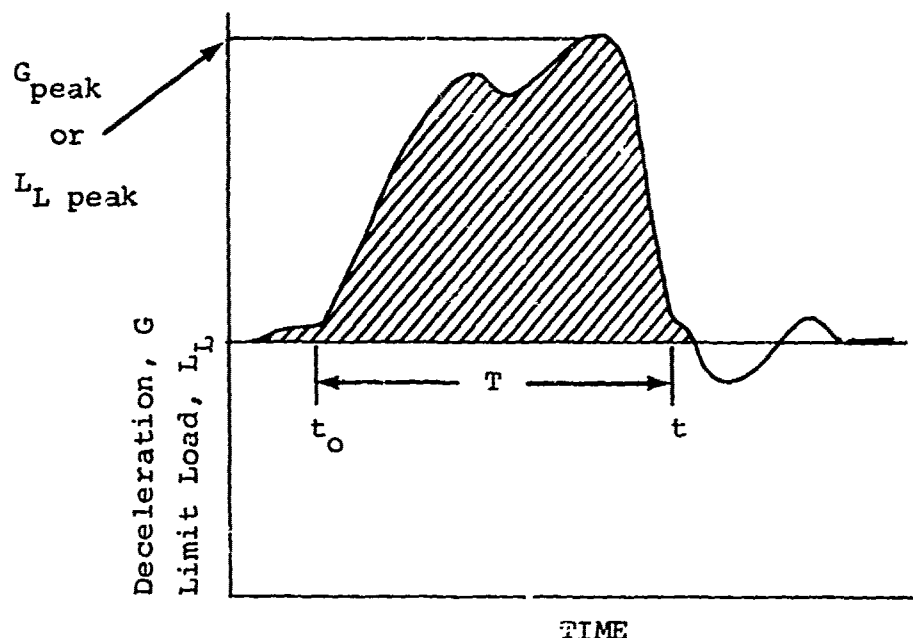
Figure 119. Peak Seat Deceleration Versus Rate of Onset.

167

$$\eta = \frac{\dfrac{1}{T}\displaystyle\int_{t_o}^{t} G\,dt}{G_{peak}} = \frac{\dfrac{1}{T}\displaystyle\int_{t_o}^{t} L_L\,dt}{L_{L_{peak}}} \qquad (23)$$

The average slopes of the onset and offset sides of the pulse were extended to where they cross the abscissa, which in all cases was the time scale for the event. Duration was then measured between these slope intercepts. Average values were obtained by integrating the area under the curves thus defined and dividing the area by the time duration measured. This average value was then divided by the maximum or peak value of the abscissa measured along the ordinate, which in this case was either the deceleration in G or, in the case of the energy-absorber calculations, the force.

Figure 120 shows efficiencies thus calculated as a function of test number. The average efficiencies of the chest (also included in Figure 120) and the seat are seen to be relatively close, although the chest efficiency is lower. The efficiencies measured on the pelvis are still lower and indicate wider fluctuation and interaction with the seat bucket. Use of a seat cushion which would provide better shock attenuation between the pelvic section of the dummy and the rigid seat pan
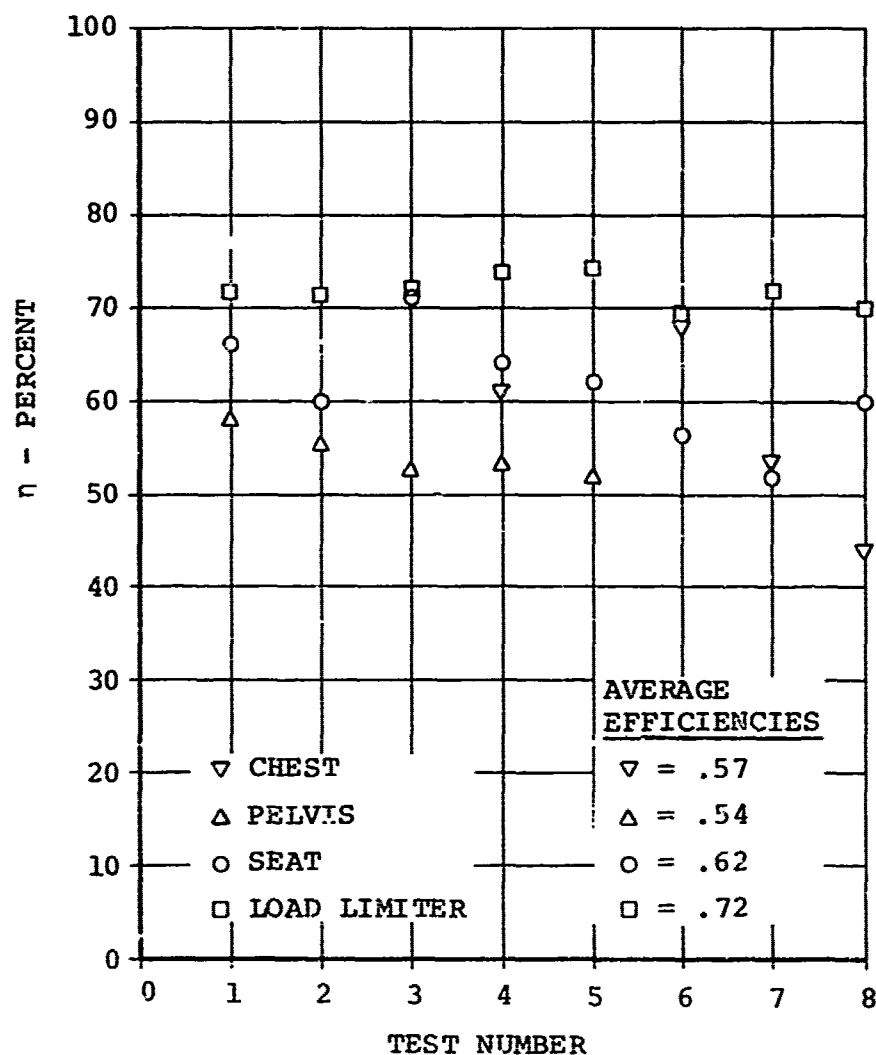
168

Figure 120. Efficiency Versus Test Number for the Chest, Pelvis, Seat, and Energy Absorber.

would be expected to reduce the magnitudes of the deceleration spikes and raise the efficiency.

It can be seen that the efficiency of the tensile tube energy absorber is on the order of 0.72. This is a rather high efficiency, falling rather close to the concepts producing more trapezoidal-shaped curves such as the rolling torus. Efficiencies roughly computed by the same method described for sample rolling torus energy absorbers fell between 0.8 and 0.9. Thus, the use of energy absorbers such as these could be

169

expected to provide the same velocity change for roughly 9- to
18-percent less stroke, providing the response of the occupant
to the higher rate of onset and initial load overshoot, typi-
cal of these energy absorbers, did not produce a decreased
efficiency. Decreased efficiency would require lowering the
limit deceleration factor, which would again increase the
stroke.

The efficiencies were used to check the validity of the decel-
eration design limit factor of 14.62G previously obtained by
use of the data plotted in Figure 120. Since the efficiency
was defined as the ratio of the measured average value of a
parameter divided by the measured peak value of the same param-
eter, dividing the limit deceleration factor by the seat pan
efficiency provided an indication of the expected peak values
that might be imposed on the seat occupant. Thus, on the
average,

$$G \text{ peak} = \frac{\bar{G}}{\eta} = \frac{14.62}{0.62} = 23.6G \tag{24}$$

which is slightly over the   human tolerance level. This
shows that a deceleration .   . factor of around 14.5G will be
required to limit the deceleration imposed on the seat and
occupant to within human tolerance limits.

Average efficiencies for the purely vertical direction, the
triaxial loading direction, and the overall average have been
computed and tabulated in Table XX. A comparison of the
average efficiencies for the purely vertical tests with the
average efficiencies for the triaxial tests yielded no signi-
ficant difference. It can be seen that the averages for the
triaxial direction were slightly lower than for the purely
vertical; however, the magnitudes are probably insignificant.

Chest deceleration data were lost in Tests 1, 2, 3, and 5 and
are therefore marked as not available in the table.

As previously explained, the rectangular box configuration of
the sophisticated test dummy used in these tests tipped and
the corner cut through the cushion, resulting in an impact
blow against the rigid seat bucket in the triaxial tests.
This resulted in extremely high aeceleration spikes. The
pelvic data for the triaxial pulses is therefore marked NU, or
not usable, as it is not representative of a human occupant.
Chest decelerations, while also affected by the harder blows
received by the pelvis, are included. They are, however,
marked with an S to stand for suspect data. The efficiencies
of the chest deceleration for these two test pulses would

170

TABLE XX. EFFICIENCY OF SYSTEM COMPONENTS				
	Efficiency, η			
Test No.	Chest	Pelvis	Seat	Load Limiter
1	NA	.58	.66	.72
2	NA	.55	.60	.72
3	NA	.52	.71	.72
4	.61	.53	.64	.74
5	NA	.52	.62	.74
Average η Vertical	.61	.54	.65	.73
6	.68S	NU	.56	.69
7	.53S	NU	.52	.72
8	.44S	NU	.60	.70
Average η Triaxial	.55		.56	.70
Average η Overall	.57	.54	.62	.72
NA Not Available NU Not Usable S Suspect Data				

probably have been higher if the pelvic box section had not
transmitted the impact decelerations into the chest section
of the dummy.

5.4   COMPONENT PERFORMANCE

5.4.1   ENERGY ABSORBERS

The energy absorbers performed as expected. Observation of
the static load deformation data and the dynamic load data
shows that very little difference exists between the static
and dynamic performance. This agreed with previous findings[25]
and thus supported the design analysis.

171

The energy absorbers, as expected, provided little rebound control; in most cases, the seat rebounded, bending the tube in the process. This created no problem in analysis of the data, as the rebound phenomena were easily identifiable in the traces. No failures were experienced with the energy absorbers, and they performed their function efficiently.

As stated previously, selection of the tensile tube energy absorber was made to provide replacement, substitution, and testing flexibility in the system. The nature of the matrix test program required the energy absorbers to be designed using a conservative characteristic elongation and for strokes in excess of 12 inches. Over 1 foot could be cut from the overall height of the experimental seat by simply designing the tensile tube energy absorber for its known capability. In a flight system, however, the basic drawback of the tensile tube device is that it provides little or no rebound capability, which is a distinct disadvantage of this system. The specific energy of these devices is so high, however, that an additional mechanism could perhaps be provided to limit rebound with no weight penalty on the system. Although the tensile tube energy absorbers showed very little sensitivity to local damage, it is felt that a more rugged type should be chosen for operational designs.

5.4.2 CARRIER BEARINGS AND GUIDANCE MECHANISM

The carrier bearings and guidance mechanism performed extremely well, actually exceeding design expectations. Past seats using this same general overall concept implementing friction bearings failed to provide the degree of protection required. This was caused by variations in frictional resistance to vertical loading as a result of loading direction and binding in the frame. Changes in loading direction, of course, changed the loads at the sliding bearings and, thus, the frictional resistance. Racking and binding of structures added to the variation in resistive load, depending on the degree and amount of racking.

The carrier bearings designed for this seat, as explained previously, provided an almost frictionless carrying mechanism which probably would be capable of stroking successfully even in the presence of frame racking. The combination of contouring the roller surfaces to provide line contact instead of point contact, the use of four rollers per bearing and four bearings per seat to distribute the load to the best advantage, and hard anodized coating of the aluminum guide tubes to prevent metal deforming which could have resulted in increased rolling friction, successfully defeated the problems associated with friction systems. In addition, the increased resistance to motion resulting from cross-sectional distortion of

172

either a tight-fitting sleeve bearing or the internal guide
tube was eliminated by the design of the roller bearing and
bearing block. Based on the previously mentioned factors and
the performance of this experimental seat, it is felt that
rolling type bearings should be used exclusively in guided
seats in place of sliding types.

5.4.3 CUSHIONS

The rate-sensitive foam cushions used in the experimental seat
were extremely temperature sensitive as discussed previously.
The extent of property variation noted in the cushions used
would seriously degrade their ability to perform the design
function. Exposure to direct sunlight resulted in a reduction
of stiffness to the point that the rate-sensitive property was
essentially lost. On the other hand, exposure to low tempera-
tures during testing resulted in an extremely rigid member,
which would be very difficult to sit on until the body tempera-
ture warmed the cushion.

Although a cushion having the room temperature properties re-
ported for these materials is definitely desirable, it appears
that the temperature sensitiveness and the design of this
specific cushion was inadequate to provide the desired func-
tions. Material properties should be adjusted to decrease
temperature sensitivity, and design modifications should be
made to increase the shock isolation capability of the seat
pan cushion system for use in integral armored seats.

5.4.4 RESTRAINT SYSTEM

Although the restraint system performed its required function,
it was cumbersome, difficult to use, and inefficient. Wrin-
kling and folding of the webbing combined with webbing compact-
ing in the sides of fittings is extremely undesirable, in that
decreased restraint system area is imposed on the occupant,
thus increasing localized loading. Further, wrenching of the
webbing leads to local edge loading and can result in tearing
of the webbing.

In one of the tests, the inertia reel failed to perform its
function. As explained previously, it loaded up to an initial
level of 1,050 pounds and then released, permitting the dummy
to jackknife forward and be restrained by lap belt alone.
Close examination of the inertia reel revealed that the tops
of two ratchet teeth and the ratchet pawl were chipped as
shown in Figure 121. Normally this would not have prevented
the reel from remaining locked, but in this particular case
the ratchet pawl was apparently forced back into an inter-
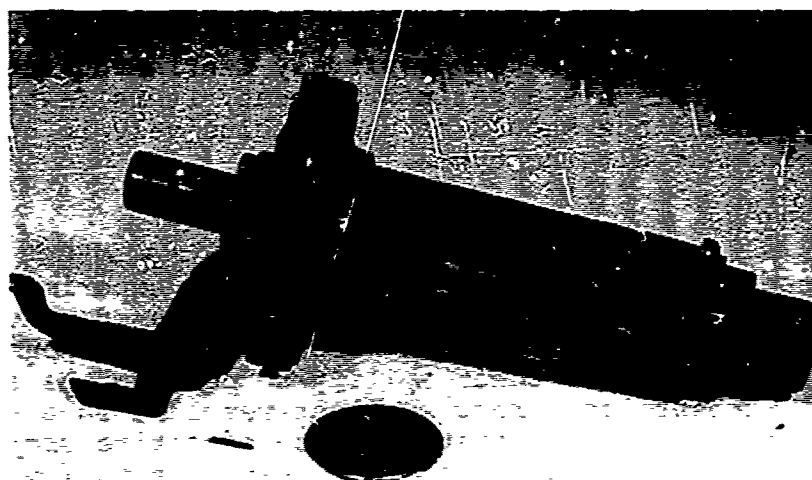mediate position which would not allow it to latch either

173

Figure 121. Inertia Reel Ratchet Failure.

manually or automatically. There is some speculation that the broken chips of teeth may have momentarily blocked the ratchet pawl, but there is no proof to substantiate this. Posttest manipulation of the inertia reel indicated that it returned to a normal manual and automatic latching operation even with the chipped teeth.

5.4.5 BUCKET

The composite bucket performed its function very well, duplicating the areal density of the composite armor and carrying repeated decelerative loads during testing. It resulted in a much superior armor simulation technique than that resulting from previously used combinations of metal and wood.

5.4.6 SUPPORT STRUCTURE

The support structure performed its intended function well. Its design provided guide tube support at both the top end above the top carrier bearings and at the center between the bearings, thus limiting beam bending of the guide tubes as a result of longitudinal and lateral loading. Its friction fitting attachment block to the guide tubes performed as

174

desired in two tests, permitting controlled racking of the frame resisted by frictional force provided by the four clamp fittings around the guide tubes.

Initially the design of the racking-resistant members in the plane of the guide tubes consisted of two 7-inch-wide strips of aluminum sheet extending the length of the guide tubes, one on each side of the seat as shown in Figure 82. The sheets were attached by rivets and bonded to crossmembers at the bottom, top, and center of the guide frame. The racking plates' performance during static testing (illustrated in Figure 100) resulted in their elimination from the design. They were replaced with a single X located between the bottom and center crossmembers which can be seen in Figure 88. This system performed successfully during the dynamic testing although some racking was sustained during the 95th percentile biaxial test as shown in Figure 110.

The crushable collar placed between the bolt head and the top of the cluster tube at the back frame support member (visible in Figure 34) was not worked during testing. The posttest condition of the collar can be seen in Figure 92. It was provided to permit some controlled deformation if the loads resulting from high longitudinal moments became excessive. Measured dynamic loads in the bolt indicated that if loaded under static conditions, the collar would have progressively crushed; however, the dynamic loads imposed were insufficient to cause crushing of the column. Although this type of provision was not needed in the design tested, it is considered to be good design practice to provide these "safety valves" to limit loads wherever possible in the seat structure.

Considerable weight could be removed from the system by optimization of the support structure. Neither the guide frame attachment nor the structure itself was optimized during design, as the primary system being tested was the energy-absorbing mechanism associated with the movable integral armored bucket. Although the frame was of the flight type, production design practices could remove considerable weight and result in a much more efficient system.

5.4.7 FLOOR ATTACHMENTS

The floor attachments successfully solved the problem of permitting angular rotation of the floor relative to the seat support without imposing bending on the seat members. The spherical rod ends permitted angular misalignment exceeding the ±10-degree requirement.
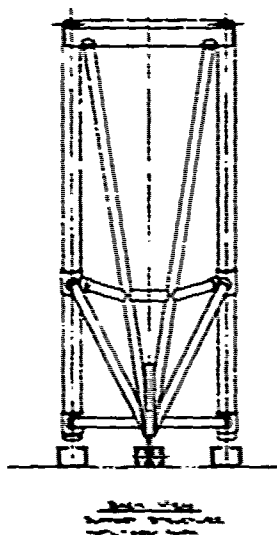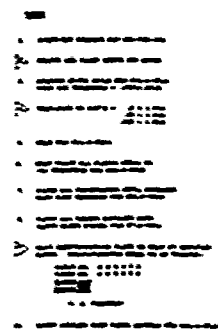
175

The three-point seat mount successfully solved the problem related to racking of the seat structure with floor warpage. Four-legged seats cannot be designed simply to permit floor warpage, because any three legs define a plane in which the fourth must also lie in order to eliminate the requirement for frame racking. Three-legged seats, however, can adjust through tipping without imposing the racking loads.

Combinations of the spherical rod ends and the three-point mount can provide the desired seat capability to assure maintenance of seat restraint in aircraft whose floors are buckling and warping within the 95th percentile survivable accident definition. Disadvantages are that longitudinal moments must be resisted by a single leg instead of two, thus increasing the strength requirements of the attachment and floor structure in that area. This requires an additional adapter or special provisions at that location on the aircraft floor. At present, however, this appears to be a reasonable compromise for solution of the floor warpage problem.

5.5 PROJECTED SEAT DESIGN

Figure 122 is the top assembly of a preliminary design of an operational type crashworthy integrally armored crew seat. This preliminary design was prepared as an application of the technology developed in this program to a specific retrofit requirement. The seat design does not have the required 12 inches of stroke, as considerable space was used by the requirement for a survival kit used as a seat cushion and because the system was required for application in existing aircraft. Existing limitations of these aircraft therefore limited the flexibility of the design.

The seat design incorporates the technology developed in the program discussed herein and results in a seat configuration projected to weigh on the order of 170 to 180 pounds. As stated in Chapter 2, this weight is entirely competitive with the heavy-weight armored crew seat used in some UH-1's at the present time which weigh on the order of 170 pounds while containing no crashworthy features. This UH-1 seat does not provide as complete a ballistic coverage envelope and does not have the handicap of providing room for parachute and survival kit as does the preliminary design shown in Figure 122. As a result, it can be seen that the next generation of integral armored crashworthy crew seats can be competitive with existing systems and still provide the protection required to increase the chances of survival of crew members involved in crashes.

Figure 122.   Top Assembly Preliminary Design of Operational
Crashworthy Armored Crew Seat.

177

NOTES

1. ████████ ████████ ███ ███-███-███

2. ████ ███ ████ ████ ███ ████

3. ████ ███ ████ ███ ███-█-███
   ███ ███ ████████ █ ████/████

4. ████████ ██ ███ █ █   ██ ± ████
                      ██ ± ████

5. ████ ███ ███-█-████

6. ██ ██ ████ ███ ████ ██
   ██ ████████ ███ ███-█-███

7. ████ ███ ████ ████ ████ ████████
   ███ ████ ████████ ███ ███-█-████

8. ████ ███ ████ ████████ ████
   ████ ████ █████ ███ ███-█-███

9. ████ ████████ ████ ██ ████ ██ ██████
   █████ ████████████ ██ ██ ██ █████

   ████ ██ ██████
   ████
   █. █. ████████

10. ████ ████, █ █ ████ ██████ ███ ███-█-████

████ ████
████ ████████
████ ████ ████

5.6 CRITERIA FOR ENERGY-ABSORBER LIMIT LOAD SIZING AND CUSHION DESIGN

The results of this program indicate that the limit loads for energy-absorbing systems of integrally armored crew seats should be designed using a limit decelerative load factor of 14.5G together with the effective weight of the occupant and the weight of the stroking part of the seating system.

This criterion will probably prove to be conservative for lightweight seats, and if dynamic analysis and/or testing can show otherwise, then the load factor should be increased. The increase will result either in providing protection for a higher percentile crash pulse or in shortening the stroke required to provide protection from the 95th percentile survivable crash as it is defined at this time.

It is further recommended that a 12-inch minimum stroke be established for use in all crew seats and that single-limit-load energy-absorbing systems be designed for the 50th percentile occupant, not the 95th. A single-level load limiter could be expected to impose a 6G higher decelerative load on a 5th percentile occupant than imposed on the 95th percentile if the limit load were sized for the 95th. Design for the 50th percentile occupant would on the other hand split the range of increased hazard essentially equally between the 5th and 95th percentile occupant, meaning that the 95th percentile occupant would be decelerated at a lower level, thus providing him increased protection with a decrease in probability of injury for the lower percentile accidents. However, the seat could bottom if subjected to a full 95th percentile accident. This may not be as harmful as indicated by first appearance, however, as the deceleration pulse at this time is beginning to taper off and the energy content remaining would be relatively small. The spike resulting from bottoming may not add to the maximum deceleration imposed during the major portion of the deceleration pulse.

Design for the 50th percentile would lower the deceleration to be imposed on the 5th percentile, thus providing added protection to the lighter occupant.

It should also be recalled that most of the aviators will, by definition, be 50th percentile or be close to 50th percentile; thus, the protection will be provided for most of the seat occupants - a desirable goal.

It is apparent that an infinitely variable load limiter would be desirable; however, at this point, such a device is not available. Consequently, a recommendation for its use is not

warranted. It is recommended, however, that at least two limit loads be provided wherever energy-absorbing devices separate from the seat structures are chosen for use. It is apparent that if collapsible structure is chosen as the energy-absorbing technique, then predictable multiple limit loads are difficult to achieve. If, however, a separate device is selected, a two-level limiter is relatively simple to incorporate and does permit the effect of occupant weight range to be reduced to values within the accuracy of design control.

The two limit loads should be calculated by dividing the total effective weight range, occupant, and movable portion of the seat into two equal ranges. The limit loads should then be designed for the midpoint of each range. In use, a prospective seat occupant would be required to select a limit load based on his weight.

As an example, assume a bi-level limit-load energy absorber. The seat occupant weights of concern are as follows:

Percentile	Effective Weight (lb)
95th	166
50th	139
5th	114

Assuming a movable seat weight of 130 pounds, the total effective weight for each percentile is

Percentile	Effective Weight (lb)
95th	296
50th	269
5th	244

The limit loads should be designed for the average of each weight range, 5th to 50th and 50th to 95th percentile, to minimize the effect of off-design weight variation.

The averages of the weight ranges are as follows:

Percentile Range	Average Weight (lb)
5th - 50th	256.5
50th - 95th	282.5

The limit loads are then

Lower range limit load: (14.5) (256.5) = 3,720 pounds

Upper range limit load: (14.5) (282.5) = 4,100 pounds

The limit decelerations at each end of each range are

Lower range:

5th percentile occupant: $G_L = \frac{3,720}{244} = 15.2$

50th percentile occupant: $G_L = \frac{3,720}{269} = 13.8$

Upper range:

50th percentile occupant: $G_L = \frac{4,100}{269} = 15.2$

95th percentile occupant: $G_L = \frac{4,100}{296} = 13.8$

It can be seen that the deviation around the 14.5G limit is thus only 0.7G over the entire weight range.

Applying the average seat efficiency (n) of 0.62 from Table XX, peak seat accelerations of $\frac{15.2}{0.62} = 24.5G$ could therefore be estimated. This may not prove to be intolerable, however, as the measured peak would probably be less than 24.5G and of shorter duration than that required to produce injury.

Results of this program indicate that cushions for use in integrally armored crew seats should be designed as shock attenuators to reduce the tendency for impact loading between the boney structure of an occupant and the massive, rigid seat bucket. Rate-sensitive foams are a good candidate for use; however, material properties and design features should be adequate to eliminate the possibility of penetration. This may result in the requirements for a tough, strong layer of material under the rate-sensitive foam as well as increased energy-absorbing content of the basic cushion material.

181

CHAPTER 6

CONCLUSIONS AND RECOMMENDATIONS

6.1 CONCLUSIONS

The following conclusions were drawn as a result of this program:

1. A crashworthy integrally armored crew seat with roughly the same weight as some existing non-crashworthy armored crew seats is feasible.

2. A 95th percentile Army aviator can be protected from a 93rd percentile survivable crash in a properly designed integrally armored crew seat in which 12 inches of vertical seat stroke is provided. For 95th percentile crash pulses, 14-1/2 to 15 inches of stroke distance is required.

3. A limit load factor of 14.5G should be used together with the movable seat weight, 80 percent of the occupant weight, and the weight of all clothing and equipment carried on the upper portion of the body for sizing an energy-absorber limit load. The load thus calculated represents total force resisting vertical movement and thus includes friction, binding, etc.

4. Energy-absorber limit loads should be adjustable to provide comparable protection for all crewmen.

5. Roller bearings eliminate the negative aspects normally found with guided-stroke, energy-absorbing seat systems by minimizing the effects of unpredictable resistance to stroking through frame racking and friction.

6. Three-point floor attachments with swivel joints increase structural integrity under warped floor conditions.

7. A shock-attenuating, low-rate-of-return seat cushion is necessary in integrally armored seats to provide a proper interface between the occupant and the heavy armored bucket.

8. Existing types of military lap belts used in Army aircraft rope and fold during loading. Also, webbing bunches in one end of fitting attachments, resulting

182

in edge loading of the webbing. In this configuration, the buckle can gouge into the inner thighs of the occupant.

9. Existing types of military restraint systems used in Army aircraft permit excessive movement of the occupant under decelerative loading, permit submarining, and are cumbersome and inefficient.

6.2 RECOMMENDATIONS

The following recommendations are made as a result of this program:

1. Future procurement of new Army aircraft should incorporate the requirement for crashworthy crew seats designed to the criteria existing today in the proposed Military Specification[5], as modified by the findings of this program.

2. Integrally armored crew seats should be designed to provide a minimum of 12 inches of vertical stroke.

3. Seats should be designed to maximize available stroke distance, including the increase resulting from upward seat adjustment.

4. The limit load of the energy-absorbing system should be designed using a load factor of 14.5G, the weight of the movable section of the seat, and the effective weight of the occupant, calculated as specified in this report (80 percent of the occupant weight and clothing, exclusive of boots and including 100 percent of all equipment and clothing carried on the upper portion of the body).

5. If a separate energy-absorber device is used in the design, at least a bi-level limit load should be incorporated to provide more comparable protections for all crewmen regardless of weight.

6. If a collapsible-structure energy-absorbing technique is used in the seat, the limit load should be designed for the 50th percentile occupant, not the 95th.

7. If the stroking portion of the seat is guided, low-friction roller bearings should be used to eliminate friction and binding due to racking.

183

8. The floor attachments should be designed to permit buckling and rotation of the aircraft floor without imposing racking on the seat structure or local bending of the attachment structure at the floor interface.

9. Additional development should be conducted on shock-attenuating cushions for use as an interface between occupants and the massive armored bucket on integrally armored seats.

10. Existing types of military restraint systems used in Army aircraft should be replaced by a more efficient system.

11. A development program should be conducted to optimize the configuration and weight of the subject prototype seat design for application to future aircraft and for retrofit.

12. Flight-weight versions of the subject seat design should be designed and developed for retrofit to all existing Army aircraft requiring armored seats. Since the retrofit effort will be limited by existing cockpits, the design philosophy should be to provide the maximum protection permissible within existing aircraft limitations, thus increasing survivability in present aircraft to the maximum.

13. Integral armored crashworthy crew seats should be incorporated into aircraft scheduled for combat use. Wherever use permits, however, crashworthy crew seats of high occupant-to-movable seat weight ratios should be used to maximize crash protection.

184

LITERATURE CITED

1. Rothe, V. E., et ál, CREW SEAT DESIGN CRITERIA FOR ARMY AIRCRAFT, Aviation Crash Injury Research of Flight Safety Foundation; TRECOM Technical Report 63-4, U. S. Army Aviation Materiel Laboratories*, Fort Eustis, Virginia, February 1963.

2. CRASH SURVIVAL DESIGN GUIDE, Dynamic Science; USAAMRDL Technical Report 71-22, Eustis Directorate, U. S. Army Air Mobility Research and Development Laboratory, Fort Eustis, Virginia, October 1971, AD 733358.

3. Weinberg, L. W. T., and Turnbow, J. W., SURVIVABILITY SEAT DYNAMIC TEST PROGRAM, Aviation Crash Injury Research of Flight Safety Foundation; USAAVLABS Technical Report 65-43, U. S. Army Aviation Materiel Laboratories, Fort Eustis, Virginia, July 1965.

4. Peterson, Richard L., and Ducker, George W., STATIC AND DYNAMIC EVALUATION OF AN EXPERIMENTAL NET CREW SEATING AND RESTRAINT SYSTEM, TM-68-1-FDFR, Air Force Flight Dynamics Laboratory, Air Force Systems Command, Wright-Patterson Air Force Base, Ohio, February 1968.

5. MIL-S-58095(AV), SEAT SYSTEM: CRASHWORTHY NON-EJECTION, AIRCREW, GENERAL SPECIFICATION FOR.

6. ANTHROPOMETRY OF ARMY AVIATORS, Quartermaster Research and Engineering Center, Technical Report EP-150, Natick, Massachusetts, June 1961.

7. Dotseth, Walter, D., SURVIVABILITY DESIGN GUIDE FOR U. S. ARMY AIRCRAFT, North American Rockwell Corporation, USAAMRDL Technical Report 71-41, Eustis Directorate, U. S. Army Air Mobility Research and Development Laboratory, Fort Eustis, Virginia, November 1971.

8. Hertzberg, H. T. E., et al, ANTHROPOMETRY OF FLYING PERSONNEL - 1950, Wright Air Development Center, Dayton, Ohio, September 1954.

9. Morgan, C. T., et al, HUMAN ENGINEERING GUIDE TO EQUIPMENT DESIGN, Joint Army-Navy-Air Force Steering Committee, 1963.

---

*Now Eustis Directorate, U. S. Army Air Mobility Research and Development Laboratory

10. Draft Standard, U. S. ARMY ARICREWMAN AND INFANTRYMAN CLOTHING AND EQUIPMENT, U. S. Army Human Engineering Laboratories, Aberdeen, Maryland, March 1969.

11. MALE PHYSICAL DIMENSIONS FOR CONSTRUCTION AND INDUSTRIAL EQUIPMENT DESIGN - SAE J833, Society of Automotive Engineers, June 1962.

12. Military Standard 1333, AIRCREW STATION GEOMETRY FOR MILITARY AIRCRAFT.

13. TM55-1520-210-10, OPERATOR'S MANUAL, ARMY MODEL UH-1D/H HELICOPTER, Department of the Army, Washington, D. C., May 1969.

14. Auyer, Walter Leon, and Turnbow, James W., A STUDY OF THE DYNAMIC RESPONSE OF A DAMPED, MULTI-DEGREE OF FREEDOM, SPRING MASS SYSTEM WHICH SIMULATES A SEAT, SEAT CUSHION, AND SEAT OCCUPANT SUBJECTED TO A VERTICAL IMPACT ACCELERATION, Dynamic Science Report 69-8, June 1969.

15. Carr, R. W., and Phillips, N. S., DEFINITION OF DESIGN CRITERIA FOR ENERGY ABSORPTION SYSTEMS, Report No. NADC-AC-7007, Beta Industries, Inc., Dayton, Ohio, Contract N00156-70-C-1374, 11 June 1970.

16. Schwartz, Marcus, COMPARATIVE STUDY OF BODY DISPLACEMENTS IN BOTH HUMANS AND ANTHROPOMORPHIC DUMMIES WHEN SIMULTANEOUSLY SUBJECTED TO CONTROLLED VERTICAL IMPACT TYPE DECELERATIONS, Naval Air Development Center, Johnsville, Pennsylvania, Report No. NADC-AC-6808, April 1968.

17. Dempster, Wilfred T., SPACE REQUIREMENTS OF THE SEATED OPERATOR, WADC Technical Report 55-159, Wright Air Development Center, July 1955.

18. Vogt, H. L. Coermann, R. R., and Fust, H. D., MECHANICAL IMPEDANCE OF THE SITTING HUMAN UNDER SUSTAINED ACCELERATION, Aerospace Medicine, Vol. 39, No. 7, July 1968.

19. Clark, W. S., Lange, K. O., and Coermann, R. R., DEFORMATION OF THE HUMAN BODY DUE TO UNI-DIRECTIONAL FORCED SINUSOIDAL VIBRATION, Human Factors, Vol. 4, No. 5, October 1962.

20. Parks, Donald L., DEFINING HUMAN REACTION TO WHOLE-BODY VIBRATION, Human Factors, Vol. 4, No. 5, October 1962.

21. Lange, K. O., and Coermann, R. R., VISUAL ACUITY UNDER VIBRATION, Human Factors, Vol. 4, No. 5, October 1962.

22. von Gierke, Dr. H. E., RESPONSE OF THE BODY TO MECHANICAL
    FORCES - AN OVERVIEW, Report No. AMRL-TR-66-251, Aero-
    space Medical Research Laboratories, Wright-Patterson
    Air Force Base, Ohio, 1966.

23. Payne, P. R., A DYNAMIC MODEL OF THE HUMAN BODY SUBJECTED
    TO SPINAL ACCELERATION WHEN SITTING ERECT, Bio Astro-
    nautics Division Technical Report, Task No. 630102, Aero-
    space Medical Laboratory, Wright-Patterson Air Force Base,
    Ohio, January 1963.

24. Steen, Ernest L., THE OPTIMIZATION OF SEAT CUSHIONS FOR
    EJECTION SEATS, Report No. AMRL-TR-68-126, Aerospace
    Medical Research Laboratories, Wright-Patterson Air Force
    Base, Ohio, February 1969.

25. Haley, J. L., Klemme, R. E., and Turnbow, J. W., TEST AND
    EVALUATION OF 1000 - 4000 POUND LOAD-LIMITING DEVICES,
    Dynamic Science, AvSER Memorandum Report M69-2, February
    1969.

APPENDIX I

TENSILE TUBE ENERGY-ABSORBER DESIGN AND SUPPORTING TESTS

This appendix presents a discussion of the analysis performed
in designing the tensile tube energy absorbers. It also de-
scribes the tests performed to establish the limit load versus
deformation characteristics of the candidate stainless steel
tubes selected for use in the energy absorbers.

I.1 TENSILE TUBE ENERGY-ABSORBER DESIGN

I.1.1 Design Loads

The design loads were as follows:

Limit Load, Light Man	= 3,400 pounds
Limit Load, Intermediate	= 3,600 pounds
Limit Load, Heavy Man	= 3,800 pounds

I.1.2 Energy-Absorbing System

The 3,400-pound limit load was supplied by tensile elongation
of a 304 series stainless steel tube. The two 200-pound incre-
ments were provided by selective connection of supplementary
energy-absorbing cables. Two cables were provided, each capa-
ble of supplying a 200-pound load increment.

I.1.3 Energy-Absorbing Cable Sizing

A 1/16-inch 7 x 7 construction cable was selected from the
available listing shown in Table XXI.

I.1.4 Energy-Absorbing Stainless Steel Tube Sizing

Figure 123 presents the before and after dimensional nomencla-
ture used in the analysis.

A relationship between limit load and tube outside and inside
diameters was established to aid selection of commercial tubing
to provide the desired 3,400-pound ultimate load. The develop-
ment was based on scaling data previously measured and re-
ported in Reference 25. The development was as follows:

TABLE XXI. ENERGY-ABSORBING CABLE - APPROXIMATE BREAKING STRENGTH AND ELONGATION (APPROXIMATE ELONGATION 45 TO 50 PERCENT)

1 x 7 Construction

Dia (in.)	Approx. Wt Per 100 Ft (lb)	Approx. Breaking Strength (lb)
1/32	.25	70
3/64	.59	140
1/16	.85	240
5/64	1.4	370
3/32	2.0	530
7/64	2.7	750
1/8	3.6	920
5/32	5.3	1,490
3/16	7.7	2,110
7/32	9.0	2,850
1/4	12.0	3,520
9/16	20.5	5,950
3/8	27.2	7,920

1 x 19 Construction

Dia (in.)	Approx. Wt Per 100 Ft (lb)	Approx. Breaking Strength (lb)
1/16	.85	260
5/64	1.4	390
3/32	2.0	550
7/64	2.7	730
1/8	3.5	940
9/64	4.1	1,100
5/32	5.5	1,140
3/16	7.7	2,170
7/32	10.2	2,930
1/4	13.5	3,760
9/32	17.0	4,770
5/16	21.0	5,780
3/8	25.3	6,440

7 x 7 Construction

Dia (in.)	Approx. Wt Per 100 Ft (lb)	Approx. Breaking Strength (lb)
1/16	.75	200
5/64	1.1	360
3/32	1.6	420
1/8	2.8	800
5/32	4.3	1,210
3/16	6.2	1,600
7/32	8.3	2,200
1/4	10.6	2,850
5/16	16.7	4,550
3/8	23.7	6,780
7/16	31.9	8,070

7 x 19 Construction

Dia (in.)	Approx. Wt Per 100 Ft (lb)	Approx. Breaking Strength (lb)
1/8	2.9	760
9/32	4.5	1,070
3/16	6.5	1,520
7/32	8.6	2,060
1/4	11.0	2,670
5/16	17.3	4,220
3/8	24.3	6,100

6 x 25 IWRC Construction

Dia (in.)	Approx. Wt Per 100 Ft (lb)	Approx. Breaking Strength (lb)
3/8	26.0	6,600
7/16	35.0	8,850
1/2	46.0	11,500
9/16	59.0	14,700
5/8	72.0	18,400
3/4	104.0	26,200
7/8	142.0	35,400
1	185.0	47,800
1-1/8	234.0	58,700
1-1/4	280.0	72,800
1-3/8	350.0	87,400

189

Subscript 1 refers to original tube dimensions.
Subscript 2 refers to yielded tube dimensions.

Figure 123.   Dimensional Nomenclature.

$$\text{(Volume of Metal)}_1 = \text{(Volume of Metal)}_2 \tag{25}$$

$$\frac{\pi}{4} (D_{o_1}^{2} - D_{i_1}^{2})\ L_1 = \frac{\pi}{4} (D_{o_2}^{2} - D_{i_2}^{2})\ L_2 \tag{26}$$

Using a design elongation of 40 percent,

$$L_2 = 1.4\ L_1 \tag{27}$$

Combining the two relationships yielded

$$(D_{o_1}^{2} - D_{i_1}^{2})\ L_1 = (D_{o_2}^{2} - D_{i_2}^{2})\ (1.4)\ L_1 \tag{28}$$

$$D_{o_2}^{2} - D_{i_2}^{2} = \frac{D_{o_1}^{2} - D_{i_1}^{2}}{1.4} \tag{29}$$

and in terms of original tube dimensions,

$$\text{(Cross-Sectional Area)}_2 = \frac{\pi}{4} \left(\frac{D_{o_1}^{2} - D_{i_1}^{2}}{1.4}\right)$$

$$= .561\ (D_{o_1}^{2} - D_{i_1}^{2}) \tag{30}$$

190

Solving for the limit load, L_L, yielded

$$L_L = \sigma A_2 = \sigma(.561)(D_{o_1}^2 - D_{i_1}^2) \qquad (31)$$

where σ equals the maximum work-hardened stainless steel tube tensile stress.

Inside and outside tube diameters for the tubes tested in Reference 25 were measured and found to be

$$D_{o_1} = 0.50 \text{ inch}$$

$$D_{i_1} = 0.46 \text{ inch}$$

$$\therefore \quad D_{o_1}^2 - D_{i_1}^2 = 0.0384 \text{ inch}^2 \qquad (32)$$

A representative ultimate static load measured in Reference 25 was determined to be 2,750 pounds, and the ultimate tube tensile stress was calculated as follows:

$$\sigma = \frac{L_L}{(.561)(.0384)}$$

$$\sigma = \frac{2750}{(.561)(.0384)}$$

$$\sigma = 127,907 \text{ psi}$$

$$\approx 128 \text{ KSI} \qquad (33)$$

Observation of the data measured and reported in Reference 25 indicated that, although there was a difference between the static and dynamic load versus deformation curves for lower deformations, no significant difference in ultimate loads existed. Consequently,

$$D_{o_1}^2 - D_{i_1}^2 = \frac{L_L}{\sigma(.561)}$$

or, for $L_L = 3,400$ pounds

191

$$\Gamma_{o_1}^{2} - D_{i_1}^{2} = \frac{3,400}{(128 \times 10^3)\,(.561)}$$

$$= 0.0473 \text{ inch}^2 \tag{34}$$

In general, then, for the purposes of this study,

$$D_{i_1}^{2} = D_{o_1}^{2} - .0473 \tag{35}$$

$$D_{i_1} = (D_{o_1}^{2} - .0473)^{1/2} \tag{36}$$

This relationship was used to select the commercially available stainless steel tube size most nearly providing the desired 3,400-pound ultimate limit load. This was done by picking available outside diameters and calculating the required inside diameter and resultant wall thickness. The various wall thicknesses available in each outside diameter were then reviewed, and the closest available one was selected. The selection of the 3,400-pound limit load tube is shown in Table XXII as an example of the procedure. The brackets enclose groups of wall thicknesses close to that desired, and the asterisks mark those meeting the requirements.

TABLE XXII. TENSILE TUBE SIZE SELECTION				
D_{o_1} (in.)		D_{i_1} Required (in.)	Wall Thickness (in.)	Wall Thickness Available (in.)
Fraction	Decimal			
7/8	.875	.849	.0130	.028
13/16	.8125	.784	.0142	.035
3/4	.750	.717	.0165	.010 .016* .020
11/16	.6875	.652	.0177	.020
5/8	.625	.586	.0195	.010 .020* .028
9/16	.5625	.518	.0222	.020
1/2	.500	.450	.0250	.020 .028 .035

I.1.5 Energy-Absorbing Tube Length Sizing

Referring to the following sketch and assuming that the tube angle with respect to vertical is θ, the elongated tube length is ε, and the vertical stroke length is S, a relationship was developed for selecting original tube length (X) as a function of both S and ε.
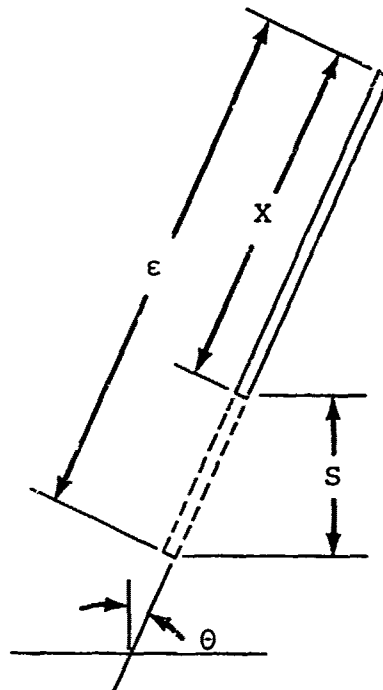
This relationship was

$$\varepsilon = X + \frac{S}{\cos\theta} \qquad (37)$$

$$\text{and } X = \varepsilon - \frac{S}{\cos\theta} \qquad (38)$$

Since ε = some factor (f) times X, ε was represented by fX.

$$X = fX - \frac{S}{\cos\theta} \qquad (39)$$

$$\text{and } X (f - 1) = \frac{S}{\cos\theta} \qquad (40)$$

193

$$\therefore \quad X = \frac{S}{(f - 1) \ (.9744)} \quad \quad (41)$$

Using this relationship, the stroke lengths and original tube lengths were developed for various percentages of elongation (f in percentage of initial length) (Table XXIII). The tube lengths tabulated have 3.0 inches added to the computed values to allow for nonworking bond lengths on each end.

TABLE XXIII. STROKE AND ORIGINAL TUBE LENGTHS AS A FUNCTION OF TUBE ELONGATION		
Elongation (percent)	Original Tube Length (in.)	Stroke Length (in.)
30	44.05	12.0
	52.66	14.5
	61.22	17.0
35	38.10	12.0
	45.52	14.5
	52.85	17.0
40	33.79	12.0
	40.20	14.5
	46.61	17.0

I.1.6 End Fitting Sizing

An epoxy bonded joint was selected for attaching the end fittings to the tubes without producing stress risers. A bond strength (σ_s) was assumed to be 1,500 psi, and the bond thickness was set at 0.005 inch. The required length (L) of bond was then calculated from the following relationship:

$$L = \frac{C \ L_L}{\sigma_s \ \pi \ D_{OF}} \quad \quad (42)$$

194

where D_{OF} = outside diameter of the fittings, inches, (0.717 inch for 3/4-inch O.D. X 0.016-inch wall thickness tubing)

L_L = ultimate strength of energy absorber, 3,400 pounds

C = factor of safety, 1.5

$$L = \frac{(1.50)\ (3400)}{(1500)\ (\pi)\ (.707)} = 1.53$$

$$\approx 1.5 \text{ inches}$$

The resulting end fitting bond designs for the 3/4- and 5/8-inch O.D. tubing were as shown in Figures 124 and 125, respectively.
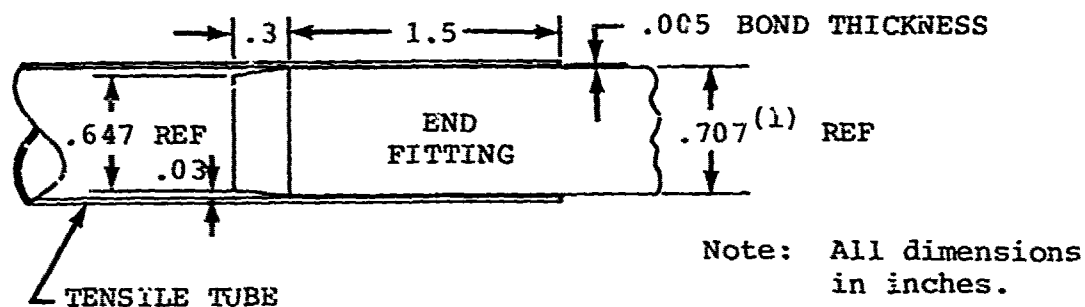
Figure 124. Bond Design for 3/4-Inch O.D. Tubing.
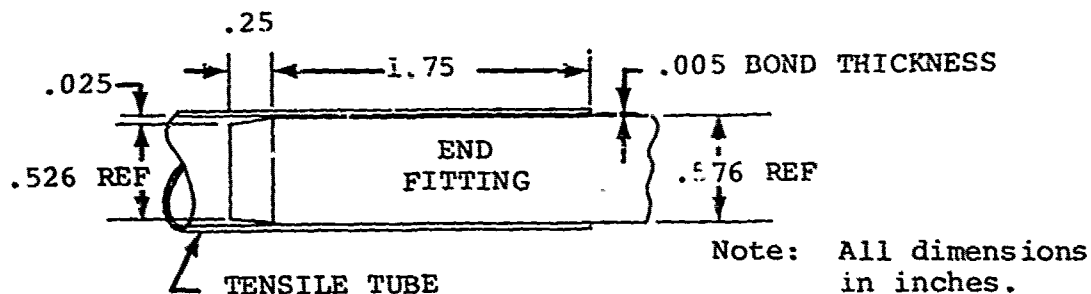
Figure 125. Bond Design for 5/8-Inch O.D. Tubing.

I.2   TENSILE TUBE ENERGY-ABSORBER DESIGN SUPPORT TESTS

Nine static tests were performed on three tube configurations
to establish the limit load versus deformation characteristics
of stainless steel tubes that were considered for use in the
energy absorbers.

I.2.1   Test Objectives

The primary objective of the test program was to obtain the
energy-absorption characteristics of a number of selected thin-
wall type 304 annealed, seamless, stainless steel tensile tube
energy absorbers.

A secondary objective was to verify attachment fitting design
and bonding procedures.

I.2.2   Test Item Description

The energy-absorber samples consisted of seamless, annealed,
type 304 stainless steel tubes which were bonded to steel end
fittings with an epoxy adhesive.   Three different tube diam-
eters and/or wall thicknesses were evaluated:

    1.   .625-inch O.D. with a .020-inch wall thickness

    2.   .750-inch O.D. with a .016-inch wall thickness

    3.   .750-inch O.D. with a .020-inch wall thickness

The tubing sizes listed above were based on calculations pre-
sented previously.   Each of the nine test specimens that were
fabricated used a 23-inch length of annealed type 304 stain-
less steel tubing two steel end fittings.   Three samples of
each tubing size were cut to the proper length and inspected
to insure that there were no surface nicks or scratches and
that the wall thickness at each end of the tube did not vary
more than .0005 inch from the desired thickness.

The steel end fittings were machined from 0.750-inch 4130
steel rod.   These end fittings were 3.17 inches long and were
machined to permit insertion in the stainless steel tube to a
depth of 1.80 inches.   A clearance of 0.005 inch was main-
tained between the inside wall surface of the tube and the
machined surface of the end fitting.   A 0.250-inch hole was
drilled in each end fitting perpendicular to the tube center-
line to permit attachment to the tensile test machine.   To aid
the bonding process, it was determined that one end fitting of
each set should be center bored to provide a small hole to

permit escape of entrapped air during the second end fitting
insertion process.

The end fittings were bonded to the tube sections with Epon
901 and B1 hardener. The contact surfaces were carefully
cleaned with methyl ethyl ketone (MEK) and a clean cloth prior
to the application of the adhesive. Adhesive was applied to
both surfaces, and the tube and end fitting were then as-
sembled. The tube assemblies were positioned in a clamping
fixture to insure that the end fittings did not creep out of
the tubes prior to adhesive cure, thereby increasing the effec-
tive tube stretch length. After removal from the test fixture,
the tube assemblies were painted with 1-inch-wide blue bands
spaced 1 inch apart. Figure 126 illustrates the nine tensile
test specimens prior to testing.
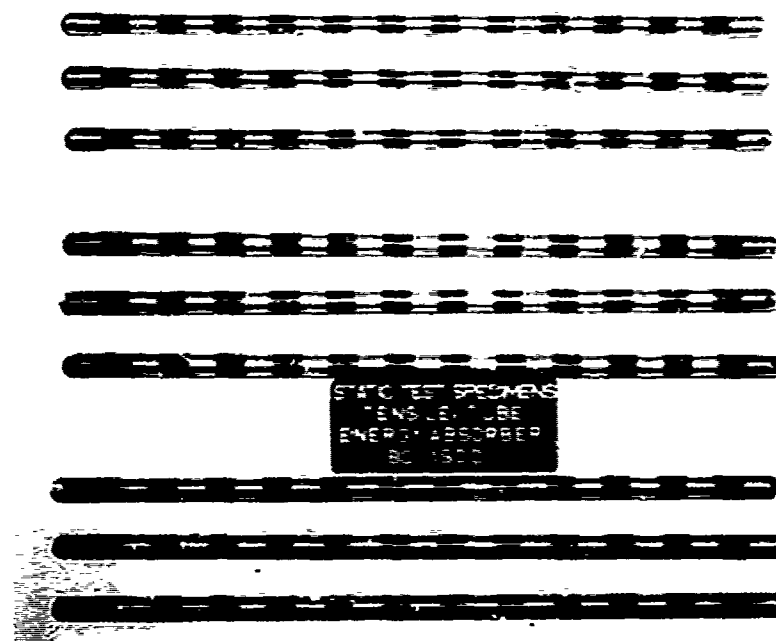
Figure 126.   Tensile Tube Energy Absorbers
Prior to Static Tests.

I.2.3   Test Methodology

All nine tests performed in this series were static tests in
which a 0-10,000-pound tensile test machine was used to apply
the failure loads. The specimen to be tested was installed in

197

the test machine as shown in Figure 127. The lower end
fitting of the energy absorber was attached to the movable
crosshead of the machine. The upper end fitting was then
attached to a 0-4,000-pound load cell located between the
upper end of the energy absorber and the top of the test
machine. The load cell data were recorded on a direct-write
oscillograph at a chart speed of 0.25 ips.
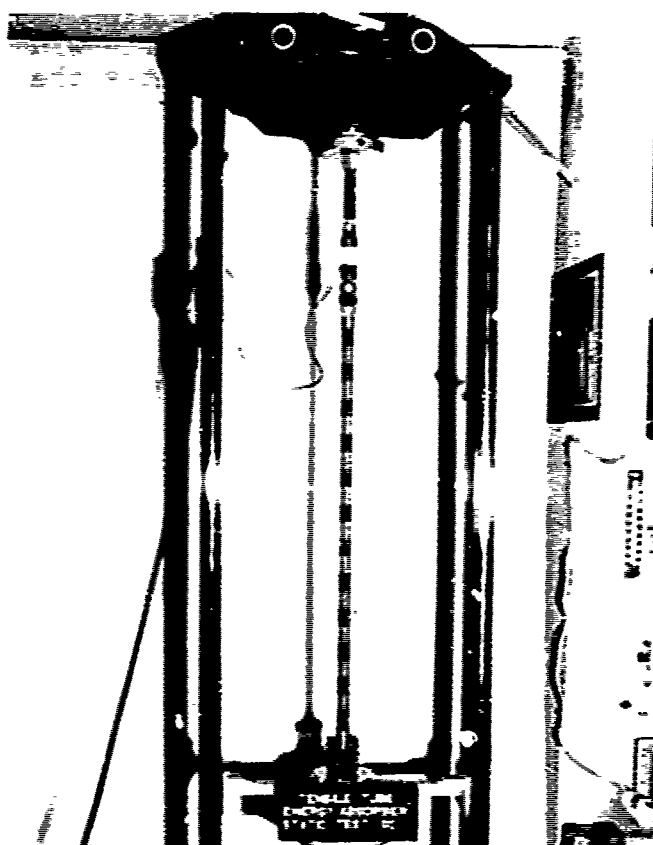
Figure 127. Static Tensile Load Application Method.

The elongation was measured by a reference pointer bolted to
the movable crosshead and a 36-inch scale clamped to the side
of the test machine. At selected increments of elongation, a
switch was manually depressed which then electrically placed
a reference mark opposite the tensile load value at that point
on the oscillograph chart.

198

All loads were applied at a rate of 1 inch per minute. Load application was maintained until ultimate failure of the tube section occurred. The peak load and the total elongation of the specimen were then recorded. Elongation was also followed throughout the load application, and the load was recorded at each 1/8 inch of travel for the first and last inch of elongation and at each 1-inch increment in between. All tests were performed at room temperature.

Black-and-white still photographs were taken of each test item before, during, and after load application. Representative test setups are shown in Figures 128 and 129.

I.2.4 Test Results

The nine energy-absorber test specimens are shown in Figure 130 following load application and removal from the fixture.

All of the specimens failed as desired in the tube section of the specimen. A summary of the ultimate loads obtained and the corresponding elongations measured for the various tube sizes is presented in Table XXIV. Tensile load versus elongation curves are presented in Figures 131, 132, and 133. Figure 134 compares the average elongation curves for the three tube sizes. Both the 0.625-inch O.D. x 0.020-inch wall tube and the 0.750-inch O.D. x 0.016-inch wall tube gave very consistent results. The 0.750-inch O.D. x 0.0.6-inch wall tube gave a greater elongation with only a slightly greater load than the 0.625-inch O.D. x 0.020-inch wall tube, and its design choice for the primary energy-absorbing device was confirmed.
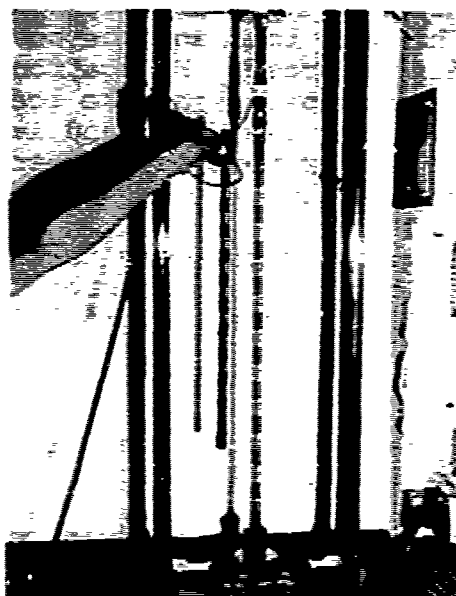
Figure 128. Typical Energy-Absorber Test Specimen
Undergoing Tensile Load Application.

Figure 129. Typical Energy-Absorber Test Specimen
Following Ultimate Failure.
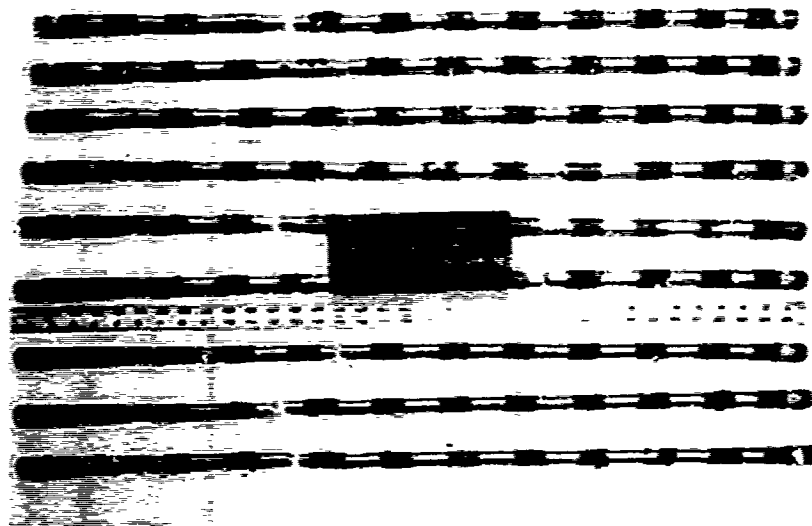
Figure 130. Tensile Tube Energy-Absorber Test Specimens
After Loading and Removal From Test Fixture.

		TABLE XXIV. ENERGY ABSORBER TEST DATA SUMMARY					
Test Specimen	Material Annealed 304 Stainless Steel	Average Elongation (pct)	Average Load (lb)	Peak Load (lb)	Total Elongation (in.)	Average Elongation (in.)	
SC-1				3345	9-1/4		
SC-2	.625-Inch O. D. x .020-Inch Wall	44.3	3382	3410	9-3/16	9-1/4	
SC-3				3390	9-5/16		
SC-4				3925	10		
SC-5	.750-Inch O.D. x .020-Inch Wall	56.4	3972	4100	9-7/8	10-1/8	
SC-6				3890	10-5/16		
SC-7				3472	10-7/16		
SC-8	.750-Inch O.D. x .016-Inch Wall	51.0	3435	3460	10-1/4	10-3/16	
SC-9				3375	9-7/8		

201
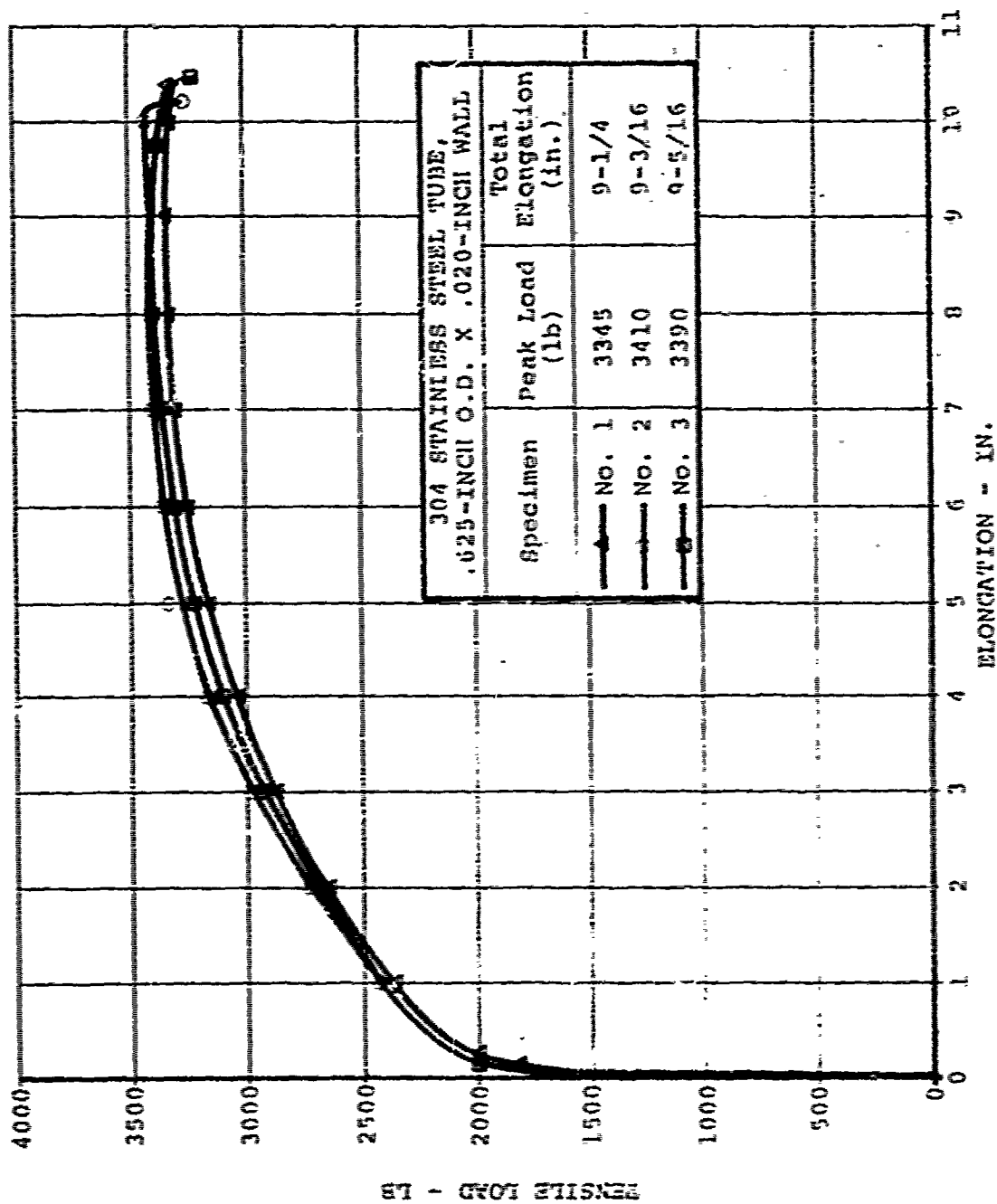
Figure 131. Load Versus Elongation Data for Test Specimens 1, 2, and 3.

The following data appears within the figure:

304 STAINLESS STEEL TUBE, .625-INCH O.D. X .020-INCH WALL

Specimen	Peak Load (lb)	Total Elongation (in.)
No. 1	3345	9-1/4
No. 2	3410	9-3/16
No. 3	3390	9-5/16

ELONGATION - IN.

TENSILE LOAD - LB

304 STAINLESS STEEL TUBE,
.750-INCH O.D. X .020-INCH WALL

Specimen	Peak Load (lb)	Total Elongation (in.)
No. 4	3925	10
No. 5	4100	9-7/8
No. 6	3090	10-5/16

TENSILE LOAD - LB

ELONGATION - IN.

Figure 132. Load Versus Elongation Data for Test Specimens 4, 5, and 6.
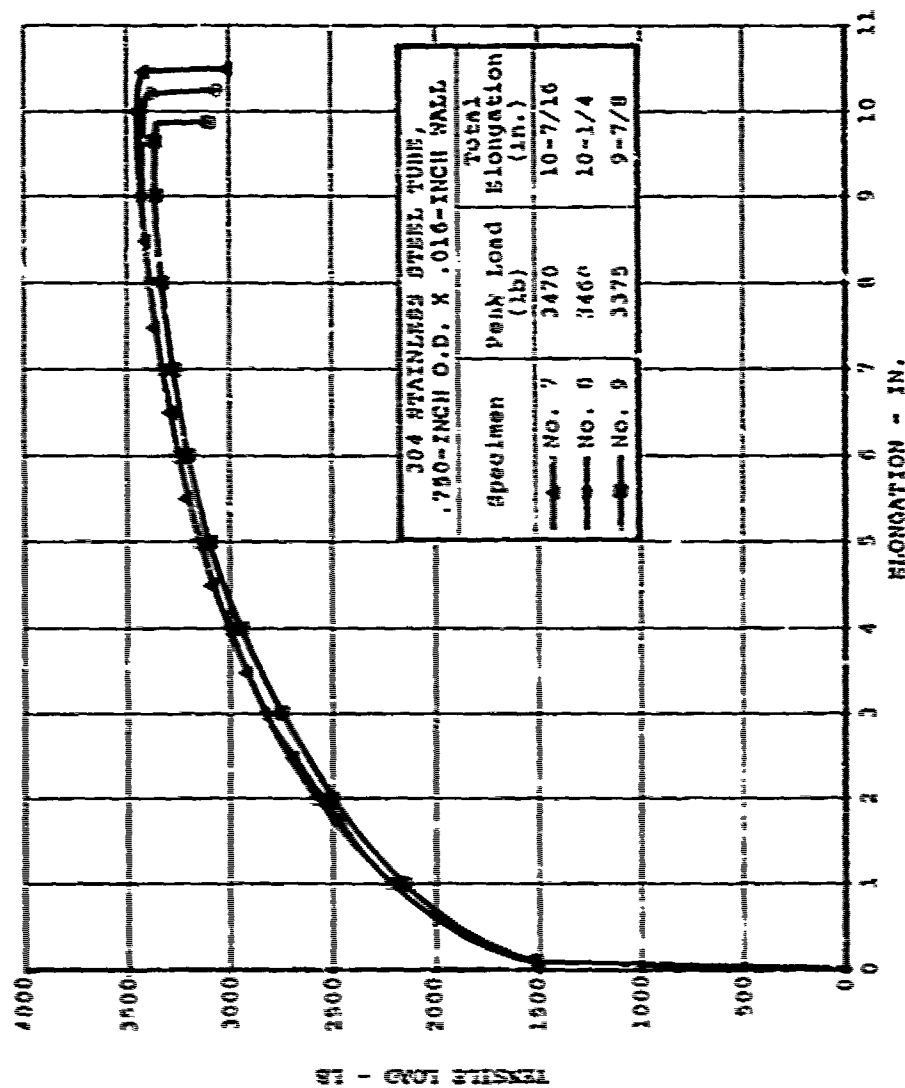
Figure 133. Load Versus Elongation Data for Test Specimens 7, 8, and 9.

304 STAINLESS STEEL TUBE,
.750-INCH O.D. X .016-INCH WALL

Specimen	Peak Load (lb)	Total Elongation (in.)
No. 7	3470	10-7/16
No. 8	3460	10-1/4
No. 9	3375	9-7/8

ELONGATION - IN.

TENSILE LOAD - LB

Symbol	Tube Size (in.)	Average Peak Load (lb)	Average Elongation (in.)
	.625 x .020	3302	9-1/4
	.75 x .020	3972	10-1/16
	.75 x .016	3435	10-3/16

TENSILE "PFT" DATA SUMMARY*
304 STAINLESS STEEL TUBES

*VALUES ARE AVERAGE OF ALL THREE TUBES FOR EACH SIZE

ELONGATION - IN.

TENSILE LOAD - LB

Figure 134. Load Versus Elongation Data Summary by Tube Sizes.

APPENDIX II

SEAT LOADING AND STRUCTURAL SIZING

This appendix presents a discussion of the calculation of the occupant and movable seat bucket loading of the guide frame assembly and an explanation of the techniques used for the sizing of the structural components of the seat.

II.1 SEAT LOADING DESIGN ENVIRONMENT

The design environments were obtained from References 2 and 5. The decelerations of the 95th percentile survivable accident and the static design load factors for the horizontal, lateral, and vertical axes are shown below:

Direction	Expected Deceleration (G)	Static Design Load Factor (G)
Horizontal	30	35
Lateral	16	20
Vertical	48	48*
		17**

II.1.1 Component Weights

The movable weight of the seat was determined from the preliminary design. The occupant weight for load calculation in the vertical direction was taken as the effective weight of the 95th percentile crewman and in the longitudinal and lateral directions as the total weight of the 95th percentile crewman. These weights were:

Movable seat weight	=	151 pounds
Effective weight of occupant	=	166 pounds
Total weight of occupant	=	211 pounds

II.1.2 Dimensions and Nomenclature

For structural sizing, the total effective weight of the occupant and movable weight of the seat were assumed to act as a

---

Fixed structure
*Load-limited structure

206

lump mass at the cg of the system. The dimensions defining
the location of the cg relative to the carrier bearing loca-
tions on the guide tubes and the symbolism used in computing
the loads are presented in the following sketch. For ease of
calculation, the axes were adjusted to coincide with the axes
of the guide tubes.
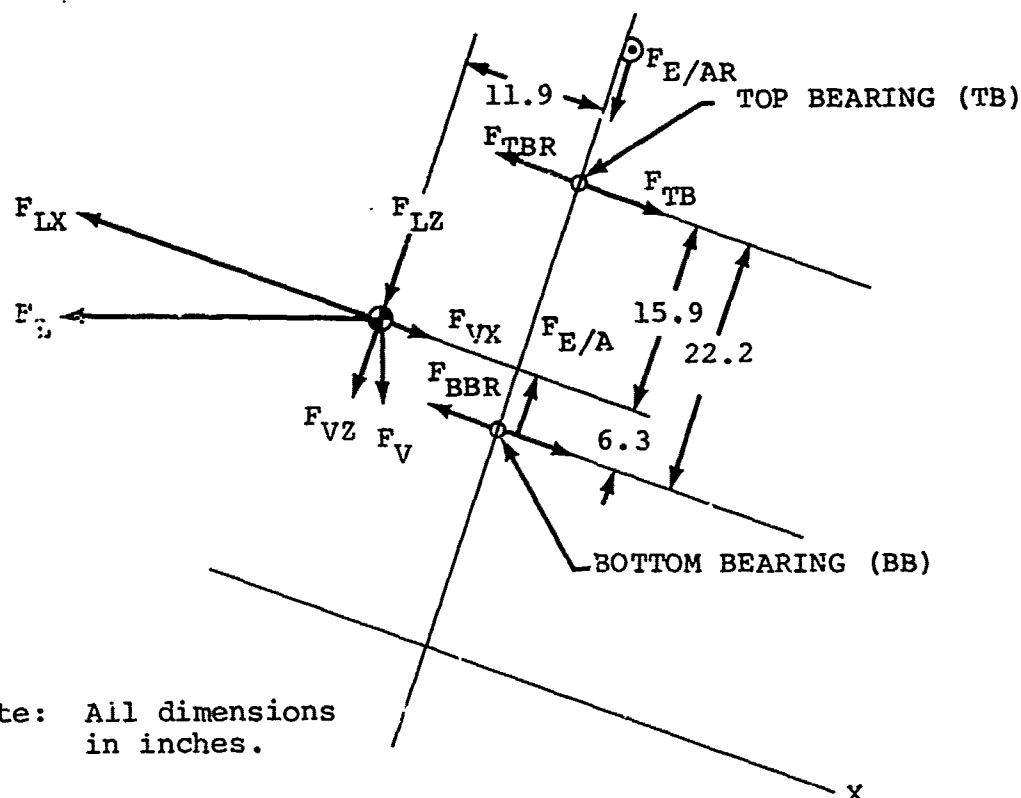
Note: All dimensions
       in inches.

where F_L = longitudinal load

       F_{L_X} = X component of longitudinal load

       F_{L_Z} = Z component of longitudinal load

       F_V = vertical load

       F_{VX} = X component of vertical load

207

F_{VZ} = Z component of vertical load

$F_{E/A}$ = energy-absorber limit load

$F_{E/AR}$ = energy-absorber limit load reaction

F_{TB} = total top bearing load

F_{TBR} = total top bearing load reaction

F_{BB} = total bottom bearing load

F_{BBR} = total bottom bearing load reaction

II.1.3 Longitudinal Loading

The inertial longitudinal load on the movable seat assembly was calculated as follows:

$$F_L = G_L [W_{T(OCC)} (O.S.) + W_{T(MS)}]$$ (43)

where F_L = longitudinal load, lb

G_L = static design load factor in longitudinal direction, G

$W_{T(OCC)}$ = weight of seat occupant, lb

O.S. = overshoot factor

$W_{T(MS)}$ = weight of movable seat, lb

For structural sizing, the overshoot factor (O.S.) was assumed to be unity, as maximum occupant loading was not expected to occur simultaneously with maximum seat load.

$$\therefore F_L = -35 [211 + 151]$$

$$= 12,670 \text{ pounds} \quad (44)$$

$$F_{LX} = -(12,670) (\cos 13°)$$

$$= -12,346 \text{ pounds} \quad (45)$$

208

$$F_{LZ} = -(12,670)\ (SIN\ 13°)$$

$$= -2,851\ \text{pounds} \tag{46}$$

and

$$F_V = \text{Total movable weight}$$

$$F_V = -362\ \text{pounds}$$

$$F_{VZ} = -(362)\ (COS\ 13°)$$

$$= -353\ \text{pounds} \tag{47}$$

$$F_{VX} = (362)\ (SIN\ 13°)$$

$$= 81\ \text{pounds} \tag{48}$$

$$\therefore \quad \sum F_X = -12,346 + 81$$

$$= \underline{-12,265\ \text{pounds}} \tag{49}$$

and

$$\sum F_Z = -2,851 - 353$$

$$= \underline{-3,204\ \text{pounds}} \tag{50}$$

The loads supported by the bearings were then calculated by summing moments about first the bottom bearing and then the top, assuming the clockwise direction as positive.

$$\sum M_{BB} = 0 \tag{51}$$

$$-(\sum F_X)\ (6.3) - (\sum F_Z)\ (11.9) + F_{TB}\ (22.2) = 0 \tag{52}$$

$$-(12,265)\ (6.3) - (3,204)\ (11.9) + F_{TB}\ (22.2) = 0$$

$$F_{TB} = \frac{77,270 + 38,128}{22.2}$$

$$F_{TB} = 5,198\ \text{pounds}$$

$$F_{TB}\ (\text{Each Bearing}) = \underline{2,599\ \text{pounds}}$$

$$\sum M_{TB} = 0 \tag{53}$$

$$(12,265) \ (15.9) - (3,204) \ (11.9) - F_{BB} \ (22.2) = 0 \tag{54}$$

$$F_{BB} = \frac{195,014 - 38,128}{22.2}$$

$$F_{BB} = 7,067 \text{ pounds}$$

$$F_{BB} \ (\text{Each Bearing}) = \underline{3,534 \text{ pounds}}$$

and the load applied to the energy absorber was

$$F_{EA} = - \ F_Z = \underline{3,204 \text{ pounds}}$$

The loads exerted on the guide tubes by each bottom bearing, by each top bearing, and by the energy absorber under longitudinal loading were therefore, respectively,

$$-F_{BB} = F_{BBR} = -3,534 \text{ pounds}$$

$$-F_{TB} = F_{TBR} = -2,599 \text{ pounds}$$

$$-F_{E/A} = F_{E/AR} = -3,204 \text{ pounds}$$

where the sign convention was
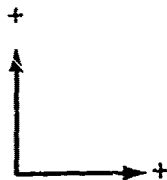
II.1.4 Vertical Loads

The inertial load on the movable seat assembly was calculated as follows:

$$F_V = [Wt_{(OCC \ EFF)} + Wt_{MS}] \ (-G_Z) \tag{55}$$

210

where G_Z = limit load factor in Z direction

$$F_V = (166 + 151)(-18)$$

$$F_V = -5,706 \text{ pounds}$$

$$F_{VZ} = (-5,706)(\cos 13°)$$

$$= -5,558 \text{ pounds} \tag{56}$$

$$F_{VX} = (-5,706)(\sin 13°)$$

$$= -1,284 \text{ pounds} \tag{57}$$

The loads supported by the bearings were then calculated by summing moments about first the bottom bearing and then the top, assuming the clockwise direction as positive.

$$\sum M_{BB} = 0 \tag{58}$$

$$-(F_{VZ})(11.9) + (F_{VX})(6.3) + F_{TB}(22.2) = 0 \tag{59}$$

$$-(5,558)(11.9) + (1,284)(6.3) + F_{TB}(22.2) = 0$$

$$F_{TB} = \frac{66,140 - 8,089}{22.2}$$

$$= -2,615 \text{ pounds}$$

$$F_{TB} \text{ (Each Bearing)} = \underline{-1,308 \text{ pounds}}$$

$$\sum M_{TB} = 0$$

$$-F_{VZ}(11.9) - F_{VX}(15.9) - F_{BB}(22.2) = 0 \tag{60}$$

$$-(5,558)(11.9) - (1,284)(15.9) - F_{BB}(22.2) = 0 \tag{61}$$

$$F_{BB} = \frac{66,140 + 20,416}{22.2}$$

$$= -3,899 \text{ pounds}$$

$$F_{BB} \text{ (Each Bearing)} = \underline{-1,950 \text{ pounds}}$$

and the load applied to the energy absorber was

$$F_{EA} = -F_{VZ} = \underline{5,558 \text{ pounds}}$$

The load exerted on the guide tubes by each bottom bearing, each top bearing, and by the energy absorber under vertical loading were, respectively,

$$-F_{BB} = F_{BBR} = 1,950 \text{ pounds}$$

$$-F_{TB} = F_{TBR} = -1,308 \text{ pounds}$$

$$-F_{EA} = F_{E/AR} = -5,558 \text{ pounds}$$

where the sign convention was
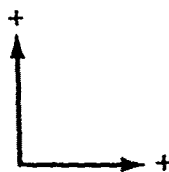
II.1.5 Lateral Loading

The inertial lateral load on the movable seat assembly was calculated as follows:

212
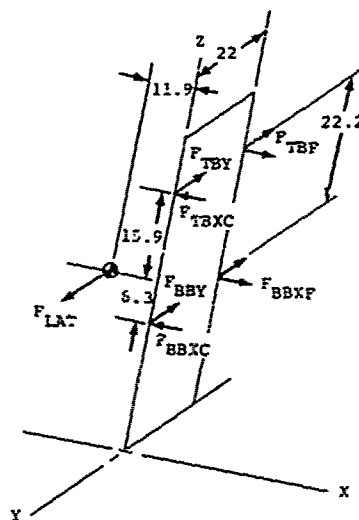
Referring to the preceding sketch,

$$F_{LAT} = F_Y = (G_Y) \ (Wt_{OCC} + Wt_{MS}) \tag{62}$$

where G_Y = static design load factor in lateral direction, G

$$F_{LAT} = F_Y = (20) \ (317)$$

$$= 6,340 \ pounds$$

The loads supported by the bearings were then calculated by summing moments about the bottom and top bearings in the X-Z plane, about the Z axis, and about the center of gravity of the occupant and movable seat.

$$\sum M_{BBX} = 0 \tag{63}$$

Assuming clockwise rotation about an axis lying in the X-Z plane as positive,

$$-F_Y \ (6.3) + F_{TBY} \ (22.2) = 0 \tag{64}$$

$$-(6,340) \ (6.3) + F_{TBY} \ (22.2) = 0$$

$$F_{TBY} = \frac{39,942}{22.2}$$

$$= 1,799 \ pounds$$

$$F_{TBY} \ (Each \ Bearing) = \underline{900 \ pounds}$$

$$\sum M_{TBX} = 0 \tag{65}$$

$$(F_Y) \ (15.9) - F_{BBY} \ (22.2) = 0 \tag{66}$$

$$(6,340) \ (15.9) - F_{BBY} \ (22.2) = 0$$

$$F_{BBY} = \frac{100,806}{22.2}$$

$$= 4,541 \ pounds$$

$$F_{BBY} \ (Each \ Bearing) = \underline{2,271 \ pounds}$$

Assuming clockwise rotation about the Z axis as positive,

$$\sum M_Z = 0 \tag{67}$$

$$-(F_Y)(11.9) + F_{BBXF}(22) + F_{TBXF}(22) = 0 \tag{68}$$

$$-(6,340)(11.9) + F_{BBXF}(22) + F_{TBXF}(22) = 0$$

Balancing moments about the center of gravity of the occupant and movable seat resulted in the following relationship:

$$(F_{BBX})(6.3) = (F_{TBX})(15.9) \tag{69}$$

and

$$F_{BBX} = \frac{(F_{TBX})(15.9)}{6.3}$$

or

$$F_{BBX} = 2.52 (F_{TBX}) \tag{70}$$

Substitution of this value for F_{BBX} into the relationship developed above for $\sum M_Z = 0$ yielded

$$-75,446 + (22)(2.52)(F_{TBX}) + F_{TBX}(22) = 0 \tag{71}$$

$$F_{TBX} = \frac{75,446}{22 (3.52)}$$

$$= \underline{974 \text{ pounds}} \text{ (Each Bearing)}$$

$$F_{BBX} = (2.52)(974)$$

$$= \underline{2,455 \text{ pounds}} \text{ (Each Bearing)}$$

The directions of the forces acting on the guide tubes are opposite to those shown as bearing loads on the previous sketch.

A summary of the pure longitudinal, vertical, and lateral loading of the guide tubes is shown in Table XXV, with arrows denoting the direction of force.

TABLE XXV. SUMMARY OF PURE LONGITUDINAL, VERTICAL, AND LATERAL LOADING ON GUIDE TUBES				
Load Identification	Longitudinal Loads* (lb)	Vertical Loads** (lb)	Lateral Loads*** (lb)	
	Close and Far Members	Close and Far Members	Close Member	Far Member
F_{TB} (Longitudinal)	2,599 ⟵	1,308 ⟵	974 ⟶	974 ⟵
F_{TB} (Lateral)	0	0	900 ⟋	900 ⟋
F_{BB} (Longitudinal)	3,534 ⟵	1,950 ⟶	2,455 ⟶	2,455 ⟵
F_{BB} (Lateral)	0	0	2,271 ⟋	2,271 ⟋
$F_{E/A}$	3,204 ↓	5,558 ↓	0	0

  *Static design load factor of 35G
 **Static design load factor of 18G (load-limited and in-
   cluding 1G to account for system weight)
***Static design load factor of 20G

II.1.6 Combined Loading

Combined loads were calculated by correcting the individual loading components by the trigonometric relationships of the planned dynamic test loading and then algebraically summing load components. Test No. 1 called out in References 2 and 5 is a vertical drop test with the seat pitched forward 30 de-grees and rolled 10 degrees with respect to the impact veloc-ity vector.

The peak input deceleration required is 48G; thus, the deceler-ative loading components are as follows:

$$G_{VERT} = (48) \ (COS \ 30) \ (COS \ 10) \tag{72}$$

$$= 40.9$$

$$41G$$

215

$$G_{LONG} = (48) \ (SIN \ 30) \tag{73}$$

$$= 24G$$

$$G_{LAT} = (48) \ (COS \ 30) \ (SIN \ 10) \tag{74}$$

$$= 7.2$$

$$8G$$

Test No. 2 called out in References 2 and 5 is a longitudinal-lateral test with the seat yawed 30 degrees to the impact velocity vector. The peak resultant deceleration required is 30G; however, for design purposes in this direction, the 35G static design load factor was used. The loading components were as follows:

$$G_{LONG} = (35) \ (COS \ 30) \tag{75}$$

$$= 30G$$

$$G_{LAT} = (35) \ (SIN \ 30) \tag{76}$$

$$= 18G$$

Correction factors were then established as the ratios of the decelerative components calculated for the specific test configurations to the static design load factors used to calculate the pure longitudinal, vertical, and lateral loading. The correction factors are shown below:

Direction	Test No. 1	Test No. 2
Longitudinal	$\frac{24}{35} = .69$	$\frac{30}{35} = .86$
Vertical	$= 1$	$= 1$
Lateral	$\frac{8}{20} = .40$	$\frac{18}{20} = .90$

The summary of combined loading of the guide tubes is presented in Table XXVI, with arrows indicating the load directions.

Sketches of the frame assembly with the applied loads are shown in Figures 135 through 139.

216

TABLE XXVI. SUMMARY OF COMBINED LOADING OF GUIDE TUBES

Load Identification	Correction Factor Used	Test No. 1 (2,5) Triaxial Loading		Test No. 2 (2,5) Biaxial Loading	
		Close Member (lb)	Far Member (lb)	Close Member (lb)	Far Member (lb)
F_{TB} (Longitudinal)	(.69)	1,793 ↓	1,793 ↓	2,235 ↓	2,235 ↓
	(1.0)	1,308 ↑	1,308 →	0	0
	(.4)	390 ↓	390 ↓	877 ↓	877 ↓
	—	2,711 ↘	3,491 ↓	1,358 ↓	3,112 ↘
F_{TB} (Lateral)	(.4)	360 (+Y or Out) ↓	360 (+Y or Out) ↓	810 (+Y or Out) ↓	810 ↘
F_{BB} (Longitudinal)	(.69)	2,438 ↓	2,438 ↓	2,039 ↓	2,039 ↓
	(1.0)	1,950 ↑	1,950 ↑	0	0
	(.4)	982 ↑	982 ↓	2,210 ↓	2,210 ↓
		494	1,470 ↓	829 ↓	5,249 ↓
F_{BB} (Lateral)	(.4)	908 ↘	908 ↙	2,044 ↙	2,044 ↘
$F_{E/A}$	1.0	5,558		2,755	

217

Note: All loads in pounds.

CLOSE MEMBER

FAR MEMBER

3,204

2,599

2,599

3,534

3,534
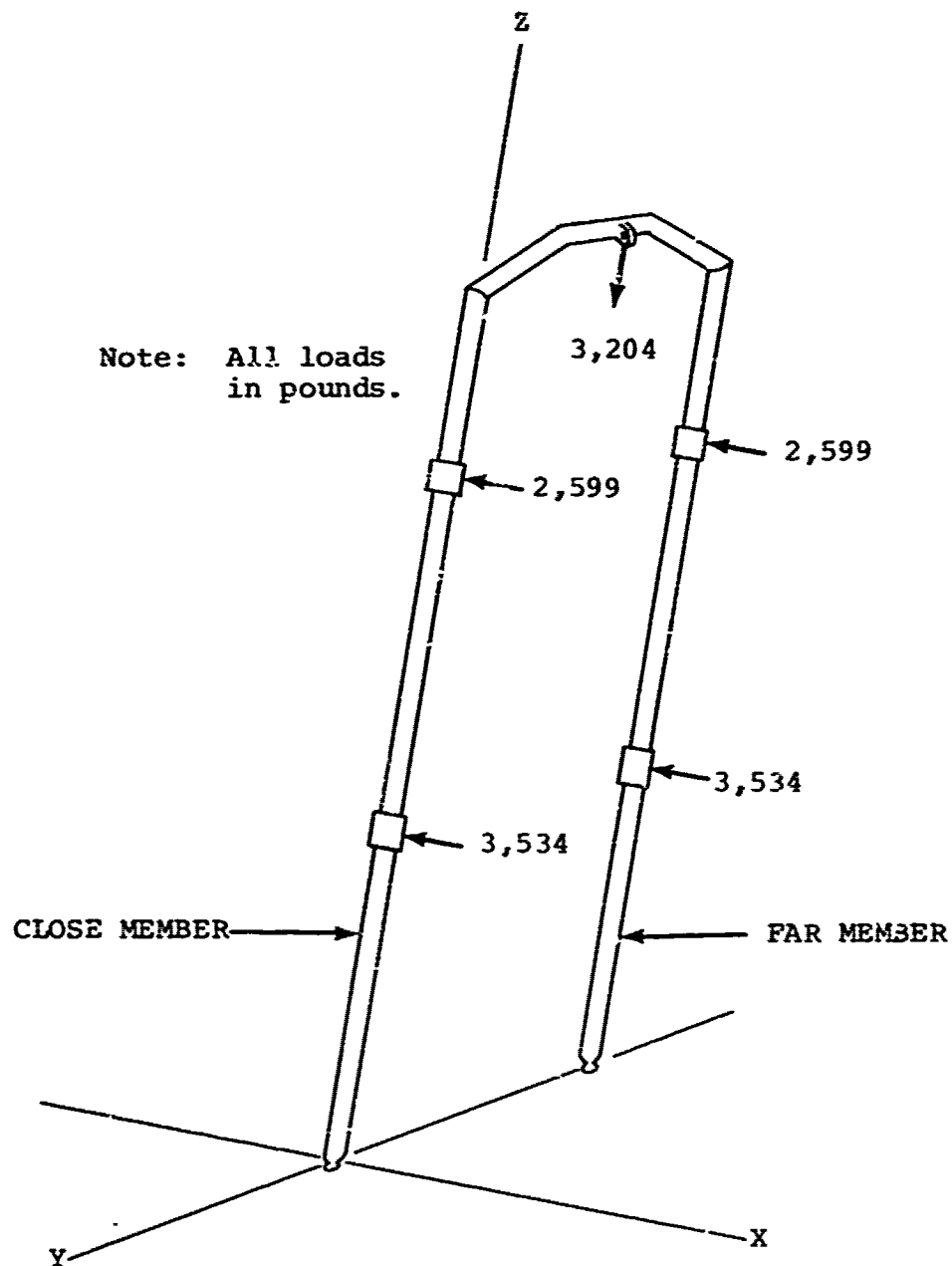
Figure 135. Applied Loading of Guide Frame Assembly - Longitudinal Loading.

218
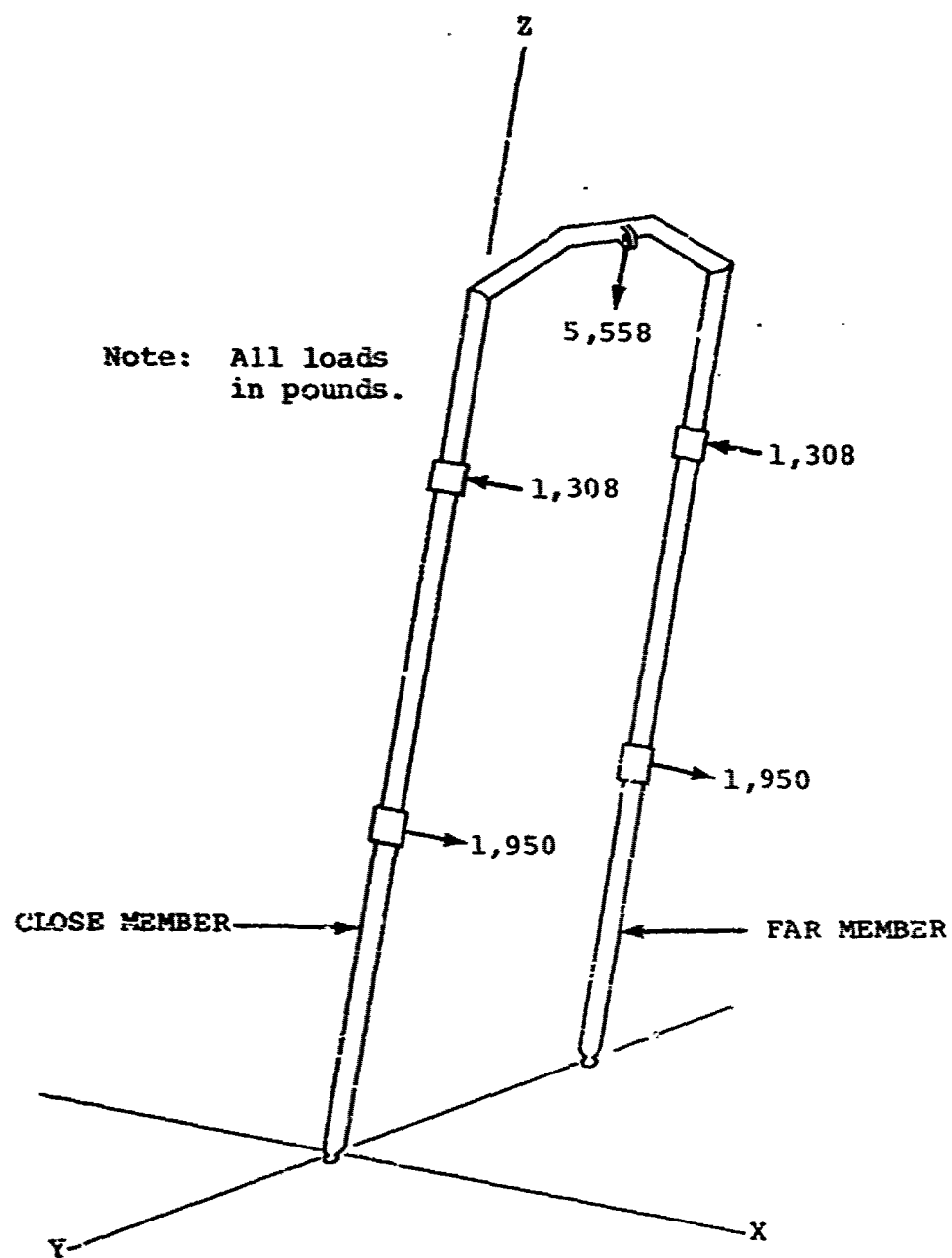
Figure 136. Applied Loading of Guide Frame Assembly -
Vertical Loading.
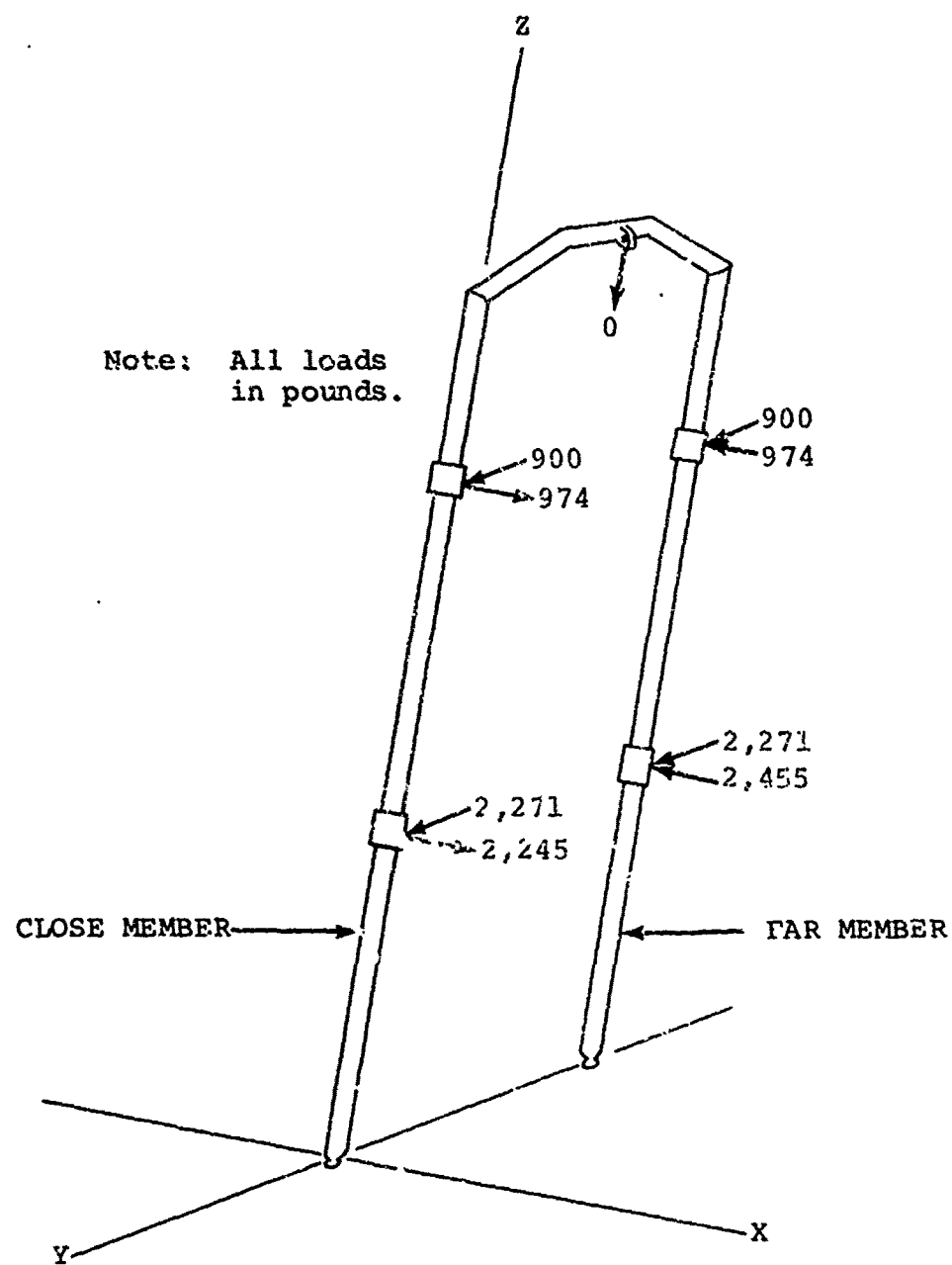
Figure 137. Applied Loading of Guide Frame Assembly -
Lateral Loading.

220
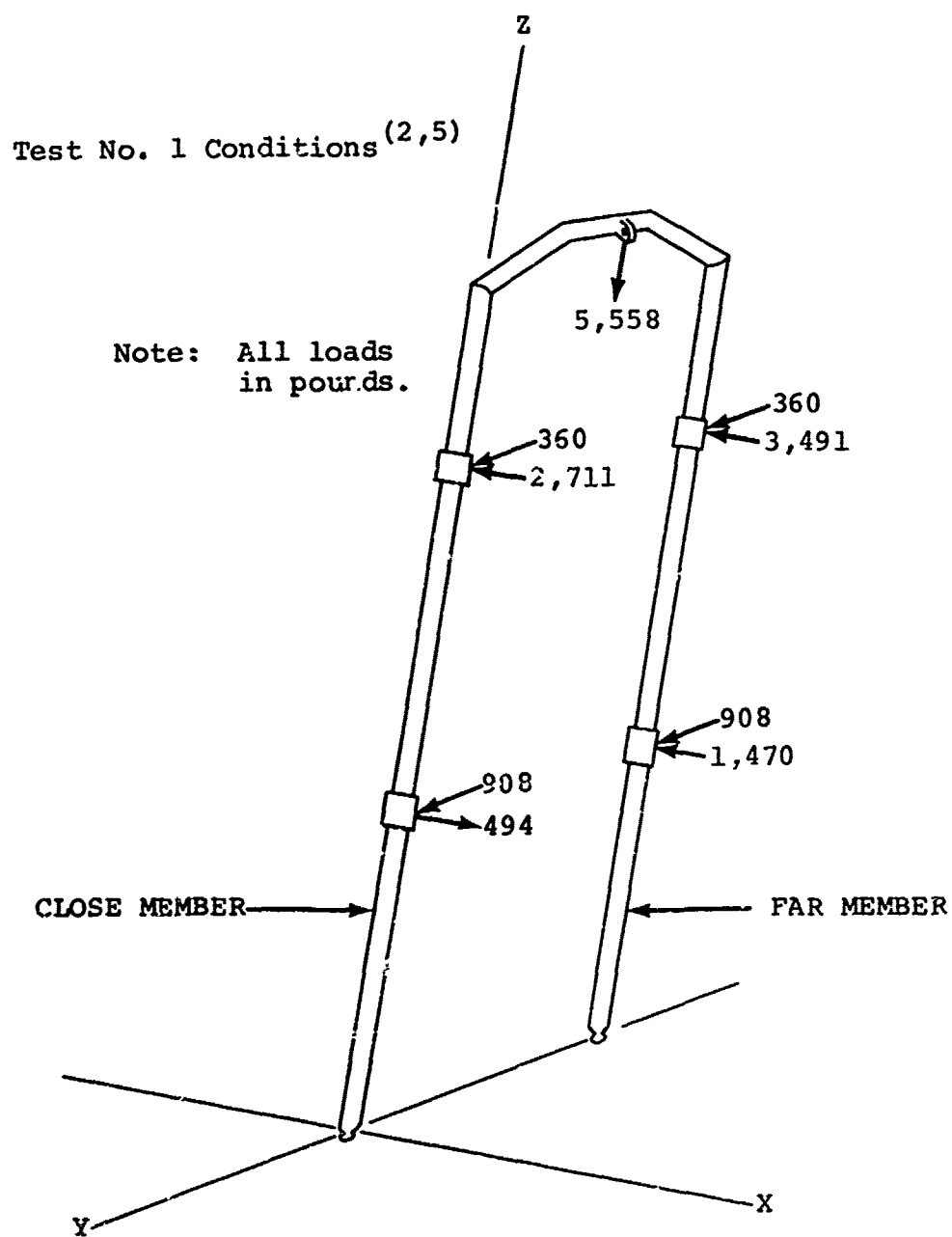
Figure 138. Applied Loading of Guide Frame Assembly –
Triaxial Test.

Test No. 2 Conditions[2,5]

Note: All loads
in pounds.

2,755

810
3,112

810
1,358

2,044
5,249

2,044
829

CLOSE MEMBER

FAR MEMBER

Z

X

Y
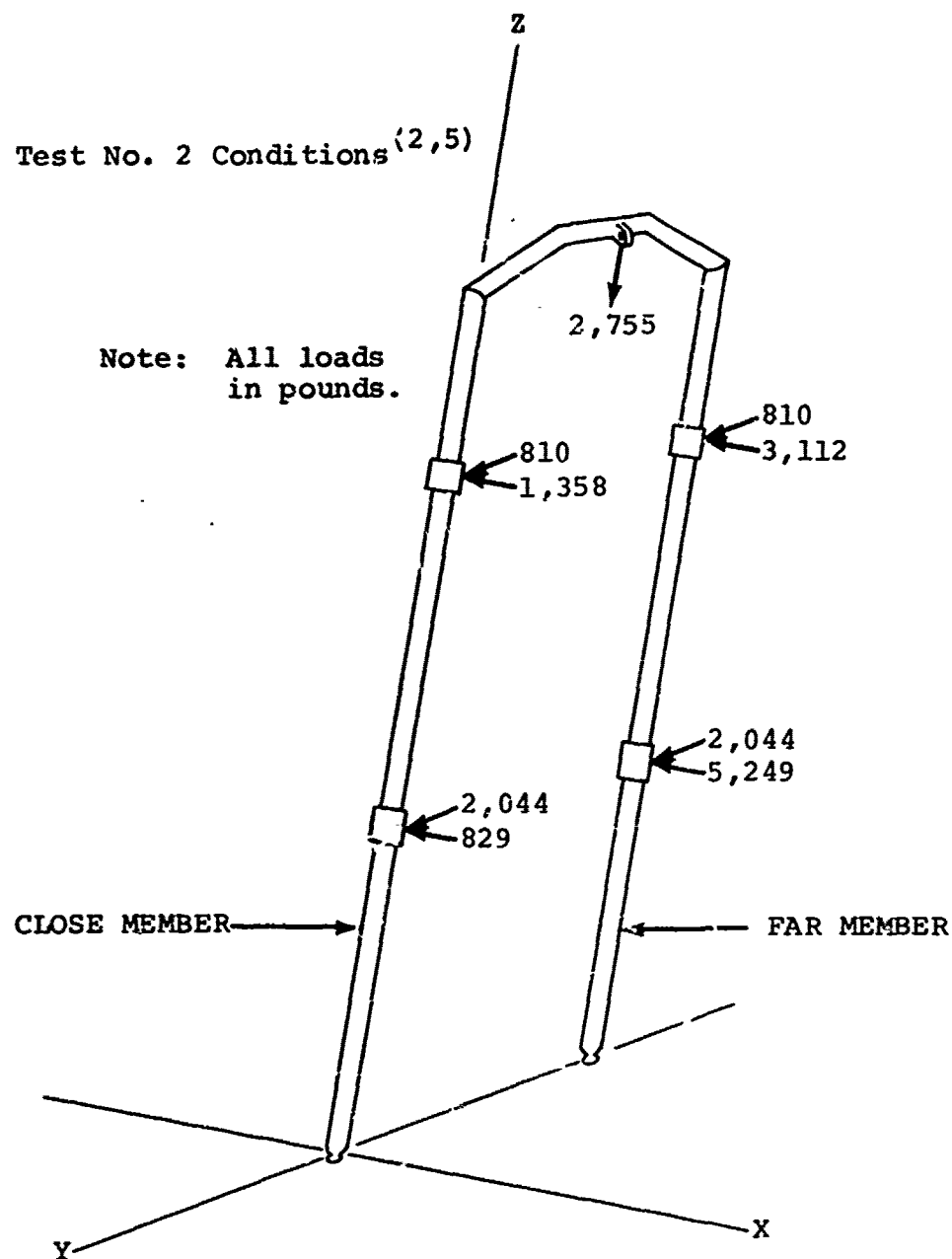
Figure 139.   Applied Loading of Guide Frame Assembly -
Biaxial Test.

222

II.2 STRUCTURAL SIZING

Support structure sizing was accomplished through use of STRESS, a computer program which performs a linear analysis of elastic statically loaded frame truss type structures. The analysis computes internal member forces and moments, joint rotations and displacements, and support reactions. The program can handle both small and large structural problems, including from 2 to over 800 degrees of freedom. This program is particularly well suited for design analysis and was therefore used in support of the design effort.

During the design development, the configuration of the seat changed considerably several times; consequently, since the analysis was being used as a design sizing support tool, analyses were repeated only in those areas which changed in a manner which would increase the loading.

Use of the analysis required establishment of the coordinates of all members and joints. Loads were then applied at representative coordinate points and the frame response was computed. Two such analyses were conducted during the design effort to check the selection of structural members and for use in computing the sizes required. Since no effort was made to optimize the weight of the support structure, some of the members were left considerably overdesigned.

Sizing of indivi al structural components such as bearings, brackets, and fasteners was accomplished in the typical design fashion using applicable formulas from Roark, "Formulas For Stress And Strain", or developed from basic relationships.

Since the seat structure was not optimized for weight, a detailed presentation of the structural design sizing calculations performed is not included in this report.

APPENDIX III

HELICOPTER CRASH TEST OF MODIFIED SEAT

III.1 TEST OBJECTIVE

The objective of this effort was to modify the test seat to be
more representative of an operational seat and to demonstrate
its performance in a full-scale helicopter crash environment.

III.2 SEAT MODIFICATION

The modification effort included replacement of the long ten-
sile tube type energy absorber with a rolling torus type.
This enabled removal of the high upper yoke on the guide frame
assembly and provided an energy absorber having rebound capa-
bility typical of a required end item device. Seat modifica-
tion effort was minimized to incorporate only those changes
necessary for inclusion of the different type energy absorber.

The rolling-torus-type energy absorber selected for this test
consisted of two concentric cylinders with a continuous wrap
of stainless steel wire interference fit between the cylinders
as shown in Figure 140. Impact energy is absorbed by cyclic
plastic deformation of the wire as the tubes are separated.
The force-elongation characteristic provided by this type of
energy absorber is essentially trapezoidal, although the ini-
tial breakout force typically exceeds the plastic force level
following it. The device is capable of absorbing energy when
stroked in either direction and will withstand several cycles
with little change in force-elongation trace shape. Typical
specific energy of this type of device is on the order of
$1,453$ ft-lb/lb^2.

The seat that was modified had previously been subjected to
several dynamic tests. The modification included removal of
the top yoke from the guide frame assembly, fabrication and
welding of an attachment bracket to the upper crossmember of
the support structure, inversion of the lower bearing cross-
member, and fabrication and fastening of another attachment
bracket to that crossmember. Inversion of the lower bearing
crossmember was used as a method of shortening the distance
between the upper energy-absorber attachment bracket and the
lower attachment bracket. In the unmodified design, the lower
energy-absorber attachment bracket was welded to the cross-
member and extended below it to increase the distance between
the lower and the upper bracket as needed for the type of
energy absorber chosen for dynamic testing. During modifica-
tion, it was desired to decrease this distance; consequently,

224
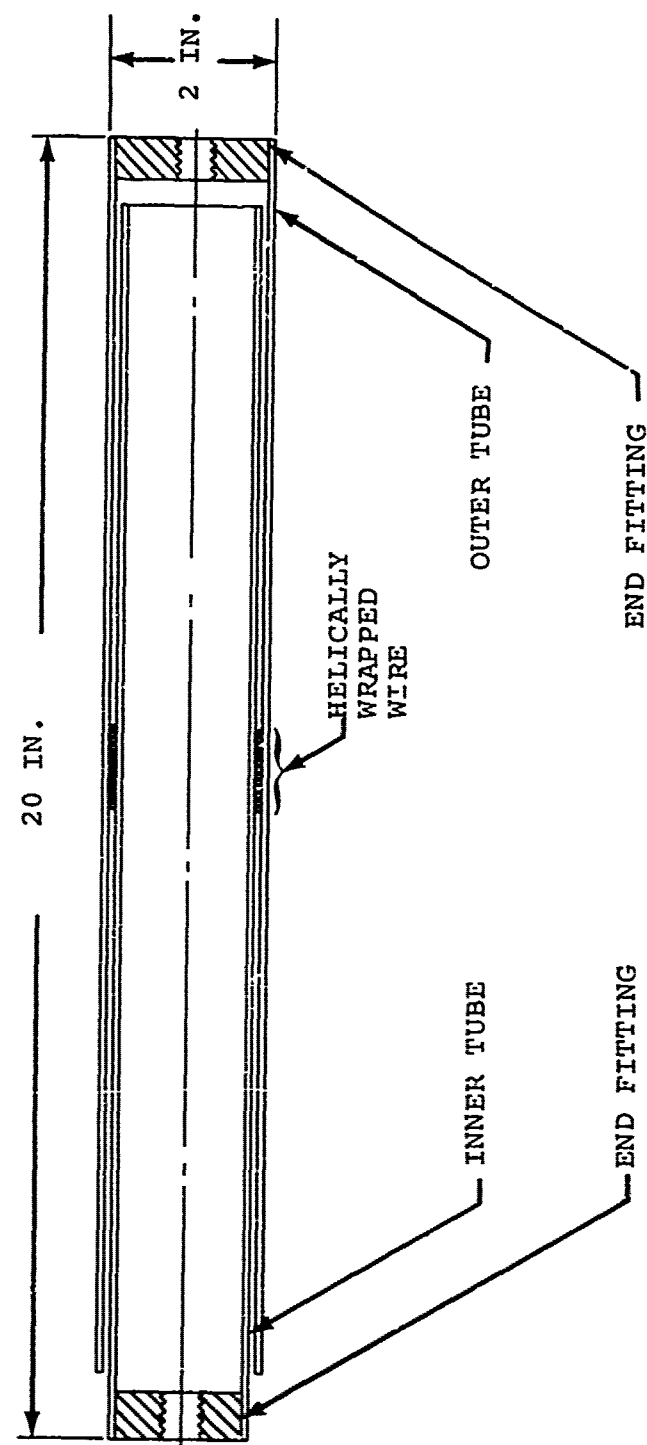
Figure 140. Section of Rolling Torus Energy Absorber.

225

the lower bearing crossmember was inverted, which extended the attachment bracket upward instead of downward as shown in Figure 141.

ORIGINAL CONFIGURATION

INVERTED CONFIGURATION WITH BOTTOM ENERGY-ABSORBER ATTACHMENT BRACKET
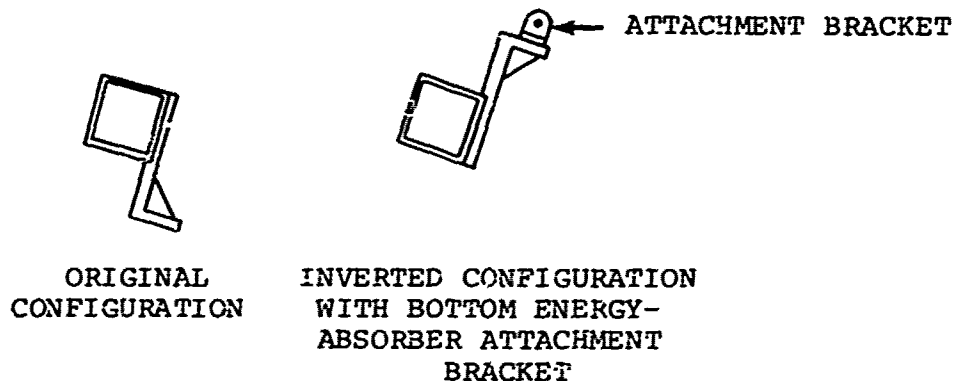
Figure 141.   Lower Bearing Crossmember, Original and Modified.

An additional bracket for the lower end of the rolling torus energy absorber was then bolted to the upper surface of the existing bracket.

A steel mounting plate was also designed, fabricated, and installed on the floor of the test helicopter (UH-1D/H) to provide a mounting surface for the seat.

The modified crew seat was installed on the plate in the co-pilot's position, and a 95th percentile anthropomorphic dummy was instrumented, clothed, and installed as the seat occupant. Views of the installation with and without occupant are shown in Figures 142 through 145. Figure 144 is a rear view showing the mounting plate, some of the floor instrumentation, and the rolling torus type energy-absorber installation.

III.3   TEST VEHICLE

The test vehicle was a UH-1D/H helicopter that was crash tested to verify the performance of the Crash Resistant Fuel System (CRFS) in a severe crash environment. Complete details of the CRFS investigation are provided in USAAMRDL Technical Report 71-47, "Evaluation of the UH-1D/H Helicopter Crash-worthy Fuel System in a Crash Environment" (being published).

226
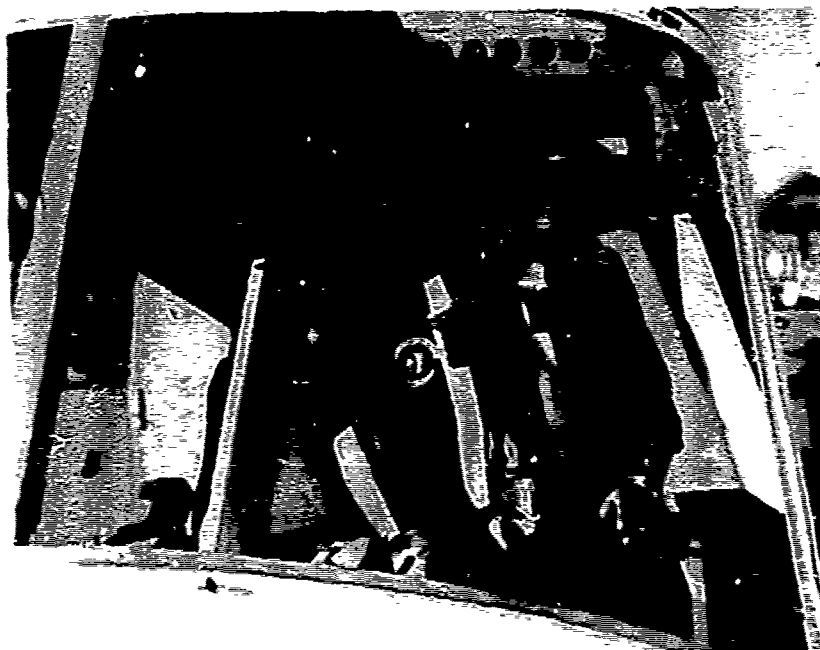
Figure 142.   Front View of Seat and Dummy.
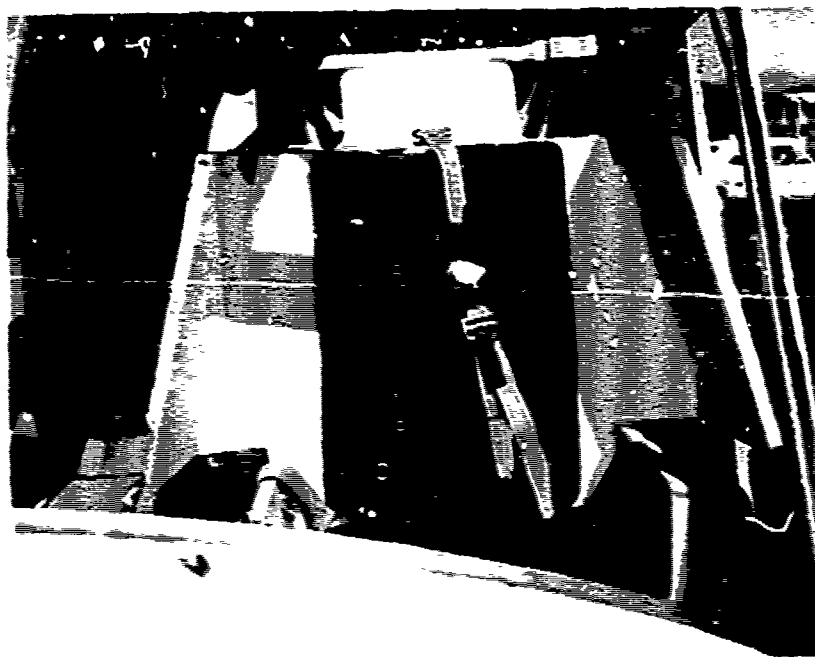
Figure 143.   Front View of Seat.

227
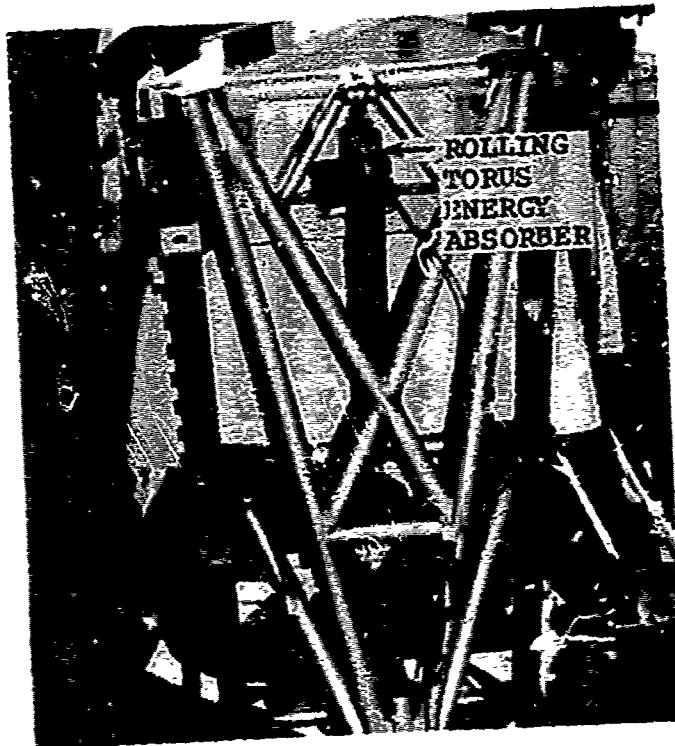
Figure 144. Rear View of Seat.

Figure 145. Side View of Seat.

228

III.4 OVERALL TEST RESULT

When the test helicopter impacted, the seat received severe loading in all three axes, including a vertical deceleration of 79.7G measured on the mounting plate at floor level under the seat support structure.

The seat withstood the longitudinal and lateral forces extremely well, restraining the occupant without evidence of incipient failure or permanent deformation. Figure 146 is a view of the seat in the stroked position after the test. Failure of the lower bearing crossmember which provided the attachment for the lower end of the energy absorber, however, resulted in failure to stroke the energy absorber and thus to obtain vertical energy-absorbing performance. This crossmember was a square aluminum tube with 0.125-inch wall thickness. Since square tubing of this size was not available when needed for fabrication of the original seats, it was formed by welding two aluminum angles together. Posttest analysis revealed that one of the welds had insufficient penetration. Figure 147 shows the deficient weld and progression of failure.

During the entire dynamic testing series to which this seat had previously been subjected, this member successfully withstood repeated loads of greater magnitude than imposed in the crash test. As previously explained, during modification to accept the rolling torus energy absorber, this member was inverted. This placed the deficient weld in a location where it was loaded differently than during the previous tests. The vertical load from the energy absorber (4,520 pounds) caused initial failure of the weld under the attachment bracket. This failure progressed to the ends of the crossmember, with the bracket peeling the top panel of the box upward and outward and eventually failing in tension.

Although the energy absorber did not stroke, sufficient energy was absorbed through progressive failure of the bearing crossmember to limit the vertical decelerative loading on the dummy to the values listed below:

Peak Chest Deceleration	Peak Pelvic Deceleration	Peak Seat Pan Deceleration
27.8G	20.6G	27.1G

Review of the time-at-G-level dependency of human tolerance indicates that these pulses would have been survivable. The energy-absorption capability was provided by progressive rather than brittle failure of the 6061-aluminum angle from which the crossmember was formed. Although the primary

229
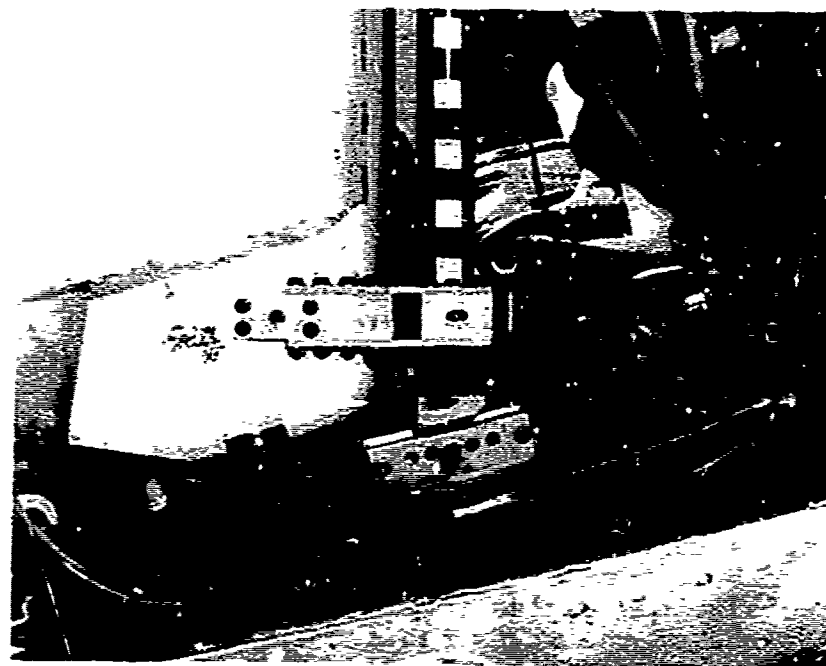
Figure 146. View of Floor Attachments and Seat in Stroked Position.
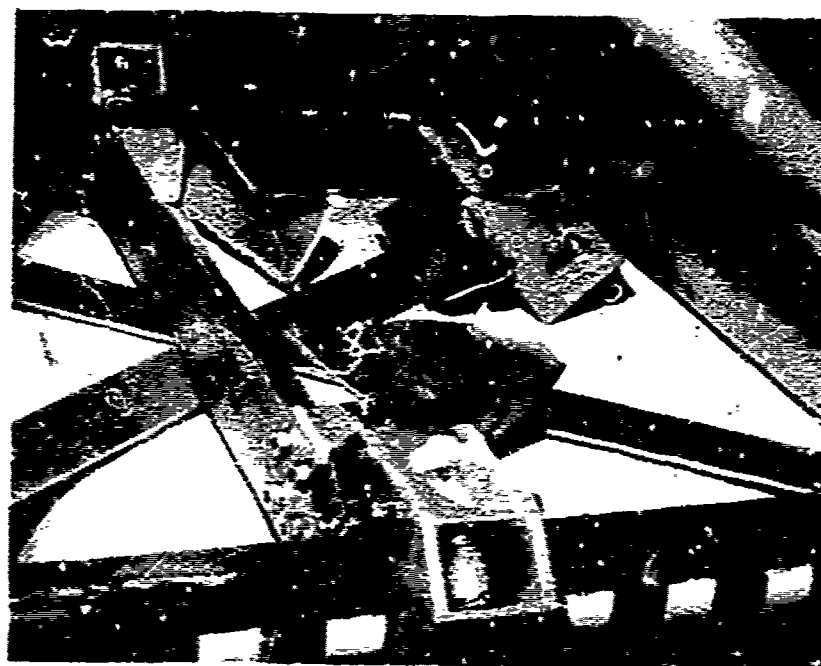
Figure 147. Lower Bearing Crossmember Failure.

objective of the test was not achieved, it is interesting to note that the occupant was protected and would have survived the crash because of adherence to the principles outlined in the Crash Survival Design Guide[2] recommending the use of ductile materials.

Table XXVII presents a summary of the peak decelerations and energy-absorber (failure strength of bearing crossmember) limit loads measured during the test.

TABLE XXVII. SUMMARY OF HELICOPTER CRASH TEST DATA			
	Peak Measurement		
Measurement	Vertical	Longitudinal	Lateral
Helicopter Floor Deceleration (G)	79.7	23.5	7.2
Seat Pan Deceleration (G)	27.1	20.3	12.1
Dummy Pelvis Deceleration (G)	20.6	30.4	11.3
Dummy Chest Deceleration (G)	27.8	43.1	17.3
Energy-Absorber Limit Load (lb)	4,520	–	–

APPENDIX IV

DYNAMIC TEST DATA

This appendix presents all the dynamic test data of interest
to the analysis of the seat performance. It includes input,
seat and dummy deceleration, energy-absorber limit, and har-
ness load-versus-time traces recorded during the dynamic tests.
Peak values were presented in Table XVII.

The sign convention used in presenting the data is consistent
with standard terminology presented in Figure 101. For ex-
ample, eyeballs out deceleration is negative in sign and eye-
balls down deceleration is positive in sign.

232
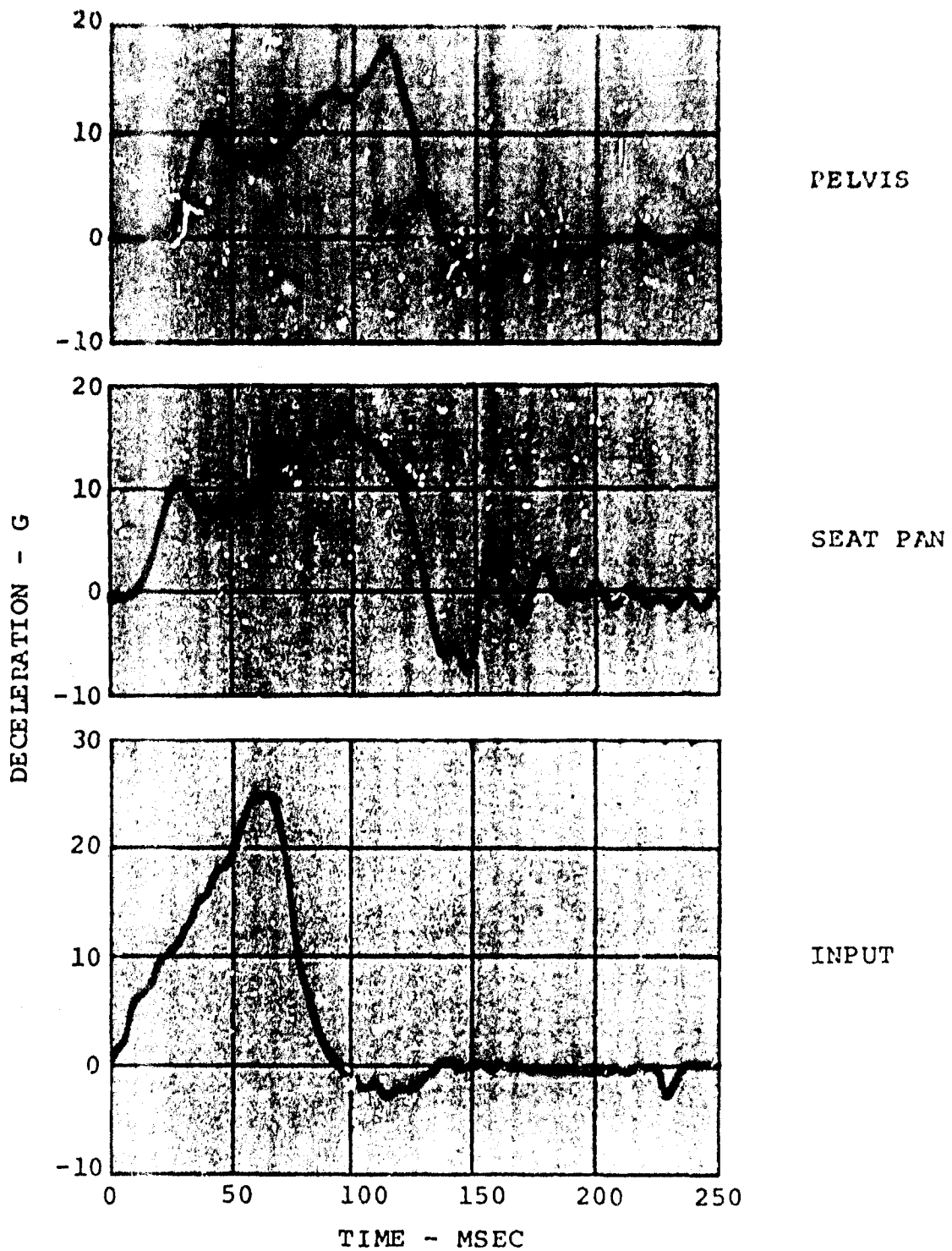
Figure 148. Vertical Pelvis, Seat Pan, and Input
Decelerations (Test 1A).
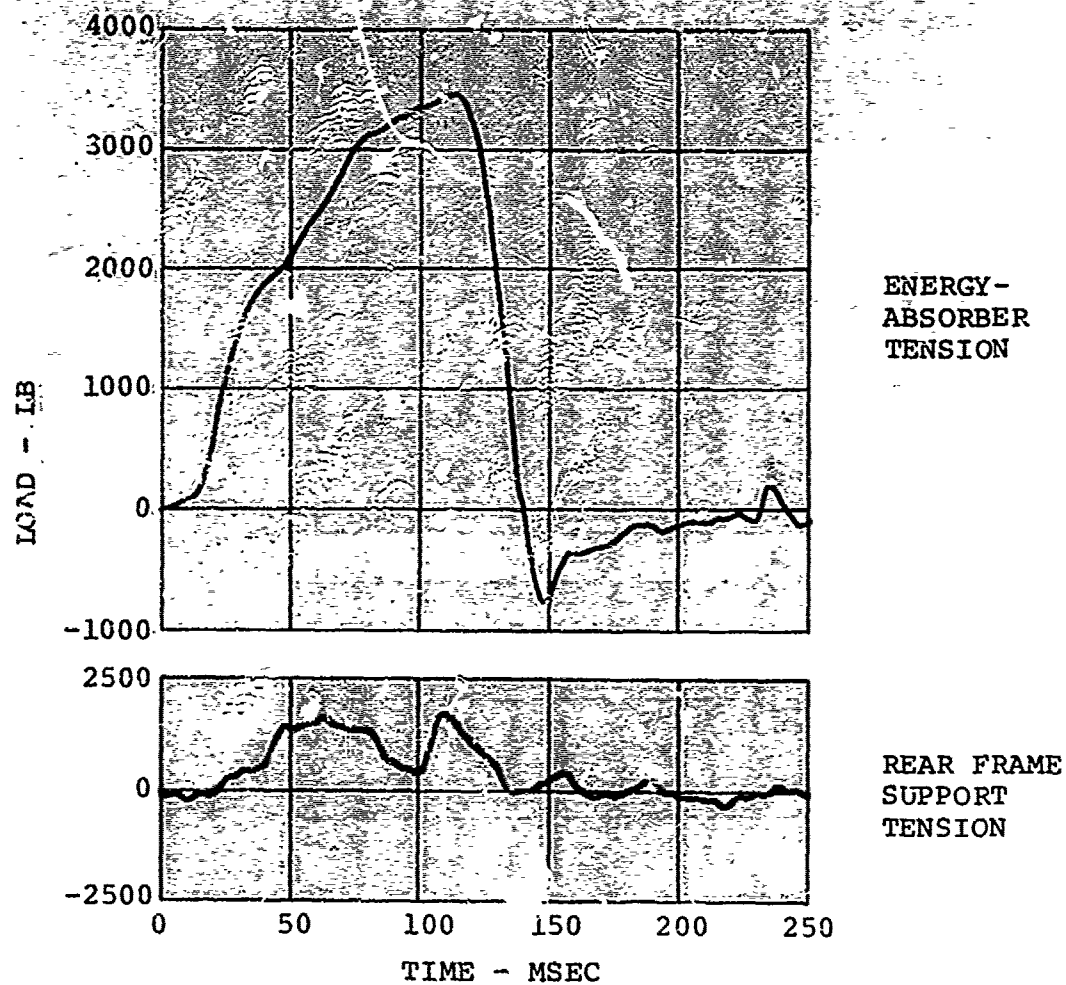
Figure 149. Energy-Absorber and Rear Frame Support Loads (Test 1A).
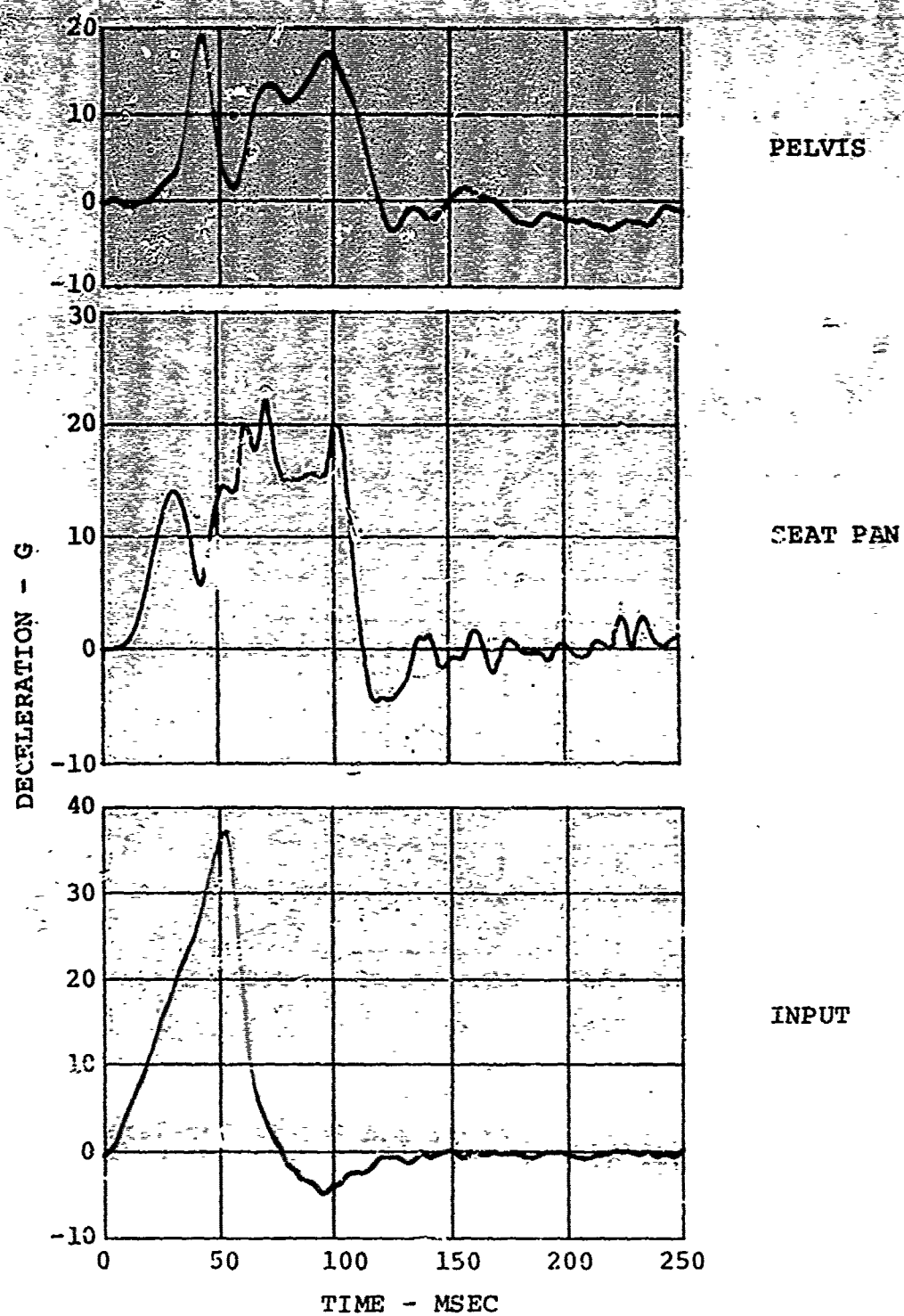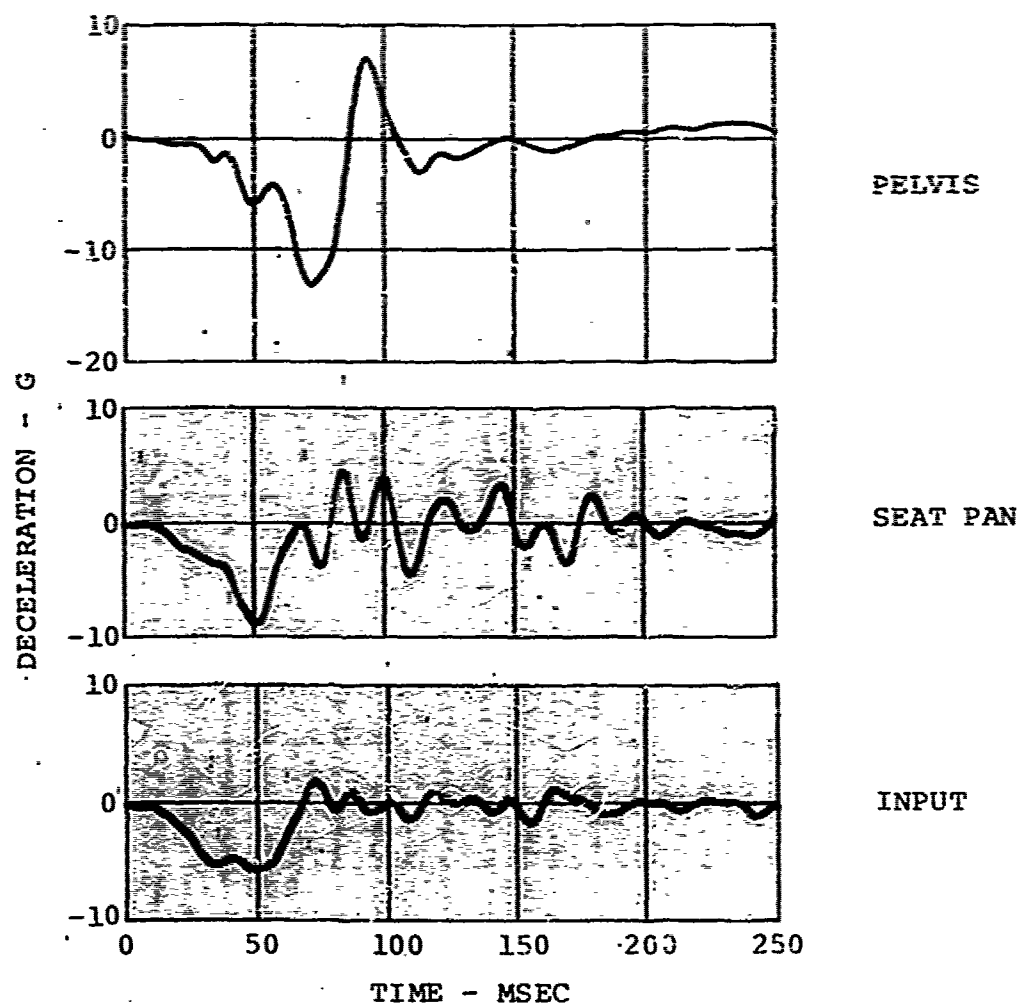
Figure 150. Vertical Pelvis, Seat Pan, and Input
Decelerations (Test 2).

235
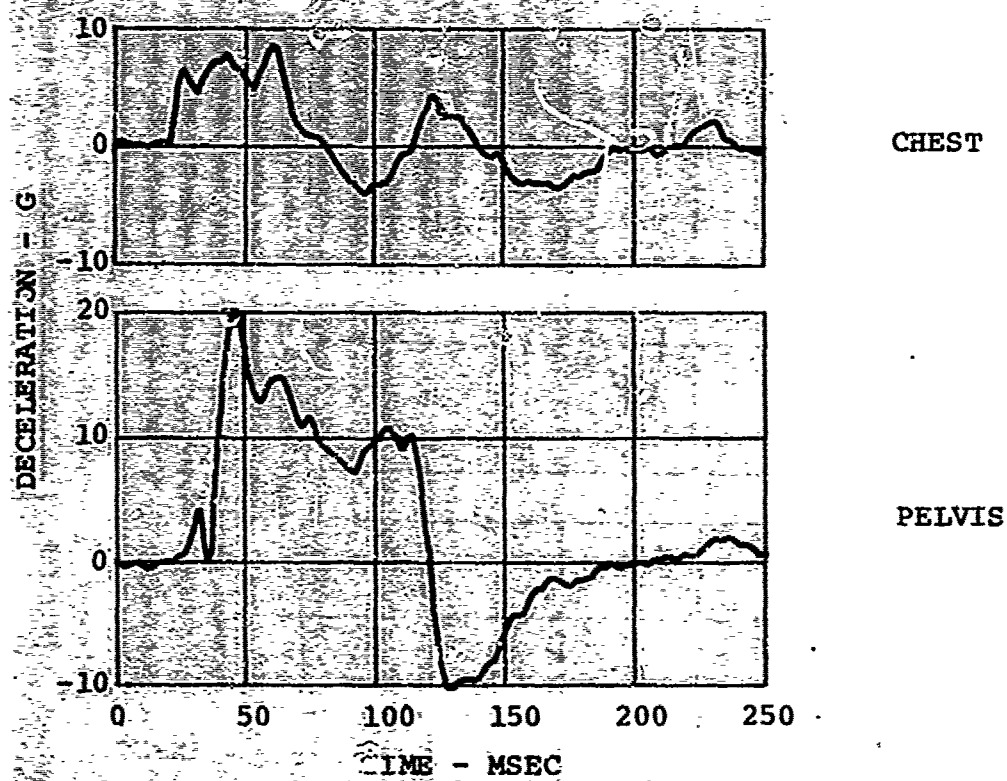
Figure 151. Longitudinal Chest and Pelvis Decelerations (Test 2).
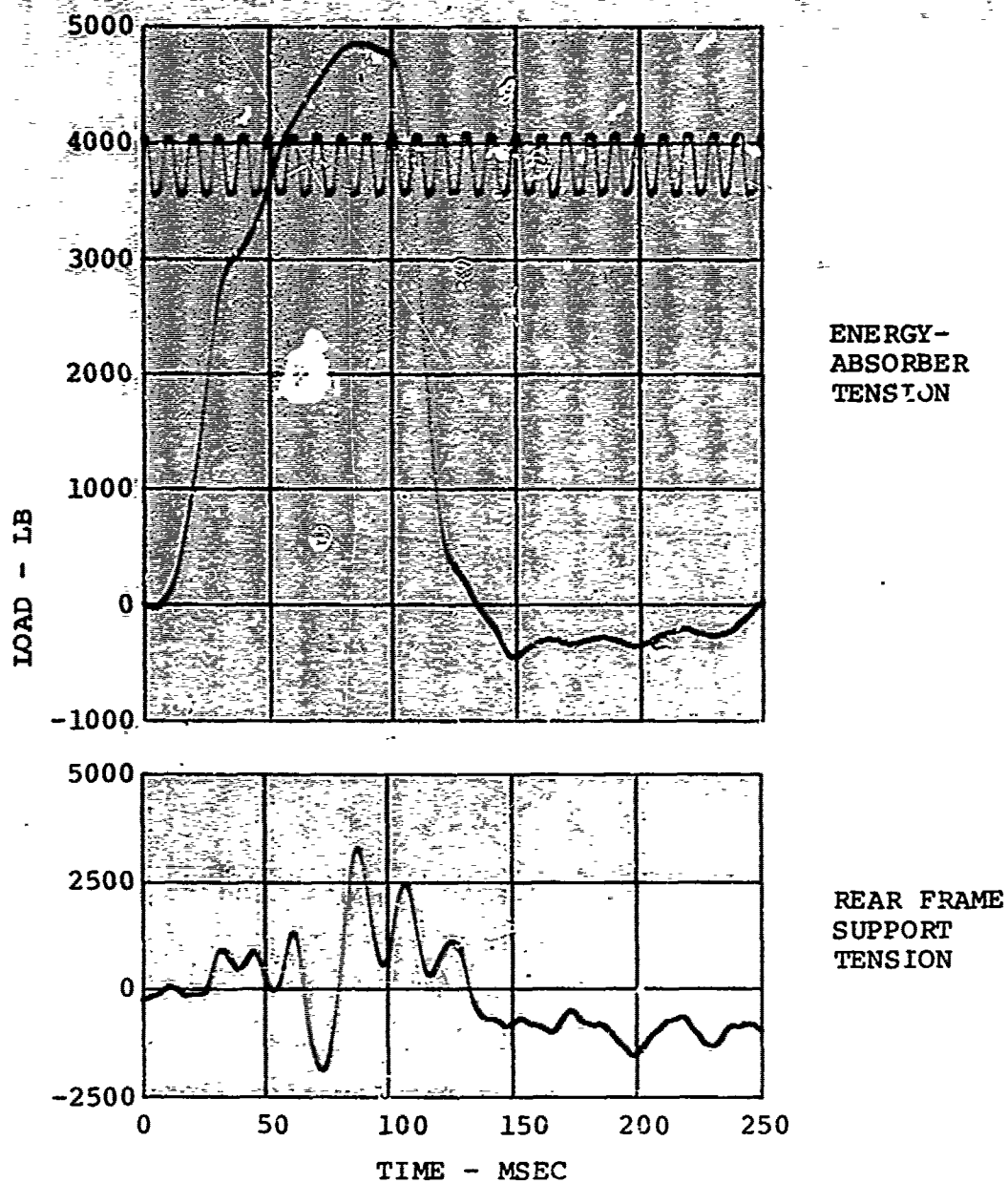
Figure 152. Energy-Absorber and Rear Frame Support Loads (Test 2).
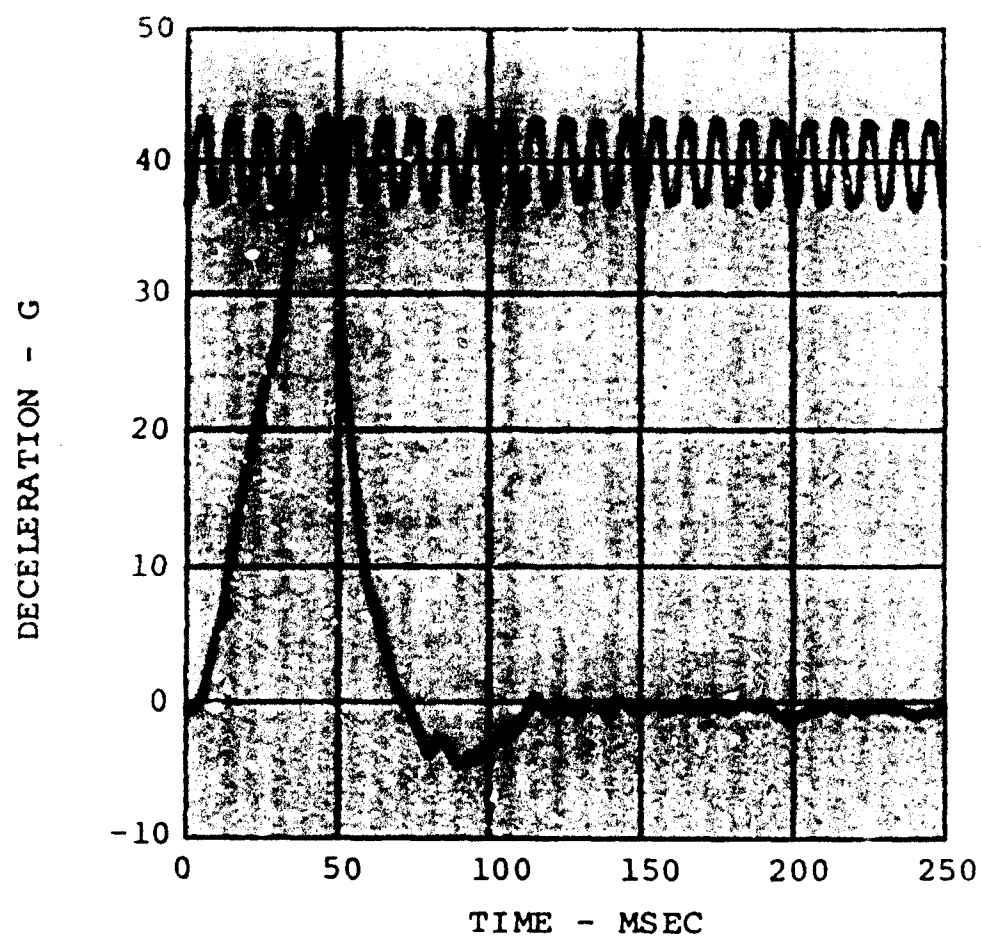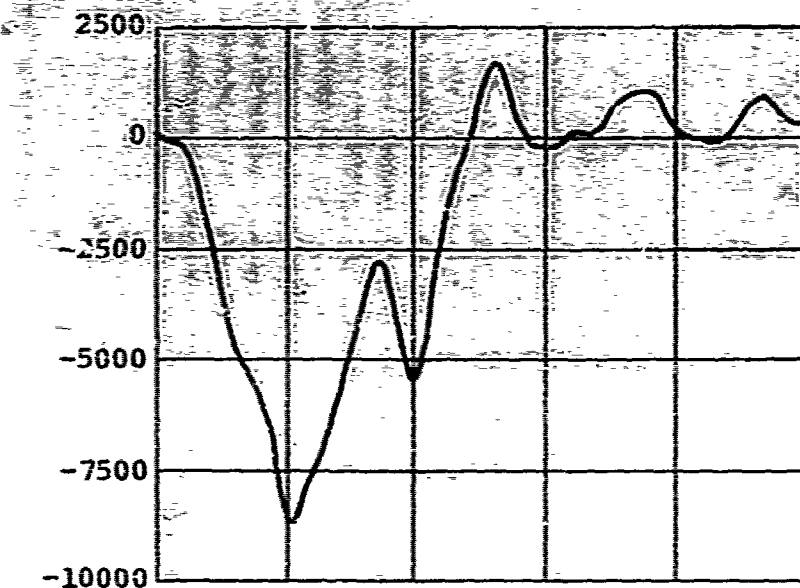
Figure 153. Vertical Input Deceleration (Test 3).

238
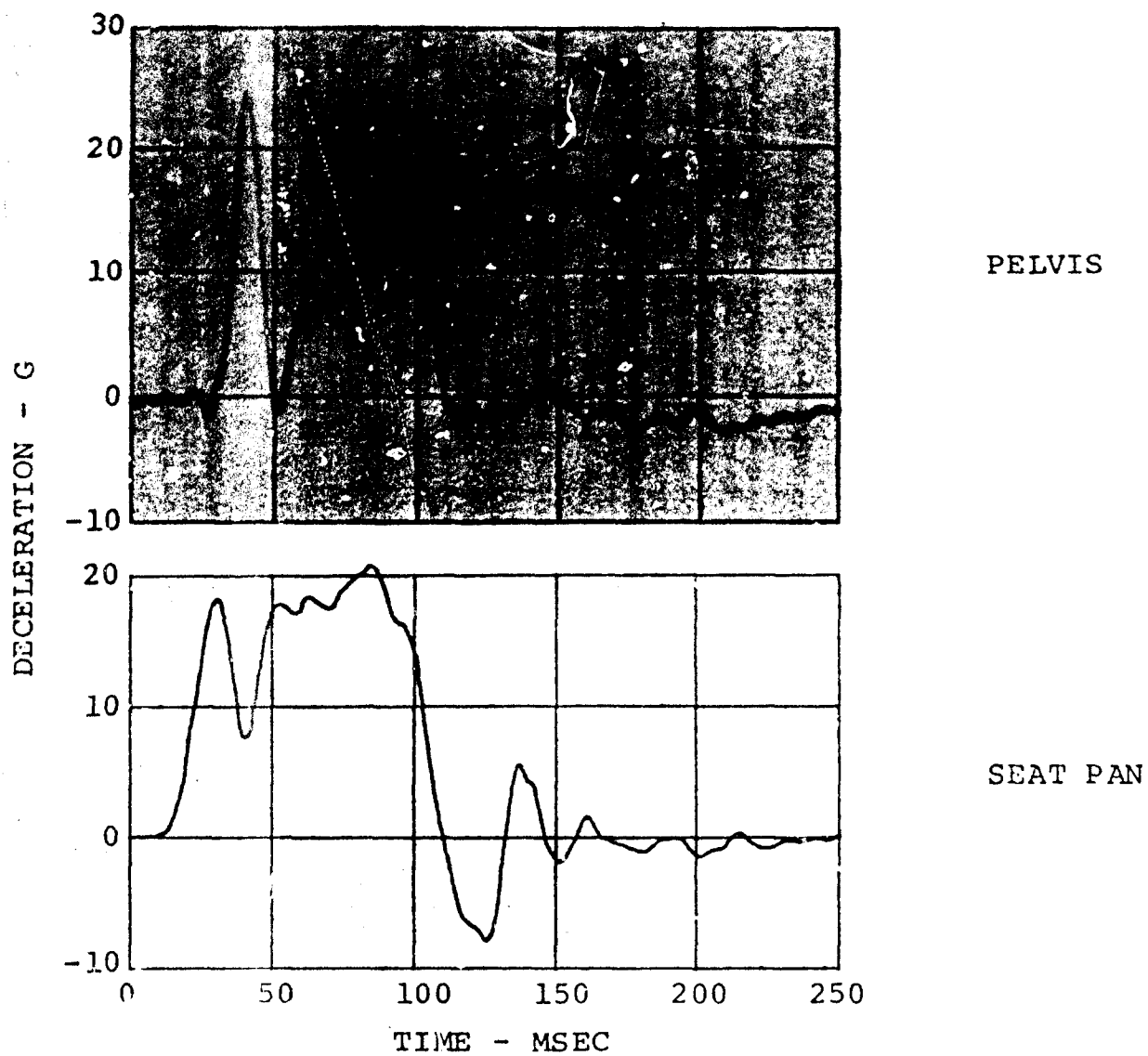
Figure 154. Vertical Pelvis and Seat Pan Decelerations (Test 3).
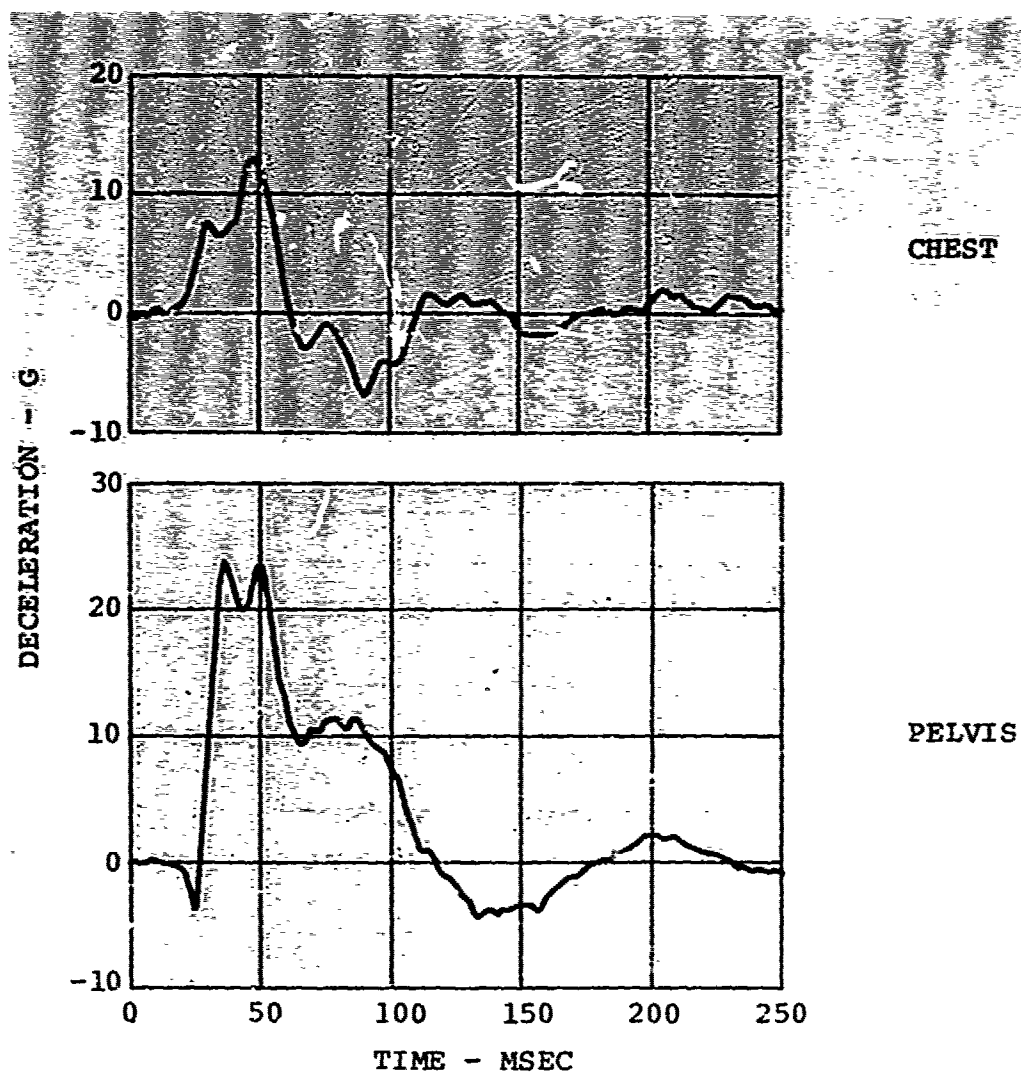
Figure 155.   Longitudinal Chest and Pelvis Decelerations
             (Test 3).

240
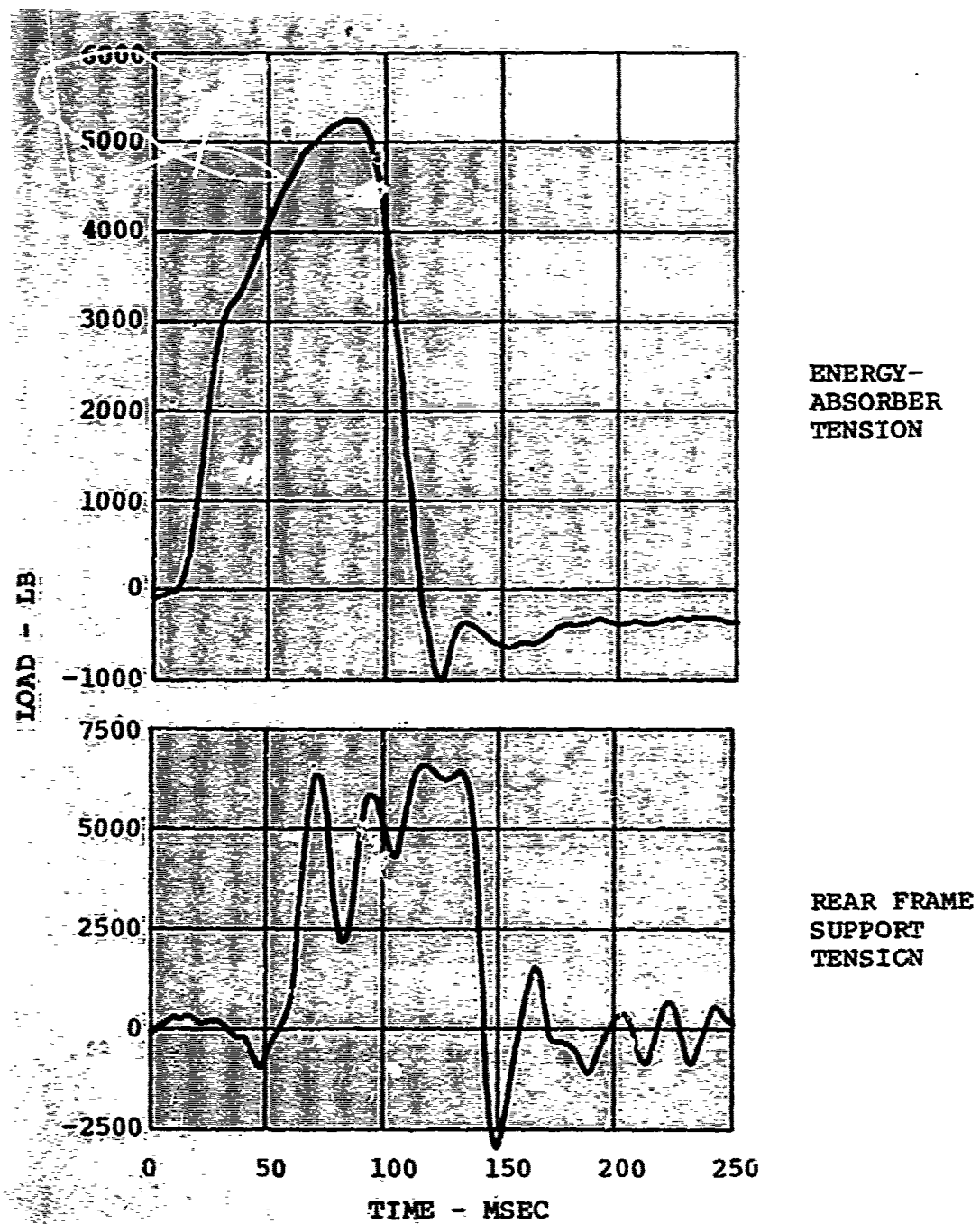
Figure 156. Energy-Absorber and Rear Frame Support Loads
(Test 3).

241
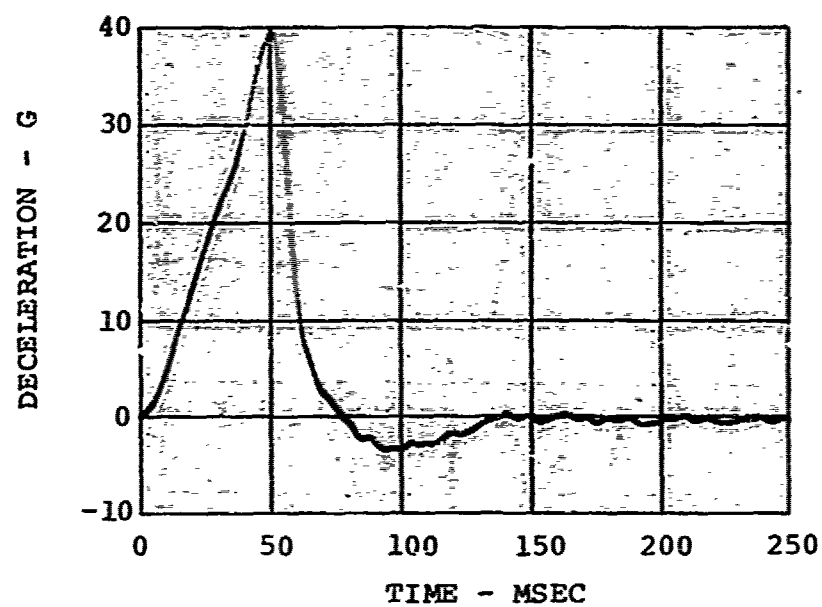
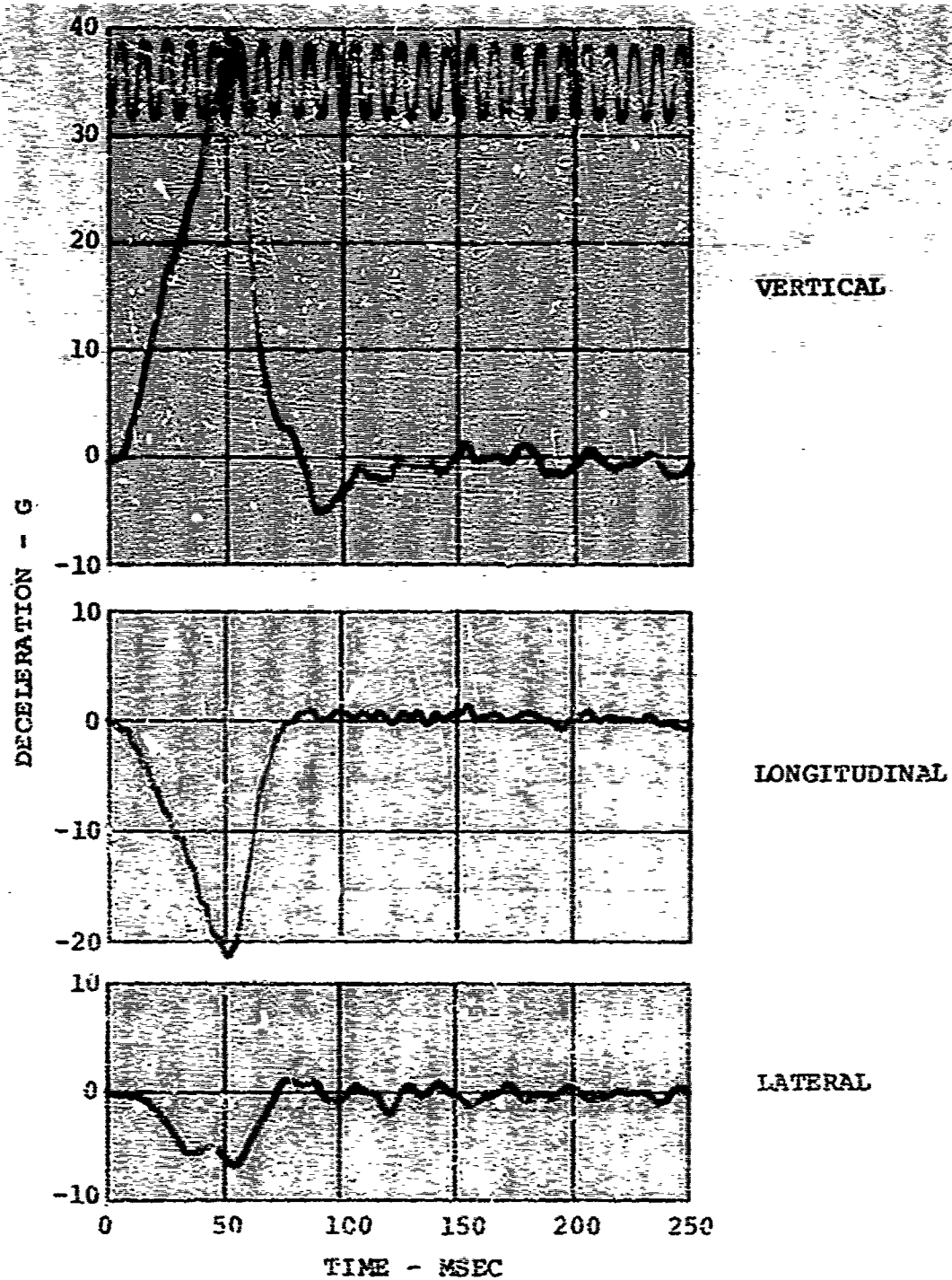Figure 157. Vertical Input Deceleration (Test 4).
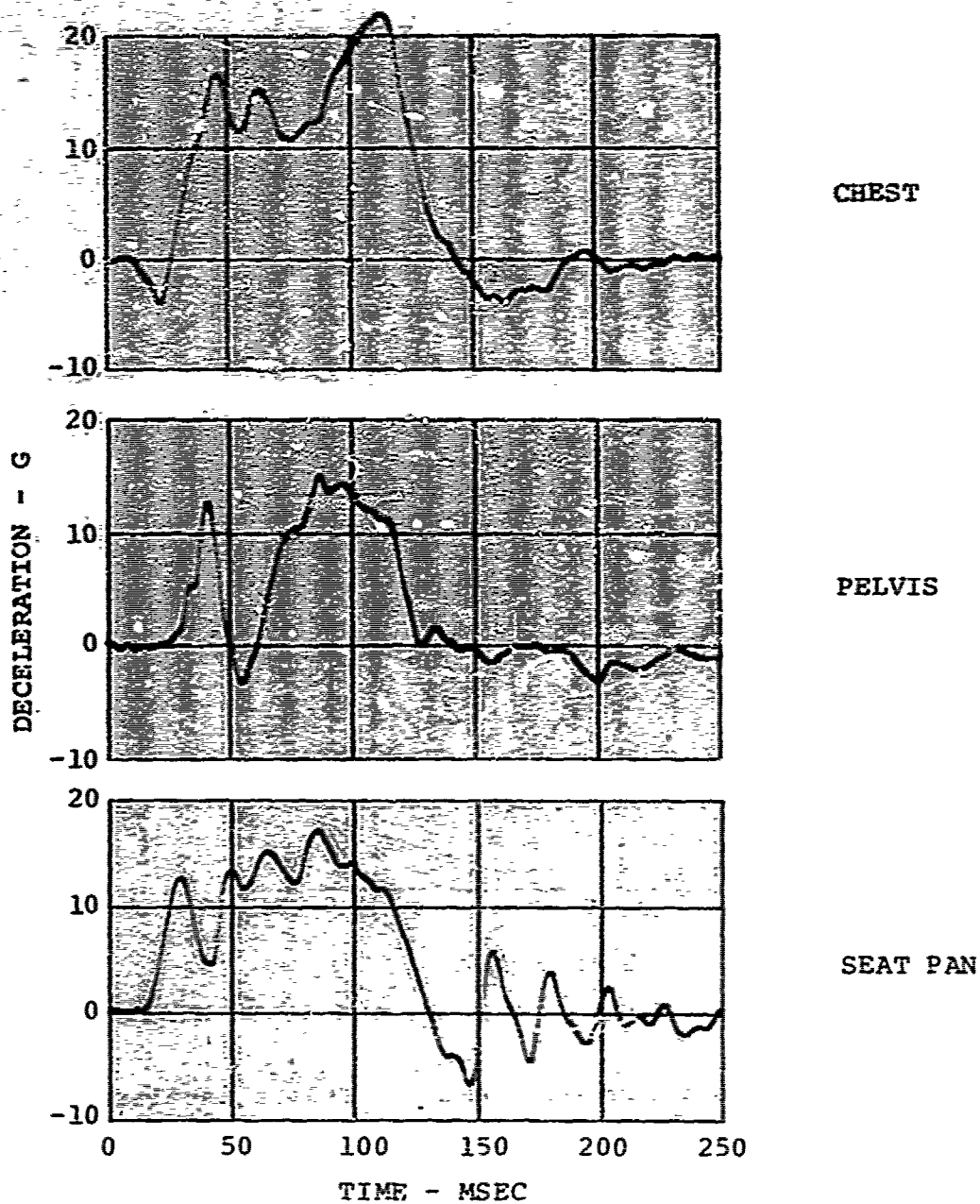
Figure 158. Vertical Chest, Pelvis, and Seat Pan
Deceleration (Test 4).

243
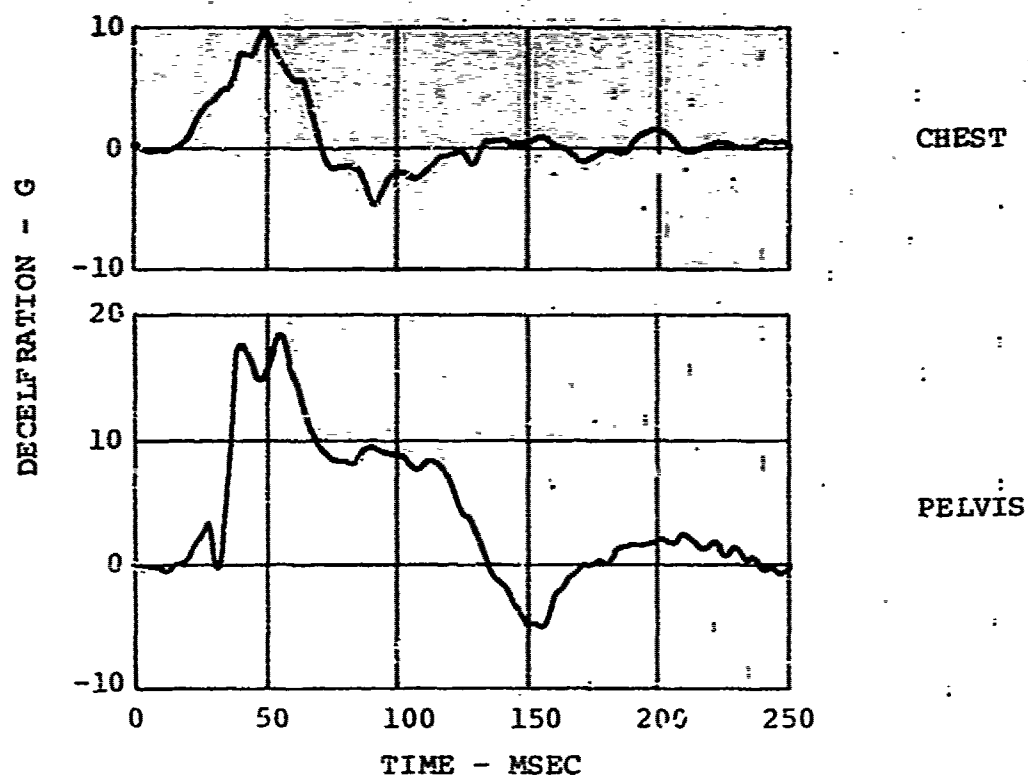
Figure 159. Longitudinal Chest and Pelvis Decelerations
(Test 4).
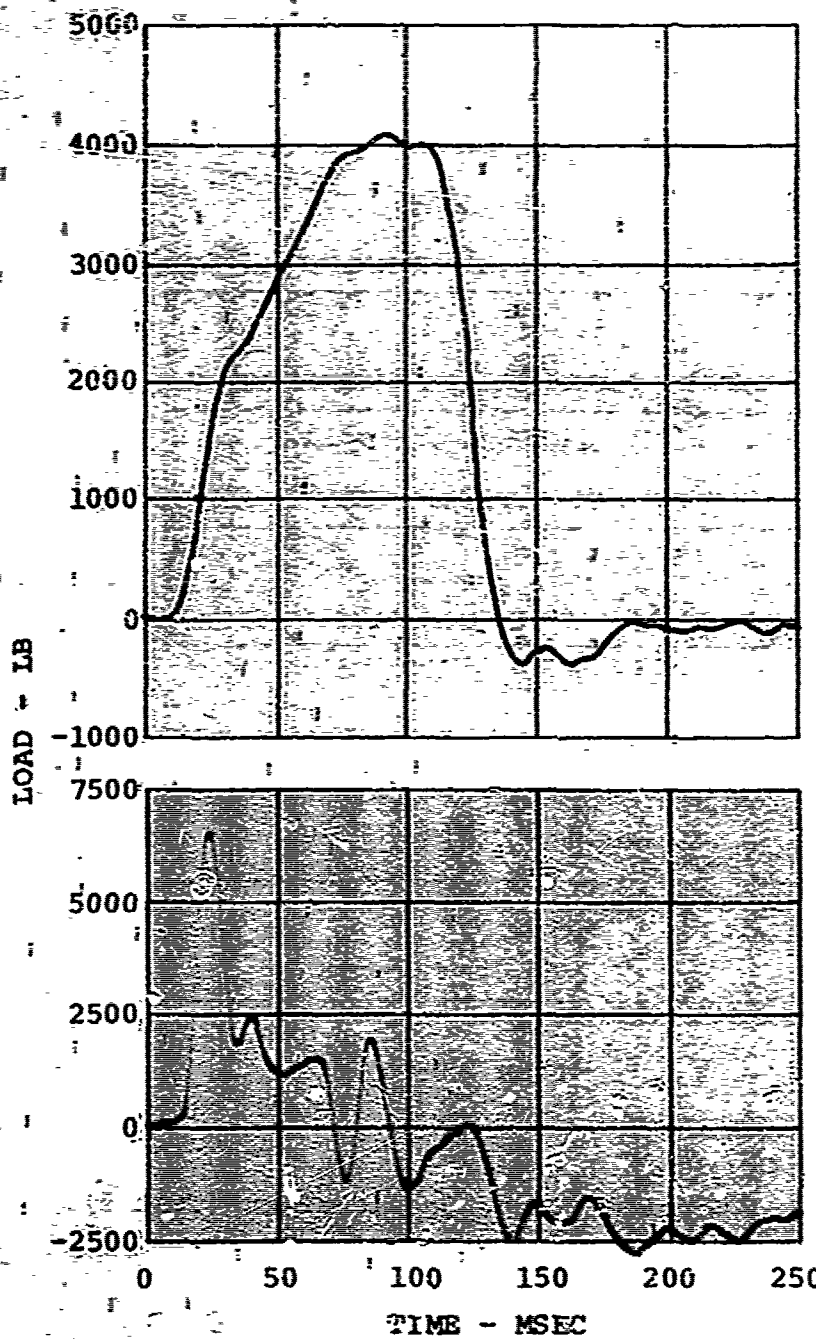
Figure 160. Energy-Absorber and Rear Frame Support Loads (Test 4).
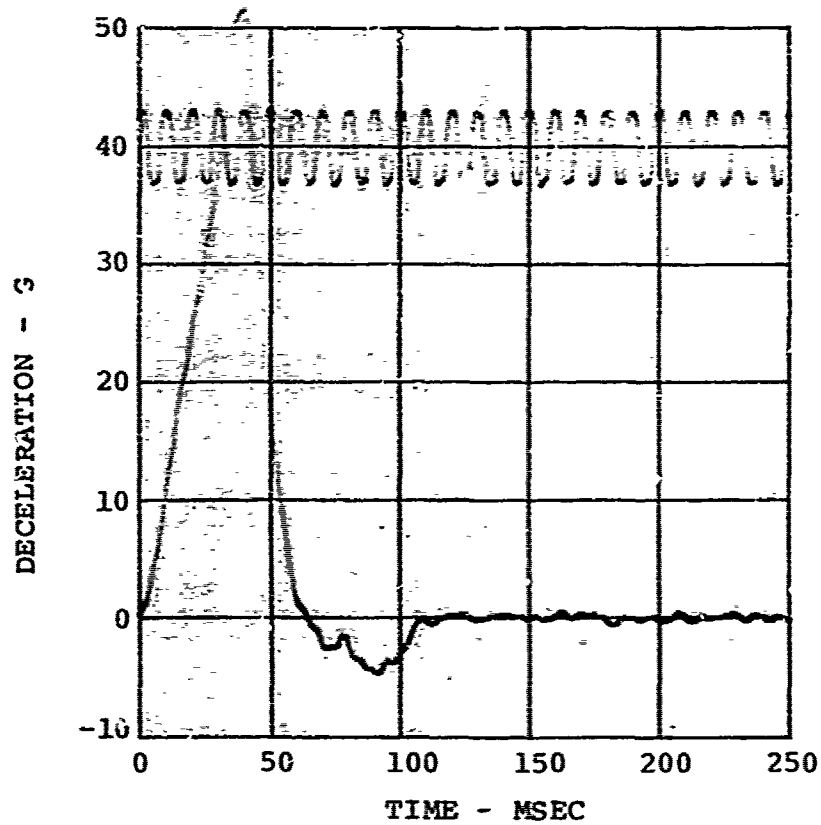
Figure 161. Vertical Input Deceleration (Test 5).

246
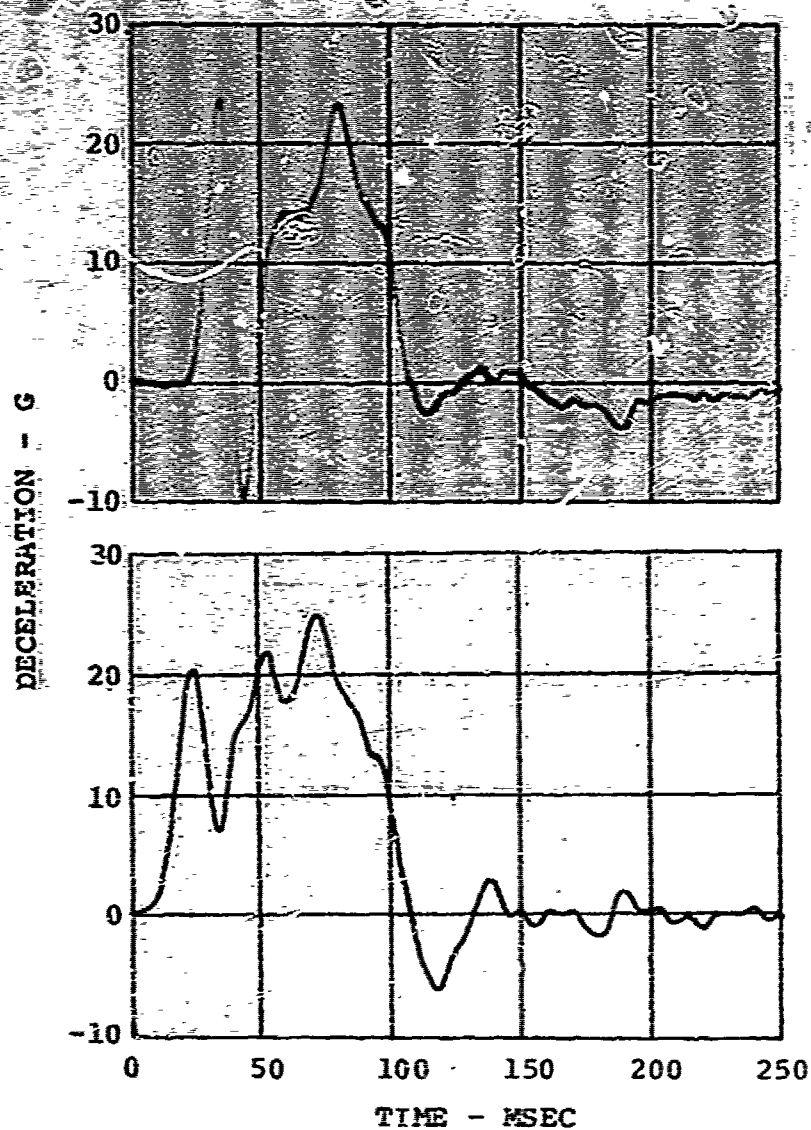
Figure 162.   Vertical Pelvi‑ and Seat Pan Decelerations
(Test 5).

247
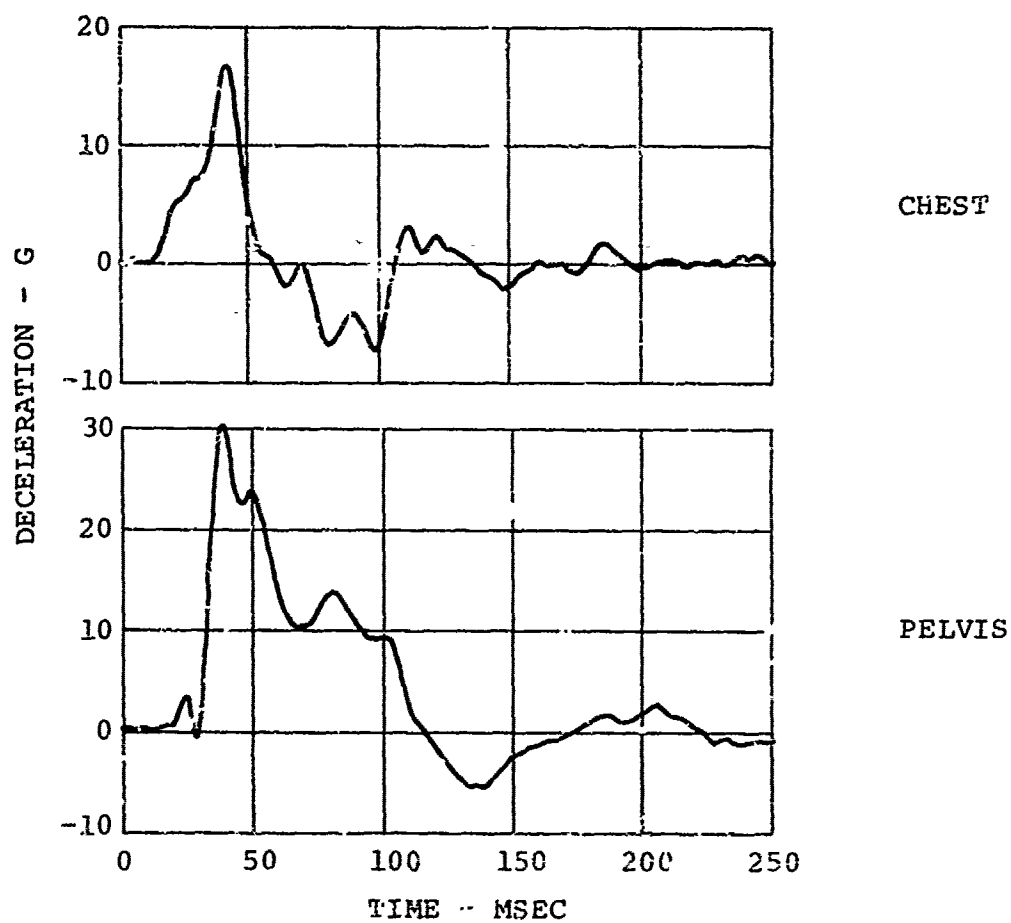
Figure 163. Longitudinal Chest and Pelvis Decelerations (Test 5).

248
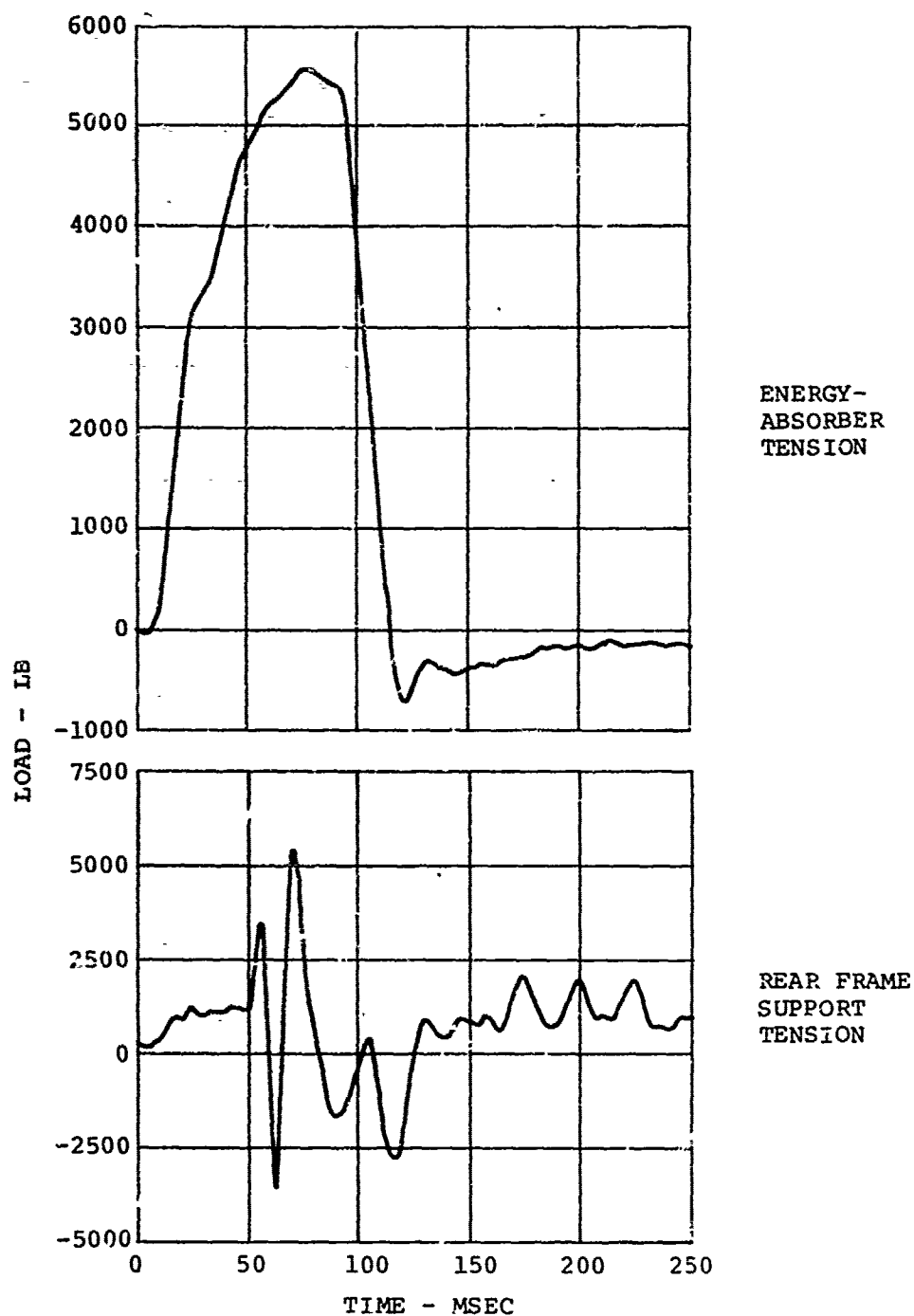
Figure 164.   Energy-Absorber and Rear Frame Support
Loads (Test 5).

249
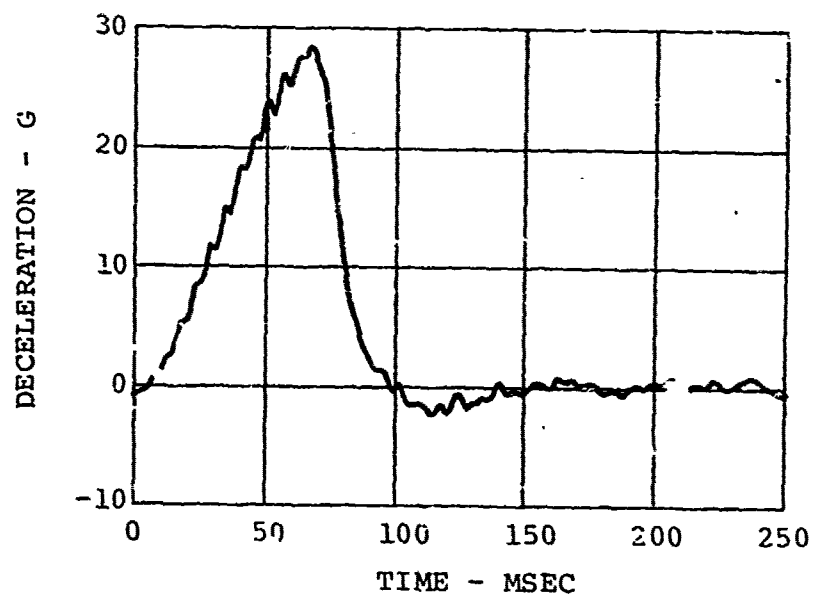
Figure 165. Triaxial Input Deceleration (Test 6).
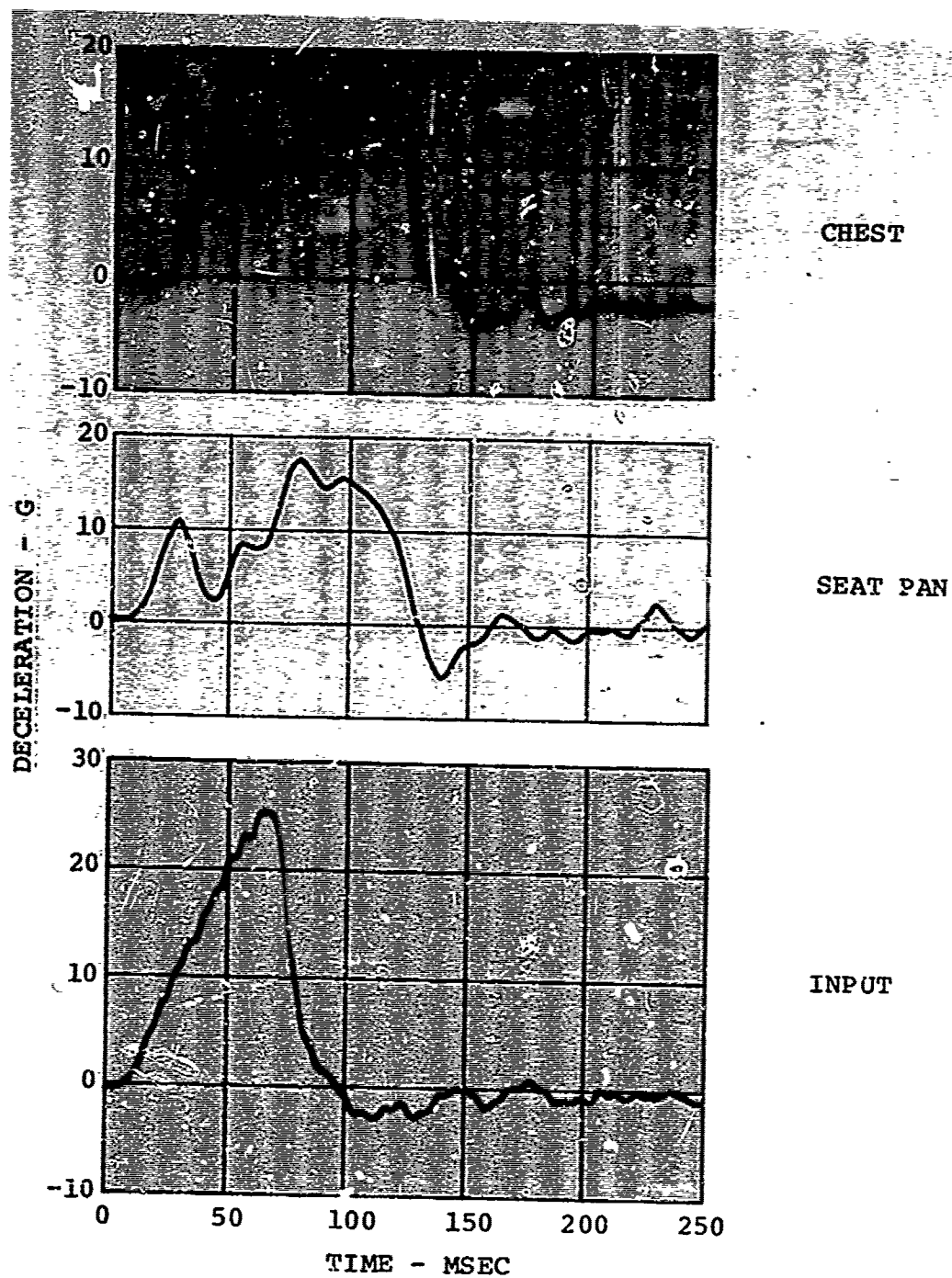
Figure 166. Vertical Chest, Seat Pan, and Input
Decelerations (Test 6).

251
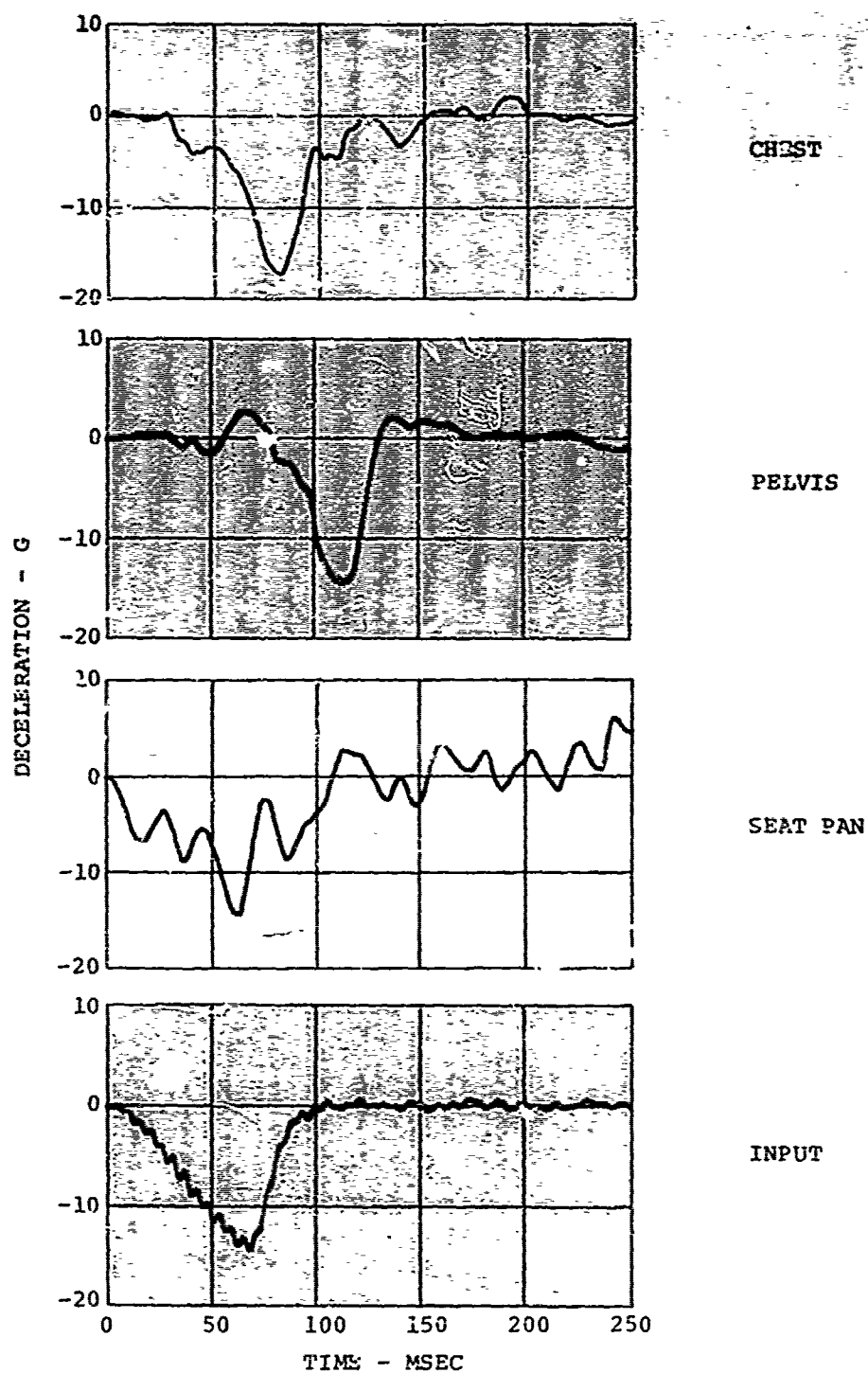
Figure 167. Longitudinal Chest, Pelvis, Seat Pan,
and Input Decelerations (Test 6).

252
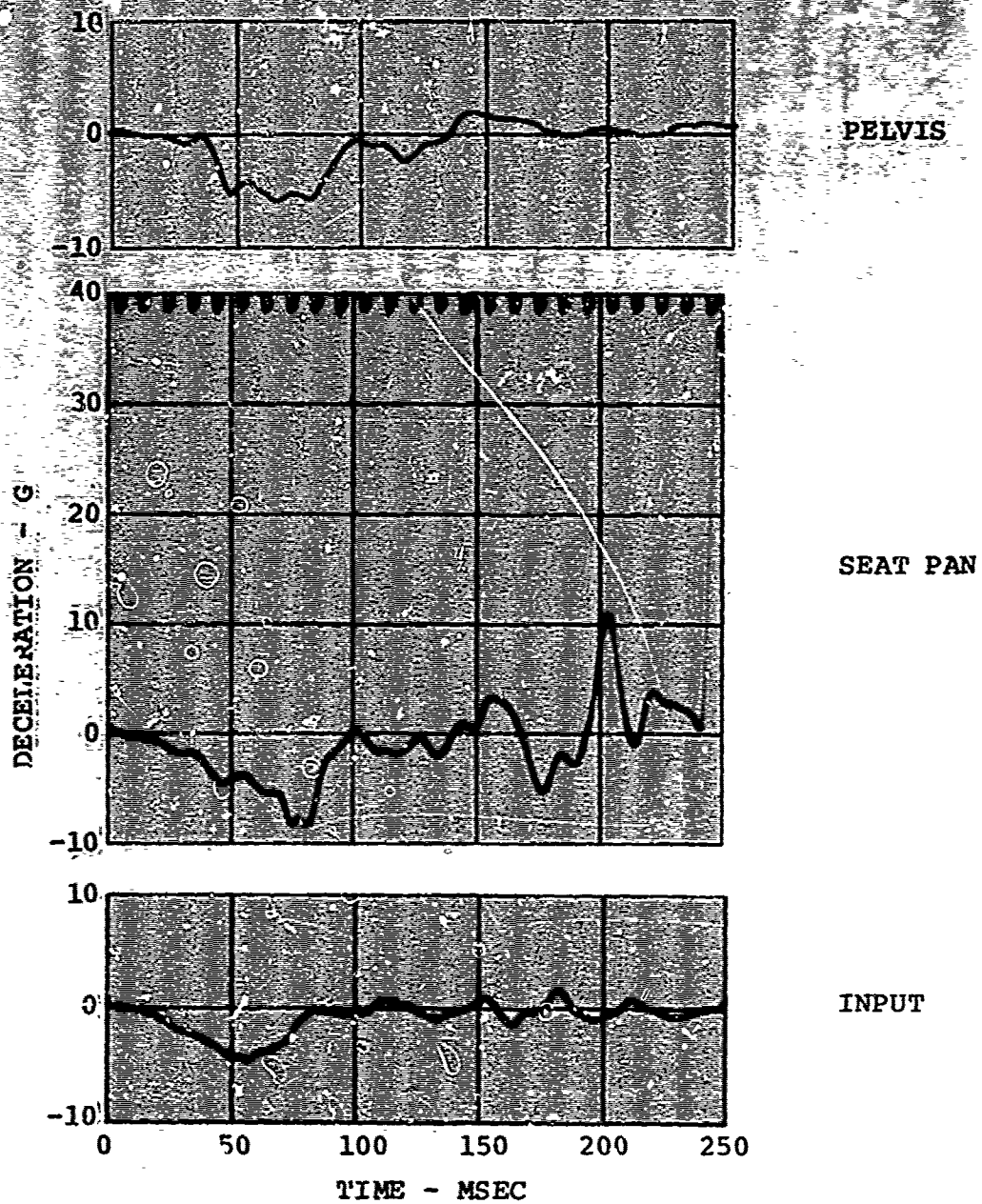
Figure 168. Lateral Pelvis, Seat Pan, and Input Decelerations (Test 6).
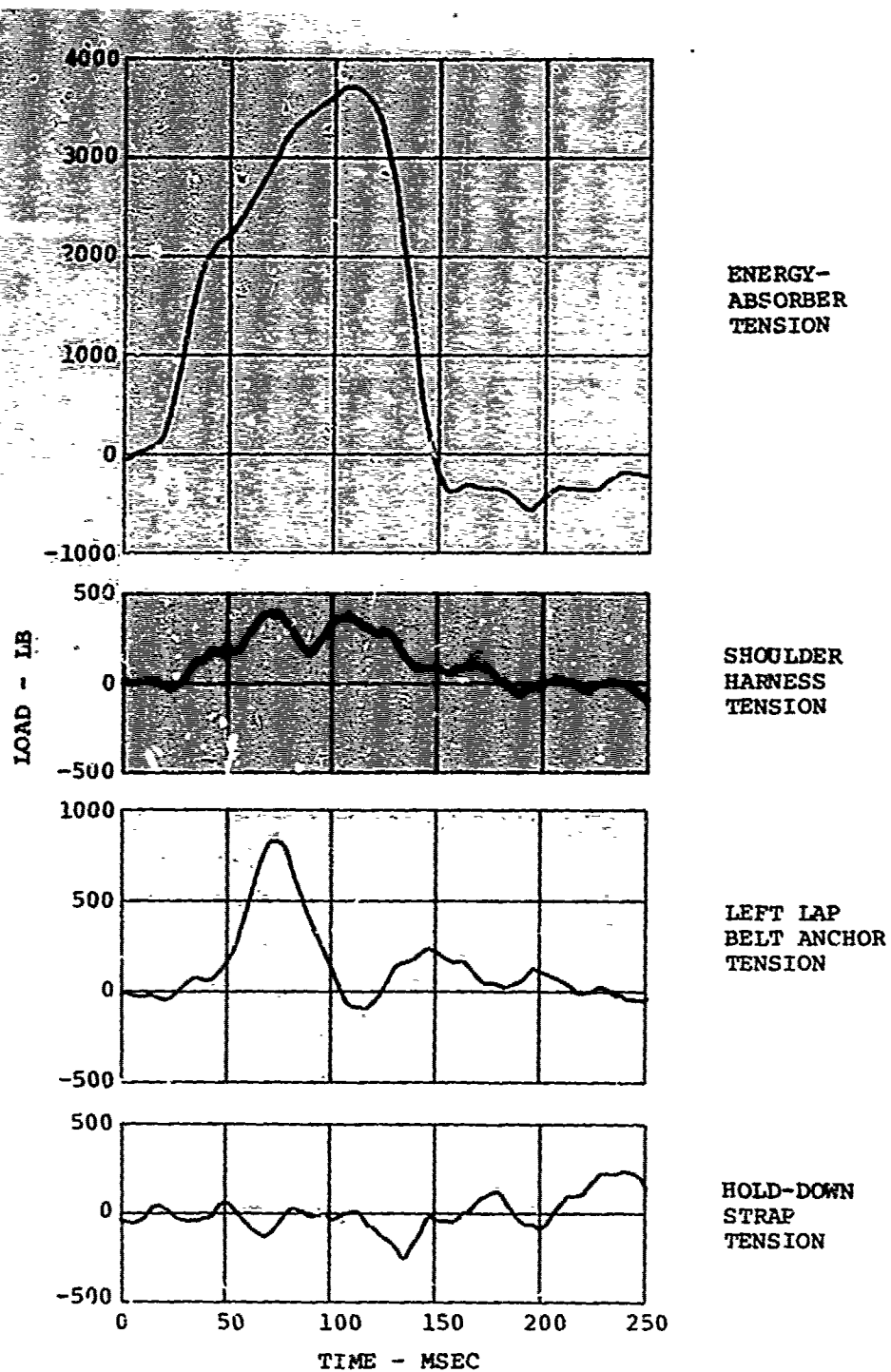
Figure 169. Energy-Absorber and Restraint
System Loads (Test 6).

254
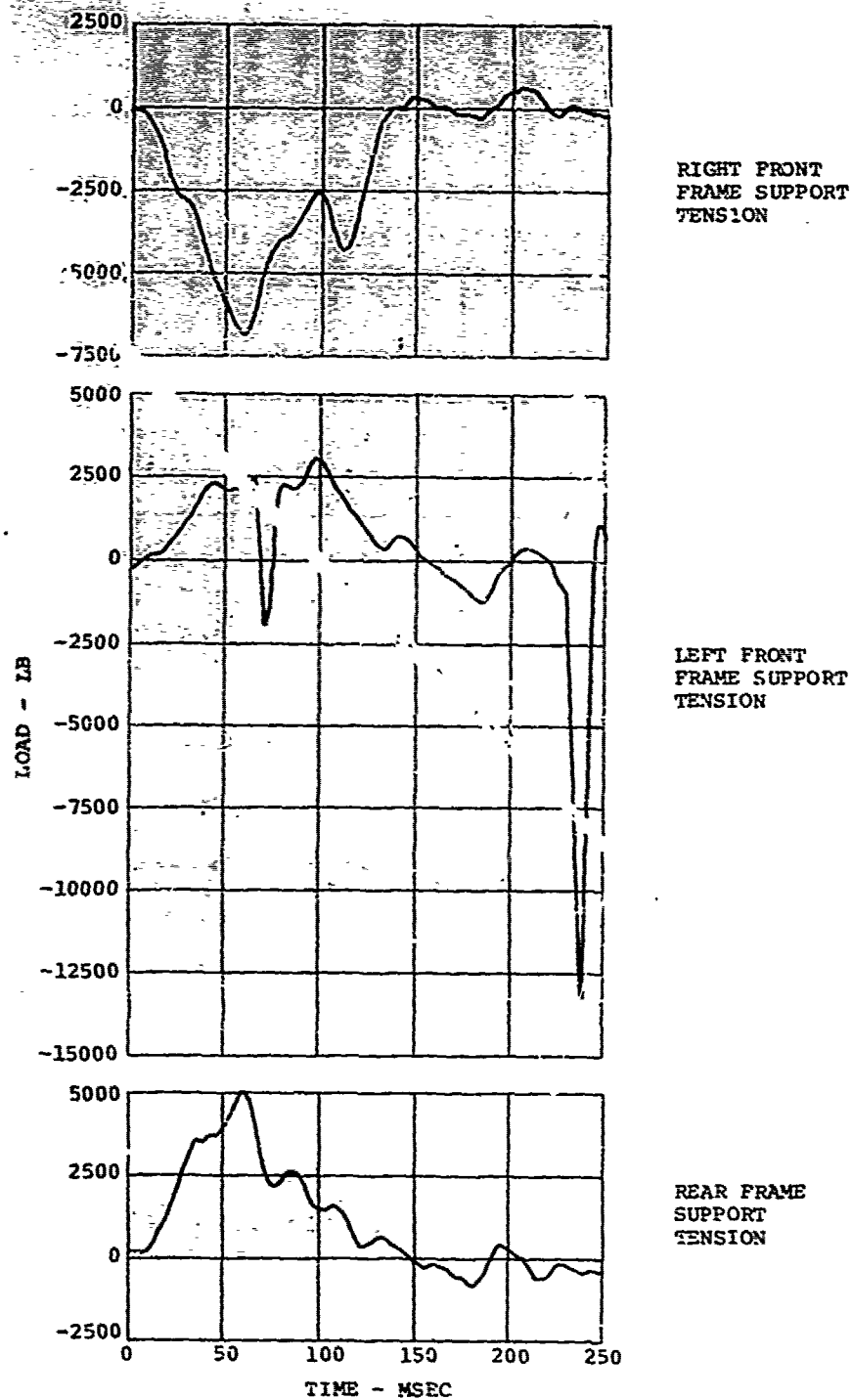
Figure 170.   Frame Support Loads (Test 6).

255
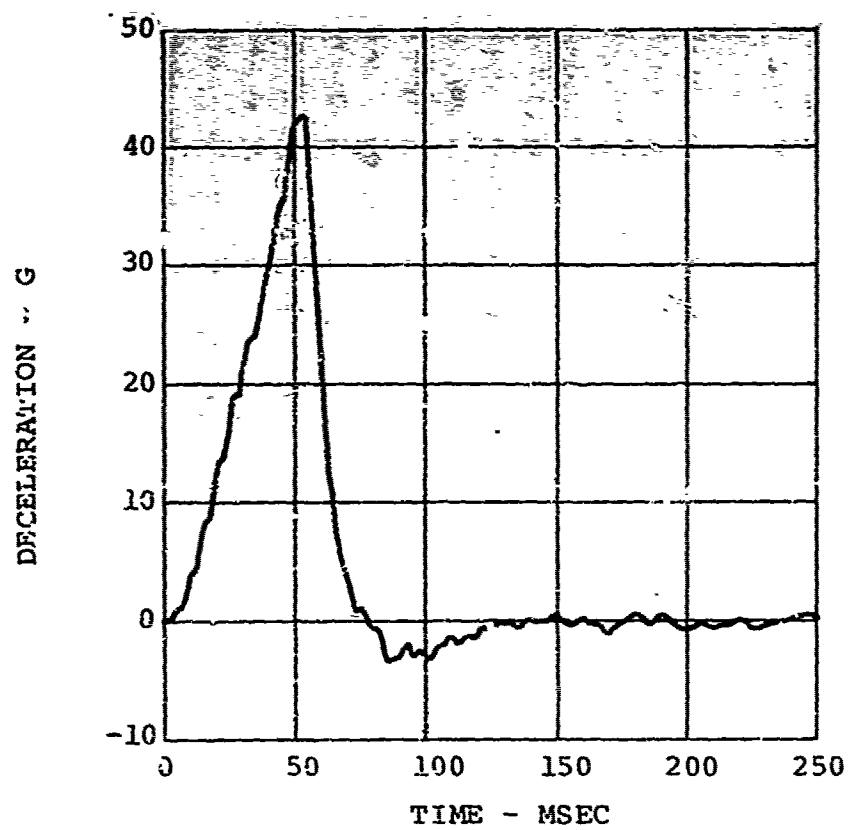
Figure 171. Triaxial Input Deceleration (Test 7).
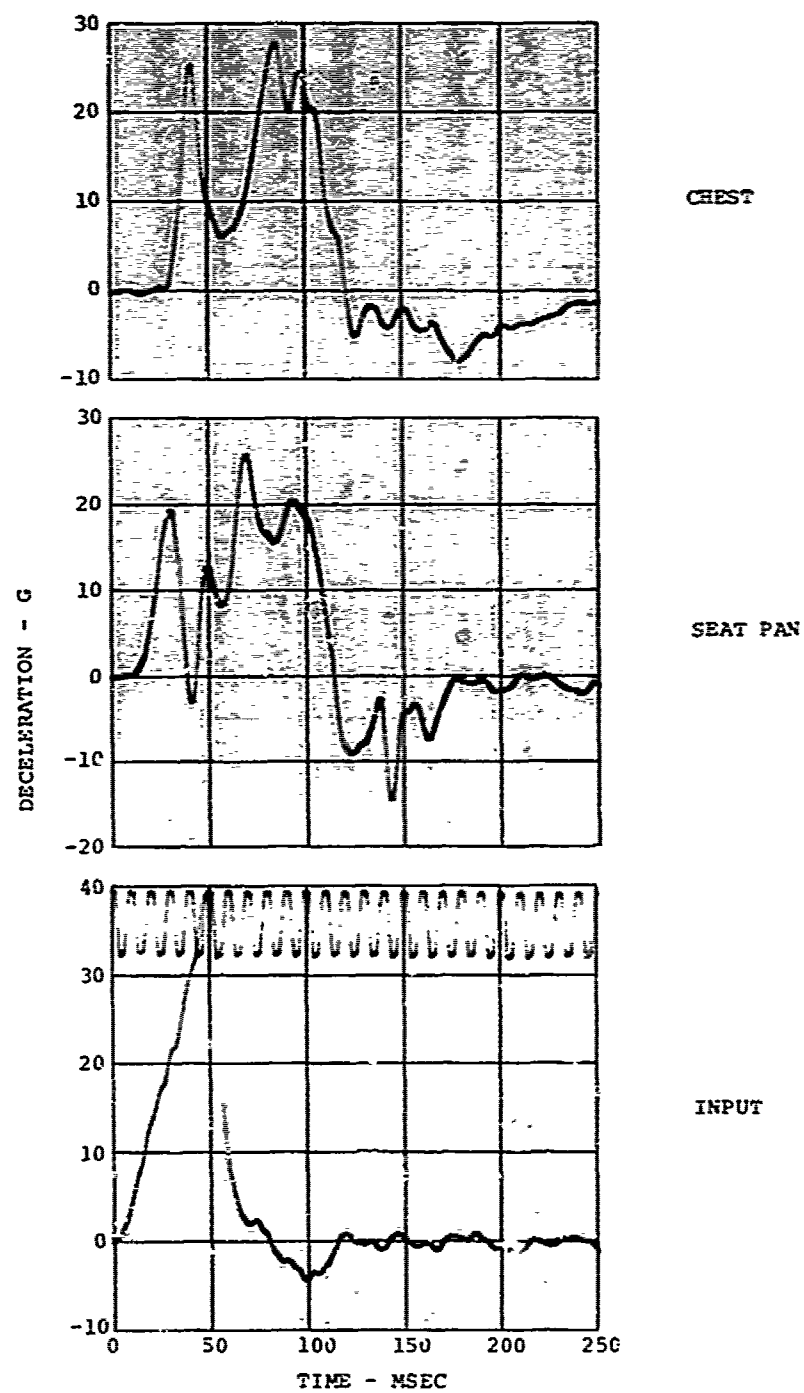
Figure 172. Lateral Pelvis, Seat Pan, and Input Decelerations (Test 7).

257
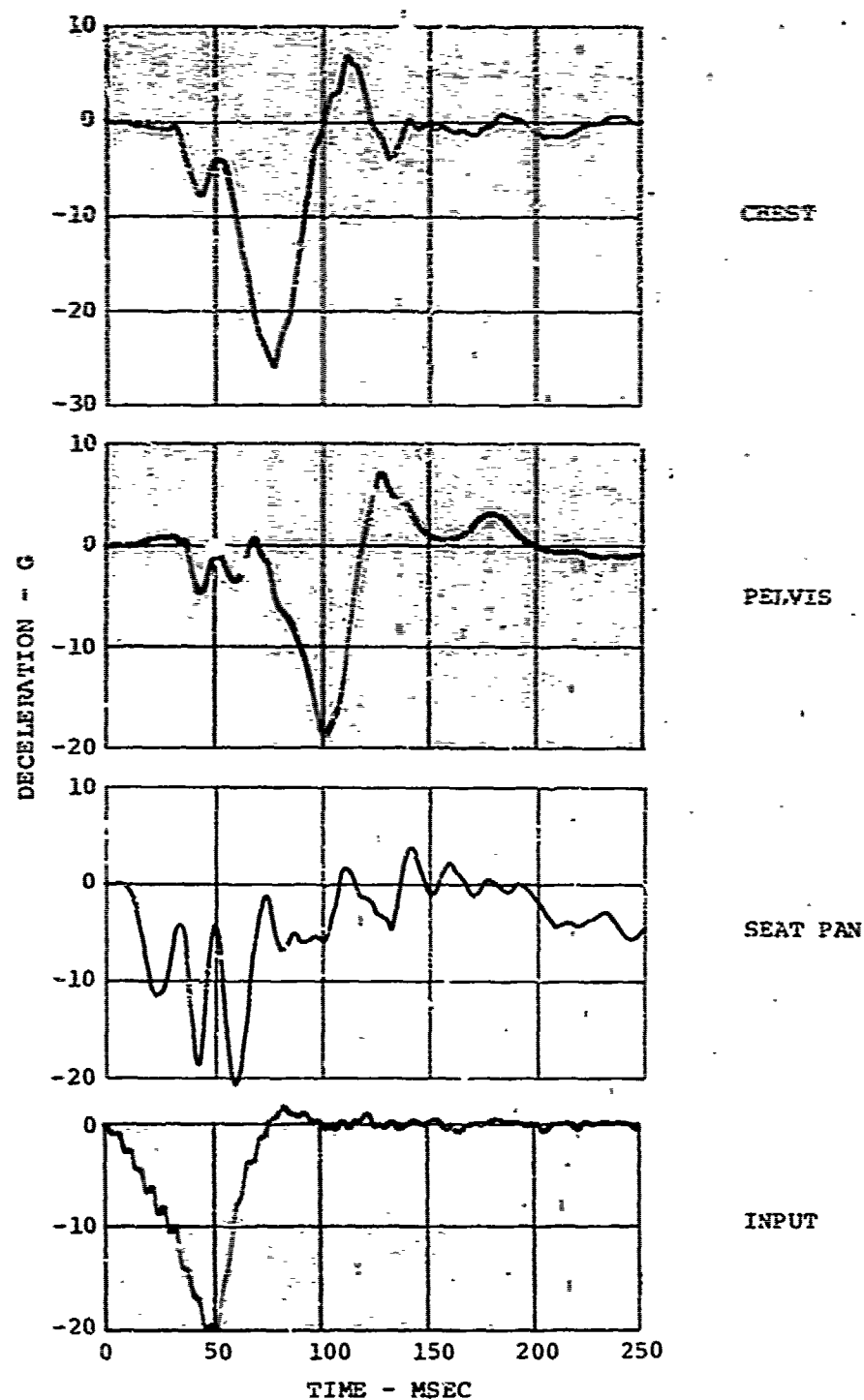
Figure 173. Longitudinal Chest, Pelvis, Seat Pan, and Input Decelerations (Test 7).

258

Figure 174.   Vertical Chest, Seat Pan, and Input
Decelerations (Test 7).

259
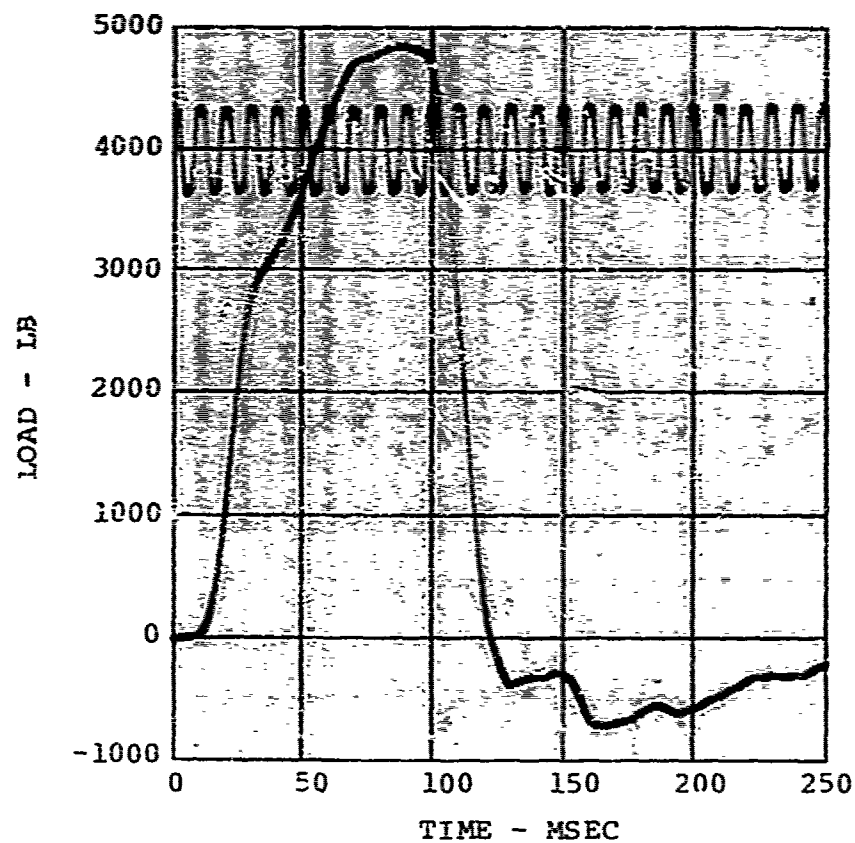
Figure 175. Energy-Absorber Load (Test 7).

260
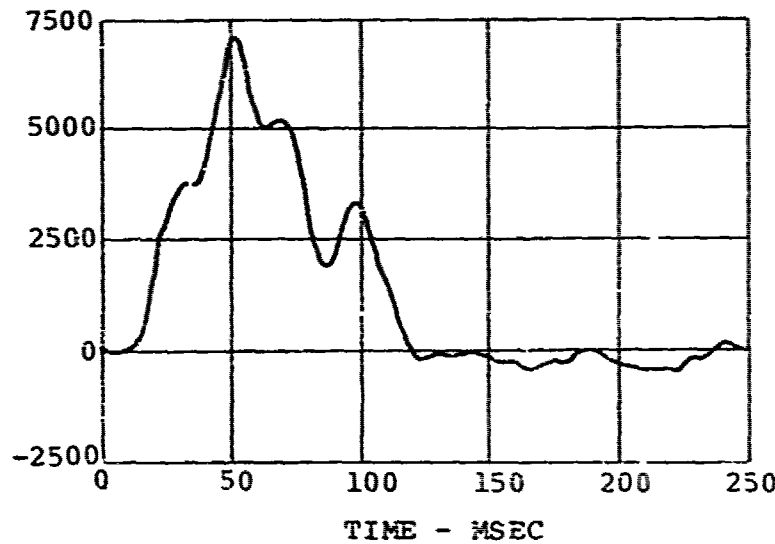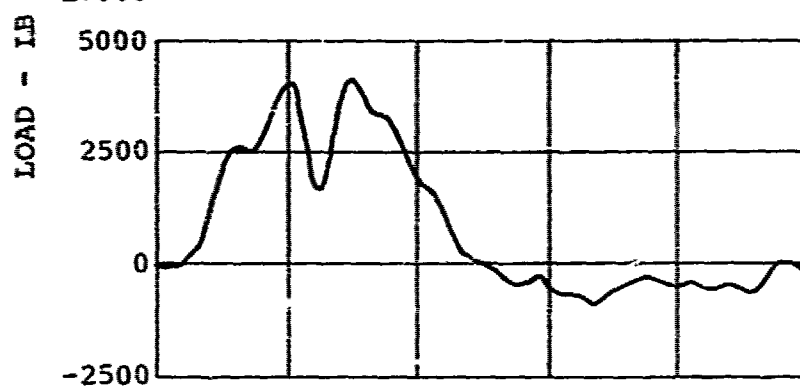
Figure 176. Frame Support Loads (Test 7).

261
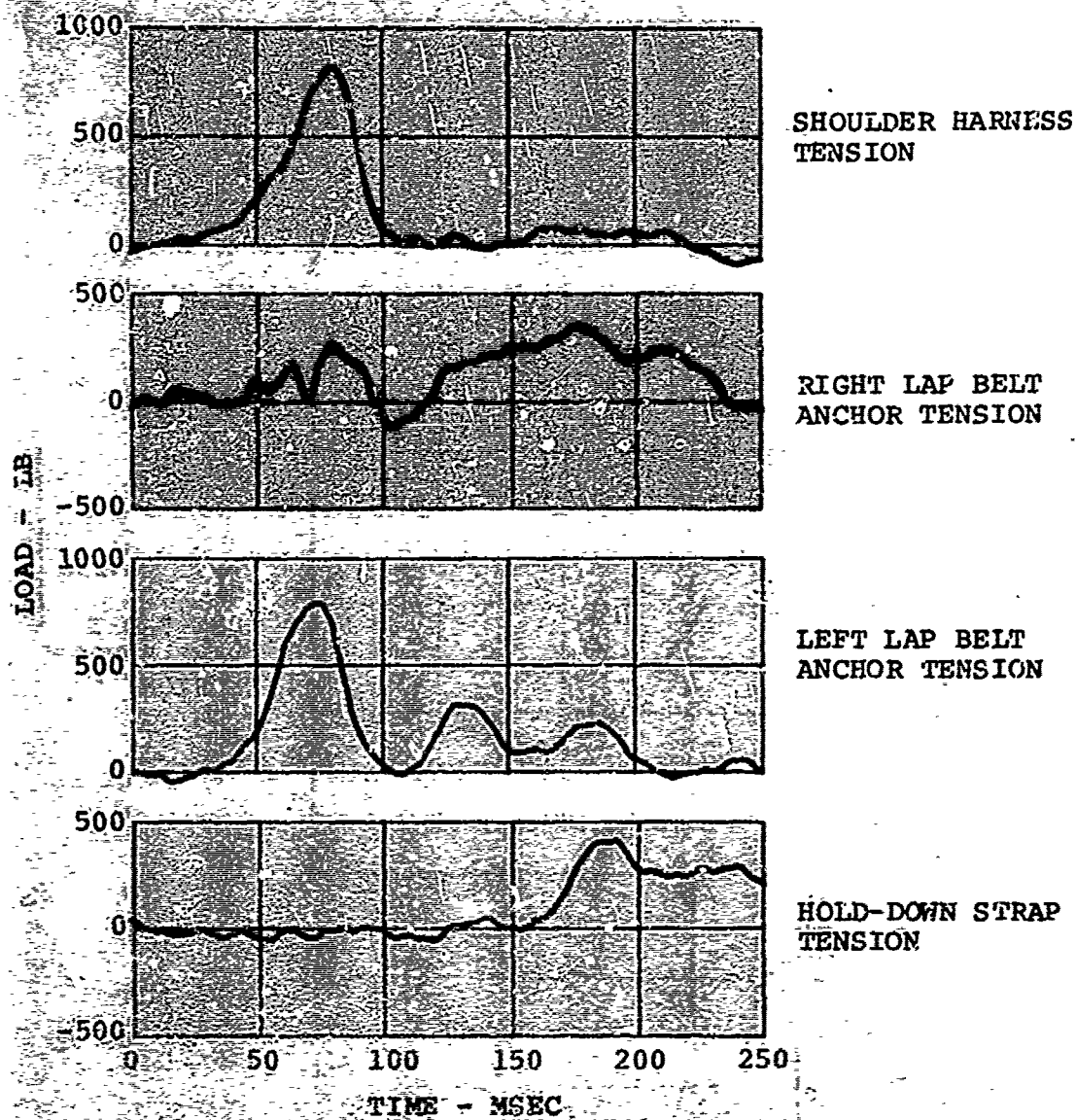
Figure 177. Restraint System Loads (Test 7).
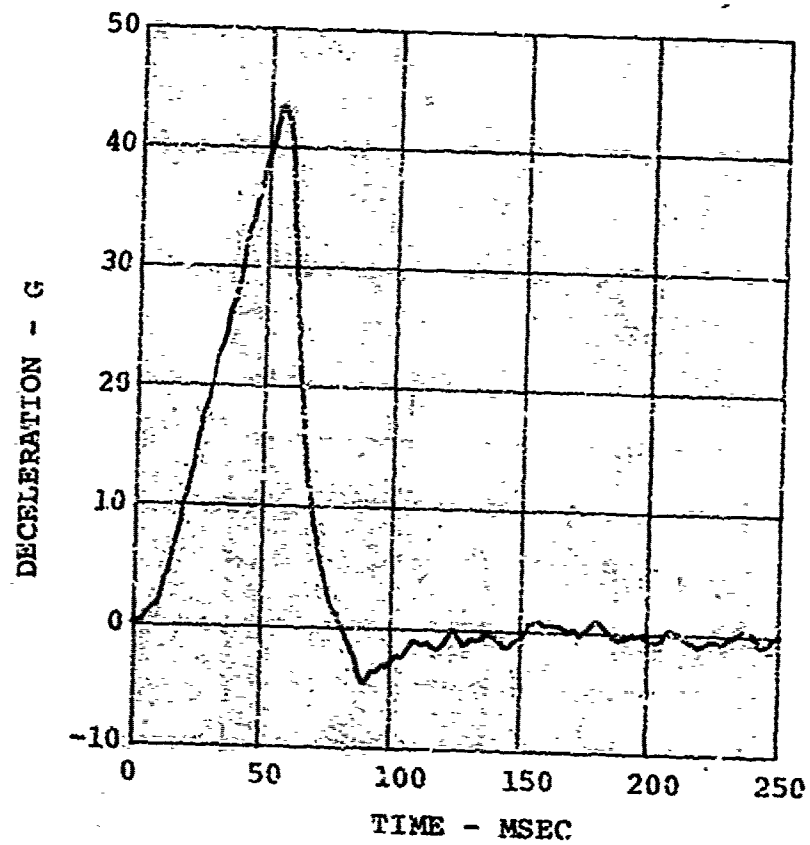
Figure 178. Triaxial Input Deceleration (Test 8).

Figure 179. Component Input Decelerations (Test 8).

264
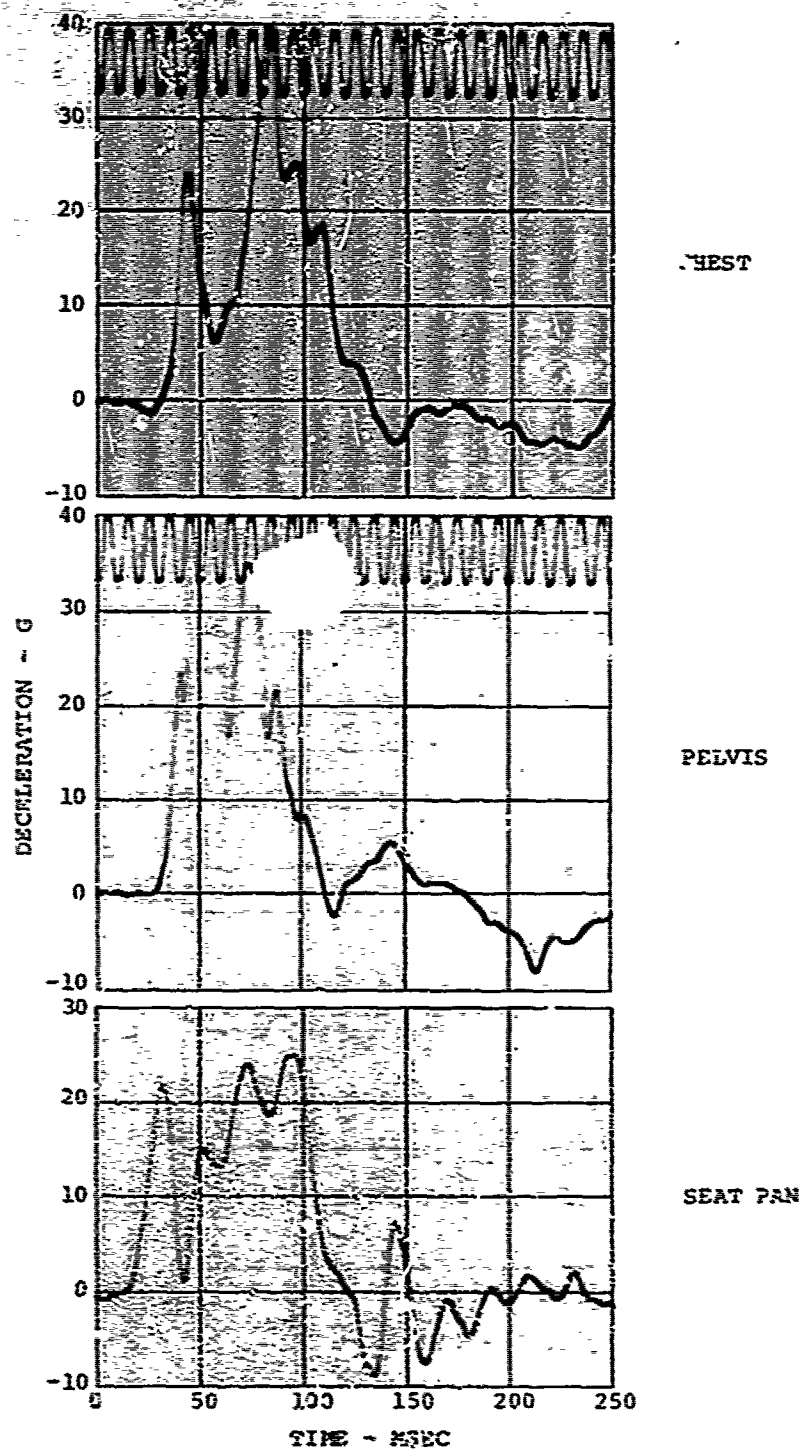
Figure 180.   Vertical Chest. Pelvis, and Seat
              Pan Decelerations (Test 8).

265
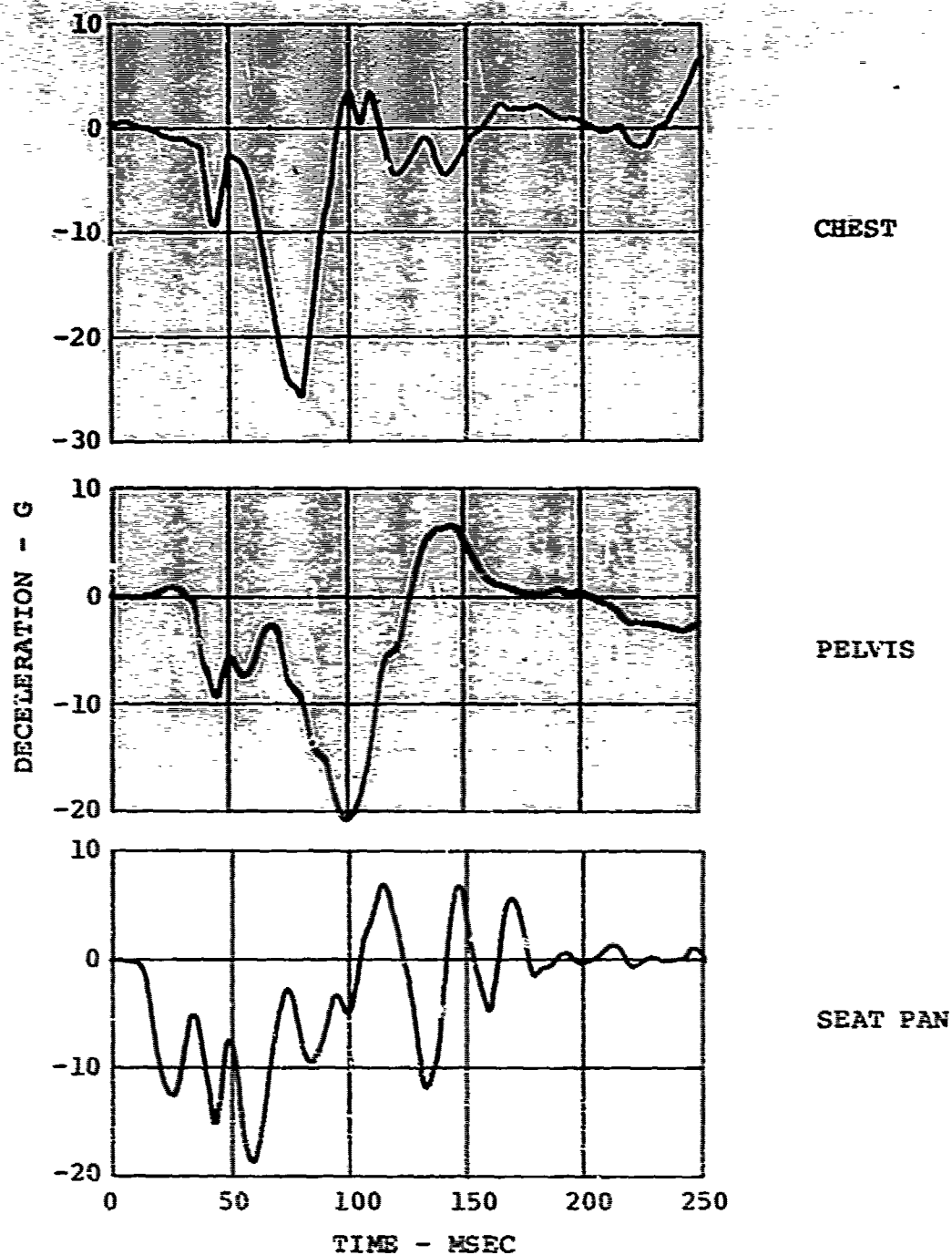
Figure 181. Longitudinal Chest, Pelvis, and Seat Pan
Decelerations (Test 8).
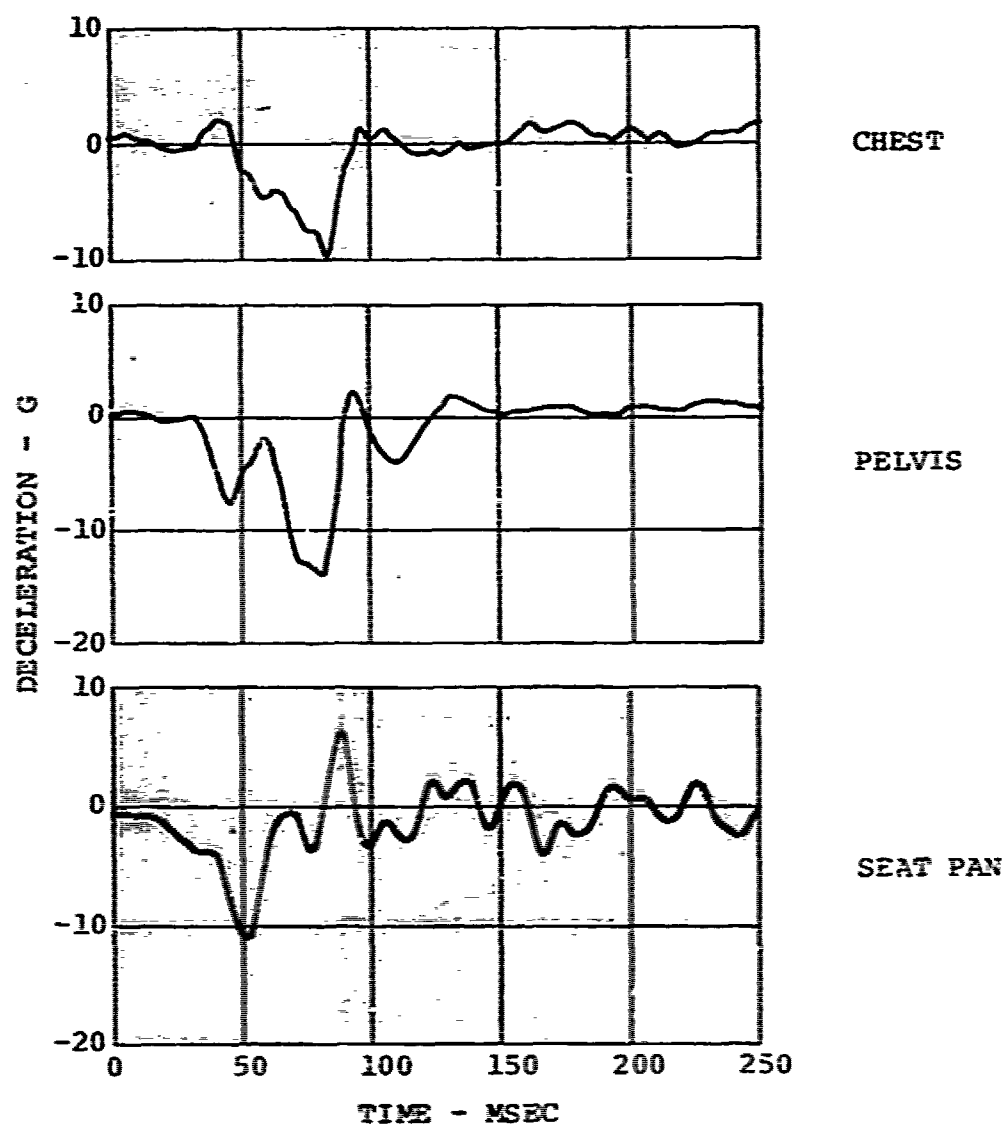
Figure 182. Lateral Chest, Pelvis, and Seat Pan
Decelerations (Test 8).

267
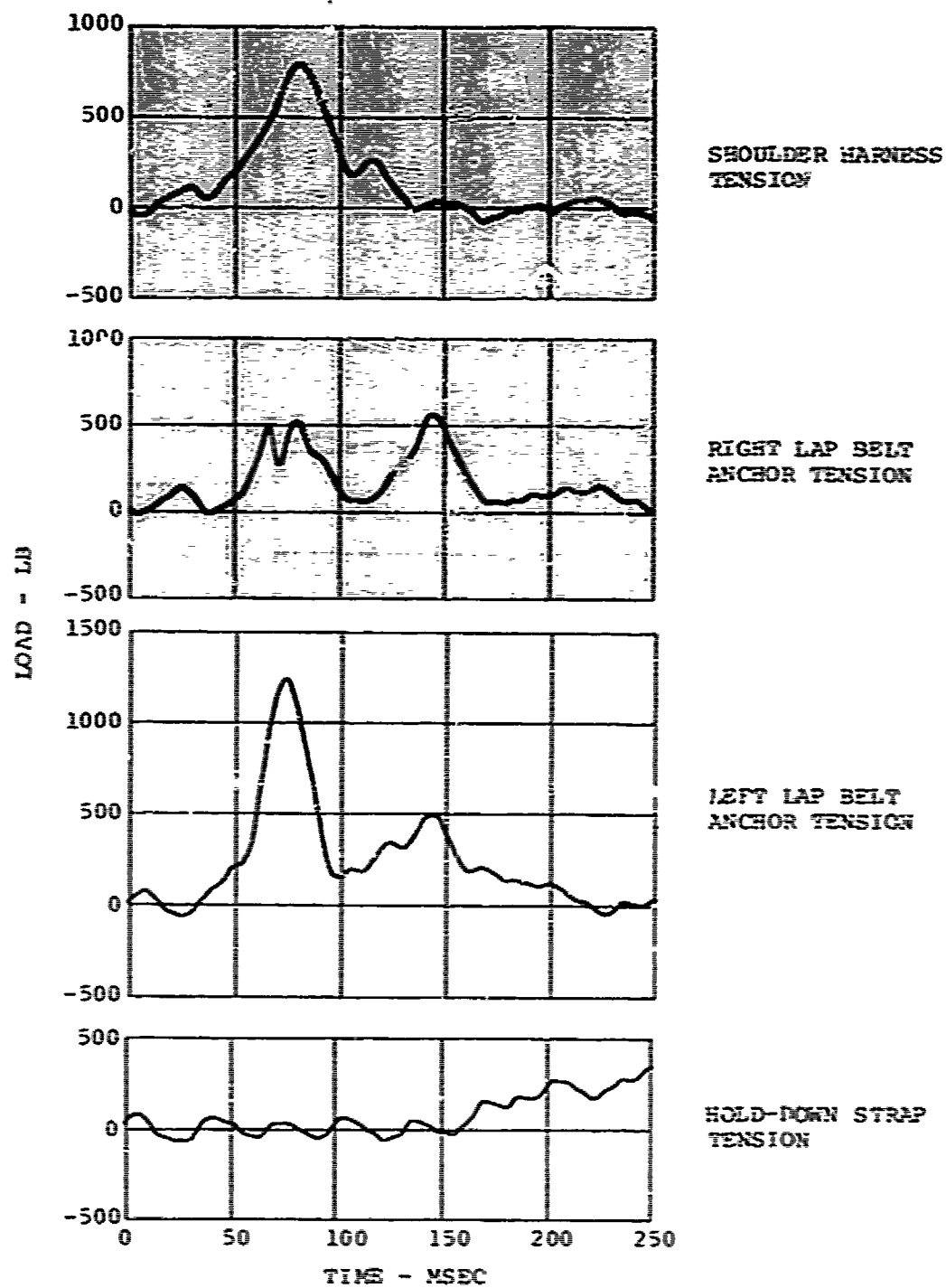
Figure 183. Restraint System Loads (Test 8).
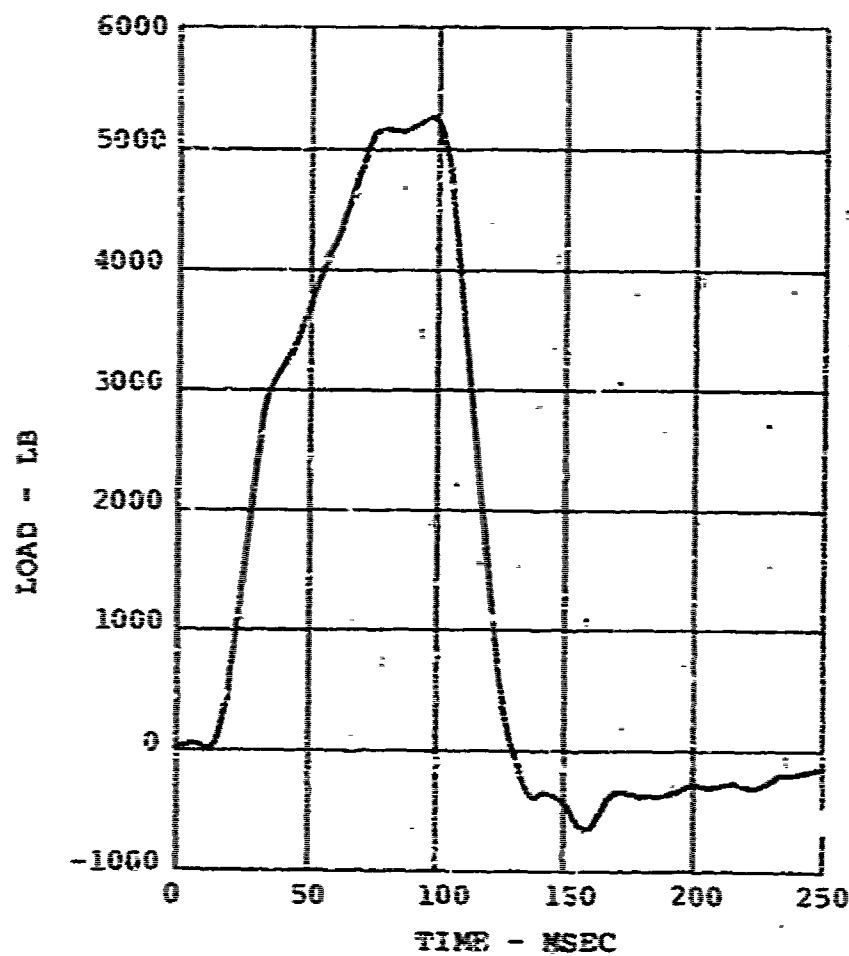
268
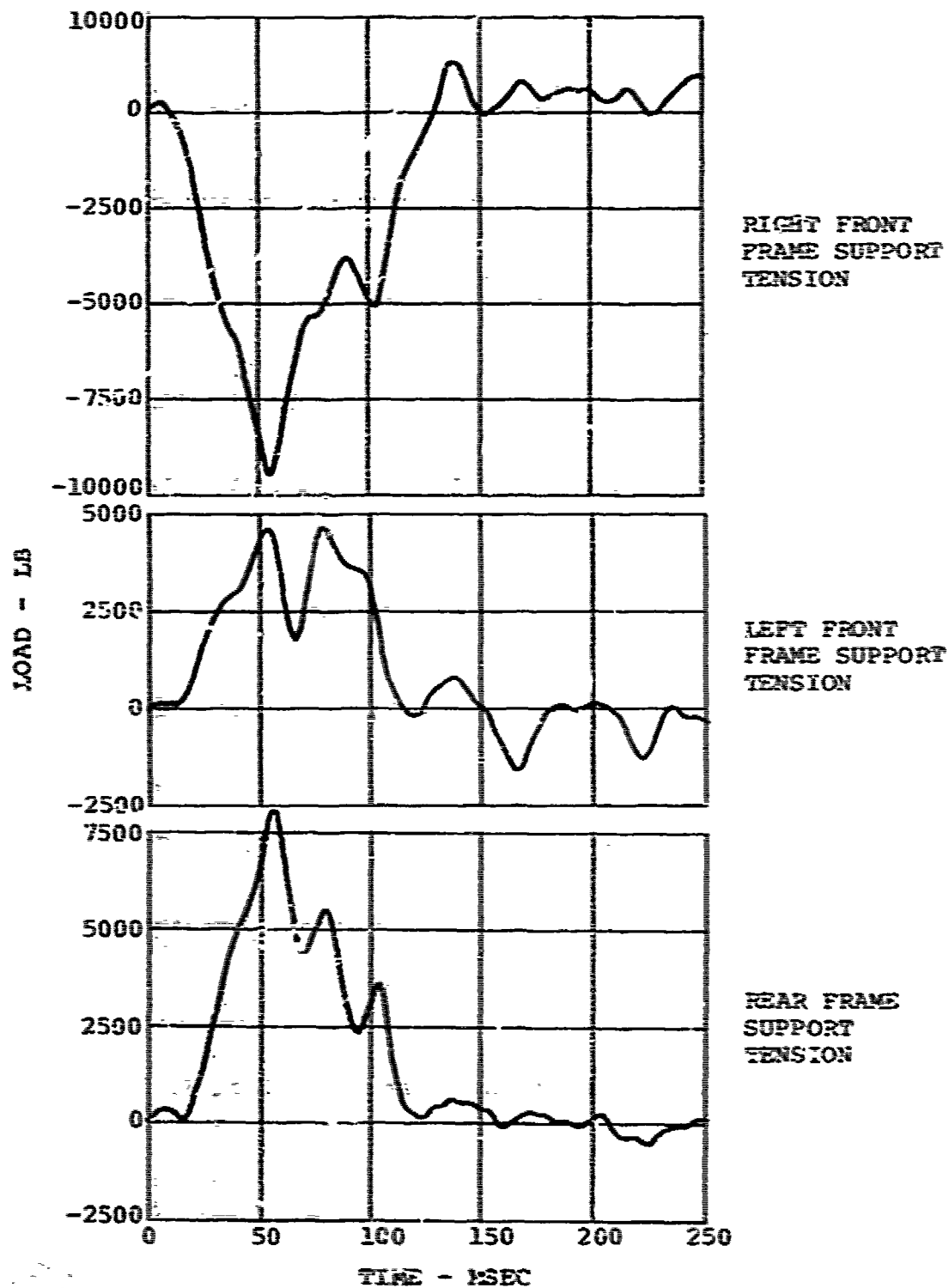
Figure 184. Frame Support Loads (Test 8).

269

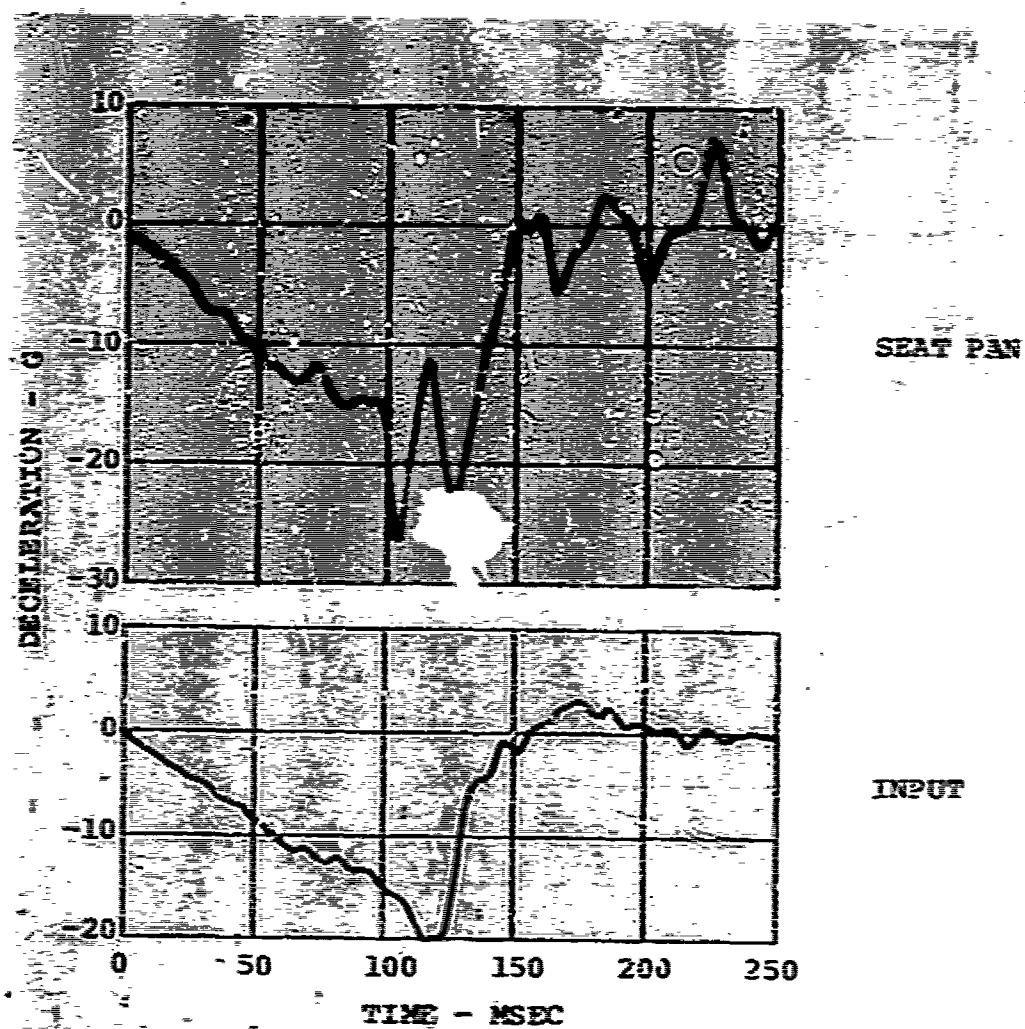Figure 185. Energy-Absorber Load (Test 8).

Figure 186. Longitudinal-Lateral Seat Pan and Input
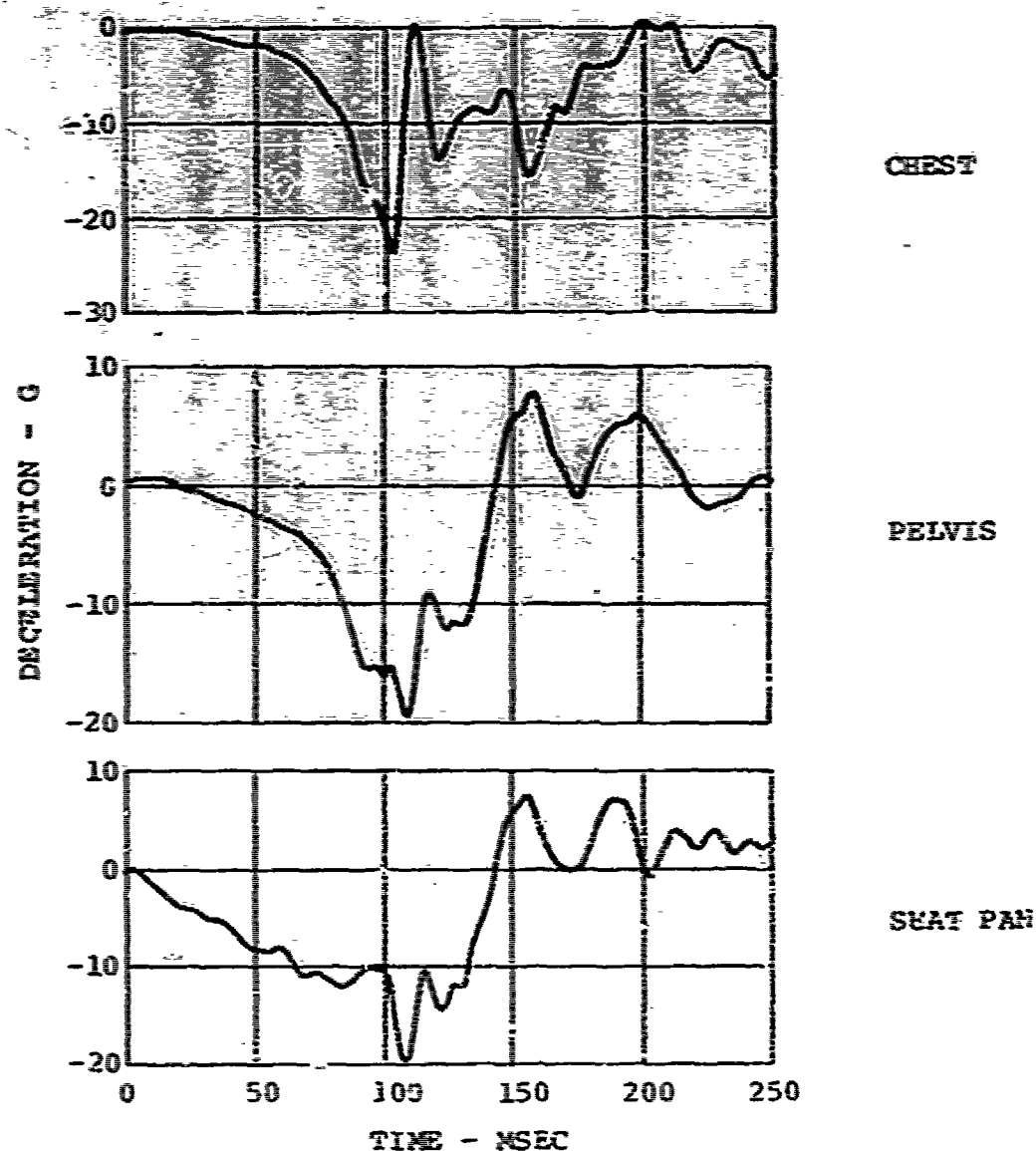Deceleration (Test 9).

271

Figure 187. Longitudinal Chest, Pelvis, and Seat Pan Decelerations (Test 9).
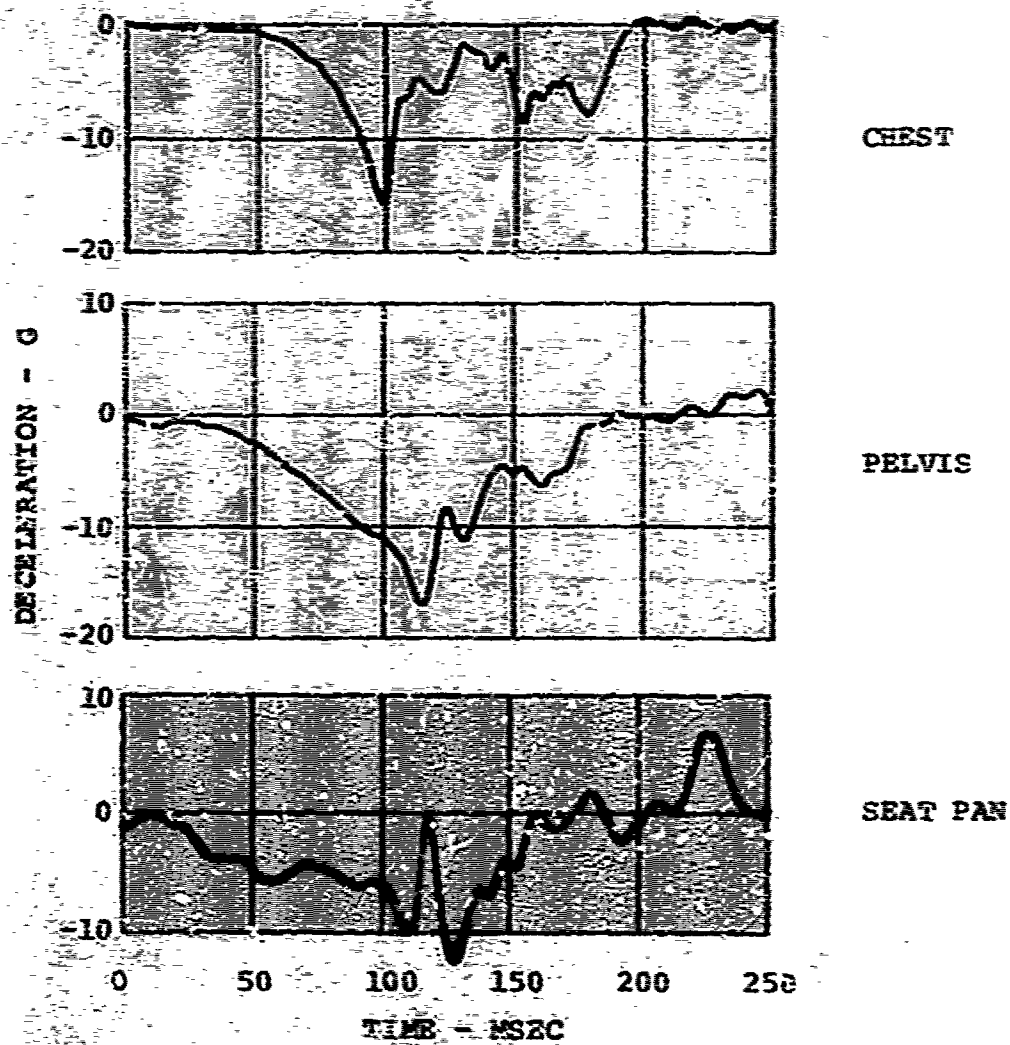
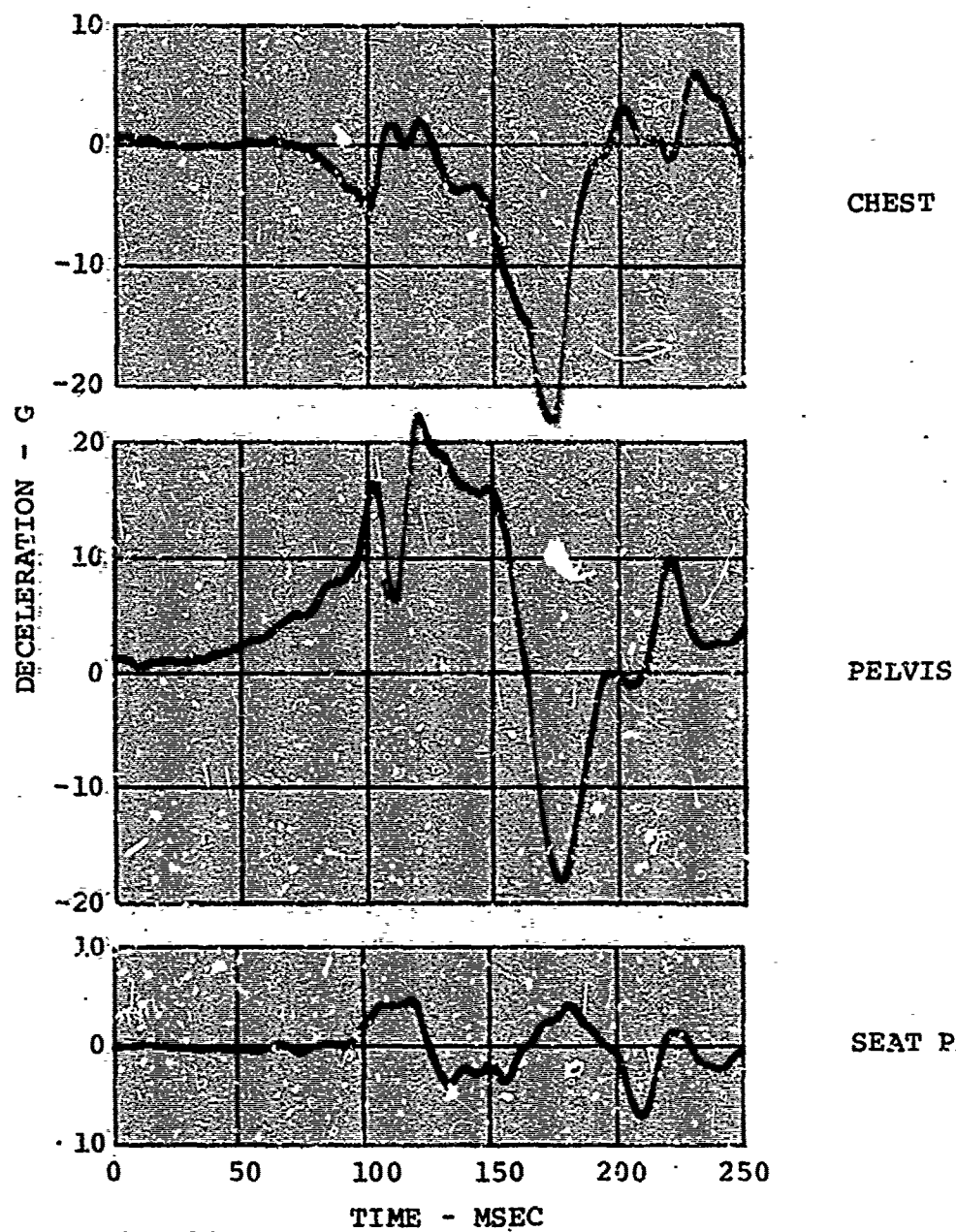Figure 188. Lateral Chest, Pelvis, and Seat Pan
Decelerations (Test 4).

273

Figure 189. Vertical Chest, Pelvis, and Seat Pan
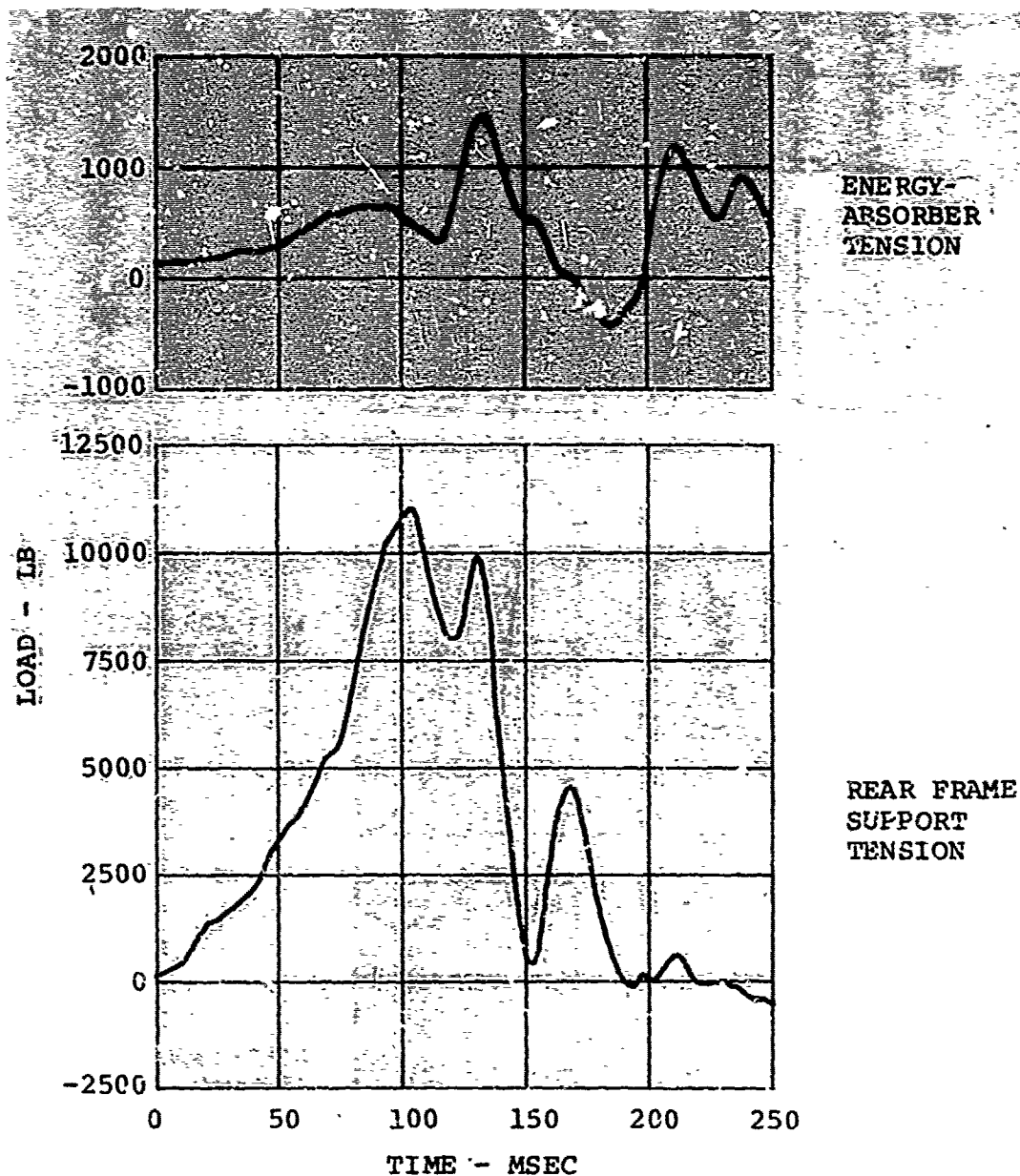Decelerations (Test 9).

274

Figure 190. Energy-Absorber and Rear Frame Support Loads (Test 9).
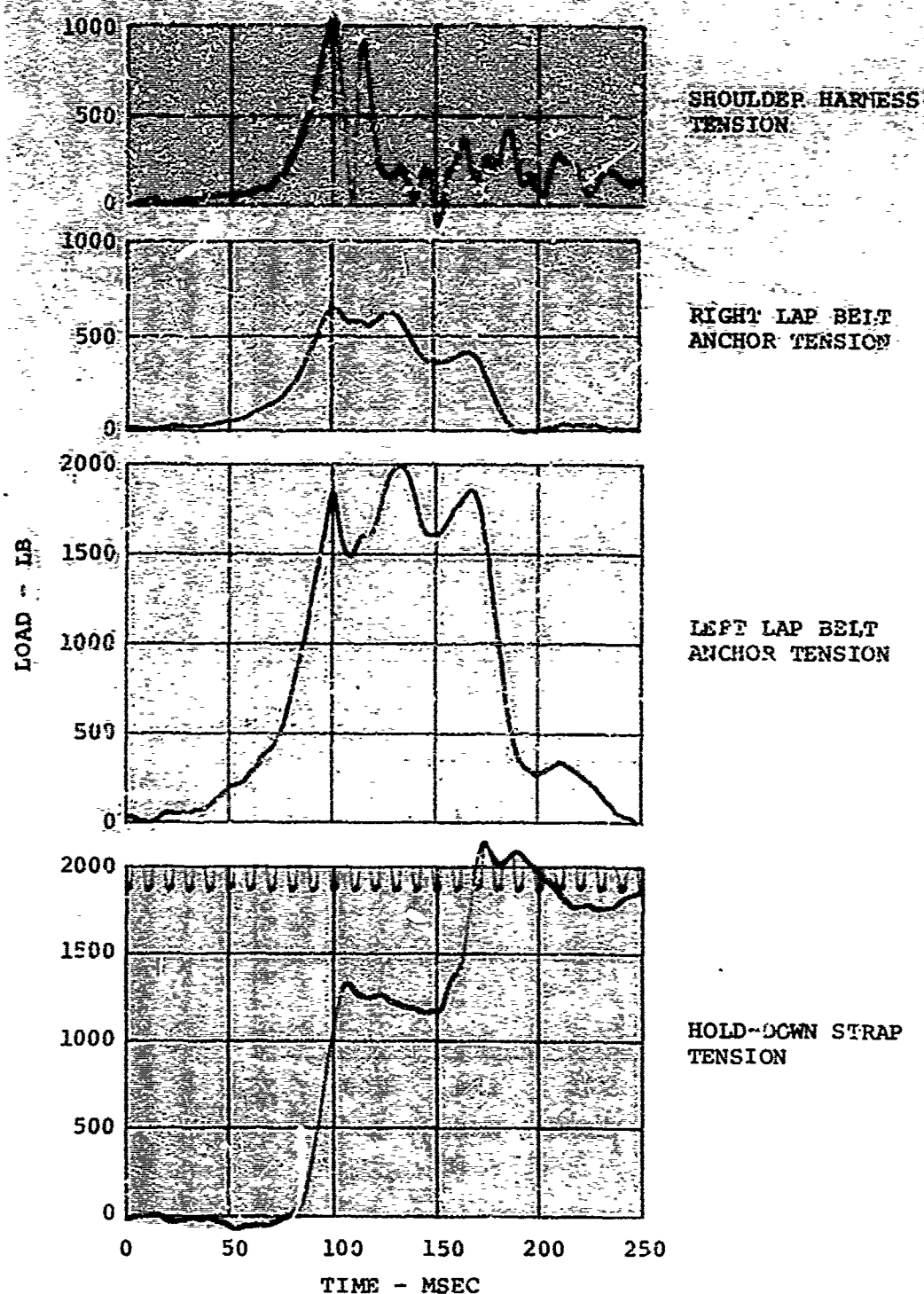
275

Figure 191. Restraint System Loads (Test 9).
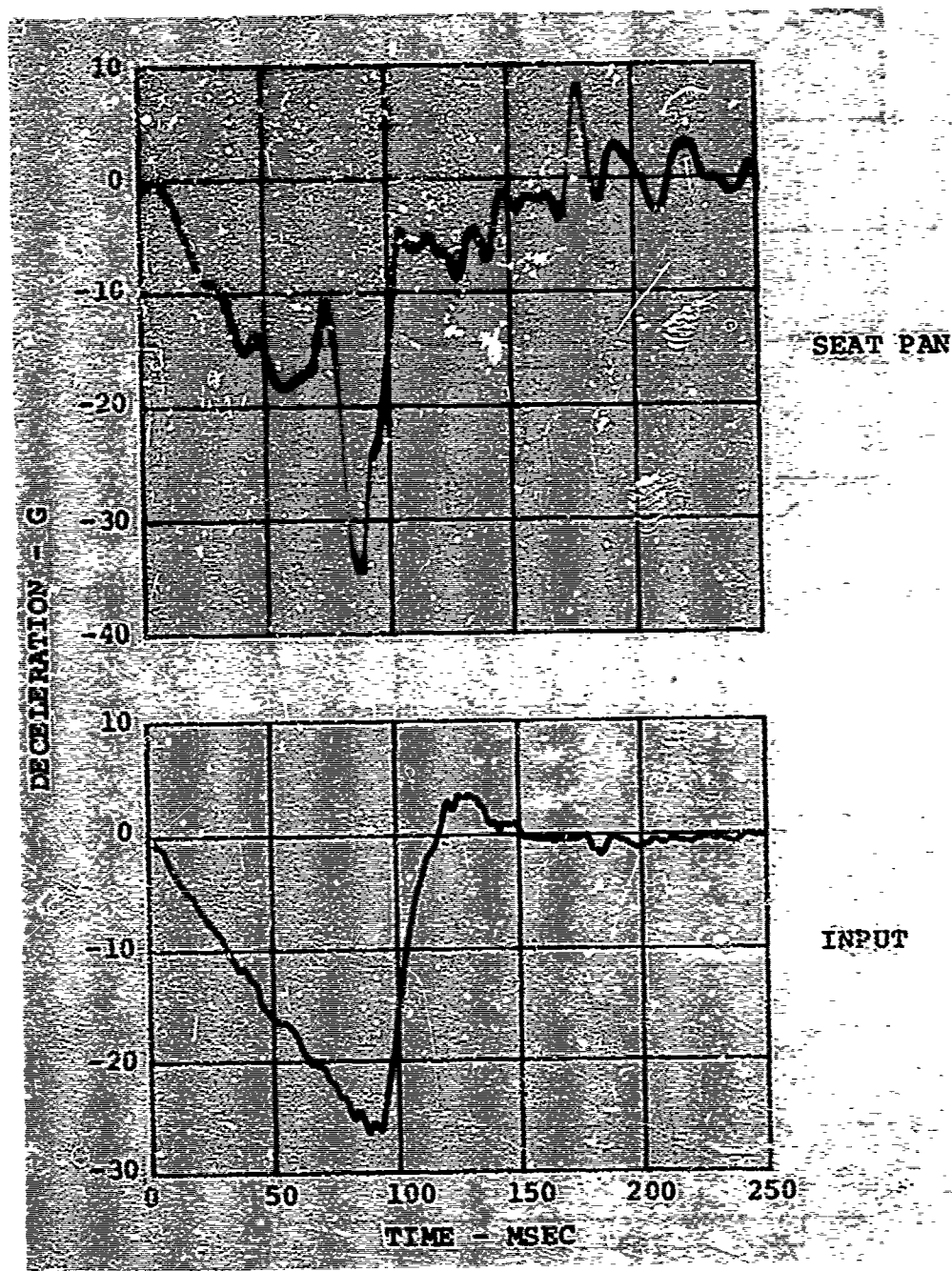
Figure 192. Longitudinal-Lateral Seat Pan and Input
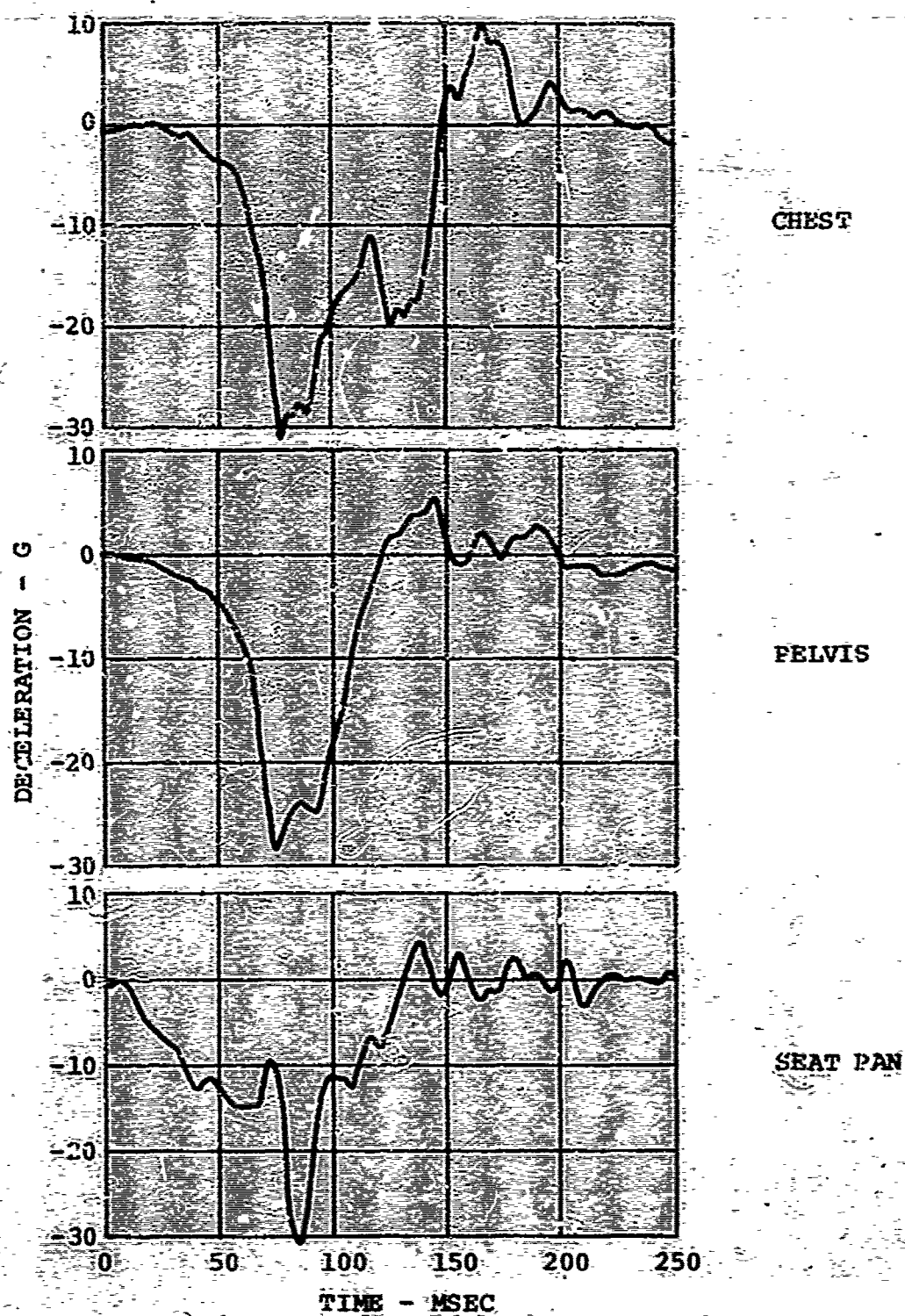Decelerations (Test 10).

277

Figure 193. Longitudinal Chest, Pelvis, and Seat Pan
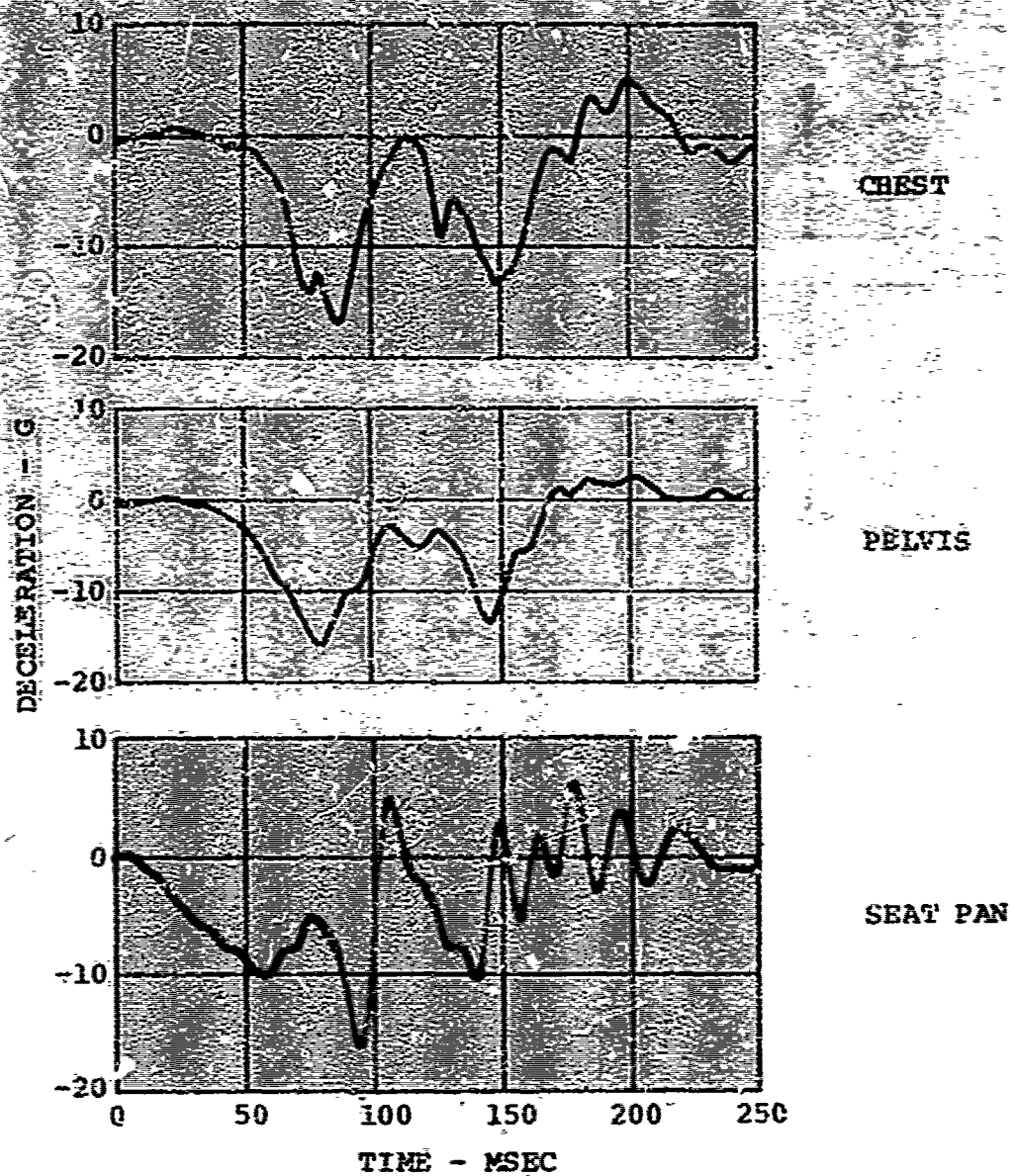Decelerations (Test 10).

278

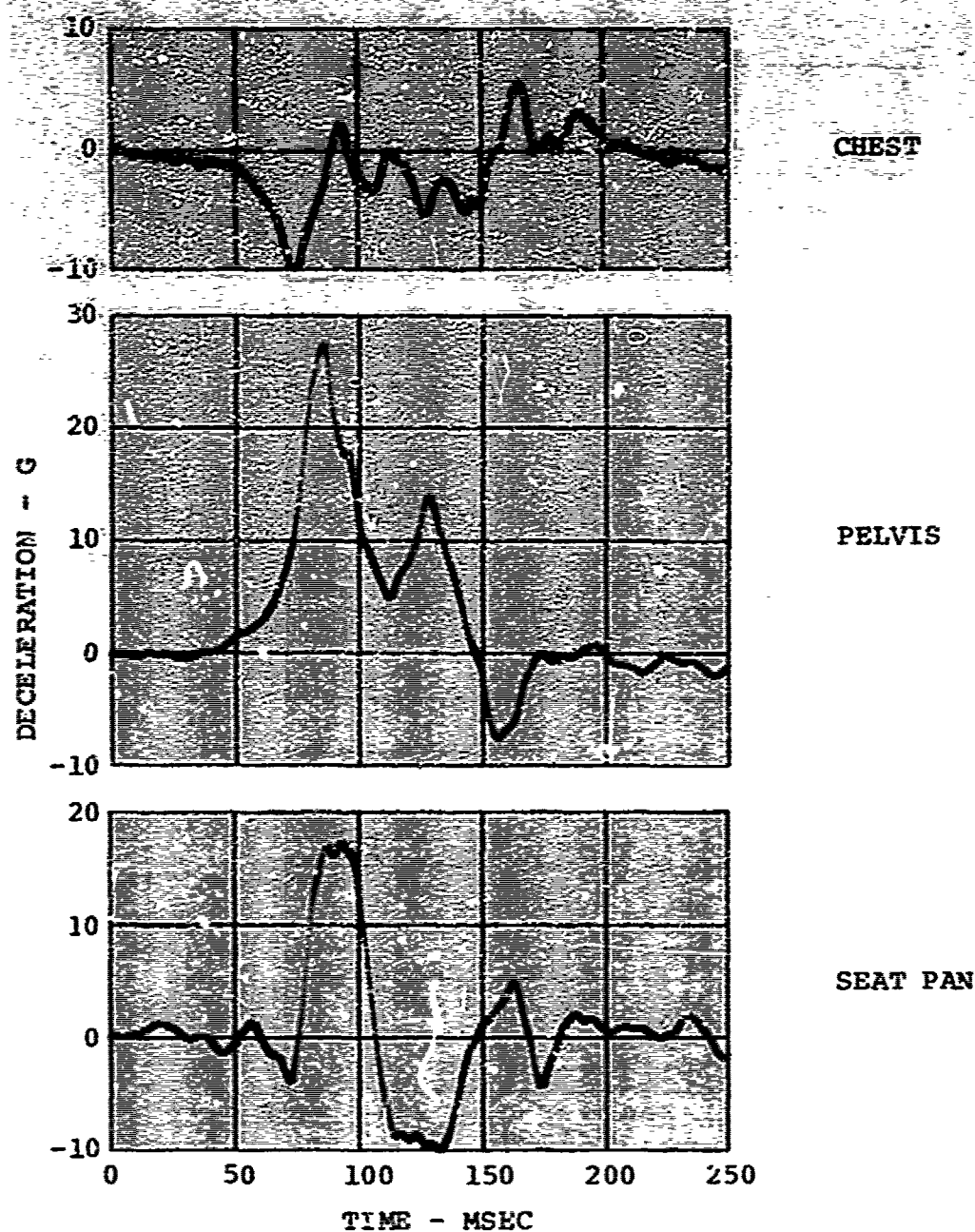Figure 194. Lateral Chest, Pelvis, and Seat Pan
Decelerations (Test 10).

279

Figure 195. Vertical Chest, Pelvis, and Seat Pan
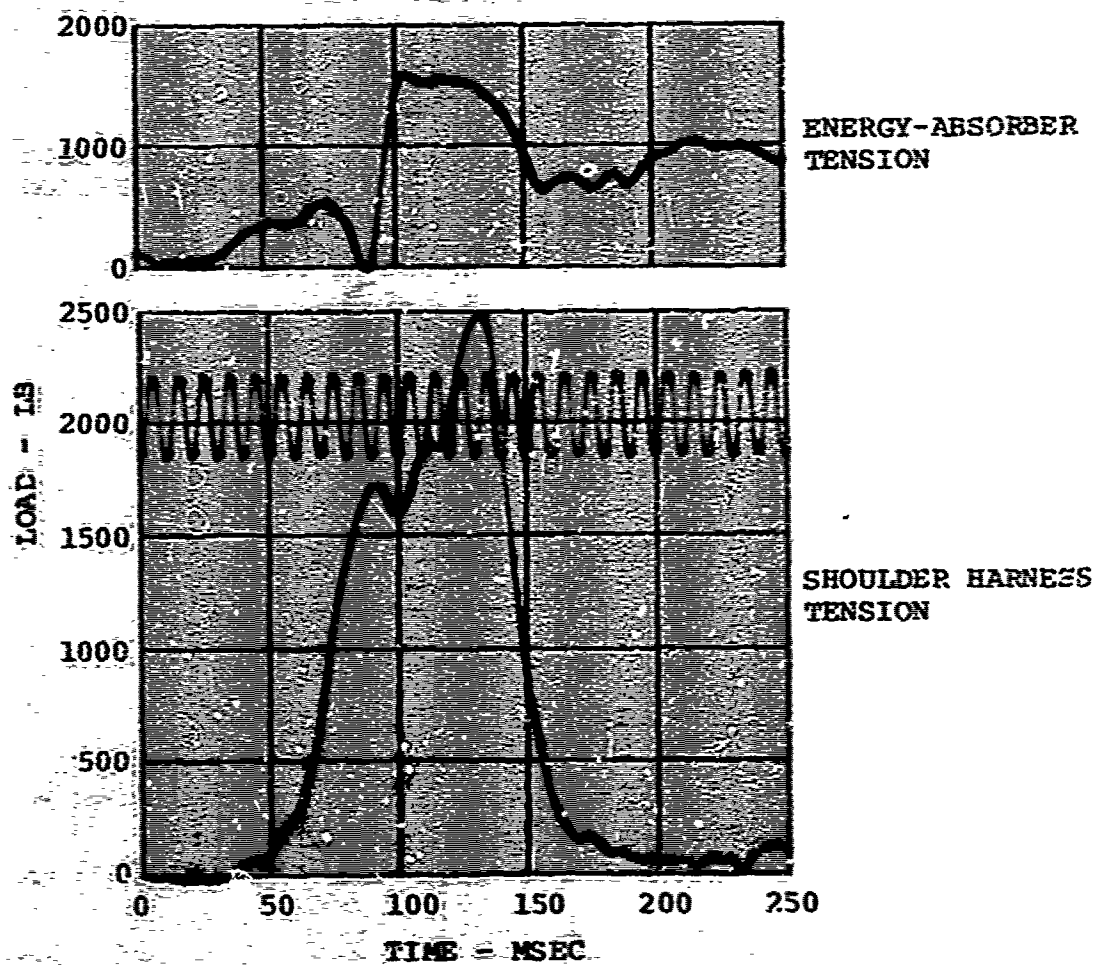Deceleration (Test 10).

280

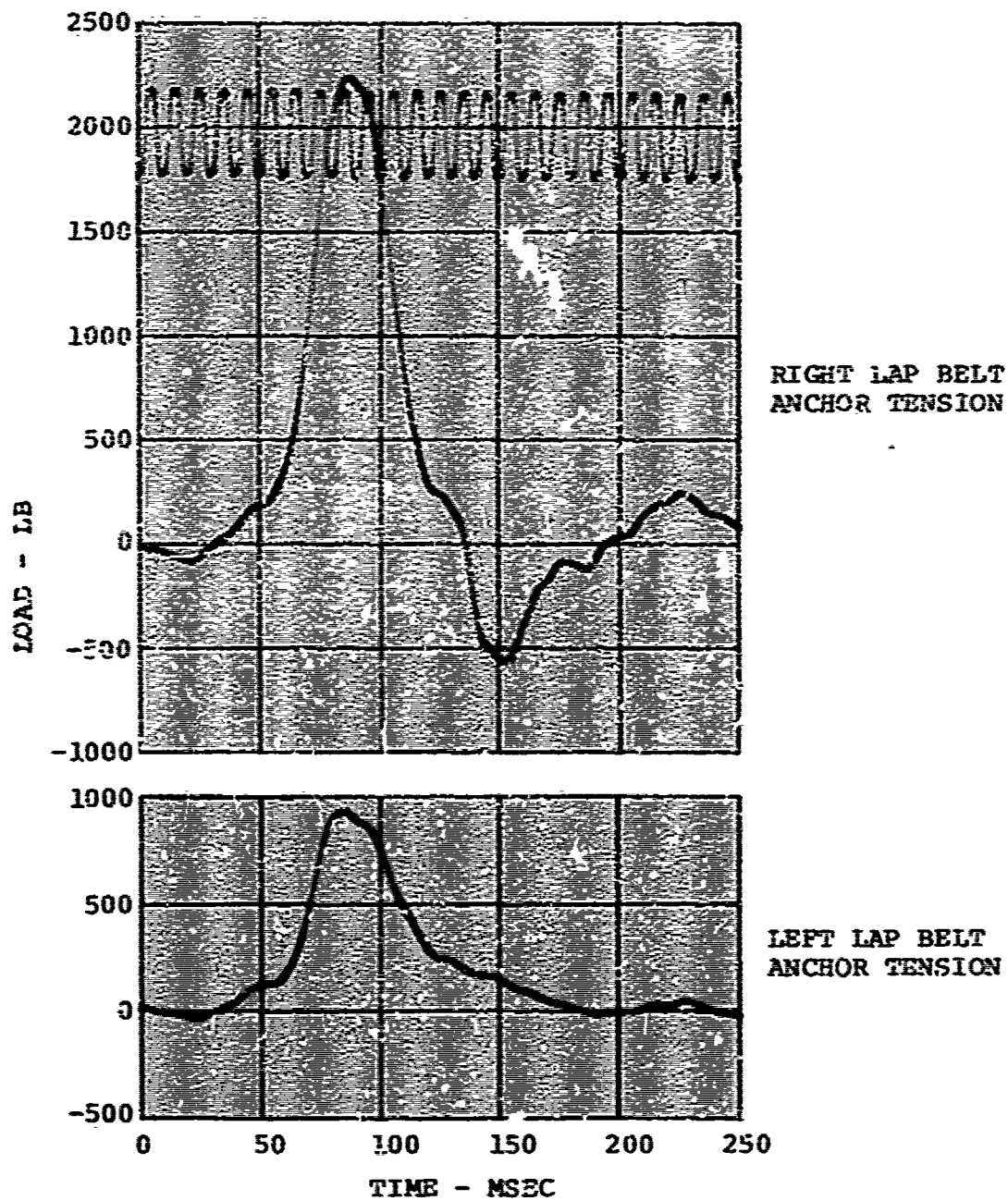Figure 196. Energy-Absorber and Shoulder Harness Loads (Test 10).

281

Figure 197. Lap Belt Loads (Test 10).

APPENDIX V

FABRICATION

V.1 BUCKET

The seat bucket was fabricated as a hand layup of woven glass
roving. A male mold was built up based on the inside dimen-
sions of the bucket. The thickness of the fiberglass was de-
termined by the ratio of the density of the simulated armor to
that of the fiberglass. This established a working thickness
of 0.83 inch of fiberglass. The actual number of layers (27)
of the woven roving glass cloth was dependent on matching the
areal density of the simulated armor.

Thin stiffener members were bonded into strategic locations in
the bucket to help the local integrity of the glass at highly
stressed points such as the lap belt anchorages. As is normal
practice with fiberglass work, the cloth and resin were laid
up beyond the edges of the finished product and then trimmed
back to the edge dimensions called out in the design drawings.
A white gel coat was initially laid down directly on the male
mold to give a white finish to the inside of the bucket.
During later stages of production, special aluminum plugs were
bonded into locations where bolts passed through the glass.
When drilled out, these plugs acted as crush tubes supporting
compression loads and preventing the glass from experiencing
compressive failure. An aluminum angle was bonded to the
front edge of the seat pan to provide the necessary longi-
tudinal restraint for the lower seat cushion to prevent it
from slipping out during a longitudinal pulse. Figure 198
shows the finished bucket installed in the seat structure.

V.2 GUIDE TUBE ASSEMBLY

The guide tubes were constructed of 2-inch-diameter, 1/4-inch
wall aluminum alloy (7075-T6). The lower end of each guide
tube was drilled and countersunk to accept four 1/4-inch flush-
head screws required for installation of the forward support
track attachment fittings. It was necessary that these screws
be flush-fitted to allow passage of the carrier bearings so
that the seat could stroke to the full bottom position, thus
maximizing stroking distance.

The upper end of each guide tube was drilled and spot faced to
accept eight buttonhead 1/4-inch screws, which attached the
guide tube to the upper yoke assembly portion of the guide
frame. After machining, the guide tubes were hard-anodized to
a 0.0005-inch penetration and a 0.0005-inch buildup to provide
a hard bearing surface.

283

Figure 198.   Bucket Installed in Seat Structure.

The upper yoke assembly was a weldment of aluminum alloy
(6061).   It consisted of two extension tubes angling upward
and inward from the top of the guide tubes.   The extension
tubes were joined at the top by a short piece of tubing posi-
tioned horizonatally.   A pair of 1/2-inch-thick brackets were
positioned and welded in the center of the horizontal tube to
accept the seat adjuster and support the energy-absorption
system.   Two angle fittings were machined from bar stock and
welded to the bottom of the extension tubes to provide spanning
structure for joining the yoke to the guide tubes.

The entire upper yoke assembly was welded, heat treated to a
T4 condition, and then installed on the guide tubes to form
the guide tube assembly.   During assembly, the holes previously
drilled in the top of the guide tubes were used as templates
for drilling and tapping directly into the portion of the angle
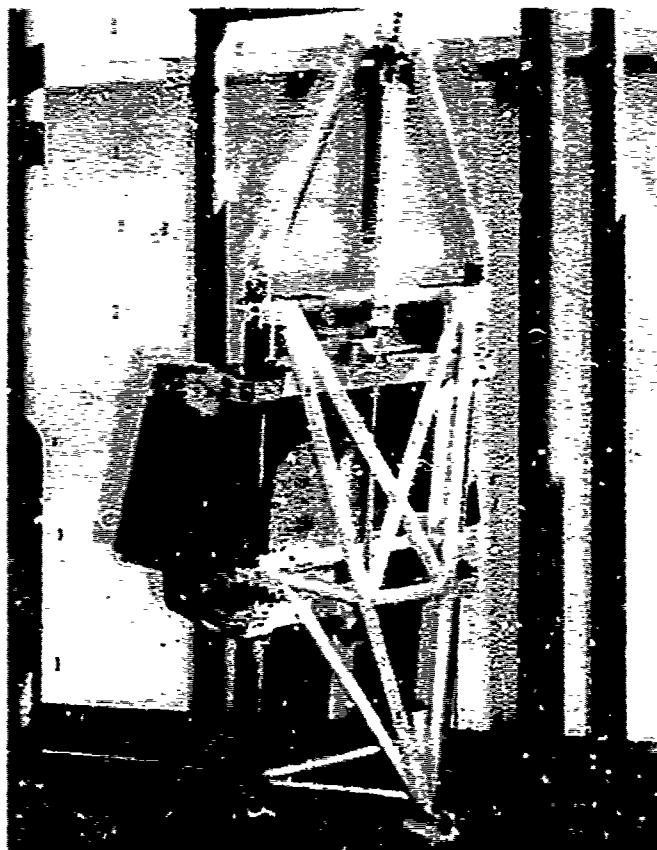fitting that fitted down inside the guide tubes.   Figure 199

284

Figure 199. Guide Frame Installation
in Seat Structure.

shows the guide frame after installation in the complete seat
structure.

V.3 CARRIER BEARINGS

Each carrier bearing was fabricated as a sandwich-type struc-
ture with cover plates machined from 1/4-inch-thick aluminum
(6061-T4). Figure 200 shows a finished carrier bearing
mounted in the seat system. The forward edge of the cover
plate was contoured to fit the back of the bucket adjacent to
where the bearing assemblies attach. (Refer to Figure 31 for
a detailed view.) The cover plates were drawn down on spacer
blocks by 1/4-inch bolts passing completely through the as-
sembly. The spacer blocks were machined from 1-1/2-inch-
thick aluminum alloy (6061-T651) plate. These blocks were
bored out to accept the shafts of the roller bearings which
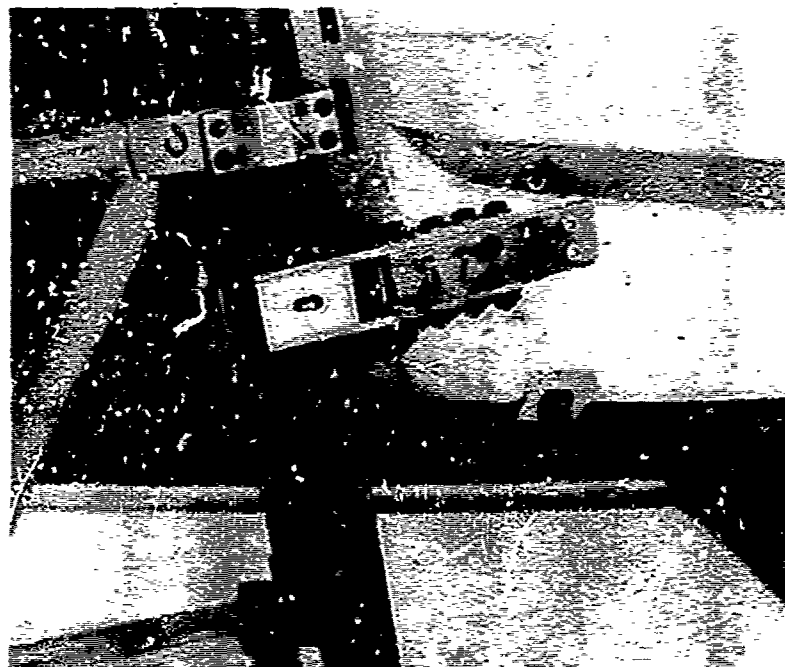rolled along the guide tube.

Figure 200. Carrier Bearing.

The roller shafts were commercially available items made from heat-treated steel alloy (4130).

The bearing assemblies were fabricated from commercially available bearing parts. They used needle bearings between the inner and outer races. The inner race was press fitted onto the bearing shaft, and the outer race was press fitted into a steel alloy (4130) ring with a concave outer surface. This outer surface was machined to fit around the guide tube and provide line contact through an approximate 40-degree arc.

The entire bearing assembly was fabricated in a small fixture simulating a section of the guide tube so that proper spacing of the bearing rollers and alignment of the cover plates and spacer blocks could be achieved. After alignment in the fixture, holes were drilled through the cover plate and spacer blocks and the unit was bolted together. This was one of the most critical adjustments in the seat system. The bearings had to be loose enough to account for any tolerance buildup or binding tendencies in the seat structure while also being tight enough to eliminate unnecessary slack in the system.

286

The square tube bearing crossmembers were formed from two pieces of 1/8-inch aluminum alloy angle (6061). The angle was then welded at the mating edges.

The bearing blocks were assembled to the crossmembers by inserting an extension (machined on the end of one of the spacer blocks) inside the square tube. The square tube crossmember had four 1/4-inch holes pre-drilled in it. These holes were used as drilling templates during final assembly of the bearings and crossmembers. Final assembly of these bearings and crossmembers was accomplished during final seat assembly. The bearings were installed on the guide frame assembly and the spacer block insert match-drilled to the holes pre-drilled in the square tube crossmember. Final attachment was made through four 1/4-inch bolts.

The inertia reel mounting plate was welded to the top surface of the top crossmember, and a small nut plate with self-locking inserts was installed on the inside to provide attachment for two No. 10 screws used on the forward side of the inertia reel. The rear of the inertia reel was attached by two No. 10 bolts which passed through an extension flange welded to the back edge of the crossmember, thereby allowing use of self-locking nuts. The lower energy-absorber attachment bracket was welded to the back side of the lower bearing crossmember and provided the primary load transfer path from the energy absorber into the seat bucket. The entire lower energy-absorber attachment bracket was a welded assembly fabricated from aluminum (6061-T6).

V.4 SUPPORT STRUCTURE

The seat support structure was built up with the aid of a welding fixture. Figure 201 shows the fixture with a nearly completed support structure installed in it. This welding fixture was built from structural materials and was used for two primary purposes: (1) to establish reference locations from which several primary parts of the seat support structure could be built up and (2) to support the welded support structure during heat treating. The weld fixture contained two tubes simulating the seat guide tubes. These tubes were fixed at three bulkheads, which established the spacing and parallelism of the basic structure. An upright extension at one end supported the cluster tube portion of the support structure. The other end of the fixture provided the reference point for assembly and welding of the upper yoke portion of the guide frame.

The three bulkheads in the welding fixture each provided a reference location for three components on each side of the
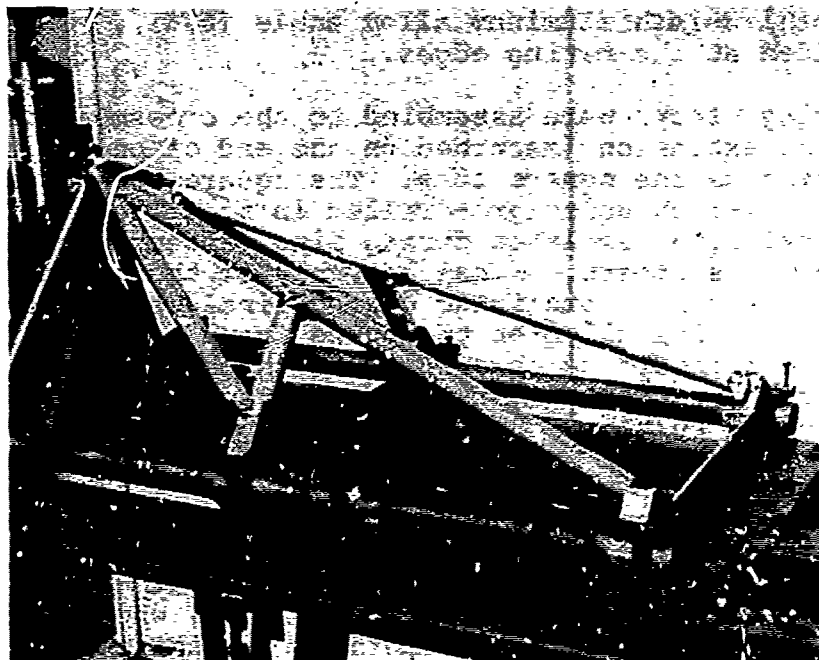
287

Figure 201. Welding Fixture With Support Structure Installed Prior to Welding.

support structure from which the rest of the support structure was built up. Two of these components initially assembled on each simulated guide tube were similar saddle blocks. Figure 202 shows the bore of the saddle block being machined. These saddle blocks provide the necessary clamping force to attach the support structure mechanically to the guide tubes. The forward support track attachment fittings were machined out of aluminum alloy (6061-T651) and then clamped to the bottom end of the guide tubes in the welding fixture. Figure 203 also shows the finished sets of saddle blocks.

The cluster tubes were turned from 1-3/4-inch-diameter round bar stock, and one was attached at the top of the lower extension of the welding fixture for each support structure that was fabricated. These seven pieces -- the two pairs of saddle blocks and the one pair of forward support track attachment fittings mounted on the two simulated guide tubes -- and the cluster tube were properly referenced against their bulkheads to provide the base for the cutting, fitting, and welding of the structural tubing used to create the support structure. Each pair of members that attached to the guide tubes had

288

Figure 202.   Machining Bore of Saddle Blocks.

Figure 203.   Post-Machining Inspection of
Saddle Blocks.

crossmembers fitted between them. The hollow tube cross-
members slipped down over round bosses that provided conti-
nuity through the welded joint. In addition, there were tubes
fitted between the initial three pairs of fittings and the
cluster tube. After these tubes were all properly sized and
located, an additional X member was built up in the plane de-
fined by the uppermost saddle blocks and the cluster tube.
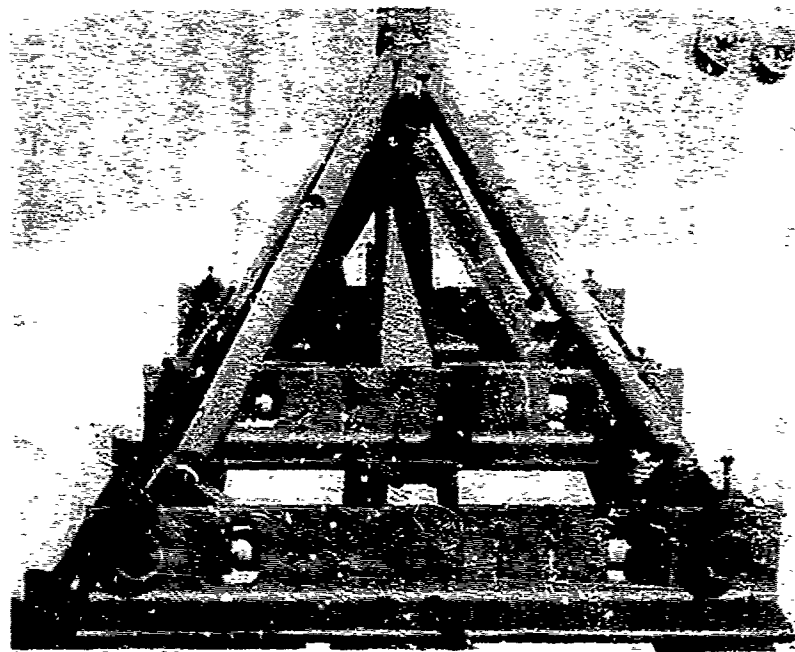Figure 204 shows the support structure before the X member was
installed.

Figure 204. Support Structure Before
Installation of X Member.

All tubing in the upper portions of the support structure was
cut from 1-1/2-inch-diameter by 1/8-inch-wall aluminum alloy
(6061-T4). The lower crossmember located between the two for-
ward support track attachment fittings was cut from 1-1/2-inch-
diameter by 1/4-inch-wall tubing of the same alloy. The two
remaining tubes that formed the triangle in the plane of the
base of the support structure were cut from 1-inch-diameter by
1/8-inch-wall tubing, also of the same alloy.

290

All joints were welded (TIG) and incorporated 100-percent penetration as defined by MIL-STD-22A. The entire structure was annealed and heat treated to the T4 condition. The saddle block caps were initially secured to the welding fixture with bolts threaded directly into the body of the saddle block. After the heat-treating process, these were removed and replaced with self-locking inserts and socket-head cap screws.

V.5 ENERGY ABSORBER

The energy-absorber tensile tube was fabricated from fully annealed stainless steel tubing (304). Considering the critical application and the fact that it was to be used in the plastic region of its stress-strain curve, extreme caution was observed throughout the fabrication process. The material specification to which the tubing was ordered required that the material be free of all nicks, scratches, and other surface imperfections.

The tubing was cut in rough lengths from the pieces of stock received. Short test samples were selected adjacent to these primary pieces for use in correlating and verifying the strength of the material. The tubing was then placed in a lathe and held in a collet chuck so as not to damage or mark the tube in any significant manner. Then, each end was cut back and dressed to give a deburred and properly sized tube. Alloy steel end plugs were turned with a 6-degree taper on the inboard end, and a 5/16-24 internal thread was tapped for fitting the rod end bearings to each end of the finished energy absorber. The O.D. of the insert was turned 0.011 inch smaller than the I.D. of the stainless steel tensile tube. This provided the necessary bond line thickness for proper bonding with the epoxy used. All parts were cleaned in acetone with a final wash of Freon TF before the end fittings were bonded into the tensile tubes.

The test samples used in the energy-absorber quality assurance tests were bonded up at the same time as the primary energy absorbers to help detect any problem in the bonding process that would be common to all members bonded at that time.

V.6 FLOOR ATTACHMENTS

Fabrication of the floor attachment system involved machining the floor tracks and the slider blocks. The floor tracks themselves were of uniform cross section and were machined from aluminum alloy bar stock (6061-T651). The section represented a shape easily produced in large quantities as an extrusion. The slider blocks were turned from alloy steel (4130).

291

The center portion of the slider block had a round shanked section that was sized to fit into the spherical bearing of the rod-ends attached to the seat support structure. The rectangular blocks that formed the ends of the slider block were milled to provide a sliding fit in the floor tracks. The slider blocks for the two forward floor attachment locations were bored to accept the quick-release pins used to lock the seat into a longitudinal position. Figure 205 shows one of the floor attachments in the static test configuration.
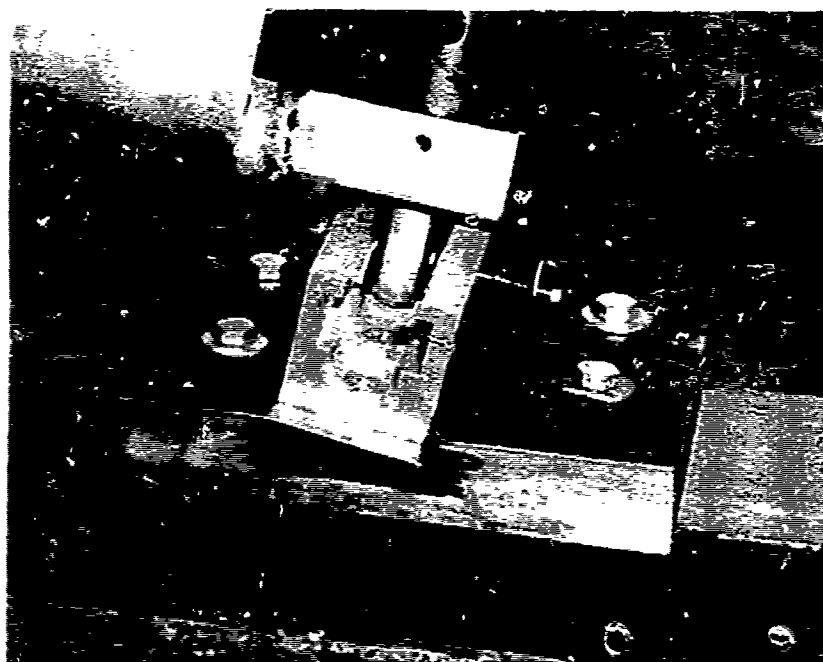

Figure 205. Floor Attachment for Static Tests.